FATIGUE CRACK INITIATION AND PROPAGATION FROM DEFECTS IN ALUMINIUM WELDS

A THESIS SUBMITTED BY PETER WOODS FOR THE DEGREE OF

DOCTOR OF PHILOSOPHY

SEPTEMBER 1976

SUMMARY

Fatigue crack initiation and propagation in aluminium butt welds has been investigated. It is shown that the initiation of cracks from both buried defects and from the weld reinforcement may be quantified by predictive laws based on either linear elastic fracture mechanics, or on Neuber's rule of stress and strain concentrations. The former is preferable on the grounds of theoretical models of crack tip plasticity, although either may be used as the basis of an effective design criteria against crack initiation. Fatigue lives following initiation were found to follow predictions based on the integration of a Paris type power law.

The effect of residual stresses from the welding operation on both initiation and propagation was accounted for by a Forman type equation. This incorporated the notional stress ratio produced by the residual stresses after various heat treatments.

A fracture mechanics analysis was found to be useful in describing the fatigue behaviour of the weldments at increased temperatures up to 300°C. It is pointed out, however, that the complex interaction of residual stresses, frequency, and changes in fracture mode necessitate great caution in the application of any general design criteria against crack initiation and growth at elevated temperatures.

ACKNOWLEDGEMENTS

I would like to thank Mr V.N.Whittaker for his continual guidance and encouragement throughout this work, and for his patience with somewhat eccentric habits and behaviour. I am indebted to Dr. Barnby for helpful discussion in the final stages of the work, and for his suggestions on the presentation of this thesis. For assistance with the practical work I am grateful to Mr.J.Foden, Mr.K.Moule, and to the many friends at the University of Aston who have helped me along the way.

Finally I thank my colleagues in the Personal Issue section at Birmingham UBO, for helping to maintain a balanced attitude during the completion of the thesis.

INDEX

CHAPTER 4 cont'd Page

INTRODUCTION

For more than a century, it has been appreciated that metal components and structures subjected to variable or repeated loads may fail in service, even though they would usually be capable of standing considerably higher loads if the loading were of a 'static' nature. This type of failure, which consists of the formation of a crack or cracks under the action of varying loads, has come to be known as fatigue. The fatigue failure of metals may therefore be defined as the formation of a crack or cracks as a result of the repeated application of loads, each of which is insufficient by itself, to cause normal static failure.

In the design of a component or structure the designer has to satisfy three conditions.

(1) It must be able to perform its specified functions as efficiently as possible.

(2) It must be capable of being fabricated economically.

(3) It must be capable of providing an adequate service life.

As a direct result of the first and second of these conditions the modern trends in engineering design are to reduce factors of safety to a bare minimum, in order to reduce weights and costs, and to increase the speed of operation of machines and production processes, in order to make the most effective use of the invested capital.

Unfortunately, both these trends tend to work against the designer in his efforts to obtain an adequate service life, particularly

in cases where fatigue failure is likely to occur. Perhaps it is therefore not so surprising that 90% of the failures which occur in engineering components can be attributed to fatigue.

When fatigue cracks do occur, they are inevitably initiated at points of stress concentration. Since all welded joints are inevitably points of stress concentration, it is axiomatic that weldments are among the structures most prone to fatigue failure.

Much recent theoretical and empirical work has concentrated on the role of fatigue crack initiation and propagation phases in the overall fatigue failure of carefully machined test pieces. For the purpose of utilizing these advances in the development of design specification for welded joints, it would appear to be essential that the predictions should be verified in the context of naturally occurring defects in practical welding situations.

2. LITERATURE REVIEW

2.1 General Description of the Fatigue Process

The first formal investigation of the fatigue process was reported by Ewing and Humphrey[1]. Their work on Swedish iron demonstrated that fatigue failure started with the development of coarse slip bands which broadened into cracks. Failure was completed by the spreading and linking of these cracks. Following this, much work was concentrated on the development of slip bands[2]. Eventually Orowan[3] turned interest towards cracking with his theory of crack growth.

It was not until 1961 that attention was paid to the physical features of initiation and growth of fatigue cracks[4]. Forsyth[4] developed the three stage classification of fatigue cracking which is still currently accepted. This was initiation, stage I or slip band growth, and stage II growth on planes normal to the maximum tensile stress. Ewing and Humphrey[1] had noted that crack initiation in plain samples took place on slip bands. Forsyth[5] found that metal was extruded from these slip bands, and simultaneously fine crevices, generally named intrusions, were formed within these bands. The intrusions develop into cracks, and initiation was accepted as the formation of a 'viable' crack from an intrusion. Little attention has been given to the number of fatigue cycles required to initiate a crack in plain samples, but the proportion of life occupied by initiation has been found to increase with total fatigue life, and may exceed 80% of the total life at 10^6 cycles.[6]. It is known[7] that surface roughness may greatly affect fatigue life, and this is explained by the presence of favourable sites for early slip-band formation at stress concentration such as surface scratches.

The presence of a notch also facilitates the nucleation process, but it has been shown that the initiation period may even so take up 65% of the total life of a notched test piece having a fatigue strength reduction factor of 1.8[8]. Much recent work has concentrated on the effect of notches on fatigue crack initiation, and this will be dealt with in a later section. No information exists on crack initiation from natural notch or crack like defects of the type found in weldments, it is generally assumed that initiation is instantaneous in these case[9].

Stage I fatigue crack growth takes place on planes of maximum resolved shear stress, and is considered by Forsyth[4] to be an extension of the reversed slip process responsible for crack initiation. Although this mode of growth may occupy a major proportion of the life of plain specimens, it is generally considered to be absent in notched or cracked test pieces, and is not therefore relevant to the present work.

Stage II crack growth takes place on planes normal to the applied stress and Forsyth[4] considered that it was controlled by the maximum principal stress operating in the region of the crack tip. The characteristic fatigue striations in stage II, first observed by Zappfe and Warden[10], appear as markings or lines on the fracture surface at right angles to the direction of propagation. It has been shown[11,12] that the striations were associated with the complex plastic deformation process occurring at the crack tip. In general each fatigue striation is produced by one cycle of the fatigue load[13,14].

Laws governing Stage II crack growth rates form the basis of life prediction techniques for components containing cracks or crack-like flaws, and this area will be covered fully in a later section.

2.2 Models of Crack Initiation

2.2.1 Application of the Range of Stress Intensity Factor

The stress intensity factor arises from Westergaard's treatment[15] of the stress analysis of a crack. He defined an Airy stress function which satisfied the equilibrium and compatibility equations for the case of a crack length 2a in an infinitely wide sheet under uniform tension [Figure 1]. The crack tip stress field at a point $P(r,\theta,)$, where r is small compared with the crack length,[16] is given by:-

$$\sigma x = \frac{K}{\sqrt{2\pi r}} \cos\frac{\theta}{2}\left[1-\sin\frac{\theta}{2}\sin\frac{3\theta}{2}\right] \quad - [1]$$

$$\tau xy = \frac{K}{\sqrt{2\pi r}} \sin\frac{\theta}{2}\cos\frac{\theta}{2}\cos\frac{3\theta}{2} \quad - [2]$$

$$\sigma y = \frac{K}{\sqrt{2\pi r}} \cos\frac{\theta}{2}\left[1+\sin\frac{\theta}{2}\sin\frac{3\theta}{2}\right] \quad - [3]$$

where K, the stress intensity factor is given by:-

$$K = \sigma\sqrt{\pi a} \quad - [4]$$

for the geometry shown in figure 1.

The stress intensity factor uniquely defines the stress field around the crack tip, and may be related to the driving force G tending to cause crack extension[16] by the relationships:-

$$K^2 = EG \text{ in plane stress} \quad - [5]$$

$$K^2 = \frac{EG}{(1-\nu^2)} \text{ in plane strain} \quad - [6]$$

where E is Youngs Modulus and ν is Poissons Ratio.

Combining equations [4] and [5] leads to the expression:-

$$\sigma = \left(\frac{2EG}{\pi a}\right)^{\frac{1}{2}} \qquad - [7]$$

This is similar to the Griffith equation[17] for the fracture stress of a brittle solid containing a crack of length 2a:-

$$\sigma_F = \left(\frac{2E\gamma}{\pi a}\right)^{\frac{1}{2}} \qquad - [8]$$

where γ is the surface energy.

However, in metals, crack extension is accompanied by plastic deformation, and the energy expended in this case is several orders of magnitude greater than the increase in surface energy of a brittle solid considered by Griffith[17].

Irwin[18] and Orowan[19] proposed a theory in which the energy of plastic deformation or crack extension force, G, replaced the surface energy as the controlling force in brittle fracture. Irwin's concept was that fracture occured when the crack extension force reached a critical value Gc, which was termed the critical strain energy release rate, or the fracture toughness.

The stress intensity factor, K, has now replaced G as the parameter used to describe the onset of brittle fracture. The solution for K differs with the geometry of the cracked body, and the correction factor to take account of interaction between the crack and the free surface of a plate of finite width, is usually expressed as a polynomial in a/w[20], where w is the plate width. Thus:-

$$K = \sigma\sqrt{af}\left(\frac{a}{w}\right) \qquad - [9]$$

Several methods are available for computing $f(\frac{a}{w})$, including conformal mapping[21], boundary collocation procedures[22], and finite element analysis[23]. Alternatively, the crack extension force G can be determined experimentally[24], since Irwin[25] has shown that:-

$$G = \frac{P^2}{2B} \frac{d}{da}\left(\frac{1}{M}\right) \qquad - [10]$$

where P is the load on the specimen

B is the specimen thickness

$\frac{1}{M}$ is the compliance, C (C = Extension/Load)

Recently Cartwright and Rooke[26] have shown that approximate stress intensity factors for complex cracked configurations may be compounded from known standard solutions.

The critical value of the stress intensity factor, K_C, at which a crack will extend, is dependent upon the condition of stress at the crack tip and is higher in plane stress than in plane strain. The plane strain fracture toughness, K_{IC}, is a constant for a particular material and is extensively used in specifying maximum tolerable defect size in structures, and in materials selection.

In the case of failure by fatigue, the maximum value of K in the cycle may exceed K_{IC}, because fracture is time dependent and complete failure does not have time to occur. Of much more practical importance, however, is the slower growth of fatigue cracks when the highest K value produced is less than K_{IC}. Much recent work has utilized the range of stress intensity factor, ΔK, in models and laws for both the initiation and propagation of fatigue cracks.

Analogous to continuum theory is the model of Weertman[27], based on a continuous distribution of dislocations. He used a model of the plastic relaxation at a crack tip[28] to show that the plastic opening displacement at the crack tip, Φ, has two components, Φ_1 and Φ_2. The component Φ_1 is reversible in that dislocations re-enter the crack, while Φ_2 accumulates dislocations beyond the crack tip on each stress reversal. His model, and that of Bilby and Heald[29] and McCartney and Gale[30], propose that damage accumulates linearly with the accumulation in Φ_2. Thus the fatigue crack initiation period depends upon Φ_2, and this is equivalent to a dependency on ΔK^2. These models thus lead to the expression:-

$$Ni = \frac{A}{\Delta K^2} \qquad - [11]$$

where Ni is the number of cycles to initiate the crack and A is a constant.

The model of McCartney and Gale[30] is consistent with the accumulation of internal stress which is eventually sufficient to rupture carbides at low stress amplitudes[31], and with the presence of characteristic dislocation structures at final failure[32].

May[33] proposed that initiation would occur when the crack tip strain, ϵ_c, reached a critical value so that at failure:-

$$N\epsilon^2 = A\epsilon_c \qquad - [12]$$

where ϵ is the strain amplitude and A is a constant. Since a given strain (ϵ) implies a given displacement (Φ) for a fixed gauge length, this relationship implies that the crack initiation period depends on ΔK^4, giving the expression:-

$$Ni = \frac{A}{\Delta K^4} \qquad - [13]$$

Analyses based on crack tip opening displacements apply strictly to sharp cracks, but Smith[34] has shown that the treatment should apply to notches of finite root radii. His analysis predicted that Φ at the notch tip is reduced by a factor of 2 when the root radius increases from zero to 0.010ins for a notch in a semi-infinite plate. Jack[35] found that the initiation criterion based on crack opening displacement was applicable to notches of up to 0.010ins root radius for mild steel. When the root radius was greater than 0.010ins, Ni could be correlated with the parameter $\Delta K/\rho^{\frac{1}{2}}$, so that the full effect of root radius on initiation is given by the following equation, which arises from the work of Allery and Birbeck[164]:-

$$Ni = \frac{A}{[\Delta K(\frac{\rho_o}{\rho})^{\frac{1}{2}}]^m} \qquad - \quad [14]$$

where A and m are constants. When the root radius ρ is less than the critical root radius ρ_o, then ρ is put equal to ρ_o. Jack[35] was able to show that the results of Weibull[36,37,37A] for aluminium were also consistent with the existence of a critical root radius. The results of Wilkins and Smith[38] lead to a similar conclusion. Taylor[39] however, found that for the titanium alloy Ti 317 if ρo exists then it has a value of less than 0.005 ins. Forman[40] proposed that the parameter $\frac{\Delta K}{Ka}$, where Ka is the apparent notch fracture toughness for a given notch root radius, could be used to correlate notch initiation data. However, since Ka is given by the expression $K(\frac{\rho}{\rho_o})^{\frac{1}{2}}$ [35], this approach is analogous to equation [14].

Much experimental evidence has been presented to support the preceeding theories, but wide variations in the value of the exponent 'm' have been reported. Jack[35] found that the value of 'm' in equation

[14] was 4 for mild steel. Taylor's[39] work on Ti 317 and on a maraging steel indicated that the initiation period was strongly dependent upon the previous material history. He found that the effect of heat treatment after machining the notch was to prolong the initiation time and reduce the 'm' value from 6 to 4 in the case of a titanium alloy, and from 4 to 2.5 in the case of the maraging steel. Taylor attributed these changes in fatigue crack initiation resistance to the relieving of residual stresses and to surface oxidation. Pearson[41] investigated the effect of notch root radius on initiation in aluminium. His results when analysed using equation [14] exhibit banding, with the sharpest root radius giving the longest lives. The values of 'm' from this work were between 3.5 and 5. Barnby et al[42] found 'm' values of 3.5 and 4 for a cast steel to BS1456A and a single phase titanium alloy respectively. They also found that the values of both 'm' and A in equation [14] were sensitive to the criterion of initiation used. When the criterion was the first deviation of electrical potential across the notch the 'm' value for the titanium alloy was 4. This value reduced to 2.5 when the criterion was the appearance of a crack of length 1.0mm. Forman[40] claimed that his data on initiation in the aluminium alloy 7075-T6, and also the results of Manson[43] could be correlated by using the parameter $\frac{\Delta K}{Ka}$, but the scatter limits of this analysis were very wide.

2.2.2 Smooth Specimen Simulation

Crack initiation is dependent upon the magnitude of the applied cyclic stresses and strains in a body. In the presence of a notch or other geometrical type of defect, high local stresses and strains are produced. In cases where both the nominal ΔS, and local, $\Delta\sigma$, stresses are elastic, they are related through the elastic stress concentration

factor:-

$$K_t \Delta S = \Delta\sigma \qquad - [15]$$

It seems reasonable to assume that this relationship could be used to correlate crack initiation behaviour in smooth and notched samples. In practice the prediction is accurate for very blunt notches, but conservative for sharper ones of high K_t. This is the well known size effect, and may be overcome by replacing K_t by K_f, the effective fatigue stress concentration factor. Thus we have:-

$$\Delta\sigma = K_f \Delta S \qquad - [16]$$

The use of K_f accounts for both the size effect and the effect of plastic deformation at the crack tip. Pearson[41] found that his results could be well correlated by a K_f approach.

Topper et al[44] proposed an alternative method for taking into account plastic deformation at the notch root. The method is based on Neubers rule[45], which states that the true stress concentration factor is equal to the geometric mean value of the stress and plastic strain concentration factors:-

$$K_t = (K_\sigma K_\epsilon)^{\frac{1}{2}} \qquad - [17]$$

Morrow et al[46] have shown that this is a good approximation for axially loaded notches. If a notched specimen is subjected to nominal stress and strain ranges ΔS and Δe, giving rise to local stress and strain ranges at the notch of $\Delta\sigma$ and $\Delta\epsilon$, then (44):-

$$K_t = \left[\frac{\Delta\sigma}{\Delta S} \cdot \frac{\Delta\epsilon}{\Delta e}\right]^{\frac{1}{2}} \qquad - [18]$$

Rearranging and multiplying both sides by Youngs Modulus, E, gives:-

$$K_t(\Delta S \Delta e E)^{\frac{1}{2}} = (\Delta\sigma\Delta\epsilon E)^{\frac{1}{2}} \quad - [19]$$

If the nominal stress is elastic then:-

$$K_t \Delta S = (\Delta\sigma\Delta\epsilon E)^{\frac{1}{2}} \quad - [20]$$

It is still necessary to account for the size effect by substituting K_f for K_t. The appropriate value of K_f is the value obtained at long lives, e.g. 10^6-10^8 cycles. This is denoted by K_f'. Thus we have

$$K_f' \Delta S = (\Delta\sigma\Delta\epsilon E)^{\frac{1}{2}} \quad - [21]$$

The left hand side of this equation contains nominal stress and strain ranges, and the right hand side contains local stress and strain ranges at the root of the notch. Consequently the relationship can be interpreted as implying that a notched specimen and a smooth specimen will form detectable cracks after the same number of cycles, provided that $K_f'\Delta S$ for the notched speimen is equal to $(\Delta\sigma\Delta\epsilon E)^{\frac{1}{2}}$ for the smooth specimen. Thus if a master curve of $(\Delta\sigma\Delta\epsilon E)^{\frac{1}{2}}$ versus crack initiation time is obtained from smooth specimens, the life of notched specimens can be obtained from the value of $K_f'\Delta S$ on the $(\Delta\sigma\Delta\epsilon E)^{\frac{1}{2}}$ axis. This correlation has been checked experimentally (46,47,48), and good agreement found between predicted and observed notch behaviour. Nevertheless, some caution is necessary in the application of the K_f' approach as a general initiation criteria. The prediction will be valid for materials where initiation is very rapidly followed by failure, i.e. in cases where the propagation phase is minimal. This is true only in limited applications. The use of K_f at failure for other purposes is only valid where K_f at failure is virtually the same as K_f at initiation. This may be the case, as for example with titanium alloys, but may not be taken as a basis

assumption. It is therefore of considerable interest to examine the application of this technique in the context of the present work on the initiation of cracks in aluminium weldments.

2.3 Models of Crack Propagation

In 1939, Orowan[3] published a theory of fatigue crack propagation based on work hardening at the crack tip. He argued that cyclic work hardening would lead to an increase in the crack tip stress until the fracture strength of the material was exceeded. Upon fracture the crack tip would advance into a non-work hardened region where the stresses were lower. The process would then be repeated at the new and subsequent crack tips until final fracture occurred. Orowan predicted that the propagation rate would depend on applied stress; neglecting the increased stress concentration effect as the crack length increased.

This concept has been utilized in a number of subsequent attempts to devise propagation laws. Head[49] suggested that the growth rate would depend on crack length, and his mechanical model which considered rigid-plastic work hardening elements ahead of the crack tip was used to predict the law:-

$$\frac{da}{dN} = \frac{C_1 \sigma^3 a^{3/2}}{(\sigma_y - \sigma) r_p^{\frac{1}{2}}} \qquad - [22]$$

Where rp is the crack tip plastic zone size, which Head considered to be constant. σ_y and σ are the yield stress and applied stress range respectively, and a is the crack length. The value of the constant C_1, which is dependent upon the strain hardening modulus, yield stress, and fracture stress was found to differ by 2 or 3 orders of magnitude from the value given by equation [22]. Weibull[50,51] suggested that the

crack growth rate should depend only on the net section stress, giving a law of the type:-

$$\frac{da}{dN} = C \sigma_{net}^{n} \qquad - [23]$$

He presented data[38] on aluminium alloys to substantiate this relationship. The results of Rolfe and Munse[52] on mild steel could also be described by equation [23].

McEvily and Illg[53] proposed that since the concentrated stress at the crack tip increased as the crack grew, even though the net stress was constant, then the concentrated stress should determine the growth rate. This gave rise to an expression of the type:-

$$\frac{da}{dN} = f(K_N \sigma_{net}^{n}) \qquad - [24]$$

where K_N is the stress concentration factor. They presented evidence to support this and also showed that the results of Head[49] and Weibull[50,51] were in agreement with their equation.

In 1958 Frost and Dugdale[54] proposed a crack growth law which was based on the assumption that fatigue crack growth was a continuous and not a two stage process; and that on elasticity considerations the crack remained geometrically similar as it propagated. They demonstrated experimentally that in thin sheets the crack tip plastic zone size was proportional to the crack length provided the crack length was small compared to the sheet width. Thus they concluded that applied stress and crack length were the only independent variables and the growth rate should be expressed as a function of these; giving a law of the type:-

$$\frac{da}{dN} = C\sigma_a^s \qquad - [25]$$

where σ is the gross stress, a the crack length, and C is a constant.

They pointed out that although the laws stemmed from different concepts, Head's[49] equation was similar to their own if it was assumed in his equation that plastic zone size was proportional to crack length.

Frost and co-workers [55,56,57,58,59] analysed data on a range of materials in terms of equation [25]. The value of the mean stress was found to affect only the value of the constant, C, but in the case of mild steel, Frost and Dugdale[54] found that mean stress had no effect on the growth rate. Frost[55] also used the parameter $\sigma^3 a$ in the analysis of data on non-propagating cracks. He concluded that there was a critical value of $\sigma^3 a$ below which if cracks formed they would not grow.

Liu[60] used a more rigorous dimensional analysis and agreed that the crack growth rate should be proportional to the crack length. Later[61] he used an idealised elastic-plastic stress-strain diagram, and with the assumption that the hysteresis loop energy absorption to failure was constant, derived the expression:-

$$\frac{da}{dN} = C\sigma^2 a \qquad - \quad [26]$$

Liu produced experimental evidence to support the equation.

More recently linear elastic fracture mechanics have been used in the interpretation of crack propagation data. Paris, Gomez and Anderson[61A] and Paris and Erdogan[62] related growth rates to the stress intensity factor. Paris suggested that the stress intensity factor, being a unique description of the stress field at the crack tip, should control the rate of crack growth. Paris and Erdogan[62] analysed data on 2024-T3 aluminium

alloy and found that it could be described by the relationship:-

$$\frac{da}{dN} = A\Delta K^4 \qquad - [27]$$

They also demonstrated that the data obtained by McEvily and Illg[53] and by Rolfe and Munse[52] could also be correlated by use of equation [27].

Since then many workers have reported that their results could be analysed in terms of the stress intensity factor, although the scatter in crack growth rates is generally large[63] and the value of the exponent 'm' may be between 2 and 6[64] McLintock[65] proposed that as the fatigue process is a plastic flow phenomenon, the crack growth rate should be proportional to the plastic zone size at the crack tip. He proposed two possible mechanisms for crack growth. The first was that of damage and repeated initiation ahead of the crack tip leading to a dependency of growth rate upon the square of the plastic zone size, and thus giving an exponent 'm' value of 4. The second mechanism was that of growth by irreversible plastic deformation at the crack tip, giving a growth rate dependency upon the plastic zone size, and an exponent value of 2 in equation [27]. McLintock found experimental evidence for both theories, but most of the data corresponded with the first mechanism.

Krafft[66,67] developed a concept of fracture process zone to show that fatigue crack growth should be porportional to $(\Delta K)^n$, and that the value of n should be 4 at low values of ΔK, and 2 at high values.

Weertman[68] and Bilby and Heald[29] used the model of plastic relaxation at a crack tip[28] to derive the expression

$$\frac{da}{dN} = \frac{5}{3}\left(\frac{\pi}{4}\right)^3 \frac{\sigma^4 a^2}{G\gamma\sigma_y^2} \qquad - [28]$$

where γ is the product of the critical plastic displacement at the crack tip and the yield stress, and G is the shear modulus. For the geometry considered,

$$K = \sigma a^{\frac{1}{2}} \qquad - [29]$$

and thus

$$\frac{da}{dN} = C(\Delta K)^4$$

Ham[69] considered that during crack extension, on the tensile stroke of the fatigue cycle the volume of material within the plastic zone is conserved, and on geometrical considerations the crack growth rate should be given by:-

$$\frac{da}{dN} = C\left(\frac{\Delta K}{E}\right)^4 \qquad - [30]$$

where E is Youngs Modulus.

This result is in close agreement with the experimental observations of Pearson[70], who found that for a number of materials:-

$$\frac{da}{dN} = C\left(\frac{\Delta K}{E}\right)^{3.6} \qquad - [31]$$

It has been found that in practice the crack growth rate does not correlate uniquely with the parameter $(\Delta K)^m$ over the full range of ΔK. The value of the exponent increases at higher values of ΔK, and also with increasing stress ratio[71,72,73,74]. Forman[75] pointed out that when ΔK or K_{max} approached K_{IC} for the material the growth rate should tend to infinity. To account for this, and the effect of mean stress he proposed the relationship:-

$$\frac{da}{dN} = \frac{C(\Delta K)^n}{[(1-R)K_c - \Delta K]^m} \qquad - [32]$$

where R is the stress ratio $\left(=\frac{\sigma_{max}}{\sigma_{min}}\right)$ and the value of 'm' is unity. Forman[75], and Hudson and Scardinia[76] found that this expression gave a good fit to data on aluminium alloys. Pearson[77] again working with aluminium alloys found that a value of $m = \frac{1}{2}$ in equation [32] gave a better fit.

Weertman[68] considered the effect of mean stress on his model of crack growth[27], and concluded that there was little effect except when the maximum cyclic stress was comparable to the fracture stress, when the rate of growth increased rapidly. The growth rate may vary from that described by equation [27] at low values of ΔK. Johnson and Paris[73] reported that growth rates of 10^{-10} ins/cycle, i.e. less than the atomic spacing, had been found to obey equation [27]. There is however, much recorded data[152,153] which shows an increase in the value of the exponent at low values of ΔK, and the existence of non-propagating cracks observed by Frost[78] is regarded by many as evidence for a threshold value of ΔK for fatigue crack growth.

2.4 Defects in Welded Joints

An assortment of treatments is available for the improvement of the fatigue life of welded joints. Barren and Hurlebaus[79] have shown that the fatigue life of a welded structure may be improved by grinding to remove notches, and by peening to produce a high residual compressive stress at the surface. Asnis and Ivoshenko[80], and Openshaw[81] have shown that post welding heat treatments can also lead to longer fatigue lives. Shavyrin[82] found that polymer coatings could significantly increase the fatigue strength of welded aluminium joints.

However, the problem remains that the fatigue strength of welded joints falls considerably short of the performance of the parent metal. This may be explained by the presence of defects which are inherent to the production of the welded joints. Much early work on the effect of these defects was reported in terms of their effect on the curve of alternating stress versus cycles to failure, or S-N curve. By plotting such curves for the sound welds and then for a range of severity of the defect being studied, fatigue strength reduction factors for any chosen severity and required life may be determined [See Figure 2].

Defects occurring in metal-inert-gas welded aluminium alloys may be classified in seven groups[83]. There follows a short description of each type with an indication of severity in terms of fatigue strength reduction.

(a) Reinforcement Shape

This is conventionally measured by the angle θ between the parent metal and the weld bead [See Figure 3]. It has been found that

for optimum performance the value of θ should be as near as possible to 180°. The strength reduction factor increases with decreasing θ, and is approximately 2 when θ is 120°[84]. Martelee[85] found that dressing the weld to give a θ value of 180° could be disastrous if pores were exposed at the surface, but Reemsnyder[86] found that the fatigue life could be increased by a factor of 4 or 5 by grinding away the reinforcement.

(b) Lack of Root Penetration

This may take the form of a buried defect in the case of a joint welded from both sides, or a surface defect if welding is from one side only. [See Figure 4]. Newman and Dawes[87] and Wilson[88] investigated the effect of the percentage area of lack of root penetration on fatigue strength reduction. They demonstrated that there was an approximately linear relationship between the fatigue strength and the reduction in area. The work of Dinsdale and Young[83] on welds in N5(Al/5%Mg) showed that the strength reduction factor was dependent upon the thickness of the welded plate, in addition to the loss of cross-sectional area.

(c) Double Operator Defect

This type of defect occurs when a plate is welded simultaneously from both sides, and takes the form of either large central pores or a line defect. Dinsdale[84] found that its effect on fatigue strength in aluminium welds was similar to that of lack of root fusion.

(d) Inclusions

Oxide inclusions in aluminium welds are difficult to detect because alumina is similar radiographically to aluminium. This has led

to a lack of clarity in the results of tests on material containing this type of defect, as sound welds may be mistakenly included in the analysis while large defects (later appearing on fracture surfaces) may be undetected. It appears, however, that the effect of inclusions on fatigue properties is a complex combination of their size, shape, and position in the weld. Dinsdale and Young[89] found that in undressed welds inclusions would not be the cause of failure unless they reduced the cross-sectional area by more than 7%.

(e) Porosity

It has been shown[84] that scattered porosity has little effect on the fatigue strength of undressed welds. However, if the reinforcement is machined off then pores which break the surface may act as crack initiation points, and lead to strength reduction[83,90]. Homes[91] found that the fatigue strength fell rapidly with increasing porosity up to 2%, but above 2% porosity the fall was more gradual. The strength reduction factor at 2% porosity was approximately 1.5.

(f) Cracks

The two main types of cracks which occur in welded joints are firstly cracking in the weld metal while it is hot and plastic, and secondly hard zone cracking in the heat affected zone after cooling. The restraints opposing movement to accommodate weld shrinkage set up the necessary cracking force. Warren[92] found that cracks could lead to strength reduction factors of 55-65%, but unfortunately the severity of individual cracks was not documented. Feldman et al[93] found that cracks exceeding $\frac{1}{3}$ of the thickness in aluminium welds reduced the strength by 50% or more.

(g) Lack of side wall fusion

The main cause of this defect is the presence of foreign matter, such as slag or scale, on the surface to be welded. This prevents the metal from reaching its required final temperature.

The work of Newman[94] shows that in some cases lack of side wall fusion seems to have little effect on fatigue properties. This, however, appears unlikely to be truein general since one would expect a similar effect to that produced by lack of central penetration defects.

2.5 Methods of Fatigue Life Prediction

Although the determination of S-N curves is useful in providing an assessment of fatigue life, and has been used to provide design criteria[95], it has limitations as a predictive technique. The severity of some types of weld defect may vary considerably. In such cases an S-N curve is of value only if the severity of the flaw can be expressed simply or specified. This approach has proved to be possible in the case of butt welds with uniform porosity, where the severity may be characterised simply in terms of the volume of the porosity[96]; and in the case of slag inclusions in arc welded joints, where the severity of the flaw depends on both its depth and length but may be characterised by the length since the depth does not vary much[97].

In general, planar flaws cannot be treated in this simple way, since the severity of the flaw depends not only on its size, but also on its shape and location, all of which may vary from one weld to the next. In order to provide a simple means of comparing the fatigue behaviour of such flaws with that of other weld details, some means of relating the relative variables is required.

The first significant attempt to predict the fatigue life of a specimen was the Coffin-Manson Relationship[98 99]. This may be written as:-

$$N_f^{\beta} \Delta\epsilon_p = \epsilon_f' \qquad - [33]$$

where N_f is the cycles to failure; β is the fatigue exponent; $\Delta\epsilon_p$ is the plastic strain range, and ϵ_f' is the fatigue ductility, that is the plastic strain range when N_f is a low number considered here to be unity[100].

Coffin based his findings originally on thermal fatigue tests on AISI 347 stainless steel, while Mansons contribution came from the results of Lui et al[101]. The relationship requires the resolution of cyclic strain into plastic and elastic components, and implies that only the plastic component is important to the fatigue process. The relationship was originally based on tests in which the plastic strain range was measurable in the test length, so that it originally applied only to short lives, but recent work on aluminium, copper and several steels has shown it to be valid to low plastic strain ranges ($2x10^{-5}$) and lives up to 10^6 cycles. Equation [33] has been found to predict the fatigue life of samples from materials of widely varying hardness, such as solders[102], lead[103] and tool steels[104]. Furthermore the relationship describes the fatigue behaviour of materials covering a great range of tensile ductility, e.g., tool steels of 3% ductility[104] and a super plastic aluminium-zinc alloy in which a tensile elongation of 500% can be obtained.[105]

A number of theories have been proposed to confirm the Coffin-Manson relationship. It is generally observed[106] that in the high strain regime microcracks nucleate and start to grow early in life, and thus equation [33] charaterises high strain crack growth. Theories along these lines have been proposed by Grosskreutz[107], Boettner et al[108] and Tompkins[109]. A high strain crack growth law, based on direct measurement was proposed by Solomon[110]:-

$$\frac{da}{dN} = Aa(\Delta\epsilon_p)^{\alpha} \qquad - \quad [34]$$

where a is the crack length, A and α are constant. Integration of this crack growth law leads to the Coffin-Manson relationship.

The elastic strain range may also be used to characterise the life to failure, through the Basquin relationship[111]:-

$$\Delta\epsilon_e = \frac{\Delta\sigma}{E} = \frac{B}{E} \; N_f^{-\beta'} \qquad - \; [35]$$

The total strain range-life relationship is then found by the sum of equations [33] and [35], and the plot of plastic, elastic and total strain ranges versus life is shown in figure 5. The point at which the plastic and elastic strain ranges cross is generally known as the transition life, N_t. When the life is greater than N_t, failure is by high cycle fatigue and may be characterised by the Basquin law, or by linear elastic fracture mechanics, when the life is shorter than N_t the failure is by low cycle fatigue and is characterised by the Coffin-Manson Law.

The relationship between strain amplitude and the number of cycles to failure has been found to hold at elevated temperatures. Swindeman's[112] results for a niobium base alloy, and Sheffler's[113] for two tantalum base alloys at temperatures greater than 1000°C could be described by equation [33]. It is found[114] that as the testing temperature increases the value of the exponent, β, increases and approaches unity; and that the life becomes strongly dependent upon the environment, being much longer in vacuo than in air [115]. As the temperature is increased, the life becomes dependent on the frequency of testing, the number of cycles to failure being greater at higher frequencies. The Coffin-Manson law may be modified to take account of this[116]:-

$$(N_f \nu^{k-1})^{\beta} \; \Delta\epsilon_p = C \qquad - \; [36]$$

where ν is the frequency and k serves as a measure of time dependency.

It is found[117] that there is a critical value of the frequency above which the crack growth rate is independent of frequency at a particular temperature. This situation gives rise to a k value of unity. There is also a lower critical value of frequency below which the life (in seconds) at that temperature is independent of frequency, giving rise to a k value of zero. At intermediate frequencies the value of k lies between zero and unity, and is constant for a given temperature (see figure 6).

Although the Coffin-Manson law is very useful for predicting the lives of fatigue test pieces, its application to the life prediction of components containing flaws has limitations. The analysis for strain at defects is very complex, and the only useful method of estimating the strain is through the use of Neuber's Rule [17] and smooth specimen simulation.

Van der Zanden et al[118] have used this approach to predict the lives of steel weldments containing internal cavities. Although their predictions were quite accurate, the technique suffered from two major drawbacks. The first of these is that it was necessary to estimate the value of K_f, the fatigue strength reduction factor. Van der Zanden was able to find a reasonable figure for this, but in the more general case the K_f value would vary considerably from weld to weld, and it would be necessary to find K_f experimentally over a range of defect severities. This would make the technique quite laborious. The second drawback is that the technique is strictly applicable only for the prediction of crack initiation, and relies on the equality between K_f for initiation and K_f for failure. The work of Van der Zanden was on specimens of small dimensions, such that the initiation period could be taken as a reasonable

estimate of the total life. In the more general case it would be necessary to take account of the growth period to achieve a reliable prediction. The most satisfactory means of doing this is by the use of linear elastic fracture mechanics.

It has frequently been assumed[119 120] that the life of a welded joint may be determined simply by consideration of the crack propagation phase (Stage II growth). On this basis an estimate of the joint life may be made by obtaining experimentally the values of the constants in the equation:-

$$\frac{da}{dN} = C(\Delta K)^m \qquad - [37]$$

for the relevant material, and then integrating to give the value of N corresponding to a particular value of ΔK.

Thus if $\Delta K = Y\Delta\sigma\sqrt{a}$ - [38]

where $\Delta\sigma$ is the amplitude of stress remote from the crack, a is the crack length, and Y is a correction factor to take account of the geometry of the cracked body,

then from equations [37] and [38]:-

$$\frac{da}{dN} = C\Delta\sigma^m (Y\sqrt{a})^m \qquad - [39]$$

Equation [39] may be integrated to provide a description of any part of the fatigue life between the initial a_i, and final, a_f, crack lengths. Thus[121]:-

$$\int_{a_i}^{a_f} \frac{da}{(Y\sqrt{a})^m} = C(\Delta\sigma)^m N \qquad - [40]$$

Since the value of the intergrand is not very sensitive to the value of a_f, the equation may be used to calculate the life of a weld containing a defect of original size a_i.

If the values of a_i and Y are constant for a particular weld, then equation [40] reduces to:-

$$(\Delta\sigma)^m N = \text{Constant} \qquad - [41]$$

This equation describes the form of a conventional S-N curve in which the defect initiating failure is controlled to within narrow limits in a series of tests. A recent analysis of fatigue test data for welded joints[122] confirmed the expected approximate equality between the index 'm' in equations [37] and [41], where equation [37] referred to crack propagation in structural steels, and equation [41] referred to the S-N curve for steel fillet welds failing from the toe of the weld. Variations in the values of initial and final crack length, and of Y, contributed to the scatter in the test results.

A severe limitation in the application of linear elastic fracture mechanics to the fatigue failure of welded structures is that the relationship between the range of stress intensity factor, loading, and geometry is unlikely to be known accurately. This problem arises partly because of difficulties in determining the relevant details about the size and geometry of the flaws detected in structures. However, from the fundamental point of view, the main problem is that a solution for K may not exist. In welded joints flaws may be irregularly shaped, and situated in complex stress fields such as may exist at the toe of a weld. In contrast solutions for K in the literature are confined to simple stress fields and regularly shaped cracks. An additional complication

is that flaws associated with welds are part embedded (surface defects) or fully embedded (buried) and few solutions for such cracks are available. The triaxial crack tip stress fields associated with embedded cracks increase the difficulty of determining K. Recent work has resulted in solutions for K which are relevant to welded joints. Maddox[123] determined a solution for K for the case of a semi-elliptical surface crack situated at the toe of a weld. Harrison[124] and more recently Frank[125] have obtained K solutions for a crack at the root of a fillet weld. These analyses were utilized by Maddox[126] to predict the fatigue life of cracked steel weldments. The test results were mainly within the confidence limits of the life prediction lines. The confidence limits, which originate from scatter in the determination of the growth rate law (equation [37]), are however, very wide, and cover a factor of approximately 5 in the fatigue life at a given stress-level. The successful fit of data within these limits does not therefore conclusively confirm that the prediction technique is sound. As had been previously suggested by Lawrence[127], Pearson[128] and Jerram[129], Maddox assumed that there was no crack initiation period in his tests. This may be reasonable since he introduced fatigue pre-cracks at the toes of the welds to form the weld defect which would lead to failure. However, since the work of Jack[85] showed that even with sharp cracks the initiation period could be up to 90% of the total life, then it is quite possible that the wide scatter bands in Maddox's work conceal a substantial initiation period. Jack[85] pointed out that in many cases, due to the scatter limits involved, the total fatigue life could be adequately described by either an initiation law or a growth law. It has been assumed[13] [131] that an approximate equality between the values of m in equations [37] and [41] is verification that the fatigue life consists entirely of propagation. This may, however, arise because the values of the exponent in the initiation

and propagation laws are approximately equal under the given test conditions.

A further problem in the application of linear elastic fracture mechanics to the fatigue failure of welded joints is the inevitable presence of high tensile residual stresses, often of yield point magnitude. This is equivalent to imposing a high mean stress in a fatigue test on a sample containing no residual stresses. Maddox[132] has shown that in the case of fully tensile loading, crack propagation is not very sensitive to mean load. The results of crack growth rate tests on C-M_n structural steel[133] show this to be so. Thus in his analysis of steel weldments, Maddox was able to neglect the effect of residual stresses. It has been shown, however, that growth rates in aluminium are mean stress sensitive[74] and hence the fatigue life of aluminium weldments should be dependent upon the level of residual stress present. Additionally, the initiation period may be mean stress sensitive, Taylor[39] has shown that in titanium and steel notched test pieces, the initiation period is very sensitive to post-machining heat treatment, and hence sensitive to the residual stress present at the notch.

Analysis of the results of Dinsdale and Young[84,88] on Al/5%Mg weldments containing central penetration defects shows that the value of the exponent in equation [41] has a mean value of approximately 5, compared with an 'm' value in equation [37] of approximately 3 for aluminium/5%Mg alloy[134]. This considerable discrepancy may be the result of either residual stresses or the existence of substantial initiation periods, and work is clearly needed to define the role of these phenomena in aluminium weldments.

Although weldments in Al/5%Mg N8 alloy retain limited mechanical properties at temperatures up to 300°C, there has been no work on the fatigue performance of this material at temperatures greater than ambient. Linear elastic fracture mechanics have only recently been used as a tool of analysis for fatigue data at elevated temperatures, and this has been confined to the conventional high temperature materials.

Yokobori[135] has proposed a model to account for the effect of temperature on growth rate, and produced the expression:-

$$\frac{da}{dN} = \frac{\epsilon M}{W} (\Delta K)^{1/mkT} \qquad - [42]$$

where k is Boltzman's constant, T is temperature in °K, and ϵ, m, W are constants which related to the material and conditions.

This relationship implies that the value of the exponent will decrease with temperature. This was found to be ~~care~~ so by Ohmura et al[136] with a cobalt base superalloy. Shahinian[137] however found that with stainless steels the value of the exponent increased with temperature. The value of C in equation [37] is found to increase with temperature, and at each temperature there is a unique relationship between ΔK and the crack growth for a given frequency[136 137 138]. Above a critical frequency, the fatigue fracture mode changes from intergranular to transgranular, and the growth rate is then independent of frequency at that temperature[136]. Shahinian[137] found that his data could be normalised by use of the expression:-

$$\frac{da}{dN} = C\left(\frac{\Delta K}{E^2}\right)^m \qquad - [43]$$

where E is Young's Modulus.

There is an absence of information on the effect of temperature on the initiation of fatigue cracks and the present work will include an investigation of the role of crack initiation at an increased temperature.

2.6 State of the Art and Objectives

There is extensive evidence that a fracture mechanics approach may be used as the basis of a predictive technique for both initiation and propagation of fatigue cracks from machined notches and artificial cracks. The present work aims to verify this for the case of natural defects in an engineering type situation. It is desirable to verify the findings of Jack in this application, i.e. that sharp cracks have definable crack initiation periods, since this would lead to the possibility of designing against initiation in welded structures, as an alternative to designing against crack growth alone.

Techniques based on Neubers rule have been shown to lead to design criteria against crack initiation. The present work aims to explore the merits of both approaches from a fundamental viewpoint and also in application to practical situations.

Information on the influence of residual stresses on the fatigue performance of welded joints is very limited, and it would appear fruitful to explore the possibility of incorporating this factor into a fracture mechanics analysis of fatigue crack initiation and propagation.

Finally it appears desirable to undertake an assessment of the elevated temperature fatigue properties of the widely used aluminium weldment, and to assess the use of the predictive techniques under these conditions.

3. EXPERIMENTAL TECHNIQUE

3.1 Material and Welding Technique

The parent metal used throughout the work was N8 plate, and the welding filler was NG6 in the form of 0.0016 metre diameter wire. The specified chemical composition of both are given in Table 1. Chemical analyses were carried out on the materials. The results from these also appear in Table 1, and show that the percentages of the two major alloying elements are within the specified ranges.

The thickness of the N8 plate was 0.025m. Each half of the welding section was 0.305m × 0.152m. A 'V' preparation was used, and to obtain sound welds the 0.0016m flats on the sections were separated by 0.0016m, as shown in Figure 7.

All the welding surfaces were thoroughly brushed and degreased immediately prior to welding. The welding was performed using the metal-inert-gas process, with commercial purity argon as the sheldinggas. After a number of trial runs, satisfactory welds were produced under the conditions of a voltage of 27, volts current of 260 amperes, a gas flow of $0.00058 m^3 sec^{-1}$, and a welding traverse speed of $0.058 m\ sec^{-1}$.

After the first weld run the plates were allowed to cool and then the reverse side of the joint was ground out so that the weld deposit was well exposed along the whole length of the weld. The second weld run was then made after the exposed surface had been thoroughly scratch-brushed and degreased. Two further runs on each side were necessary to overfill the weld. The reinforcement angle of the weld was varied by altering the traverse speed on the final runs. Each weld was radiographed to a sensitivity of better than 2%, determined by using a Deutsche Industrie Normal aluminium wire penetrameter. The ends of the

plates containing the stop-start positions were scrapped, together with any areas which revealed internal defects.

The tenacious oxide film on the unprepared plate surface was utilized in the production of central defects. Preliminary tests had indicated that it was possible to achieve complete penetration and wall fusion in the unprepared material only by using a gap between the weld flats and a slow welding speed. By using a welding speed of 0.059m sec^{-1} it was found possible to produce a continuous lack of side wall fusion defect along the whole weld length. To achieve this the faces of one plate were thoroughly brushed and degreased, while the faces of the other plate were left uncleaned and were given a thin coating of silicone grease in the regions adjacent to the flat. The plates were butted together so that there was no gap between the flats. After a weld run had been laid on both sides of the joint, there existed a buried defect which consisted of central lack of penetration and lack of fusion along one of the walls.

The severity of the lack of side wall fusion could be controlled by altering the traverse speed. It was found, however, that at increased speeds there was a tendency to increase the lack of fusion at the cleaned surface also. Consequently it was decided to vary the severity by grinding back the deposit covering the defect, before applying the subsequent weld runs. Following this grinding, all the joint surfaces were thoroughly cleaned. When the final runs were laid on both sides, a central defect through the thickness was produced. Figure 8 shows this schematically while Figure 9 shows a photograph of the defect in a fatigue specimen. The weldments were machined into specimens of 0.00635m thickness and these were individually radiographed to check the continuity of the defect. Using this technique it was possible to produce welded specimens

which contained quite uniform through thickness defects of length between 0.0045m and 0.0147m.

3.2 Static Tests

Number 12 standard Hounsfield tests pieces were machined from the NP8 plate. Tensile tests were carried out using a Hounsfield Tensometer. The direction of loading was at 90° to the direction of the weld runs, the same direction as that with the welded specimens during fatigue testing. All the test pieces were heated for one hour at 325°C, the usual stress relieving heat-treatment for N8 welds[139].

Room temperature tests were carried out using a 4984N beam, and a magnification of 16 to 1. Tests at 200°C, 300°C and 450°C were carried out on the same beam with a magnification of 4:1. The results of these tests appear in Table 2.

The fracture toughness of the material, heat treated as above, was determined using an Instron machine. Fatigue cracks were grown to within the range $0.4\frac{a}{w} - 0.6\frac{a}{w}$ in single edge notch three point bend specimens, and the value of K_c was calculated according to the method outlined in Ref[140]. Thicknesses of 0.025m, 0.0126m, and 0.0063m were tested so that any effect of thickness on the value of K_c could be noted and taken into account in the design of subsequent fatigue specimens. These results appear in Table 3.

3.3. Fatigue Testing

3.3.1 General

All the tests pieces used in the program had the common dimensions of thickness (0.0063m), width (0.0254m), and length (0.254m), except in the tests to check the effect of thickness on crack propagation results when a thickness of 0.0254m was used.

It was found to be unnecessary to employ the standard 'hour-glass' type specimen, since it was always known at which part of the test piece failure would occur. Even in the case of sound welds with the reinforcement machined off, the fatigue crack initiated inevitably from a pore or other minor defect in the weld metal, as required for subsequent application of the fracture mechanics analysis.

All the specimens were loaded axially, and tested under conditions of pulsating tension on an Amsler Vibrophore machine, using either a 20KN or 100KN dynamometer as dictated by the loading conditions. The frequency obtained in tests at room temperature with the 20KN dynamometer was in the range 105-120Hz. With the use of weights added to the upper loading beam it was possible to reduce the frequency to 40Hz. Growth rate tests at this frequency were carried out at 300°C to check for frequency effects, but except for these, all results were obtained in the 105-120Hz range.

The tests at increased temperatures utilized a small furnace designed for use with the Amsler machine. The performance of this furnace was checked by means of a thermocouple attached to the fatigue sample, and it was found that after allowing one hour for stabilization the temperature of the sample fluctuated by a maximum of $\pm 2^{\circ}C$.

3.3.2 The Measurement of Crack Growth Rates.

The crack growth rates were measured on single edge notch samples, machined from welds which contained no defects other than uniform porosity, by use of the potential drop technique described by Jack and Yeldham[141]. The method consists of passing a constant current through the sample and taking the following measurements:-

Vo, the potential drop across 0.0254m of uncracked sample

Va, the potential drop across the crack.

The value of the expression Va/VoW (where W is the specimen width) determines the effective spacing of the potential leads from the crack (the y value), and a computer program was used to give the values of a/w corresponding to a range of Va/VoW values, for a number of y values.

The potential leads used were of nichrome, and these were spot welded to the specimens at y values of 0.00254m. The potential drop across the crack was printed out on a chart recorder.

The accuracy to which the crack length may be measured is governed by the error in measurement of the Va value. Using a full scale deflection on the chart recorder of 50μV, the value of Va could be read accurately to 0.5μV. The relationship between Va/VoW and a/w is approximately linear at a/w = 0.2 (see Figure 11) and is such that:-

$$d(a/w) = \frac{d(Va)}{2.25\ VoW} \qquad [44]$$

Since Vo = Aρ/BW, equation [44] may be written as:-

$$d(a/w) = \frac{d(Va).B}{A\rho \times 2.25} \qquad [45]$$

where ρ = resistivity, A = current, B = thickness.

On the equipment available the maximum useable current was 40A, and taking the resistivity of aluminium as $3 \times 10^{-8}\Omega.m$, equation [45] becomes:-

$$d(a/w) = \frac{B}{5.3} \qquad [46]$$

Thus from equation [46] the accuracy of the crack length for a width of 0.025m should be 3.1×10^{-5}m for a thickness of 0.0063m, and 12.5×10^{-5}m for a thickness of 0.025m. This accuracy is improved when the temperature is increased, as the resistivity increases.

Measurement on welded test pieces introduces an unavoidable error in that while the value of Vo is measured across 0.0254m of typical specimen weld material, the value of Va is measured over a smaller distance and is likely to be affected by local concentrations of porosity or inclusions. The accuracy of the crack lengths was checked by measuring optically several final crack lengths. It was found that the discrepancy between the two values obtained increased with the crack length, but was not greater than 40×10^{-5}m for an a/w value of 0.7, in the 0.025m thick test pieces for which the accuracy is least.

Values of the range of stress intensity factor were calculated according to the method of Gross et al.[143] for single edge notch tensile specimens, and the values of growth rate were taken from curves of the crack length versus the number of cycles. Three specimens of 0.0063m thickness, and one of 0.0254m thickness were tested in each condition for which the growth rate curves were required.

3.3.3 Measurement of Cycles to Initiate a Crack.

Initiation measurements were carried out using the potential drop technique. With work on defects of the type used here, there is the complication that the shape of the defect varied from sample to sample. The placing of the potential leads was therefore different also. It was decided to place one electrode at 0.0025m from the centre of the defect on one side of the sample, while on the reverse side the second electrode was placed at 0.0025m from the line joining the tips of the defect. This is shown schematically in Figure 12. This configuration may lead to differing sensitivity between tests, but this is not important as the point of interest is the time when the Va output on the chart recorder shows its initial increase. This was the point at which initiation was taken to be complete, and

should be the same regardless of the position of the electrodes, which affected only the gradient of the print out of Va versus time. The subsequent gradient does however affect the accuracy to which the point of initial divergence could be traced, particularly when the initiation period was long and the subsequent rate of Va increase was very slow. To standardise the technique as much as possible, the current was adjusted from sample to sample to give the same initial Va value in each case. The estimation of the initiation time from the Va print out gave maximum and minimum values which differed by up to 30%, quite a small error when the values are plotted on a logarithmic scale. The figure for the initiation time recorded in the results was the minimum estimate in each case.

Tests using optical observation of the surface in conjunction with the potential drop technique showed that the latter indicated initiation before the crack was visible on the surface, except in samples where it was found that because of irregularity of the defect tip through the thickness the crack initiated first at the surface of the specimen.

The study of initiation from the reinforcement of welded samples introduced the complication that there were four possible points for initiation on each test piece. The crack was expected to initiate at the weld/plate interface where the reinforcement angle was greatest and the radius of curvature was least.

On samples where this was in doubt, the radius of curvature at one or more of the interfaces was increased by filing, and then smoothed with emery paper. The electrode potential leads were then placed at 0.0025m from the interface at which initiation was predicted, one on the edge of the plate, the other on the opposite edge on the weld material. As with the measurements on internal defects the value of the initiation period was taken as the point of initial

divergence on the Va print out.

3.4. Metallography and Fractography.

Standard metallographic techniques were used in the preparation of samples for examination and photography. Polishing was completed on a $\frac{1}{4}\mu$ diamond wheel, and etching was achieved in 9% hypophosphoric acid at 70°C. Photomicrographs were taken on a Vickers 55 projection microscope. The morphology of fracture surfaces and of welding defects was illustrated by means of photographs taken on a scanning electron microscope.

4. RESULTS

4.1 Crack Growth Rate Tests.

Crack growth rates were determined using single edge notch samples of 0.0063m thickness, under conditions of pulsating tension with a frequency of 100-120Hz. The crack length was taken from a table of 'a' versus Va/VoW, and plotted against the number of fatigue cycles. The gradient of this curve gave the value of da/dN for a given crack length. The value of the range of stress intensity factor, ΔK, was calculated according to the expression:-

$$\Delta K = Y \Delta \sigma \sqrt{a} \qquad [47]$$

The value of Y was taken from the analysis in ref.(148). Table 4 shows the values of Va/VoW, a, N and ΔK from which the final results of da/dN versus ΔK were derived, for the case of a test at room temperature on a test piece which had been stress-relieved at 325°C. Growth rate tests were carried out under the following conditions, and the results are plotted logarithmically as da/dN versus ΔK. The growth rate equation relates to the linear portion of the plot in each case.

(1) At room temperature in the as-welded condition, tested through the weld metal. Figure 13

$$da/dN = 10^{-10.48}(\Delta K)^{4.2} \qquad [48]$$

(2) At room temperature, stress-relieved at 325°C, tested through the weld metal. Figure 14

$$da/dN = 10^{-10.52}(\Delta K)^{3.7} \qquad [49]$$

(3) At room temperature, stress-relieved at 450°C, tested through the weld metal. Figure 15

$$da/dN = 10^{-10.46}(\Delta K)^{3.6} \qquad [50]$$

(4) At room temperature, stress-relieved at 325°C, tested through the heat affected zone. Figure 16

$$da/dN = 10^{-10.86}(\Delta K)^{3.9} \quad [51]$$

(5) At 200°C, stress-relieved at 325°C, tested through the weld metal. Figure 17

$$da/dN = 10^{-10.53}(\Delta K)^{4.1} \quad [52]$$

(6) At 300°C, stress-relieved at 325°C, tested through the weld metal. Figure 18

$$da/dN = 10^{-10.95}(\Delta K)^{5.1} \quad [53]$$

(7) At 300°C, stress-relieved at 450°C, tested through the weld metal. Figure 19

$$da/dN = 10^{-9.54}(\Delta K)^{3.8} \quad [54]$$

(8) At 300°C, stress-relieved at 325°C, tested through the heat affected zone. Figure 20

$$da/dN = 10^{-10.75}(\Delta K)^{4.9} \quad [55]$$

The units of da/dN are m/cycle and the units of ΔK are $MNm^{-3/2}$. The points plotted in Figures 13-20 result from three tests carried out under each of the conditions. The growth rates equations describe the linear regions of the curves, and represent the line of best fit from regression analysis of the three sets of results taken together.

The nature of the relationship between the growth rates and ΔK shown in Figures 13-20 shows several points of similarity under the differing test conditions. The limits of the scatter band in the growth rate at a given ΔK are quite consistent and cover a factor of approximately 3 in all cases. The curves all show a region of linearity at intermediate values of ΔK. At lower ΔK values the growth rates are slower than those expected from the simple power law relationship, while at higher ΔK values the growth rates are faster than predicted. This gives rise to the characteristic 'S'

shape.

It was found that the effect of increasing the test temperature was to increase the m value in the power law from m = 3.7 at room temperature to m = 5.1 at 300°C for welds stress relieved at 300°C. The growth rate for a given value of ΔK also increased. When ΔK was $6MNm^{3/2}$ the growth rate at room temperature was 2.2×10^{-8} m/cycle [Figure 14], compared with 4.5×10^{-8} m/cycle at 200°C [Figure 17] and 1.7×10^{-7} m/cycle at 300°C [Figure 18]. The power law relationship between the growth rate and ΔK was applicable down to a ΔK of approximately $4.3MNm^{-3/2}$ at 25°C, $3.9MNm^{-3/2}$ at 200°C, and $3.3MNm^{-3/2}$ at 300°C.

Figures 14 and 18 each show the results of growth rate tests on 0.0254m thick material. It was found that at both room temperature and 300°C the growth rates from these tests were within the scatter limits produced from tests on 0.0063m thick material.

Figure 21 shows the growth rate curve of a sample which had been stress relieved at 325°C and was tested through the weld metal at 300°C at a frequency of 45Hz. The power law relationship for the linear part of this curve was:-

$$da/dN = 10^{-10.78}(\Delta K)^{5.25} \qquad [56]$$

Comparison with Figure 18 shows that at the lower frequency the growth rate was marginally higher. When ΔK was $6MNm^{-3/2}$ the growth rate at frequency 100Hz was 1.7×10^{-7} m/cycle compared with 2.1×10^{-7} m/cycle at frequency 45Hz. This difference is well within the scatter limits of the results.

The effect of stress relieving on the results at room temperature was to reduce the value of the exponent 'm' from 4.2 in the 'as-welded condition' to 3.3 after stress relieving at 450°C. At a ΔK of $6MNm^{-3/2}$ the growth rate was 6×10^{-8} m/cycle in the as-welded condition (Figure 13) compared with 1.3×10^{-8} m/cycle

after stress relieving at 450°C (Figure 16). Stress relieving had a similar effect in tests at 300°C; the value of 'm' decreasing from 5.1 to 2.8, and the growth rate at a ΔK of $6MNm^{-3/2}$ decreasing from 1.7×10^{-7} m/cycle in the as-welded condition to 4.5×10^{-8} m/cycle after stress relieving at 450° C.

Crack growth rates through the heat affected zone were found to be similar to growth rates through the weld metal. At room temperature the value of 'm' from tests through the HAZ was 3.9, compared with a 'm' value of 3.7 for tests through the weld metal. At a ΔK value of $6MNm^{-3/2}$ the growth rate through the heat affected zone was 1.6×10^{-8} m/cycle (Figure 16) compared with 2.4×10^{-8} m/cycle through the weld metal. The growth rates were also similar through the weld metal and the heat affected zone at 300°C.

In the room temperature tests, the fracture was of a transgranular nature, giving rise to a flat fracture surface on which fatigue striations were present. Figures 22 and 23 show the crack path through the heat affected zone and weld metal respectively. The fracture surfaces at two levels of ΔK are shown in Figures 24 and 25; as may be expected the spacing of the fatigue striations increased with an increase in ΔK. Except for the presence of pores in the weld metal, there was very little difference in the fracture surfaces of the weld metal and the heat affected zone. These are shown under identical test conditions in Figures 26 and 27. The parent material and the weld filler were both non-heat treatable alloys, and stress relieving heat treatments had little effect on the metallographic structures, and no effect on the mode of fracture. Figures 28 and 29 show fracture paths through the heat affected zone and the weld metal after stress relieving at 450°C. (These may be compared with Figures 22 and 23).

When tested at 300°C, the fractures were essentially transgranular at low ΔK levels. As ΔK increased the crack paths became more intergranular in nature. Figure 30 shows the crack path through the weld metal when ΔK was $9MNm^{-3/2}$, in a sample which had been stress relieved at 325°C. The metallographic structure of the weld metal is coarser than in the room temperature tests, as a result of the prolonged holding time at 300°C (12 hours in this case). At high levels of ΔK there was also a tendency to crack branching, as indicated in Figure 31 which shows the fracture path through the weld metal when ΔK was $9MNm^{-3/2}$. The change of fracture mode was accompanied by the disappearance of the fatigue striations, and the fracture surface is shown in Figure 32.

4.2. Failure of Welded Test Pieces.

4.2.1 Determination of Strength Reduction Factors.

(a) Internal Defects.

The fatigue strength at an endurance of 2×10^6 cycles was obtained for welded test pieces from which the reinforcement had been machined, and which contained no defects other than uniform porosity. Samples containing through thickness lack of fusion of severity 0.2-0.25 a/w and 0.4-0.45a/w were then used to determine the fatigue strengths produced by these defects. Since interest was centred around only the high endurance portion of the S-N curve, 5 samples per group was sufficient for this purpose.

This procedure was carried out at room temperature, 200°C and 300°C on test pieces which had been stress relieved at 325°C. The individual test results appear in Tables 5,6 and 7 and these are plotted as $\log\Delta\sigma$ versus $\log Nf$ in

(a) contd.

Figures 33, 34 and 35 together with the lines of best fit from regression analysis.

The fatigue strength at 2×10^6 cycles at room temperature was $115 MNm^{-2}$ for sound welds, $36 MNm^{-2}$ for welds containing defects in the range $0.2 < \frac{a}{w} < 0.25$, and $26 MNm^{-2}$ when the defect severity was in the range $0.4 < \frac{a}{w} < 0.45$ (Figure 33). The effect of increasing the test temperature was to reduce the fatigue strengths so that at 300°C the strength at 2×10^6 cycles for sound welds was $71 MNm^{-2}$; for defect severity $0.2 < \frac{a}{w} < 0.25$, $24.5 MNm^{-2}$; and for defect severity $0.4 < \frac{a}{w} < 0.45$, $17.5 MNm^{-2}$ (Figure 35).

From the values of fatigue strengths at 2×10^6 cycles, the fatigue strength reduction factors (Kf) for each defect severity at room temperature, 200°C and 300°C were calculated. Figures 36, 37 and 38 show the relationships between Kf and defect severity. The determination of a fatigue limit is a process which gives rise to considerable scatter in the results. There is the natural scatter which occurs in any series of measurements, even when those measurements are carried out on the same object using the same equipment and same technique. In addition to this the fact that fatigue tests are destructive complicates the situation, since it means that no more than one measurement can be made on any sample. The production of an S-N curve therefore involved tests on several different samples, and although these were nominally identical there were small differences in defect severity. Furthermore, since each specimen in a series had to be set up individually in the testing machine, there would be small differences in the testing conditions (e.g. axiality of loading and the accuracy

(a) contd.

of measurement of the applied load) and in the environmental conditions (e.g. temperature and humidity) for each individual test. Since the result for the fatigue strength reduction factor is derived from the division of two values of the fatigue strength, the scatter limits in the Kf results are very wide. Bearing this in mind, the results indicate no marked effect of temperature on the relationship between Kf and defect severity.

(b) Reinforcement Failures.

The fatigue strength at 2×10^6 cycles was determined on welded specimens having reinforcement angles, θ, in the ranges 100-110°, 115-125°, and 130-140°. Each group contained 9 samples and tests were performed at room temperature and 300°C. Tables 8 and 9 show the individual results, which are plotted as $\log\Delta\sigma$ versus $\log Nf$ in Figures 39 and 40.

The fatigue strength reduction factors at 2×10^6 cycles, from Figure 39, at room temperature, were 1.60 for $100° < \theta < 110°$; 1.82 for $115° < \theta < 125°$; and 2.05 for $130° < \theta < 140°$. At 300°C the values of Kf from Figure 40 were 1.40 for $100° < \theta < 110°$; 1.7 for $115° < \theta < 125°$; and 1.97 for $130° < \theta < 140°$.

The stress concentration factor, K_t, for a geometrical projection similar to that of the reinforcement on a welded section has been evaluated by Neuber[148]. He related K_t to the parameter $\frac{a}{\rho}$, where a is the half width of the projection and ρ is the radius of curvature at the root of the projection (Figure 41). The relationship between K_t and $\frac{a}{\rho}$ for Neubers theory is expressed graphically in Figure 42.

The value of ρ for specimens in the current work was

(b) contd.

measured from tracings of the reinforcement root taken at a magnification of 50. Figures 43-45 show typical photographs for the range of θ values investigated. The values of $\frac{a}{\rho}$, together with the corresponding K_t from Figure 42 appear in Tables 8 and 9. From these tables the average value of K_t was 1.46 for $130° < \theta < 140°$; 1.74 for $115° < \theta < 125°$; and 2.05 for $100° < \theta < 110°$, in the room temperature tests. The average K_t in the 300°C tests were 1.44 for $130° < \theta < 140°$; 1.64 for $115° < \theta < 125°$; and 1.99 for $100° < \theta < 110°$. These values of K_t closely resemble the fatigue strength reduction factors obtained from Figures 39 and 40.

4.2.2 Initiation Results.

(a) Internal Defects.

The number of cycles taken to initiate a crack from the central lack of penetration and lack of fusion defects appear in Tables 5,6,7,10,11 and 12. The length of the original defect was measured, and the figure used in subsequent calculations was the average of the lengths measured on both surfaces of each fatigue test piece. The difference between these two values was never greater than 0.001m, and the defect tip was quite uniform through the thickness of the test pieces, as shown in Figures 46 and 47. Also the defects were centrally positioned through the width of the weld, as shown in Figure 9. Thus for the purpose of a fracture mechanics analysis, the defects could be treated as central through thickness cracks, loaded under uniform tension. A solution for $f\left(\frac{a}{W}\right)$, or Y, in equation [9] for this configuration has been found by Forman and Kobayashi[144], and this is shown graphically in

(a) contd.

Figure 48. Using this analysis a value of ΔK was determined for each test piece. In the present work, the defects were aligned along the angle of the weld preparation, at 60° to the tensile axis. Tanaka[145] has recently shown that for this configuration the effective value of ΔK is given by:-

$$\Delta K_{effective} = (\Delta K_1^4 + 8\Delta K_2^4)^{\frac{1}{4}} \quad [57]$$

where $$\Delta K_1 = \Delta K_A \sin^2\alpha \quad [58]$$

and $$\Delta K_2 = \Delta K_A \sin\alpha \cos\alpha \quad [59]$$

The value of ΔK_A in equations [58] and [59] is that given by the analysis of Forman and Kobayashi[144], and α is 60° in the present work. This value of $\Delta K_{effective}$, appears in Tables 5,6,7,10,11,12 as ΔK_o, the value of the stress intensity factor range before crack initiation. The initiation results are plotted graphically as logNi v log ΔK_o in Figures 49-54, and the lines of best fit from linear regression analysis gave the following relationship:-

(1) At 25°C, as welded, Figure 49

$$Ni = 10^{6.80}(\Delta K_o)^{-5.0} \quad [60]$$

(2) At room temperature, stress relieved at 325°;

Figure 50

$$Ni = 10^{7.30}(\Delta K_o)^{-4.25} \quad [61]$$

Regression Coefficient, $R_s = 0.978$

(3) At room temperature, stress relieved at 450°C

Figure 51.

$$Ni = 10^{7.20}(\Delta K_o)^{-3.60} \quad [62]$$

(4) At 200°C stress relieved at 325°C. Figure 52

$$Ni = 10^{7.20}(\Delta K_o)^{-5.10} \qquad R = 0.972 \quad [63]$$

(5) At 300°C As-welded Figure 53

$$Ni = 10^{7.35}(\Delta K_o)^{-5.5} \qquad R = 0.979 \quad [64]$$

(6) At 300°C, Stress-relieved at 450°C Figure 54

$$Ni = 10^{6.60}(\Delta K_o)^{-3.4} \quad [65]$$

(a) contd.

Since the relationship between the initiation period and ΔK appeared to be linear over the whole range studied, the equations above were taken from the complete sets of data for each condition. The effect of stress relieving was to decrease the value of the exponent in the power law and increase the initiation period at a given value of ΔK. Taking values from the lines of best fit, figures 49 and 51, at a ΔK of $8MNm^{-3/2}$ Ni increases from 25,000 cycles in the as welded condition to 260,000 cycles when stress relieved at 450°C, and tested at room temperature. Figures 53 and 54 show that stress relieving at 450°C increased the initiation period from 12,000 cycles to 130,000 cycles, at a ΔK of $3MNm^{-3/2}$ when tested at 300°C. Increasing the test temperature decreased the initiation period. At a ΔK of $3MNm^{-3/2}$, Ni was 38,000 cycles at 300°C, compared with 180,000 cycles when tested at room temperature (Figures 50 and 53). The scatter limits on the data were quite consistent and covered a factor of approximately five.

Tables 5,6 and 7 contain values of the parameter $K_f'\Delta\sigma$ for each sample. The K_f' corresponding to the relevant initial defect size was taken from the graphs in Figures 37 and 38. The initiation periods at room temperature, 200°C and 300°C, are plotted against $\log K_f'\Delta\sigma$ in Figures 55,56 and 57. From these, the initiation periods may be expressed numerically as:-

(1) At room temperature, stress relieved at 325°C

Figure 55

$$Ni = 10^{14.62}(K_f'\Delta\sigma)^{-4.70} \qquad R = 0.952 \qquad [66]$$

(2) At 200°C, stress relieved at 325°C Figure 56

$$Ni = 10^{15.04}(K_f'\Delta\sigma)^{-5.06} \qquad R = 0.941 \qquad [67]$$

(a) contd.

(3) At 300°C, stress relieved at 325°C Figure 57

$$Ni = 10^{15.53}(K_f'\Delta\sigma)^{-5.64} \quad R = 0.946 \qquad [68]$$

The scatter limits produced by the K_f' method of correlating the initiation data covered a factor of approximately 7 or 8 in Ni at a particular $K_f'\Delta\sigma$ value. This scatter is greater than in the ΔK approach, as shown by the lower values of R in equations [66,67,68] compared with the R values in equations [61,63,64]. The values of the exponents for $K_f'\Delta\sigma$ are all greater than the values of the exponents for ΔK under the same test conditions.

(b) Initiation From Reinforcement.

Examination of fracture surfaces revealed defects at the root of the reinforcement which were approximately 0.00025m deep. These were weld intrusions which varied in shape. Figures 58,59 and 60 show typical defects. Maddox[123] has recently developed a solution for K in the case of a semi-elliptical surface crack situated at the toe of a weld. The general solution may be written as:-

$$K = \frac{M_s M_t M_K}{\Phi} \sigma\sqrt{\pi a} \qquad [69]$$

where M_s is the correction for crack front shape

Φ is the complete elliptical integral

M_t is the correction factor for crack front position

M_K is the correction to take account of weld profile stress concentration

The relationship between the parameter $M_s M_t/\Phi$ and a/B is shown in Figure 61. Curves relating M_K and a/B are shown in Figure 61. Using these figures, and assuming that the original defect was approximately hemispherical, a value for the original range of stress intensity factor, ΔK_o, was calculated for each

(b) contd.

of the weld reinforcement tests, and the results appear in Tables 8 and 9. Figures63 and 64 show the plots of $\log\Delta K_o$ versus logNi at room temperature and at 300°C for welds which had been stress relieved at 325°C. The lines of best fit from these graphs lead to the following expressions:-

(1) At Room Temperature:-

$$Ni = 10^{8.095}(\Delta K)^{-4.98} \quad R = 0.982 \qquad [70]$$

(2) At 300°C

$$Ni = 10^{7.73}(\Delta K)^{-5.96} \quad R = 0.986 \qquad [71]$$

Tables 8 and 9 show the values of $K_t\Delta\sigma$ for each test piece. K_t was derived from the measurement of the radius at the reinforcement root and the relationship expressed in Figure 42. This was preferred to the use of the K_f values obtained on the grounds that it gave individual values of K_t for each test piece and it has been shown[148] that K_f is equal to K_t for values of K_t less than 2.3. The values of K_f obtained in the present work indicate an approximate equality. Figures 65 and 66 show Ni plotted logarithmically against $K_t\Delta\sigma$. Regression analysis of this data gave the following expressions:-

(1) At room temperature:-

$$Ni = 10^{16.33}(K_t\Delta\sigma)^{-5.29} \quad R = 0.969 \qquad [72]$$

(2) At 300°C:-

$$Ni = 10^{17.097}(K_t\Delta\sigma)^{-6.16} \quad R = 0.957 \qquad [73]$$

Comparison of Figures 63 and 64 shows that the initiation period is decreased at a constant ΔK_o when the temperature is increased; from 850,000 cycles at room temperature to 90,000 at 300°C when ΔK_o was $3MNm^{-3/2}$. The value of the exponent in the power laws, equations 70 and 71 is increased by increase in temperature. As with the results for initiation from internal defects, the scatter-

(b) contd.

bands are wider and the correlation coefficients lower in the $K_t\Delta\sigma$ approach compared with the ΔK_o approach, and the exponents in the power laws are higher in the $K_t\Delta\sigma$ approach.

4.2.3 Crack Growth Life Results.

A prediction of the life of a test piece after crack initiation was obtained by integration of the relevant crack growth law. To facilitate comparison of results from test pieces of differing thickness , equation 40 may be expressed, to include the $\frac{1}{2}$ section width,W, as

$$\int_{\left(\frac{a}{W}\right)_i}^{\left(\frac{a}{W}\right)_f} \frac{d\left(\frac{a}{W}\right)}{\left(Y\sqrt{\frac{E}{W}}\right)^m} = C(\Delta\sigma)^m W^{\frac{m}{2}-1} .N. \qquad [74]$$

Referring to the integral as I, equation 74 may be written as

$$\left[\Delta\sigma\left(\frac{W^{\left(\frac{m}{2}-1\right)}}{I}\right)^{1/m}\right]^m N = \frac{1}{C} = \text{Constant} \qquad [75]$$

$$\text{or } [\Delta\sigma^*]^m N = \text{a constant} = \frac{1}{C} \qquad [76]$$

$$\text{where } \Delta\sigma^* = \Delta\sigma\left(\frac{W^{\frac{m}{2}-1}}{I}\right)^{1/m} \qquad [77]$$

Maddox[126] used this approach, and referred to $\Delta\sigma^*$ as the generalised stress parameter.

The value of the integral, I, is not based on a closed form solution, and was therefore computed graphically. In the case of internal defects, the Y values used were taken from Figure 48. Graphs showing I versus $(a/W)_o$ for the range of values of the exponent 'm' in equations 48,49,50,52,53 and 54 are shown in Appendices 1-6. In the case of reinforcement failures, the value of Y was taken as

$\frac{M_s M_t M_K \sqrt{\pi}}{\Phi}$, as in equation 69, using the assumption that the crack grew with an average length to width ratio ($^a/_{2c}$ value) of 0.3. This assumption is reasonable as the average crack length measured on the 0.0063m thick samples was 0.002m when the crack had grown to the edges of the samples. Graphs showing I versus $(^a/_B)_o$ for the reinforcement angles 135°, 105° and 120° shown in Appendices 7 and 8, for the values of the exponent 'm' relating to crack growth through the heat affected zone at room temperature and 300°C. Using the relevant value of I, and the value of C from equations 48-55, the predicted growth life as a function of $\Delta\sigma^*$ was calculated for each of the test conditions. The value of $\Delta\sigma^*$ for individual test pieces is given in Tables 5-12. Figures 67-74 show $\Delta\sigma^*$ plotted logarithmically against the growth life N_G, together with the life predicted from the growth rate law relevant to each testing condition, as follows.

Figure 67 - Growth from internal defects in the as-welded condition, at room temperature

Figure 68 - Growth from internal defects, stress relieved at 325°C, at room temperature

Figure 69 - Growth from internal defects, stress relieved at 450°C, at room temperature

Figure 70 - Growth from internal defects, stress relieved at 325°C, at 200°C

Figure 71 - Growth from internal defects, stress relieved at 325°C, at 300°C

Figure 72 - Growth from internal defects, stress relieved at 450°C, at 300°C

Figure 73 - Growth from reinforcement, stress relieved at 325°, at room temperature

Figure 74 - Growth from reinforcement, stress relieved at 325°, at 300°C

All these figures show that at short lives and up to lives of approxmately 500,000- 800,000 cycles most of the individual results lie within the predicted scatter limits resulting from the growth rate

tests. At longer lives the actual life exceeds the predicted value.

5. DISCUSSION

5.1 Crack Initiation

5.1.1 Methods of Analysis

The correlation of initiation data and subsequent formulation of predictive equations for initiation periods is dependent upon the accuracy to which the initiation period is measured, and the accuracy to which the correlating parameter, ΔK or $K_f^1\Delta\sigma$, may be calculated or measured. In the present work it was assumed that the initiation had occurred at the point where the potential drop across the defect showed its first increase. The maximum error in the determination of this point was $\pm$ 20% Ni, which is small when Ni is considered on a logarithmic scale.

Errors arise in the calculation of ΔK because of difficulties in assessing the initial defect size. In the case of the internal defects, where the crack front variation through the thickness was small this error is not large. However, in the case of initiation from reinforcement defects the value of ΔK was calculated on the assumption that each test piece contained a hemispherical surface defect of 0.00025m depth. Since defects in the depth range 0.00012m to 0.0005m were found on fracture surfaces it is relevant to examine the error implicit in this assumption. The ΔK values were calculated from:-

$$\Delta K = \frac{M_s M_t M_k \Delta\sigma\sqrt{\pi a}}{\Phi} \qquad - [69]$$

Figure 61 shows that for small crack length ($<$ 0.0025m for a width of 0.025m) the parameter M_sM_t/Φ is independent of crack length for a given value of a/2c. Thus for a given value of the stress range the expression

may be written as

$$\Delta K = C\ Mk\sqrt{a} \qquad - [78]$$

Taking values of Mk from figure 62, it is calculated that the value of $Mk\sqrt{a}$ and thus of ΔK, increases by a factor of 1.2 when a increases from 0.00012m - 0.0005m. Thus variation in a_o could lead to an error of 0.08 ($\pm$ 0.04) in the values of log ΔK plotted in figures 63 and 64. Figure 61 shows that the value of $MsMt/\Phi$ and hence that of ΔK is increased by a factor of 1.4 as the value of a/2c decreases from 0.5 to 0.2. This would lead to an error of 0.14 ($\pm$0.07) in the value of ΔK plotted. Defects were found at the reinforcement root which had $a/2_c$ values of greater than unity, while the lowest values found were 0.4. Since a lower $a/2_c$ figure gives rise to a higher ΔK, initiation occurs preferentially from defects having the lower $a/2_c$ value, and the figure of 0.5 taken for the calculation of ΔK would normally be subject to a smaller error than that described above.

The accuracy of $K_f'\Delta\sigma$ is governed by the accuracy to which the fatigue strength at $2x10^6$ cycles could be determined. The scatter limits on the plots of $\log\Delta\sigma$ v Life to failure in figures 33, 34 and 35 cover approximately $\pm$ 0.04 on the $\log\Delta\sigma$ axis. Since the figure for K_f' results from the division of two results for $\Delta\sigma$ at 2×10^6 cycles, the total error in log K_f' is therefore, $\pm$ 0.08. This is the maximum error in $K_f'\Delta\sigma$ in the initiation plots.

The value of K_t derived from Neuber's theory for the case of failure from the weld reinforcements is dependent only upon the accuracy to which the radius at the reinforcement root was measured. This could be done to less than a 10% error and the nature of the relationship between

K_t and a/ρ (figure 42) is such that the error in K_t from this would be a maximum of 3%. These theoretical values of K_t assume a perfectly smooth root radius, and it may be expected that the presence of the small sharp defects in the reinforcement roots would increase the value of K_t. However, the values of K_f' from the present work are approximately equal to the predicted K_t values, and this is confirmed by the work of Dinsdale and Young[89] on similar material. It therefore, appears reasonable to use K_t as the correlating factor in this case. A complication in the study of initiation from the reinforcement was that initiation occasionally occurred at more than one site. This tended to happen more at the higher values of $K_t\Delta\sigma$, and is shown in figure 75 where three cracks have formed at the reinforcement and grown on different planes until they met and formed a single crack front. This effect is likely to affect subsequent propagation data rather than initiation data.

5.1.2 Present Work

Figures 50 and 63 indicate that ΔK may be used to correlate the initiation data from both central defects and reinforcement defects in welds which had been stress relived at 325°C. The 'm' values from the power laws are slightly different (m=4.25 for central defects, m = 4.70 for reinforcement defects), and the initiation periods from the central defects generally fall on the lower limit of the scatterband from the reinforcement data. However, figure 76, showing both sets of data together, indicates that ΔK has successfully correlated the data from these geometrically different defect types. The scatter limits cover a factor of approximately 6 in Ni.

Correlation of the same data with $K_f'\Delta\sigma$ (or with $K_t\Delta\sigma$, where

$K_t = K_f'$ in the case of reinforcement failures) in figures 55 and 63 indicates that for a given initiation period $K_f'\Delta\sigma$ is about 20% higher for reinforcement failure than for initiation from internal defects. Again the 'm' value in the power law is slightly greater in the case of reinforcement failures, m = 5.64 compared with m = 5.5 for the internal defects. Figure 77 shows that the use of $K_f'\Delta\sigma$ to correlate both sets of data leads to a scatterband covering a factor of about 12 in N_i, and thus the $K_f'\Delta\sigma$ approach does not correlate initiation data from the different geometries as successfully as the ΔK approach.

Jack[55] has shown that N_i may be correlated by $\Delta K \Big/ \left(\rho/\rho_o\right)^{\frac{1}{2}}$ as discussed in section 2.2.1. The value of ρo for aluminium was shown to be 0.0002m from the results of Wibull[56], while Pearson[41] found a value of ρo between 0.000125m and 0.00025 for aluminium alloy BSL65. When ρ is less than ρo, ρ is put equal to ρo, and the data is then correlated by ΔK. In the present work the radii at the defect tips were much less than ρ_o (Figures 78, 79). The results may be presented in the form $\Delta K/\rho^{\frac{1}{2}}$, therefore, simply by multiplying the ΔK results by $\frac{1}{\rho_o 17a}$ values of $\Delta K/\rho^{\frac{1}{2}}$ obtained in this way are shown in Figure 76.

The parameters $\Delta K/\rho^{\frac{1}{2}}$, $K_t\Delta\sigma$ and $K_f'\Delta\sigma$ all have the units of stress, and it is of interest to compare their numerical values. Using Peterson's[147] work on theoretical stress concentration factors, values of $K_t\Delta\sigma$ corresponding to $\Delta K/\rho^{\frac{1}{2}}$ for the case of elliptical through notches and single edge notch tensile specimens may be calculated. These are compared in Figure 80, and it is apparent that for the single edge notch geometry $\Delta K/\rho^{\frac{1}{2}}$ is approximately equal to $K_t\Delta\sigma$ for values of K_t greater than 4, while for the central notches $K_t\Delta\sigma$ is between 1.3 times and 1.5 times $\Delta K/\rho^{\frac{1}{2}}$ for values of K_t greater than 4. The relationship between $K_f'\Delta\sigma$ and $\Delta K/\rho^{\frac{1}{2}}$ is less clearly defined. At

very low K_t values, K_t is approximately equal to K_f', but for sharper notches and the crack like defects in the present work K_f' becomes increasingly less than the theoretical value of K_t. This is the result of plastic deformation at the crack tip, reducing the effective value of the local stress. It is furthermore well known that K_f' is dependent on section size for a given geometry, and also upon the life to failure at which it is measured. Thus equality between $K_f'\Delta\sigma$ and $\Delta K/\rho^{\frac{1}{2}}$ is not expected. However, if $K_f'\Delta\sigma$ were proportional to $\Delta K/\rho^{\frac{1}{2}}$ then it would correlate the initiation data as successfuly as $\Delta K/\rho^{\frac{1}{2}}$. In the present work it is relevant to compare $K_f'\Delta\sigma$ with $\Delta K/\rho_o^{\frac{1}{2}}$, since the values of ρ were all less than ρ_o and the radius is therefore not considered as a variable.

Figure 81 shows the curves of $\Delta K/\rho_o^{\frac{1}{2}}$ and $K_f'\Delta\sigma$ versus a_o/w for the case of internal defects. Over the range of original defect lengths investigated ($0.16 < a/w < 0.60$) $\Delta K/\rho_o$ increases from 2.3 times to 2.7 times the value of $K_f'\Delta\sigma$. Thus $K_f'\Delta\sigma$ is not exactly proportional to $\Delta K/\rho^{\frac{1}{2}}$. At a constant value of $\Delta\sigma$, the log of $\Delta K/\rho^{\frac{1}{2}}$ increases by 0.38 as a/w increases from 0.16 to 0.60, the increase in log $K_f'\Delta\sigma$ over the same range is 0.30. This means that if $\Delta K/\rho_o^{\frac{1}{2}}$ is the true correlating parameter, then this discrepancy will lead to increased scatter when $K_f'\Delta\sigma$ is used as the parameter, and also accounts for the increased value of m, since a given range of Ni values is covered by a smaller change in $K_f'\Delta\sigma$ than in $\Delta K/\rho_o^{\frac{1}{2}}$.

Figure 82 shows the relationships of $\Delta K/\rho_o^{\frac{1}{2}}$ and $K_f'\Delta\sigma$ with the reinforcement angle, θ. The ratio of $\Delta K/\rho_o^{\frac{1}{2}}$ to $K_f'\Delta\sigma$ increases from 1.95 to 2.3 as θ decreases from 135° to 105°. This indicates that the equality found between the K_t values from Neuber theory and the K_f' values was purely fortuitous since if K_t were really equal to K_f' then $K_f'\Delta\sigma$ should be equal to $\Delta K/\rho_o^{\frac{1}{2}}$. This discrepancy

was expected since the presence of the crack-like defects at the root must increase the true value of K_t. A discrepancy similar to that found with the central defects exists between the change in $\log\Delta K/\rho_o^{\frac{1}{2}}$ and $\log K_f'\Delta\sigma$, and again this explains the increased scatter and increased 'm' value in the $K_f'\Delta\sigma$ approach.

5.1.3 Comparison with Other Work.

While there is a lack of information relating to the initiation behaviour of natural defects in practical situations, there have been a number of investigations into crack initiation from notches. Jack's[35] correlation of initiation data in mild steel gave an 'm' value of 4 in the power law (equation 14). Barnby et al.[48] found 'm' values of 3.5 and 4 for a cast steel and a single phase titanium alloy respectively. These values of the exponent are in close agreement with the m value of 3.6 for welds stress relieved at 450°C in the present work. The results of Barnby et al. also show good correlation with $K_t\Delta\sigma$. The results of Pearson[41] on notched bend specimens of aluminium alloy, when analysed using a value of $\rho_o = 0.002$m are shown in Figure 83. The value of m from this is 3.9. Comparison of this with Figure 51 shows that the initiation response of BS.L65 is almost identical to that of the fully stress relieved N8 welds, when the correlating parameter used is $\Delta K/(\rho/\rho_o)^{\frac{1}{2}}$. Pearson's data is correlated with $K_f'\Delta\sigma$ and the line of best fit from this appears in Figure 84. From Figures 83 and 84 it is seen that for Pearson's data $\Delta K/\rho^{\frac{1}{2}}$ is only marginally greater than $K_f'\Delta\sigma$. Thus the correlation of $K_f\Delta\sigma$ with Ni for BS.L65 is very different from that for the welded joints. This is because in Pearson's work the notches were such that the full value of the theoretical stress concentration factor could be realised, resulting in K_f' values which were almost equal to K_t, so that for the majority of this data $\Delta K/\rho^{\frac{1}{2}}$ was equal to

$K_f'\Delta\sigma$. This is a very different situation to that of the data for the N8 welds, and it is clear that great care is needed in the application of the $K_f'\Delta\sigma$ analysis to predictive techniques. In the present work the value of K_f' was taken at 2×10^6 cycles. From Figure 33 it can be seen that the fatigue strengths were still falling at lives greater than this. If it is assumed that the strength in terms of $\log\Delta\sigma$ continued to fall linearly with logNf (in practice the decrease would normally be less severe), then the K_f values at 10^8 cycles would be about 1.5 times greater than at 2×10^6 cycles. This maximum increase leaves the values of $K_f'\Delta\sigma$ still considerably less than the values of $\Delta K/\rho_0^{\frac{1}{2}}$ for the welded joints.

5.1.4 General Discussion of Initiation Criteria.

It has frequently been assumed that the natural crack like defects present in welds begin to propogate as fatigue cracks on the first cycle of stress, and that the fatigue life may be predicted simply by considering the relevant crack growth law. However, the present work confirms the findings by Jack[35] on work with mild steel, that even with sharp cracks there is a definable initiation period. In the case of failure from weld reinforcement this initiation period may be 50% of the life for the section size in the present work.

In certain cases, particularly when the working stresses are high and the growth life following initiation is small, it may be desirable to design against crack initiation rather than using a fail safe criteria which would necessitate frequent inspection of the growing crack.

Barnby et al.[49] found that the parameter $K_t\Delta\sigma$ successfully correlated their initiation data in work on machined notches, and that this approach could provide useful design data. This approach is not applicable to the present work, in which the higher values of K_t for the sharp defects are not realised.

Van der Zanden[118] showed that a $K_f'\Delta\sigma$ approach gave satisfactory correlation of his initiation data for steel weldments containing lack of fusion defects, although he used an estimate of K_f' rather than an experimentally achieved value. The present work indicates that the correlation between $K_f'\Delta\sigma$ and Ni is not unique for a given material, but may depend upon the crack geometry. The success of $K_f'\Delta\sigma$ as a correlating parameter is dependent on a directly proportional relationship between K_f' and K_t. Since K_f' is subject to the well known size effect this relationship cannot always be assumed. Empirical relationships between K_f' and K_t have been proposed. Typical of these is the expression derived by Neuber[148]:-

$$\frac{K_f - 1}{K_t - 1} = q = \frac{1}{1 + (A/\rho)^{\frac{1}{2}}} \qquad [79]$$

where q is the notch sensitivity

and A is a material constant

Khun[149] has attempted to determine the value of the constant A in equation [79], but his results gave rise to considerable scatter in the values of K_f' predicted, and in practice it is necessary to measure the K_f' experimentally for each defect type and severity. This is a laborious process, and the results are subject to the usual errors in fatigue data, particularly in the case of real defects where there may be difficulty in reproducing the required size and shape of the defect for a test series.

In view of these difficulties it may be preferable to use the linear elastic fracture mechanics approach. As previously mentioned there is strong evidence that the parameter $\Delta K/\rho^{\frac{1}{2}}$ may be used to correlate initiation data from both notches and sharp cracks. The present work suggests that ΔK successfully correlates initiation data from different geometries. This is not surprising since the relevant solutions for ΔK take account of crack size, shape and

specimen geometry.

The theoretical models of crack tip plasticity[27-30] discussed in Section 2.2.1 predict that Ni should be dependent upon ΔK^{-2}. The present results and much reported data show a dependency on ΔK^{-4}. This is the dependency predicted by May's[33] model of critical crack tip strain. Since all the theoretical models are dependent on the assumed material behaviour, it may be expected that metallurgical and microstructural factors of different materials would result in variations on the ΔK dependency. It may prove possible to incorporate these factors into the theoretical models to achieve more accurate predictive theories.

However, it is apparent that the ΔK approach does have considerable theoretical justification, and it is therefore gratifying that ΔK may be used as an effective design parameter. Using the data shown in Figures 50, 63 and 76, it is possible to draw a line below which initiation will not occur. Using the appropriate solution for ΔK, design stresses for the relevant geometry may then be calculated, and by moving back from the line, any desired safety factor may be incorporated.

5.2 Crack Growth

5.2.1 Propagation Rates.

In order to ensure consistency in the results from crack growth tests, it is desirable to gather data which is all under plane strain conditions. In fatigue, this condition is satisfied when[150]:-

$$B > 2.5 \left(\frac{\Delta K}{2\sigma_Y}\right)^2 \qquad [80]$$

where B is the specimen thickness.

Thus for the 0.0063m thick specimens used in the present work, the plane strain criteria is satisfied up to a ΔK of

$17 MNm^{-3/2}$. The value of ΔK exceeded this figure in some of the tests, but in practice the criterion is conservative. The fact that K_C for the material shows little decrease with increasing thickness (Table 3), together with the flat appearance of the fatigue fracture faces at the highest ΔK values used, indicate that the whole of the data does in fact relate to plane strain conditions.

Figures 13-20 show that the relationship between log growth rate and logΔK is linear only over a limited range, about two orders of magnitude in the growth rate. At higher ΔK the growth rate accelerates. This is expected since as K_{max} approaches K_C the growth rate should tend to infinity[151]. At lower ΔK values growth is slower than predicted by the simple power law. This phenomenon has been observed by many workers[150,155] and is probably associated with non-uniform propagation across the crack front. As ΔK is reduced toward a threshold value where the growth rate is zero, growth occurs in bursts at preferential sites on the crack front. If growth from each of these sites obeys the power law, then the average growth rate for the whole crack will be slower than predicted.

Frost[71] reported growth rates down to 10^{-9} m/cycle in the Aℓ/5%Mg alloy, which showed linearity of logΔK with log growth rate, but the results of Pearson[72] on RR58 aluminium alloy (of similar toughness to N8) indicate a deviation from linearity at 5×10^{-8} m/cycle. In the present work the log of the growth rate was found to be linear with logΔK down to about 5×10^{-8} m/cycle.

The value of the exponent 'm' in the power law was 2.7 in Frost's work[71], and 3 in Pearson's work[72]. Thus there is a small difference between these and the figure of m = 3.3 for the fully stress relieved weld metal in the present work. Frost[74]

reported growth rates which were faster than those found here (e.g. for a growth rate of 2.5×10^{-8} m/cycle, Frost found that ΔK was $5.5 MNm^{-3/2}$ compared with the value of $7 MNm^{-3/2}$ for fully stress relieved weld metal). This may be a result of the higher R values (R = 0.44) used by Frost, but this in turn should lead to higher values of the exponent, whereas the value of m in Frost's work was lower. Thus it is apparent that there are considerable differences in the crack propagation behaviour between the welded and unwelded aluminium/5% magnesium alloy.

Figures 14 and 16 indicate that crack propagation is faster in the weld metal than in the heat affected zone, by the small factor of about 1.5. Thus the behaviour of aluminium welds in this respect is similar to that of steel weldments[126].

The models of crack tip plasticity[27-30] discussed earlier suggest that the value of the exponent in the growth power law should be equal to 4, but there are few materials for which this has been found to be exactly so. Many attempts[154,156] to deduce a law of fatigue crack propagation theoretically have been made, but none has been found to agree with observed crack propagation. It is therefore apparent that for the purpose of fatigue life prediction, it is necessary to obtain empirical crack growth data which is relevant to the particular material and conditions.

5.2.2 Growth Life Predictions

It is apparent from figures 68 and 73 that the $\Delta\sigma^*$ approach gives a good means of predicting the growth life to failure for welds containing both internal defects and reinforcement defects. For lives up to about 5×10^5 cycles the lives obtained are within the scatter bands of the lives predicted from the crack growth laws. At longer

lives the predicted value becomes less than that obtained. This fits well with the crack growth rate curves (figures 14 and 16), which indicate that the log growth rate is proportional to logΔK down to a ΔK of $3.5 MNm^{-3/2}$. Tables 5 and 8 indicate that it is generally the test pieces having an initial ΔK of less than $3.5 MNm^{-3/2}$ which gave results outside the scatter limits. Deviation of the growth law from linearity at the higher ΔK values does not affect the present results, since the lives affected would be shorter than those considered here.

The $\Delta\sigma^*$ approach is extremely useful in correlating data from different section sizes. Dinsdale and Young[84] have carried out S-N curve determinations on N5 welds of width 0.005m-0.0125m containing central lack of penetration defects of varying severity. Using the relevant growth rate data from the present work, these results are presented as $\Delta\sigma^*$ v N_f in figure 85. It should be noted that here N_f refers to the total life, including both initiation and propagation. As will be shown later, the percentage of total life taken up by initiation increases as the width decreases, and would be about 40% in the 0.005m thick sections. Thus the lives plotted in figure 85 overestimate the growth life by up to 67%. This error is not great compared with the scatter in the results. The scatter from this analysis is considerably greater than in the present work, and this arises from the calculation of $\Delta\sigma^*$, as the defects were not uniform and varied across the section. Bearing these points in mind, the analysis gives reasonable agreement with the present results, and the trend towards longer lives than predicted at the lower $\Delta\sigma^*$ values is also evident.

A fracture mechanics analysis indicates that for welds containing uniform defects, the gradient of the plot of log$\Delta\sigma$v log N should be equal to the value of 'm' in the growth law. Analysis of the individual graphs produced by Dinsdale and Young[84] gives an average gradient of 4.8,

compared with m = 3.7 in the growth law. The slow growth at lower ΔK explains this discrepancy, and since the prediction at the longer lives is conservative, added confidence is given to the $\Delta\sigma^*$ approach as a design criterion.

Dinsdale and Young[89] also carried out S-N curve determinations on the effect of the reinforcement angle on the life to failure. The results from this are presented in figure 86 as log $\Delta\sigma^*$ v Nf. $\Delta\sigma^*$ was calculated, as in the present work, on the assumption that failure would originate from a surface defect of depth 0.00025m. Again the results all lie in or near the limits predicted from the growth law for the heat affected zone found in the present work. This again demonstrates the effectiveness of the $\Delta\sigma^*$ approach in predicting fatigue lives from sections of different geometries.

5.3 Prediction of Total Fatigue Life

The present work indicates that fatigue crack initiation from central defects does not occupy a significant part of the total fatigue life. Thus the common assumption that the life of a welded joint consists of crack propagation appears to be justified, at least in the case of the 0.025m wide sections considered here.

However, as the width is decreased the percentage of life taken up by crack initiation increases. The initiation period may be taken from the line of best fit in figure 50, or calculated directly from the empirical relationship:-

$$N_i = 10^{7.3} (\Delta K)^{-4.25} \qquad - [61]$$

The growth life is derived from the integration of the relevant growth law, and is taken from the line of $\Delta\sigma^*$ versus predicted life in figure 68.

The case of a welded joint which had been stress relieved at 325°, and tested at room temperature with an initial ΔK of $5MNm^{-3/2}$, is used to typify the effect of section width on the contribution of initiation and growth to total life, Figure 87 shows the relationship in the case of a central defect of a constant 2a/w value of 0.3. Figure 88 relates to a central defect of constant crack length of 0.003m.

In both cases it is clear that in thin sections the initiation period may occupy over 50% of the total life. Under these circumstances a conservative estimate of the total life could be obtained by using the initiation data alone.

Using the empirical data presented here it would also be possible to calculate the contribution of both crack initiation and growth to total life for other defect types, e.g. surface lack of fusion and reinforcement defects. Clearly the linear elastic fracture mechanics approach provides a very powerful tool, both in cases where design against fatigue crack initiation is required, and where the growth life of an existing crack must be estimated.

It is of interest to note at this point that to utilize a K_f' approach as the basis of an initiation prediction technique for welds of differing section size would entail the determination of K_f, for each size of test piece. This is so since K_f, will vary as the proportion of growth in the total life varies. To complete the prediction of total life it would then be necessary to use a fracture mechanics determination of the growth phase. It would appear to be far more elegant to apply the fracture mechanics approach, with its built in geometric considerations, to the prediction of both phases of the total life.

5.4 The Effects of Stress Relieving on Fatigue Life

It has been found[139] that during the production of a butt weld, tensile residual stresses are set up in the region of the weld deposit as a result of differential cooling and shrinkage. In thick sections these stresses will be of yield point magnitude[139] and are superimposed on the applied stress during fatigue testing. Thus the test consists of the applied stress amplitude cycling downwards from the yield point and gives rise to an effective high value of the stress ratio in a test where R is nominally zero. The effect of stress relieving is to reduce the residual stress to the level of yield stress of the material at the stress relieving temperature. Hence as this temperature is increased, the effective R value in the subsequent fatigue tests is decreased. Thus stress relieving should lead to a decrease in crack growth rate, and this was found to be the case, as shown by figures 13, 14 and 15.

Forman[75] has shown that the effect of R value on the rate of crack propagation may be accounted for in a relationship of the type:-

$$\frac{da}{dN} = \frac{C\ \Delta K^n}{[(1-R)Kc-\Delta K]^m} \qquad - \ [32]$$

It is possible that the present results may be rationalised by equation [32], but such an approach would be of little value in the prediction of fatigue life. It is reasonable to assume that the residual stress across the net section remains constant as the magnitude of a defect or the length of a growing crack is increased, then since the applied alternating stress on the net section is increased, the effective R value is different from sample to sample, and also decreases during the test. Clearly it is relevant in this case to consider the effect of the R value for each test piece on the growth life to failure.

Tiffany[157] has shown that a plot of the original stress intensity factor, ΔK_o, versus the growth life will give a satisfactory characterisation of growth life for a given section size. This is not as accurate as the $\Delta\sigma^*$ approach, but is a fair approximation since most of the growth life is accumulated in the early stages of crack growth, and over a small increment of crack length, ΔK may be considered constant. An assessment of the error involved may be obtained by comparing the growth lives obtained at a constant ΔK_o for initial crack lengths of $a/_w = 0.16$ and $a/_w = 0.60$, the extremes used in the present work. For the case of welds stress relieved at 325°C, with an original ΔK of $5 MNm^{-3/2}$ the value of $\Delta\sigma^*$ is 29.5 for the short crack and 31.5 for the long crack. The corresponding predicted lives are 120,000 cycles and 90,000 cycles respectively. This difference is small compared with the general fatigue life scatter.

On the assumption that the magnitude of the residual stress after stress relieving could be taken as the value of the yield stresses given in table 2, an initial value for the stress ratio was calculated for all the tests recorded in tables 5,10 and 11. Analogous to the Forman growth rate equation is an expression accounting for the effect of R value on growth life, of the form:-

$$N_G = \frac{A[(1-R)K_c - \Delta K_o]^m}{\Delta K_o{}^n} \qquad - [81]$$

Thus if the analysis is valid, the plot of $\log \frac{N_G}{[(1-R)K_c - \Delta K_o]^m}$ versus $\log \Delta K_o$ should give a straight line relationship. Forman[75] said that the value of 'm' in equation [32] should be unity, while Pearson[77] found that a 'm' value of 0.5 gave a better fit to data on aluminium alloys.

It was found that in the present work the data from the three conditions of heat treatment were best correlated by using a 'm' value of unity in equation [82]. This is shown in figure 89.

It is apparent from figures 49,50 and 51 that fatigue crack initiation is more sensitive to stress relieving heat treatments than crack propagation. Using the initial R values calculated for the crack propagation data, this data was rationalised by the expression:-

$$Ni = \frac{C[(1-R)K_c - \Delta K_o]^m}{\Delta K_o^{\,n}} \qquad - [82]$$

The best correlation was achieved by using a 'm' value of 2 in equation [82]. Figure 90 shows the plot of log $\frac{Ni}{[(1-R)K_c-\Delta K_o]^a}$ versus log ΔK. The results indicate that stress relieving at 450°C greatly increases the resistance of the welds to fatigue crack initiation and so if design against initiation is necessary it is clearly desirable to use a stress relieved weld if possible. Further, because crack growth is less sensitive to heat treatment, the portion of total life occupied by crack initiation increases with stress relieving, as shown in figure 91. This shows the comparison of the percentage life taken up by initiation for welds of different widths, in the case of a constant a/w value of 0.3 and a ΔK of $5MNm^{-3/2}$. Clearly it is more important to account for the initiation period in the total life prediction when referring to stress relieved joints. The effect of stress relieving on total life is shown in figure 92, for the condition of a constant a/w of 0.3 and a ΔK of $5MNm^{-3/2}$. In thick sections where the life consists almost entirely of crack propagation, stress relieving at 450°C increases the life by a factor of about 5. This factor increases to 10 as the width decreases to 0.005m and the initiation period becomes increasingly more important in the stress relieved joints.

5.5 Effect of Increasing Temperature on Fatigue Properties

Jeglic et al[158] investigated fatigue crack propagation in an aluminium/2.6% magnesium alloy between room temperature and 300°C. They showed that crack propagation was controlled by volume diffusion. The activation energy for volume diffusion (Q_o) was lowered by the applied stress intensity range ΔK, so that

$$Q(\Delta K) = Q_o - C_1 \log \Delta K \qquad - [83]$$

The driving force for the process is inversely proportional to the square of the stress intensity range, so that

$$A(\Delta K) = C_2 \, \Delta K^{-2} \qquad - [84]$$

This led to an expression for the crack propagation rate as a function of temperature and stress intensity factor:-

$$\frac{da}{dN} = C_2 \, \Delta K^{-2} \exp \left[\frac{Q_o - C_1 \log \Delta K}{RT} \right] \qquad - [85]$$

Jeglic[158] claimed that the results of Wei[159] on 7075 aluminium alloy could also be fitted by this formula.

Equation [85] implies that the dependency of crack growth rate on ΔK decreases as the temperature increases, and in Jeglic's work the value of m in the simple growth rate power law, equation [37], decreased from 4.35 at 26°C to 2.07 at 300°C.

This at first appears to be in direct conflict with the present results, equations [49],[52],[53] which indicate that the growth rate through the weld metal became more sensitive to ΔK as the temperature increased to 300°C. In fact, crack growth rate at elevated temperatures is dependent upon a more complex combination of factors than those of simply temperature and ΔK. The growth rate may still be described

phenomenologically by the power law:-

$$\frac{da}{dN} = B\Delta K^{m} \qquad - [37]$$

However, the variables which are inherent in the elevated temperature fatigue testing of welded joints must affect the values of B and m. A change in fracture mode from transgranular to intergranular cracking is accompanied by an increase in growth rate, and hence in B, since intergranular cracking involves less distortion of the structure[160]. The value of 'm' in equation [37] is also increased in intergranular cracking.[161] Furthermore, the effect of residual stresses, which is equivalent to an applied mean stress, increases the 'm' value[72], and also promotes intergranular cracking. Welds which were stress relieved at 325°C and tested at 300°C would contain residual stresses of almost yield point magnitude. In the present work it was found that cracking became more intergranular as ΔK was increased. This together with the effect of residual stresses accounts for the increased dependency of growth rate on ΔK. In welds which had been stress relieved at 450°C the growth rate decreased and the m value was markedly reduced. The cracking was predominantly transgranular to higher ΔK values. Comparison of equations [50] and [54] shows that in welds stress relieved at 450°C the m value decreased at the higher temperature, although the decrease from 3.3 to 2.8 was not as great as in Jeglic's work[158].

Other work on the effect of temperature on crack propagation, while showing that growth rates increase with temperature indicate no general trend of the effect of temperature on the m value. Shahinian[157] found that m increased from 3.6 to 4.8 as temperature increased to 427°C for Type 304 stainless steel welds. James[159] found that with Type 304 plate the m value was the same at 538°C as at room temperature. Ohmura et al[156] found that m decreased from 6.6 to 5.5 with the cobalt based superalloy HS-188 as the temperature was increased to 880°C.

Shahinian[137] found that the effect of temperature on growth rate in Type 316 stainless steel could be normalised by dividing ΔK by the square of Youngs Modulus. Variations in the m value lead to scatter of the results. The effect of frequency also suggests that this could not be a successful general correlating parameter. As the frequency of testing is decreased, the growth rate at room temperature remains virtually constant, whereas at higher temperatures the decreased frequency leads to increased growth rate. Thus a different power of Youngs Modulus would be needed at each frequency. This frequency effect will also change the constants and the activation energy in equation [85], so that a seperate equation would be necessary for each frequency.

It would appear unlikely that any predictive technique could account simultaneously for the effect of temperature, frequency, mean load, mode of failure, and processing variables. Therefore, for the purpose of a design criteria, it is apparent that crack growth data must be gathered under the conditions which are relevant to the particular service conditions ofa component. Thus the constants B and m in equation [37] should be determined under the appropriate conditions, and the expression obtained may not be used as a general criteria for any other combination of variables.

Henry et al[162] have shown that the fatigue life of notched samples in the high strain regime may be predicted by the use of Neuber's rule and the frequency modified Coffin-Manson relationship, so that:-

$$K_f \Delta S = (E \Delta\sigma \Delta\epsilon)^{\frac{1}{2}} = \text{Notch stress range}$$

where

$$\Delta\sigma = A \Delta\epsilon_p^{n_\nu} k$$

$$\Delta\epsilon_p = C_a (N_f \nu^{k-1})^{\beta}$$

$$\Delta\epsilon = \Delta\epsilon_p + \frac{\Delta\sigma}{E}$$

Interpretation of this relationship is difficult because of the existence of a small plastic zone or 'Neuber Particle', which makes the stresses and strains difficult to determine. Nevertheless, Henry et al were able to obtain a good fit for total life data from A286 specimens at 593°C. As with the room temperature work, the use of K_f is subject to the reservation that strictly speaking the K_f value used should be that obtained from initiation data and not from total life data. The total lives in the work of Henry et al may comprise a predominant initiation phase, but in the present work the existence of substantial growth periods in the total lives is a restriction to the application of the K_f approach for initiation prediction.

In the assessment of the use of ΔK as the basis of a predictive technique for fatigue crack initiation and propagation, it is desirable for the purpose of comparing results that all the data should relate to plane strain conditions. In the present work the production of reasonably uniform defects through the specimen thickness limited the thickness to 0.0063m. The criterion for plane strain, equation [80] is satisfied for values of ΔK up to 6 $MNm^{-3/2}$ for this section size tested at 300°C. This ΔK was exceeded in many of the tests. The increased growth rate found in 0.025m thick sections, and the presence of shear lips on the fracture surface of the 0.0063m thick specimens tested at 300°C indicates that failure in the thinner sections was under conditions of mixed plane stress and plane strain. Under plane stress conditions the toughness of the material is increased, and consequently the fatigue properties found in the present work will be superior to the properties of thicker sections.

Thus, it is not possible to extrapolate the results, in terms

of percentage initiation and growth periods, to other section sizes. The presence of plane stress fracture also adds a further complication to the comparison with the room temperature results, which were all collected under conditions of plane strain.

In the present work, equipment limitations dictated that the minimum and maximum frequencies available were 45Hz and 100Hz. Figures 18 and 21 indicate that over this limited range there was no appreciable effect of frequency on the crack growth rates. This indicated that the results fall in the time independent regime of figure 5. Consequently it was not possible to investigate the effect of frequency on crack initiation or propagation in the present work, and all the data included in this discussion was obtained at a test frequency of 100H2.

Figures 52-54, and 56-57, show that the initiation data from the elevated temperature tests may be correlated by either $K_f'\Delta\sigma$ or by ΔK_o. The correlation coefficients from the lines of best fit, equations [63-65] and [67-68] indicate that as at room temperature the ΔK_o approach gives a better fit. The value of the exponent 'm' follows the same trend as m in the growth law for the corresponding conditions, i.e. m increases with temperature but is greatly reduced by stress relieving at 450°c. Figures 64 and 66 show that for failure from the reinforcement, ΔK_o produces a better correlation of the initiation data than $Kt\Delta\sigma$.

The plots of $\Delta\sigma^*$ versus growth life to failure, produced by integration of the relevant growth laws are shown in figures 70-74. Good agreement of predicted and actual lives is obtained in all cases.

Figures 71 and 74 indicate that growth from the central defects and from the reinforcement could be accurately predicted by one value of $\Delta\sigma^*$, so that $\Delta\sigma^*$ may be used to predict growth from different geometries at 300°C. It is gratifying that linear elastic fracture mechanics may be used to quantify the high cycle fatigue failure of welds having different heat treatment and fracture mode, at elevated temperature.

James[163] has shown that the effect of frequency on growth rate at a specific temperature may be accounted for by an expression of the type:-

$$\frac{da}{dN} = B(\Delta K)^m \qquad - [86]$$

where B is a function of the frequency.

Clearly it should be possible to use equation [86] to incorporate frequency effects into growth life prediction, and thus provide a comprehensive picture of the growth life of welded joints from growth rate tests under the relevant service conditions.

6. CONCLUSIONS

Two techniques for the prediction of crack initiation and propagation from defects in aluminium weldments have been examined. The predictive technique based on the fatigue strength reduction factor, K_f', is found to give a reasonable correlation of data from a specific geometry. The solution is however, not a general criteria, since K_f' must be determined separately for other section sizes and geometries. The application of fracture mechanics as the basis of a crack initiation prediction technique is preferable on theoretical grounds and leads to a marginal improvement in the fit of experimental data. This approach also has the considerable advantage that a criterion for initiation established with any geometry and section size may be applied to other configurations, provided that the geometry of the defect may be approximated to one for which a solution is available for the stress intensity factor, K.

The K_f' approach may not be used to predict the total fatigue life except in cases where the life comprises predominantly the initiation phase, this is rarely the case in the context of the fatigue failure of welded joints. A fracture mechanics approach, based on the integration of crack growth laws, is found to provide a successful technique for the prediction of the life of a weldment following fatigue crack initiation.

Thus it is shown that a fracture mechanics approach may be used to predict the contribution of both initiation and propagation of cracks to the total fatigue life. This is significant in that it permits design criteria for defective weldments to be derived from the results of tests on conventional machined test pieces.

It is shown that in thick sections, a satisfactory conservative prediction of total life may be obtained from a consideration of the propagation stage alone. However, as the section size decreases for a specific cracked geometry, the initiation period becomes more significant and eventually exceeds the propagation period.

Residual stresses arising from the welding process are found to have a significant effect on both the initiation and propagation of fatigue cracks from welding defects. Stress relieving heat treatments lead to delays in both stages of failure, the effect being more pronounced in the initiation of the cracks. A simple approximation of the magnitude of the residual stresses allows both the initiation and propagation laws to be modified to account for the effective stress ratio introduced into the fatigue cycle by the residual stresses.

Increasing the temperature of testing leads to decreases in both crack initiation and propagation times. Under the conditions of high frequency testing in the present work it is found that the room temperature techniques for crack initiation and propagation could be applied at temperatures up to 300°C. However, the combined effects of residual stresses and changes in fracture mode profoundly effect the constants in the empirical laws which form the basis of the predictive techniques. It is concluded that the formulation of a general crack initiation or propagation criterion to account for the variables of temperature, frequency, residual stresses and mode of failure, is unlikely to be achieved.

7. FURTHER WORK

The analysis of the proportions of crack initiation and growth in the total fatigue life of defective welds indicates that section thickness is an important variable in predicting the fatigue life of N8 weldments. It would be desirable to confirm the predictions with work on thicker sections. The work of Jack[85] indicates that similar size effects are found in mild steel, and work on steel weldments is suggested in order to establish whether the initiation/propagation contribution to the fatigue failure of welded joints may be regarded as a general phenomenon.

In practical situations the prediction of fatigue failure in weldments is complicated by the fact that the exact nature of the defect which initiates failure is not known until after the joint has failed. Consequently, approximations of the type used in the present work, for example the approximation of the size and shape of defects at the reinforcement root, will always be a necessity. In the construction of design specifications, it is therefore, essential that all possible information is gathered regarding the size, geometry and location of defects which are expected to arise from the specific material/welding combination being used. However, from the fundamental viewpoint the main problem is that a solution for K may not exist, and further theoretical work is needed to establish K-callibrations which are relevant to welding defects.

The present work indicates that the effect of residual stresses in aluminium welds is more pronounced than in steel weldments, and the magnitude of the residual stresses may greatly influence the

fatigue life of the joints. In view of this, it is desirable that the analysis used here should be refined. The use of photo-elastic models would enable a full analysis of the pattern of the residual stresses in the region of the weld. This, coupled with an investigation into the effects of stress ratio on crack initiation and propagation through the weld material, would lead to a more rigorous analysis of the effect of stress-relieving on the fatigue life of aluminium welds.

Although it is found that a fracture mechanics analysis may be used to quantify the fatigue failure of aluminium welds at temperatures up to 300°C, the analysis is severely limited by the phenomenological aspects of elevated temperature fatigue failure. In particular, fundamental work appears to be necessary in order to determine the effect of the transition from transgranular to intergranular fracture on crack growth rates. Many materials exhibit 'notch strengthening' under creep conditions,[165] and this phenomenon may affect initiation under conditions of low frequency. Consequently an investigation into the effect of frequency on both crack initiation and growth would be necessary before the construction of any generalised design criteria for the elevated temperature fatigue failure could be attempted. At the testing frequencies employed in the present work, a linear elastic fracture mechanics analysis is valid at temperatures up to 300°C. However, at reduced frequencies and/or at higher temperatures, the conditions necessary for the valid application of the analysis may be violated, and the use of strain analysis techniques would become necessary.

Table 1 Chemical Analysis

A. Specified Chemical Composition (% by weight)

	N8 base	NG6 filler
Copper	0.1 max	0.1
Magnesium	4 - 4.9	4.5 - 5.5
Silicon	0.4	0.3
Iron	0.4	0.5
Manganese	0.5 - 1.0	0.5
Zinc	0.2	0.2
Chromium	0.25	0.25
Titanium	0.2	0.2
Aluminium	Balance	Balance

B. Chemical Analysis of the Material (% by weight)

	N8 base	NG6 filler
Magnesium	4.25	4.62
Manganese	0.62	0.47

Table 2 Tensile Tests

Each result is the average of three tests on Hounsfield No.12 test pieces.

Temperature	25°C	200°C	300°C	450°C
UTS (MNm^{-2})	302	234	110	35
0.2% Proof Stress (MNm^{-2})	150	126	87	24
% Elongation	24	38	96	-
Reduction in Area	30	51	88	-

Table 3 Fracture Toughness Tests

Each result is the average of three tests

Thickness (m)	0.0063	0.0125	0.025
K_Q ($MNm^{-3/2}$)	24	20.9	23.8

Table 4. Derivation of Data for Crack Growth Rate Results

The data relates to a sample stress-relieved at 325°C and tested at room temperature with a constant stress amplitude of 16.3 MNm^{-3}

$\frac{Va}{V_oW}$	$\frac{a}{w}$	a (10^{-3}m)	N (cycles)	$\frac{da}{dN}$ (m/cycle)	ΔK ($MNm^{-3/2}$)
0.540	0.244	6.1	0	1.8×10^{-9}	3.63
0.605	0.276	6.9	440,000	3.8×10^{-9}	4.16
0.673	0.308	7.7	650,000	8.6×10^{-9}	4.71
0.744	0.340	8.5	743,000	1.5×10^{-8}	5.30
0.817	0.372	9.3	796,000	3.1×10^{-8}	5.96
0.894	0.404	10.1	822,000	3.4×10^{-8}	6.76
0.974	0.436	10.9	846,000	5.3×10^{-8}	7.75
1.058	0.468	11.7	861,000	9.8×10^{-8}	8.81
1.146	0.500	12.5	869,200	1.1×10^{-7}	9.82
1.238	0.532	13.3	876,500	3.0×10^{-7}	11.40
1.334	0.564	14.1	879,200		

Table 5 Failure from Central Defects at Room Temperature

a_o (10^{-3} m)	$\Delta\sigma$ (MNm^{-2})	Ni (10^3 cycles)	N_f (10^3 cycles)	LogΔKo	Kf'	LogKf'Δσ	Δσ*
2.68	31	220	3,200	0.466	3.19	1.995	16.72
2.92	39	120	1,400	0.541	3.19	2.095	21.95
3.04	46.5	32	700	0.674	3.19	2.171	26.72
3.18	46.5	27	300	0.683	3.19	2.171	27.32
3.04	62	8	120	0.798	3.19	2.296	35.63
5.30	23.5	170	3,700	0.527	4.42	2.016	19.06
5.98	31	36	900	0.691	4.42	2.136	27.90
6.10	31	22	410	0.699	4.42	2.136	28.57
5.46	39	10	160	0.757	4.42	2.236	32.12
6.10	46.5	4	60	0.874	4.42	2.317	42.86
4.56	62	2	24	0.907	4.00	2.395	44.93
6.62	46.5	4	26	0.909	4.72	2.341	46.98
2.04	85.5	2	31	0.942	2.64	2.354	41.66
3.70	85.5	3	14	0.981	3.64	2.493	53.87
4.96	62	1.5	34	0.929	4.14	2.409	47.80
7.78	62	<1	4	1.109	5.06	2.496	76.88
6.86	31	20	190	0.749	4.80	2.173	32.94
7.26	39	5	48	0.847	4.91	2.282	44.09
2.28	62	16	160	0.729	2.82	2.243	31.49
4.06	46.5	9	110	0.748	3.78	2.245	30.96
Sound	156		49				
Sound	140		190				
Sound	125		480				
Sound	117		1800				
Sound	109		>4000				

Table 6 Failure From Central Defects at 200°C

a_o (10^{-3}m)	$\Delta\sigma$ (MNm^{-2})	Ni (10^3 cycles)	Nf (10^3 cycles)	$\log\Delta K_o$	Kf'	$\log Kf'\Delta\sigma$	$\Delta\sigma^*$
2.66	21	770	4,000	0.287	3.52	1.868	9.72
2.92	27	65	2,150	0.448	3.52	1.977	12.91
2.80	27	100	1,050	0.428	3.52	1.977	12.76
3.04	31	28	540	0.500	3.52	2.037	15.19
2.80	39	40	500	0.571	3.52	2.137	18.43
5.34	16	180	2,950	0.331	4.89	1.893	11.14
5.72	21	70	1,280	0.500	4.89	2.011	15.54
5.47	21	81	670	0.480	4.89	2.011	14.96
6.08	27	12	395	0.631	4.89	2.120	21.49
5.47	31	13	102	0.662	4.89	2.180	22.08
2.40	62	<1	31	0.740	3.20	2.297	27.88
4.56	46	2	42	0.780	4.41	2.307	28.36
4.96	31	10	96	0.625	4.58	2.152	20.46
6.62	31	<1	27	0.731	5.23	2.209	26.63
2.02	62	4	120	0.701	2.86	2.248	26.35
7.50	16	54	610	0.487	5.49	1.944	16.41
3.80	23	210	2,400	0.425	4.04	1.968	12.88
3.42	78	<1	9	0.925	3.85	2.477	40.48
7.62	46	<1	3	0.972	5.53	2.406	48.10
4.20	55	<1	15	0.831	4.24	2.367	32.16
0	78		>4,000				
0	86		1,700				
0	93		1,500				
0	93		780				
0	109		260				

Table 7. Failure From Central Defects at 300°C

a_o (10^{-3}m)	$\Delta\sigma$ (MNm^{-2})	N_i (10^3cycles)	N_f (10^3cycles)	$\log\Delta K_o$	K_f'	$\log K_f'\Delta\sigma$	$\Delta\sigma^*$
2.80	24	120	>4000	0.347	2.92	1.841	8.72
3.18	28	60	1230	0.450	2.92	1.913	10.91
2.68	28	125	520	0.418	2.92	1.913	9.98
2.91	35	22	190	0.538	2.92	2.010	13.15
3.18	43	3	84	0.647	2.92	2.051	16.76
5.48	12	950	74000	0.224	4.12	1.694	6.67
5.00	18	90	1900	0.437	4.12	1.870	9.28
5.86	18	130	930	0.430	4.12	1.870	10.59
5.34	24	47	185	0.528	4.12	1.995	13.11
5.86	32	2	28	0.684	4.12	2.120	18.88
4.56	68	<1	<1	0.954	3.71	2.402	32.53
7.88	24	3	28	0.683	4.75	2.057	20.34
3.94	62	<1	5	0.863	3.45	2.320	27.07
6.84	46	<1	1	0.926	4.45	2.311	32.28
2.16	78	1	7	0.812	2.44	2.279	26.16
3.68	62	<1	5	0.843	3.33	2.314	26.16
7.14	39	<1	2	0.868	4.54	2.248	28.51
2.41	70	<1	10	0.792	2.62	2.263	24.20
6.60	16	75	1300	0.428	4.39	1.847	10.94
4.40	24	42	480	0.453	3.64	1.941	11.17
Sound	94		460				
Sound	78		1010				
Sound	70		1300				
Sound	70		2900				
Sound	62		74000				

Table 8. Failure From Reinforcement Defects at Room Temperature

$\Delta\sigma$ ($MNm^{-3/2}$)	θ°	$\frac{a}{\rho}$	Kt	LogKt$\Delta\sigma$	Ni (10^3 cycles)	Nf (10^3 cycles)	ΔK_o ($MNm^{-3/2}$)	$\Delta\sigma^*$
156	137	5.5	1.46	2.358	9	31	6.32	46.7
140	134	5.9	1.48	2.313	18	54	5.68	41.9
124	139	5.2	1.44	2.249	40	95	5.03	37.2
109	131	6.2	1.49	2.206	63	118	4.42	32.7
93	137	6.2	1.49	2.141	120	350	3.77	27.9
93	137	5.4	1.43	2.123	102	198	3.77	27.9
78	132	4.7	1.41	2.038	400	1300	3.16	23.4
78	133	6.4	1.50	2.068	280	630	3.16	23.4
62	136	6.0	1.48	1.960	910	74000	2.51	18.6
70	130	6.0	1.48	2.015	1100	3300	2.84	21.0
156	116	15.2	1.80	2.445	3	15	8.33	54.1
140	118	15.3	1.80	2.401	5	24	7.31	48.6
124	125	9.8	1.63	2.304	18	48	6.62	43.0
109	127	11.1	1.67	2.283	24	90	5.82	37.8
109	123	12.7	1.73	2.275	19	51	5.82	37.8
93	122	12.4	1.71	2.201	56	126	4.97	32.3
78	121	8.5	1.58	2.087	210	560	4.16	27.1
62	119	18.6	1.89	2.067	280	1980	3.31	21.5
62	124	13.1	1.75	2.035	510	1280	3.31	21.5
54	117	15.0	1.79	1.985	780	74000	2.88	18.8
140	103	28.2	2.13	2.472	2	11	9.41	54.0
124	106	25.7	2.06	2.406	4	15	8.34	47.8
109	106	31.3	2.19	2.374	8	46	7.33	42.0
93	109	21.9	1.98	2.264	8	54	6.23	35.8
93	111	21.0	1.95	2.258	10	200	6.23	35.8
78	103	20.8	1.94	2.175	19	260	5.24	30.1
62	110	22.8	2.00	2.092	132	940	4.17	23.9
62	105	26.3	2.08	2.110	70	670	4.17	23.9
54	104	29.0	2.16	2.067	280	3050	3.63	20.8

Table 9. Failure from Reinforcement Defects at 300°C

$\Delta\sigma$ (MNm^{-2})	$\theta°$	$\frac{a}{\rho}$	Kt	$LogKt\Delta\sigma$	Ni (10^3 cycles)	Nf (10^3 cycles)	ΔK_o ($MNm^{-a/a}$)	$\Delta\sigma^*$
109	134	5.0	1.43	2.193	8	18	4.42	24.0
93	136	4.8	1.42	2.121	20	38	3.77	20.4
78	140	5.6	1.46	2.054	63	115	3.16	17.1
78	137	4.8	1.42	2.044	28	50	3.16	17.1
62	136	5.3	1.45	1.953	240	510	2.51	13.6
62	131	5.4	1.45	1.953	130	245	2.51	13.6
54	138	6.0	1.48	1.904	620	1340	2.19	11.9
54	135	4.8	1.42	1.885	720	2920	2.19	11.9
47	137	5.6	1.46	1.830	1120	>4000	1.86	10.3
93	124	9.3	1.62	2.177	7	14	4.97	23.8
78	125	14.7	1.78	2.138	12	27	4.16	20.0
62	119	8.6	1.59	1.992	65	140	3.31	15.9
62	122	9.5	1.62	2.002	24	58	3.31	15.9
54	124	11.4	1.68	1.958	130	310	2.88	13.8
47	120	9.8	1.63	1.880	410	1100	2.48	12.1
47	118	10.3	1.64	1.883	170	450	2.48	12.1
39	118	10.1	1.64	1.806	920	2200	2.04	10.0
39	123	8.4	1.58	1.790	850	4150	2.04	10.0
93	103	20.8	1.94	2.256	1	4	6.25	27.2
78	109	22.4	1.99	2.187	2	9	5.24	22.8
78	105	25.2	2.05	2.204	3	22	5.24	22.8
62	106	26.0	2.07	2.108	8	38	4.17	18.1
62	104	22.0	1.97	2.087	14	79	4.17	18.1
54	108	23.4	2.02	2.038	22	110	3.63	15.8
47	109	20.7	1.94	1.953	70	420	3.13	13.7
39	110	21.6	1.95	1.881	120	920	2.62	11.4
39	109	20.7	1.94	1.879	190	2410	2.62	11.4

Table 10. Failure From Central Defects at Room Temperature (As-Welded Condition)

a_o (10^{-3}m)	$\Delta\sigma$ (MNm^{-2})	N_i (10^3 cycles)	N_f (10^3 cycles)	$Log\Delta K_o$	$\Delta\sigma^*$
2.16	78	1	8	0.812	32.37
2.41	70	1	16	0.792	30.21
7.88	24	3	52	0.683	25.46
3.18	43	3	73	0.647	20.90
2.91	35	9	153	0.538	16.18
5.34	24	25	295	0.528	16.27
4.40	24	29	451	0.453	14.00
3.18	28	39	420	0.450	13.61
6.60	16	42	1890	0.428	13.56
2.68	28	60	3180	0.418	12.54
2.80	24	120	2400	0.347	11.01

Table 11. Failure From Central Defects at Room Temperature (Stress-Relieved at 450 °C)

a_o (10^{-3}m)	$\Delta\sigma$ (MNm^{-3})	N_i (10^3 cycles)	N_f (10^3 cycles)	$\text{Log}\Delta K_o$	$\Delta\sigma^*$
7.78	62	2	9	1.109	92.35
3.70	85.5	6	33	0.981	64.48
6.62	46.5	6	46	0.909	55.47
7.26	39	12	58	0.847	52.66
3.04	62	25	101	0.798	42.26
2.28	62	51	203	0.729	37.97
3.18	46.5	44	974	0.683	32.40
5.30	23.5	310	3620	0.527	22.66
2.68	31	270	2770	0.466	20.05

Table 12. Failure From Central Defects at 300 °C
(Stress-Relieved at 450 °C)

a_o (10^{-3}m)	$\Delta\sigma$ ($MNm^{-3/2}$)	N_i (10^3 cycles)	N_f (10^3 cycles)	$\log\Delta K_o$	$\Delta\sigma^*$
3.70	85.5	2	12	0.981	86.3
6.62	46.5	5	26	0.909	77.3
4.20	55	6	25	0.831	61.6
4.56	46	9	72	0.780	53.3
2.40	62	36	175	0.740	51.1
2.02	62	18	110	0.701	46.8
5.47	31	25	130	0.662	41.7
2.80	39	70	370	0.571	35.0
5.72	21	80	460	0.500	29.2
2.92	27	170	900	0.448	25.1
3.80	23	290	2700	0.425	23.9
5.34	16	360	74000	0.351	21.1

FIGURE 1. Distribution of Stresses around a crack in a Semi-Infinite Plate

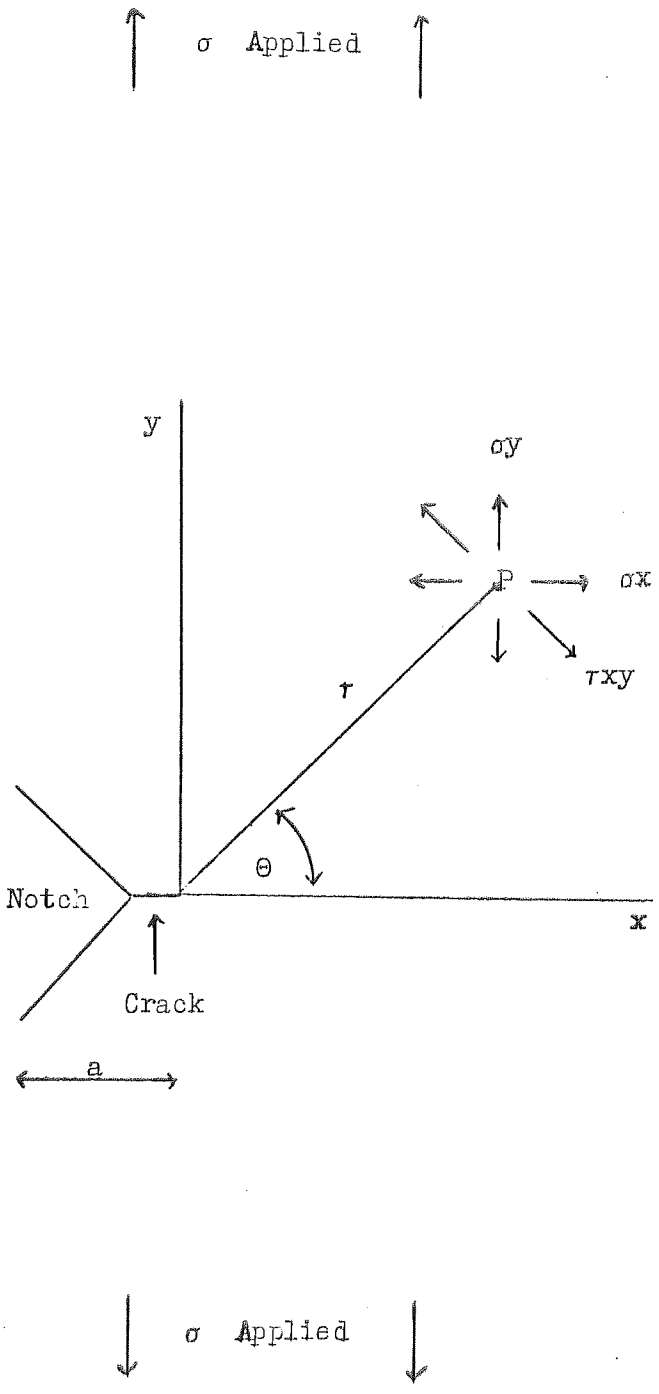

FIGURE 2. General S-N Curve,

Showing a fatigue Limit for

Sound and Defective Material.

$Kf = \frac{\sigma_1}{\sigma_2}$

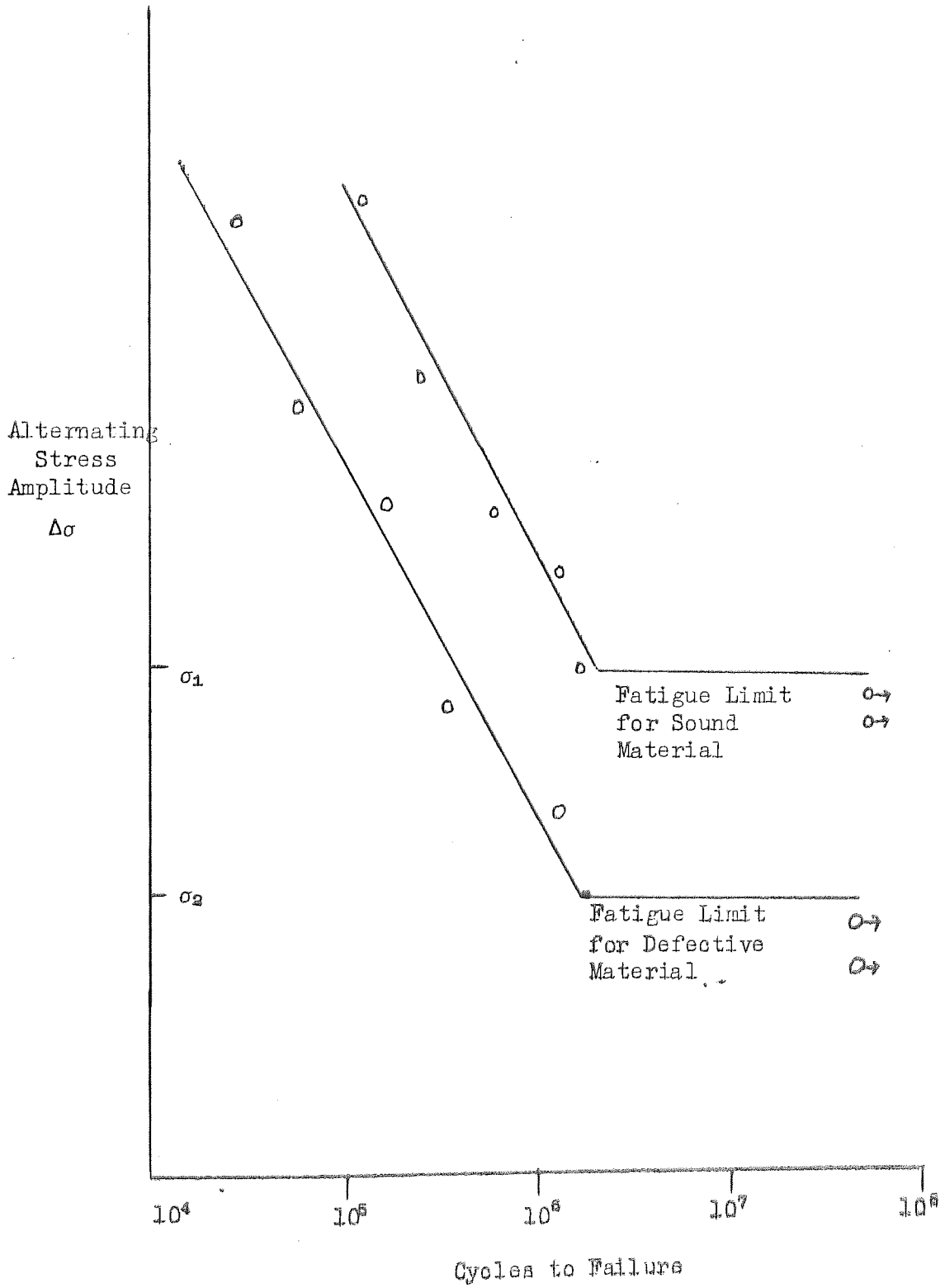

FIGURE 3. Schematic Illustration of Reinforcement Angle, θ

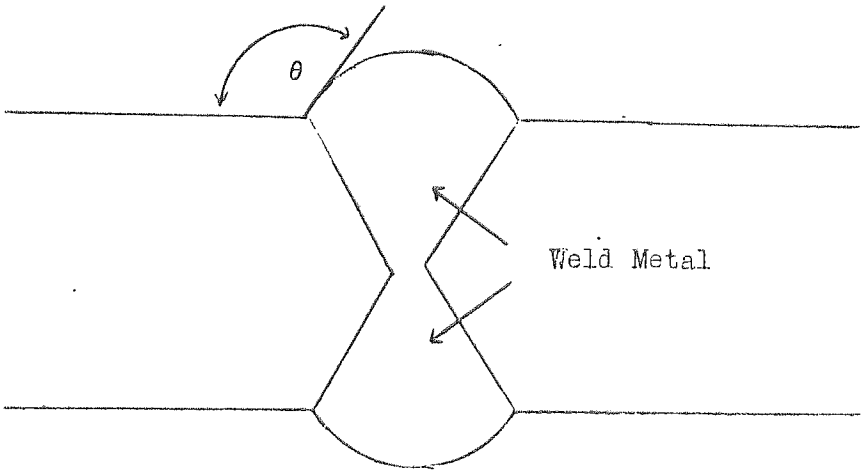

FIGURE 4A. Schematic Illustration of Edge Lack of Fusion

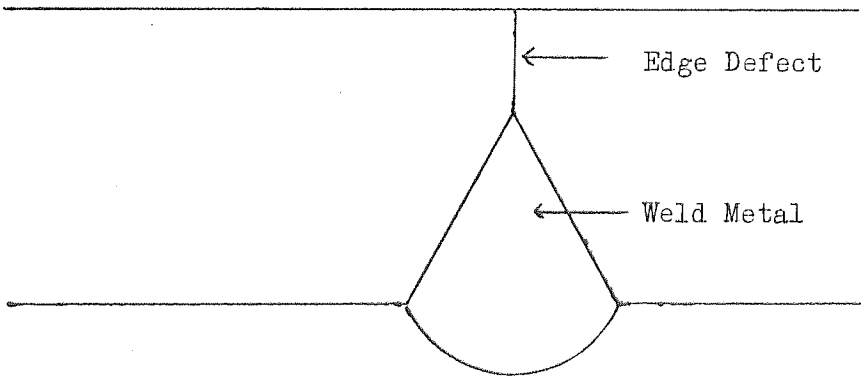

FIGURE 4B. Schematic Illustration of Central Lack of Fusion

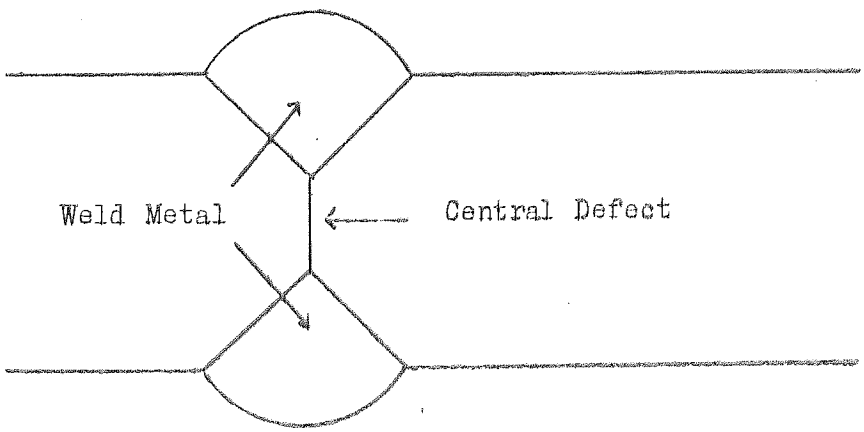

FIGURE 5. Representation of effect of Elastic, Plastic, and Total Strain Ranges on Fatigue Life. Ntr is the Transition Life.

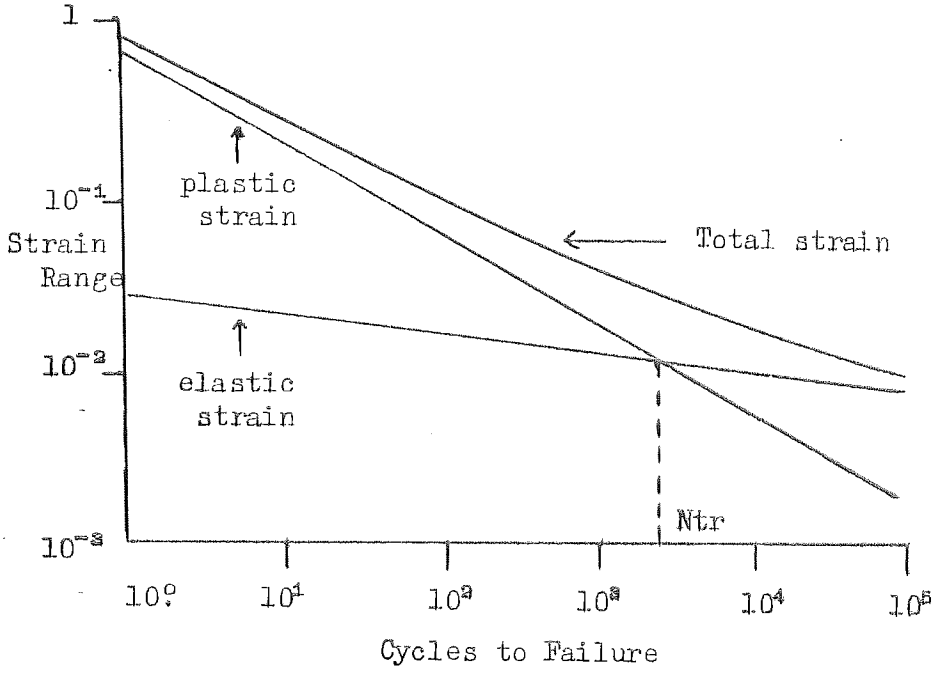

FIGURE 6. Schematic Representation of Effect of Frequency on Time to Failure, Identifying Three Frequency Regimes.

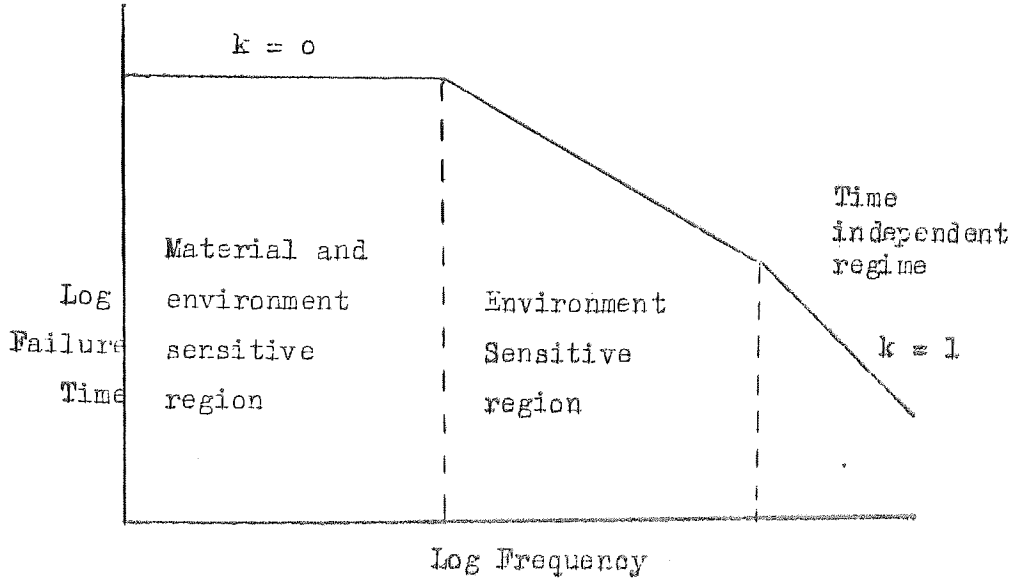

FIGURE 7. Schematic Representation of the 'V' Preparation for Welding.

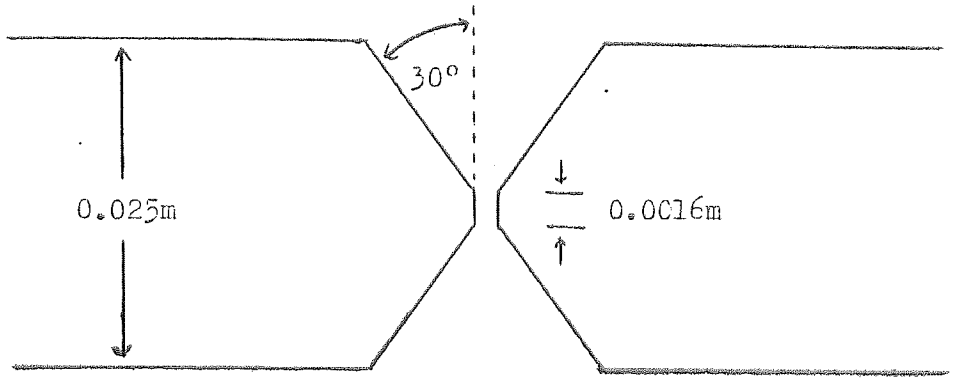

FIGURE 8. Schematic Representation of Central Defects Investigated in the Present Work.

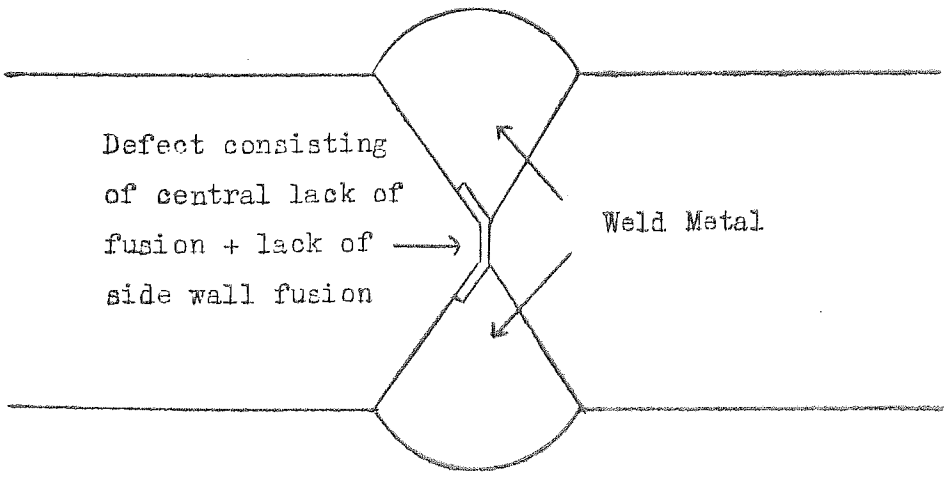

Figure 9. Fatigue Cracking from a Central Lack of Fusion and Lack of Penetration Defect. Magnification x 12.

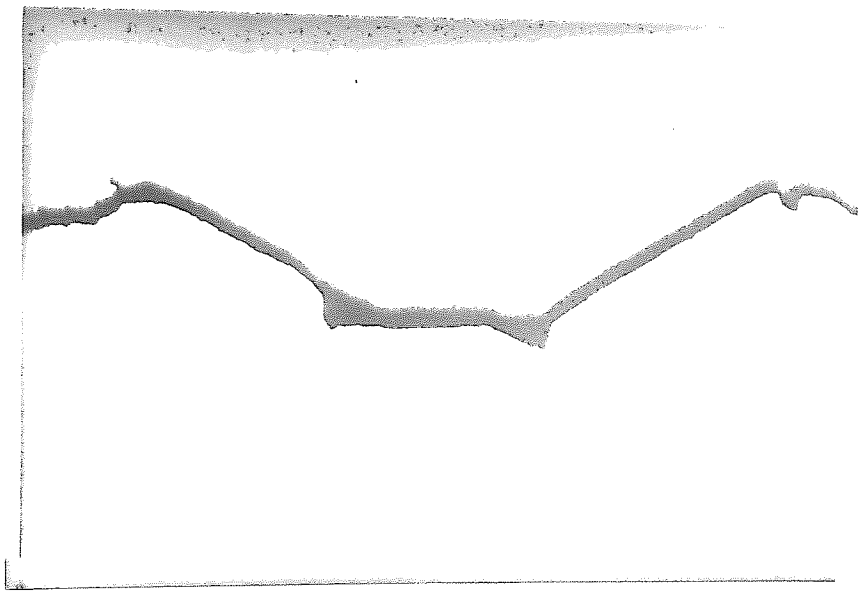

FIGURE 10 K-Callibration. Curve for a Single Edge Crack in a Plate under Uniform Tension.

$$Y = 1.99 - 0.41\left(\frac{a}{W}\right) + 18.7\left(\frac{a}{W}\right)^2 - 38.48\left(\frac{a}{W}\right)^3 + 53.85\left(\frac{a}{W}\right)^4$$

$$= \frac{K_I\, BW}{P\sqrt{a}}$$

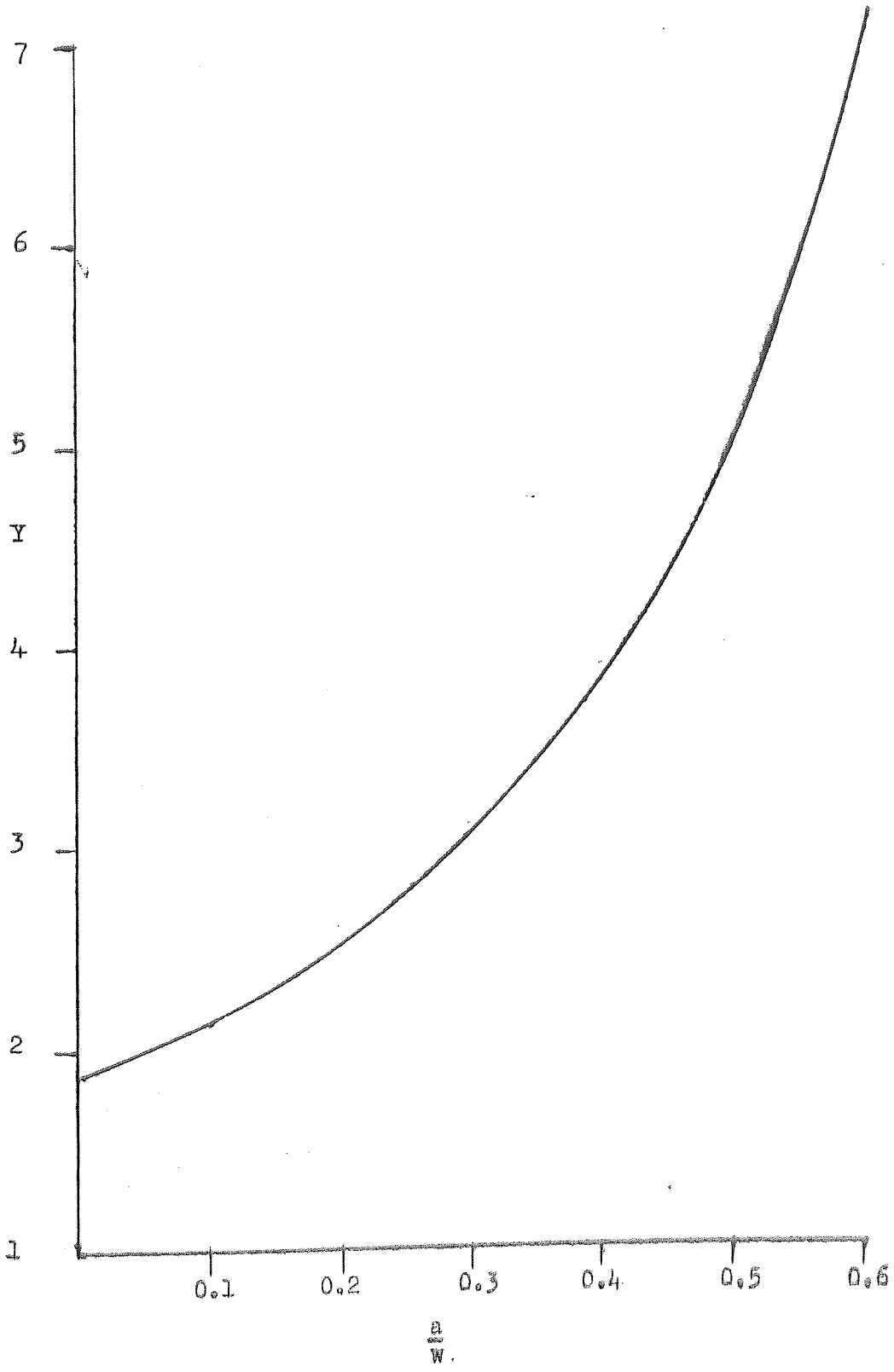

FIGURE 11 Relationship between $\frac{Va}{VoW}$ and $\frac{a}{w}$ (For y = 0.100)

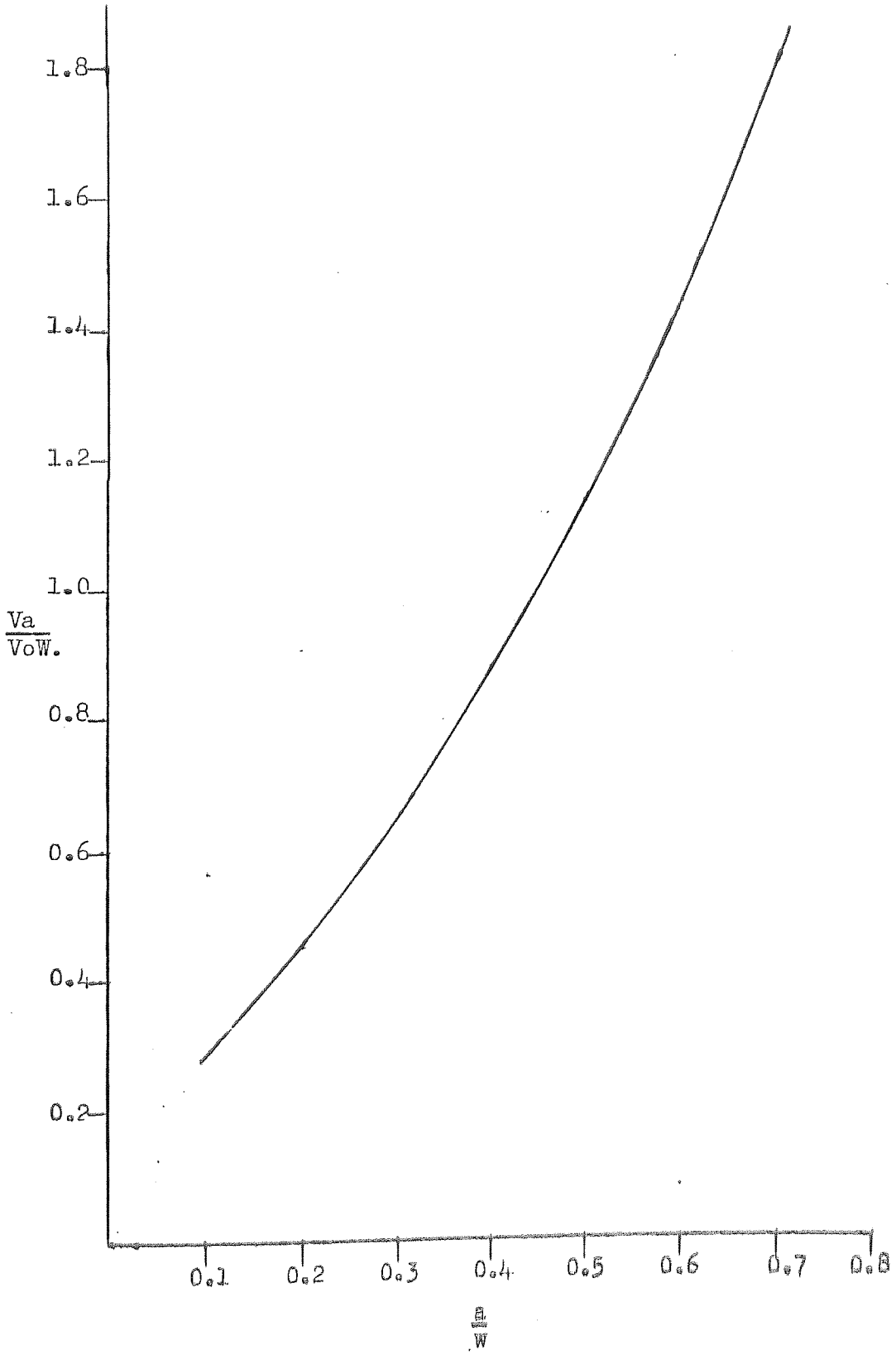

FIGURE 12 Schematic Representation of the Position of the Electrical Potential Leads on a Sample containing a Central Defect.

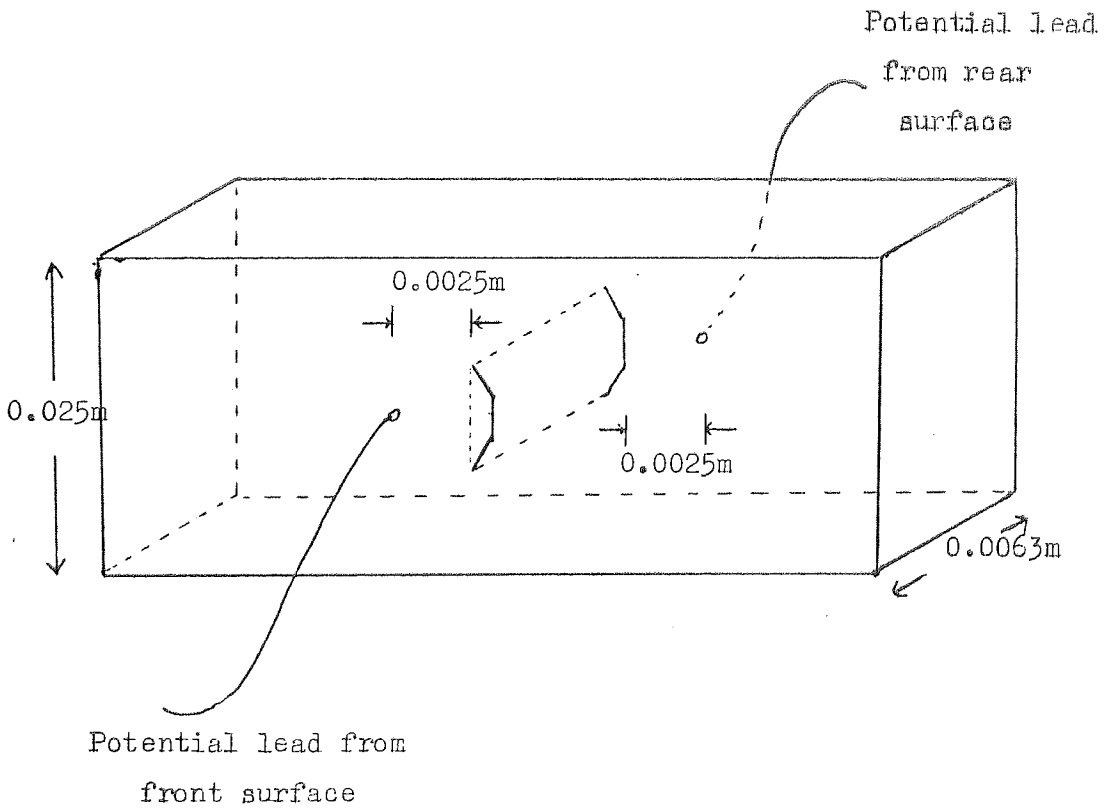

FIGURE 13. Effect of ΔK on Crack Growth Rate through the Weld Metal. Tested at Room Temperature in the As-Welded Condition.

In the Linear Region:-

$$\frac{da}{dN} = 10^{-10.48}(\Delta K)^{4.2}$$

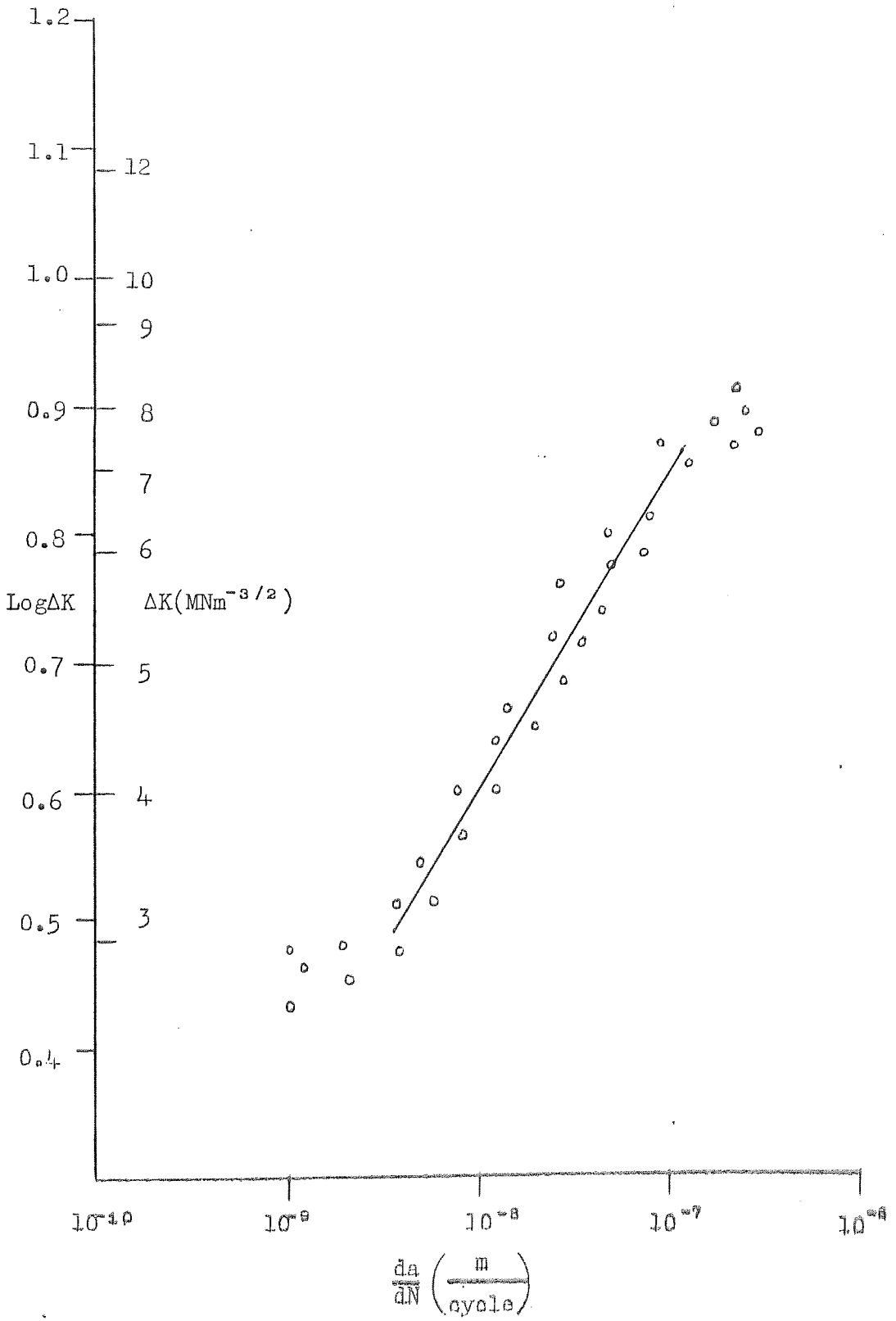

FIGURE 14. Effect of ΔK on Crack Growth Rate through the Weld Metal Tested at Room Temperature after Stress-Relieving at 325°C In the Linear Region:-

$$\frac{da}{dN} = 10^{-10.52} (\Delta K)^{3.7}$$

for the Thickness of 6.28×10^{-3} m

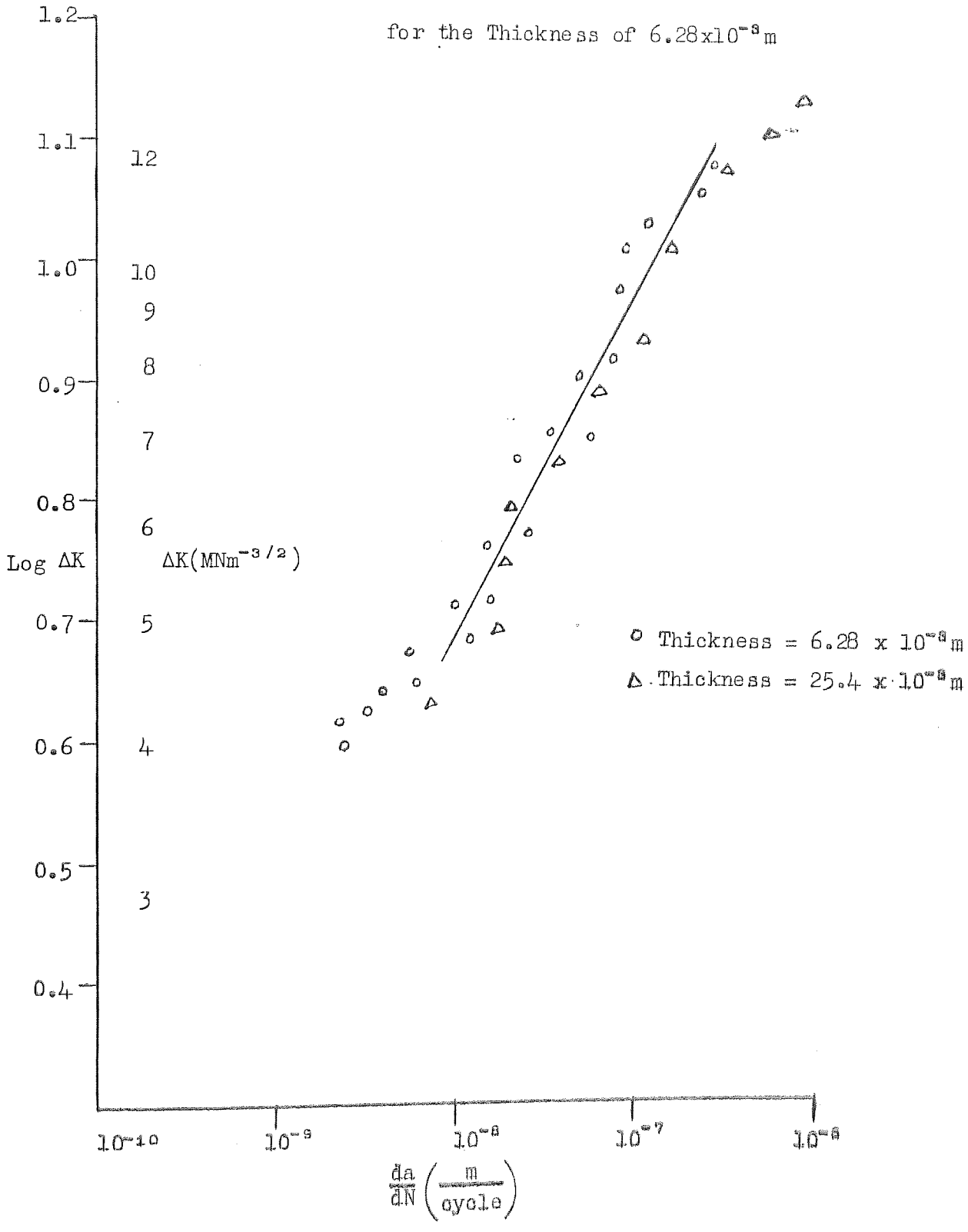

FIGURE 15. Effect of ΔK on Crack Growth Rate through the Weld Metal Tested at Room Temperature after Stress-Relieving at 450°C. In the Linear Region.

$$\frac{da}{dN} = 10^{-10.46} (\Delta K)^{3.3}$$

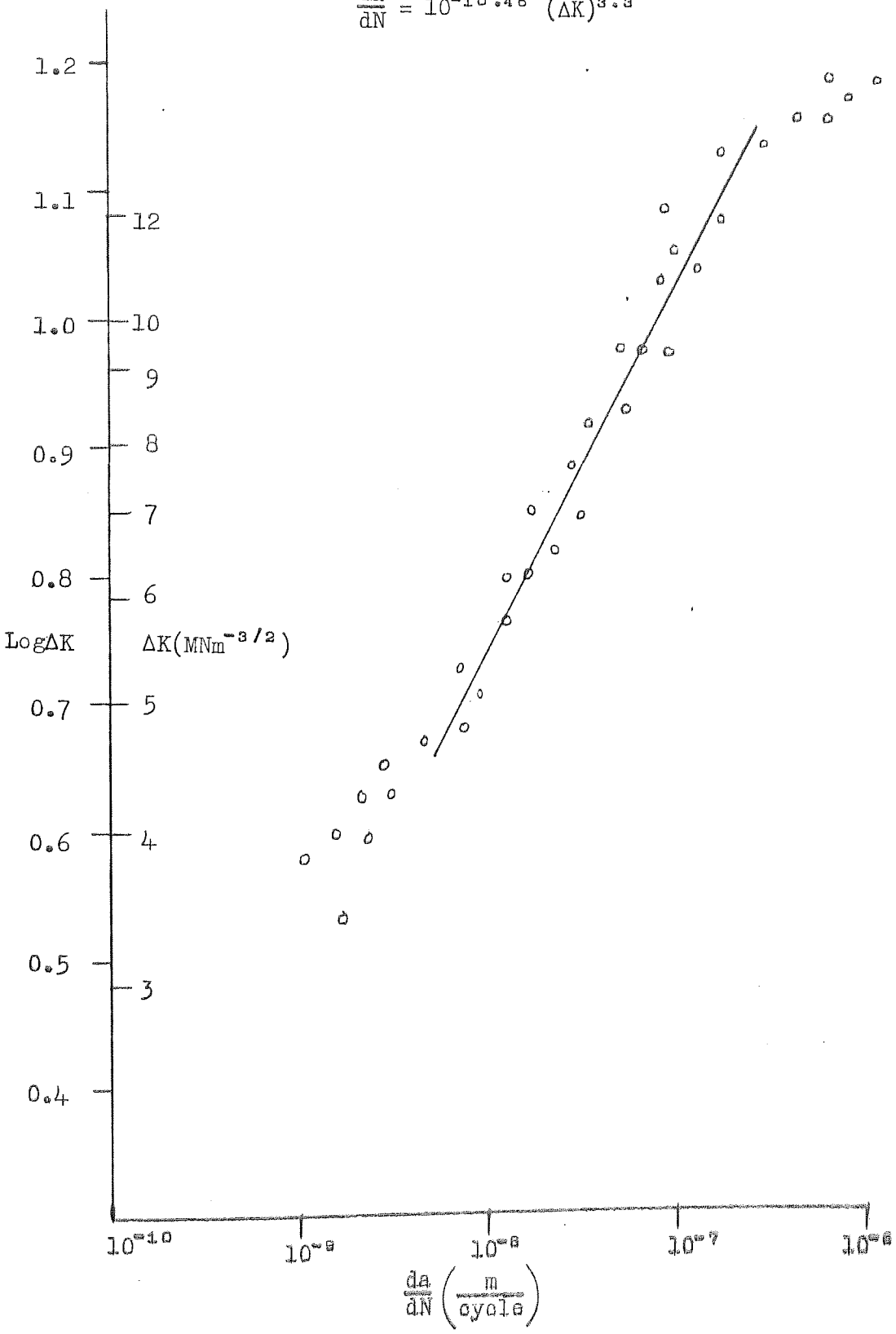

FIGURE 16 Effect of ΔK on Crack Growth Rate through the Heat Affected Zone Tested at Room Temperature after Stress-Relieving at 325°C In the Linear Region

$$\frac{da}{dN} = 10^{-10.86}(\Delta K)^{3.9}$$

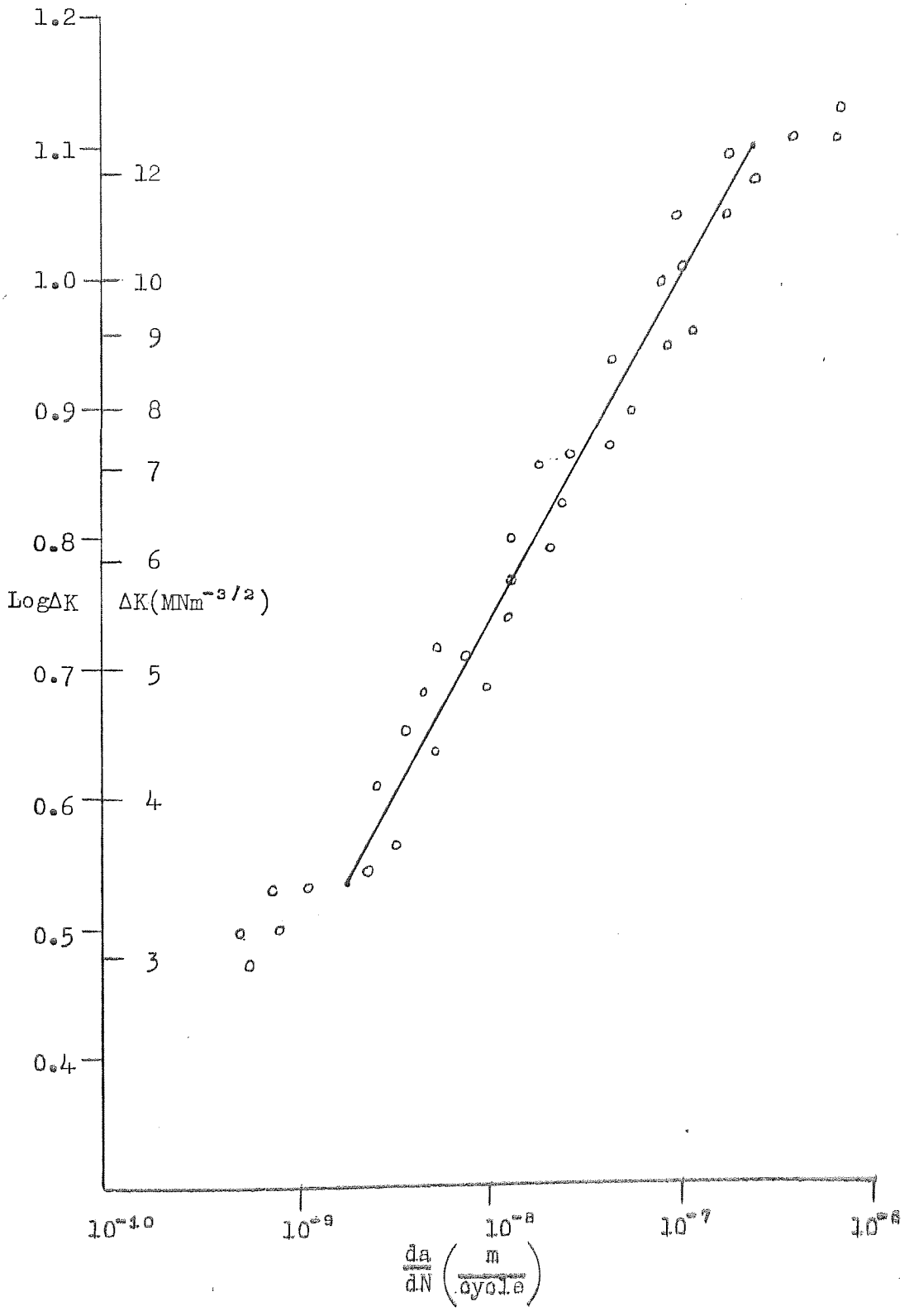

FIGURE 17 Effect of ΔK on Crack Growth Rate through the Weld Metal Tested at 200°C after Stress Relieving at 325°C

In the Linear Region:-

$$\frac{da}{dN} = 10^{-10.53}(\Delta K)^{4.1}$$

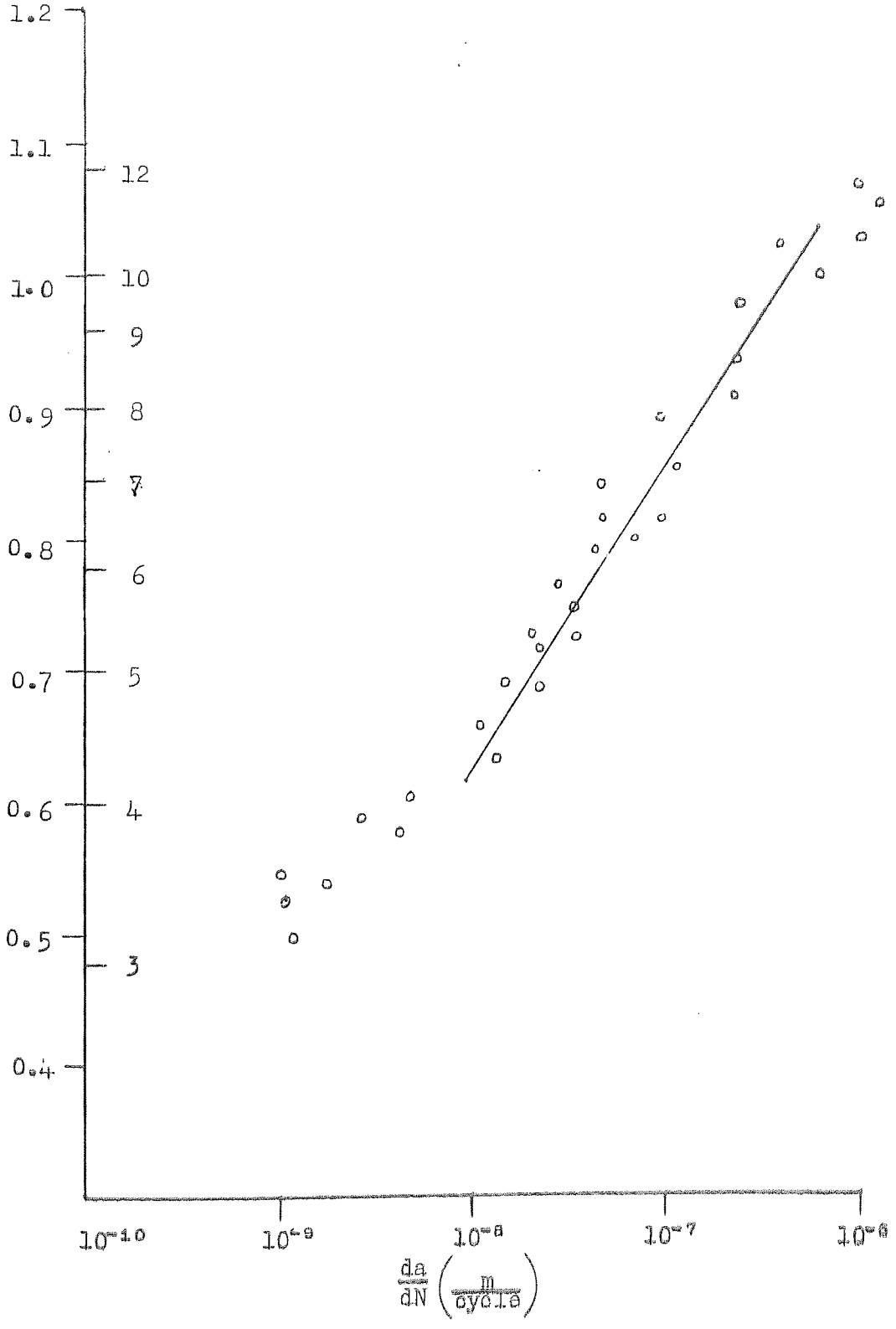

FIGURE 18 Effect of ΔK on Crack Growth Rate through the Weld Metal. Tested at 300°C after Stress-Relieving at 325°C.

In the Linear Region:-

$$\frac{da}{dN} = 10^{-10.75} (\Delta K)^{5.1}$$

for thickness of 6.28×10^{-3} m

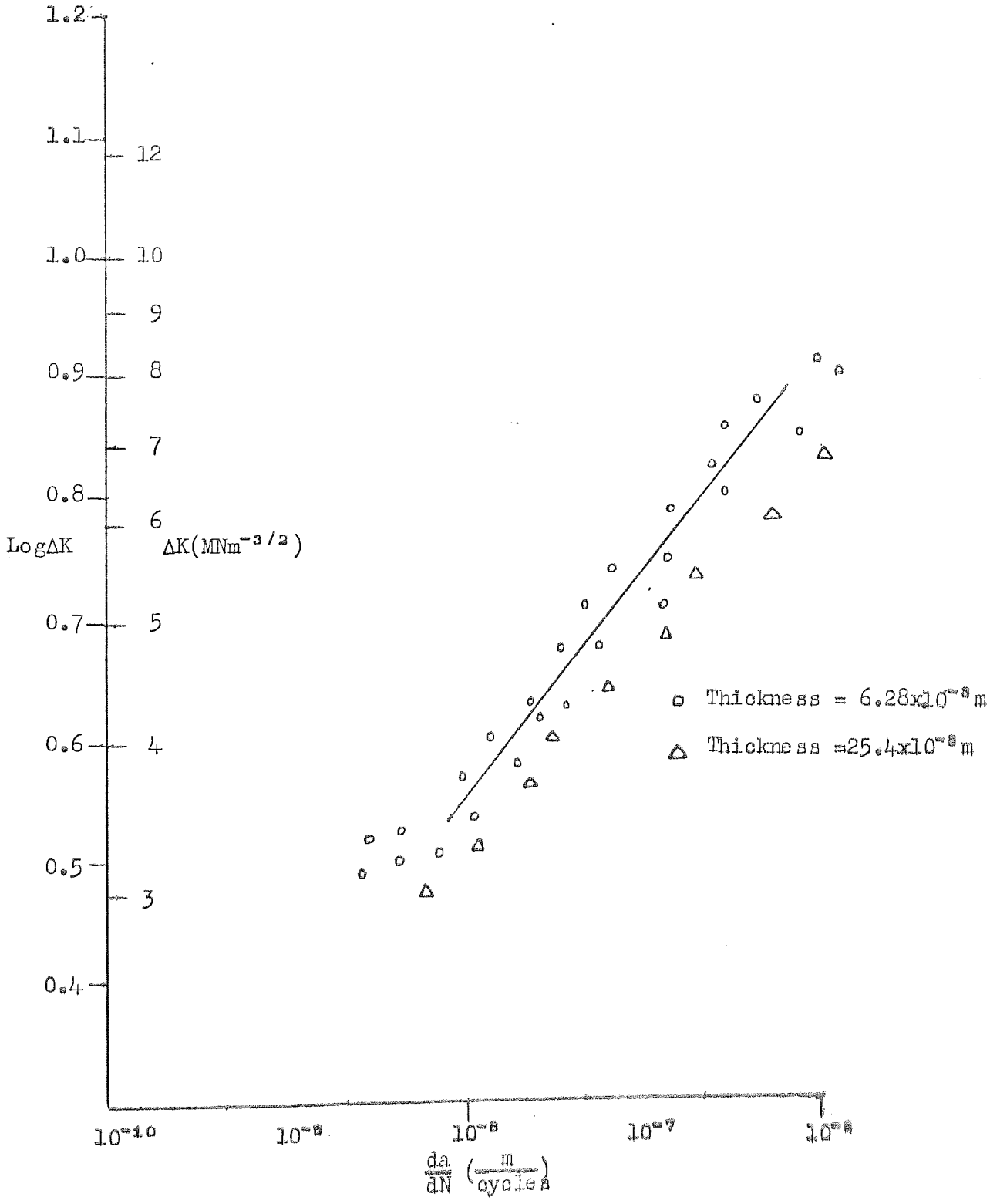

FIGURE 19 Effect of ΔK on Crack Growth Rate through the Weld Metal.
Tested at 300°C after Stress-Relieving at 450°C.
In the Linear Region

$$\frac{da}{dN} = 10^{-9.54} (\Delta K)^{2.8}$$

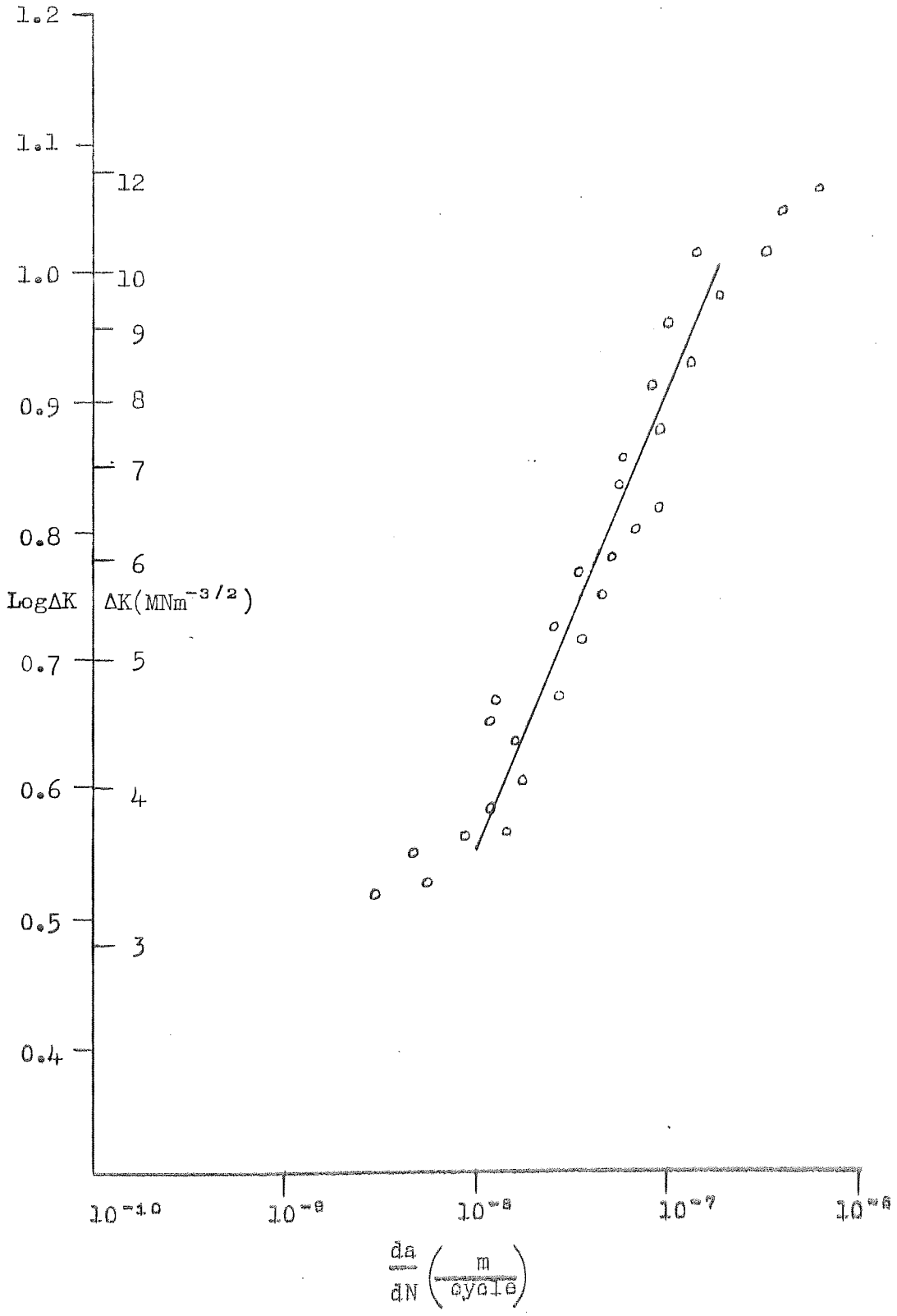

FIGURE 20 Effect of ΔK on Crack Growth Rate through the Heat Affected Zone Tested at 300°C after Stress-Relieving at 325°C

In the Linear Region:-

$$\frac{da}{dN} = 10^{-10.75}(\Delta K)^{4.9}$$

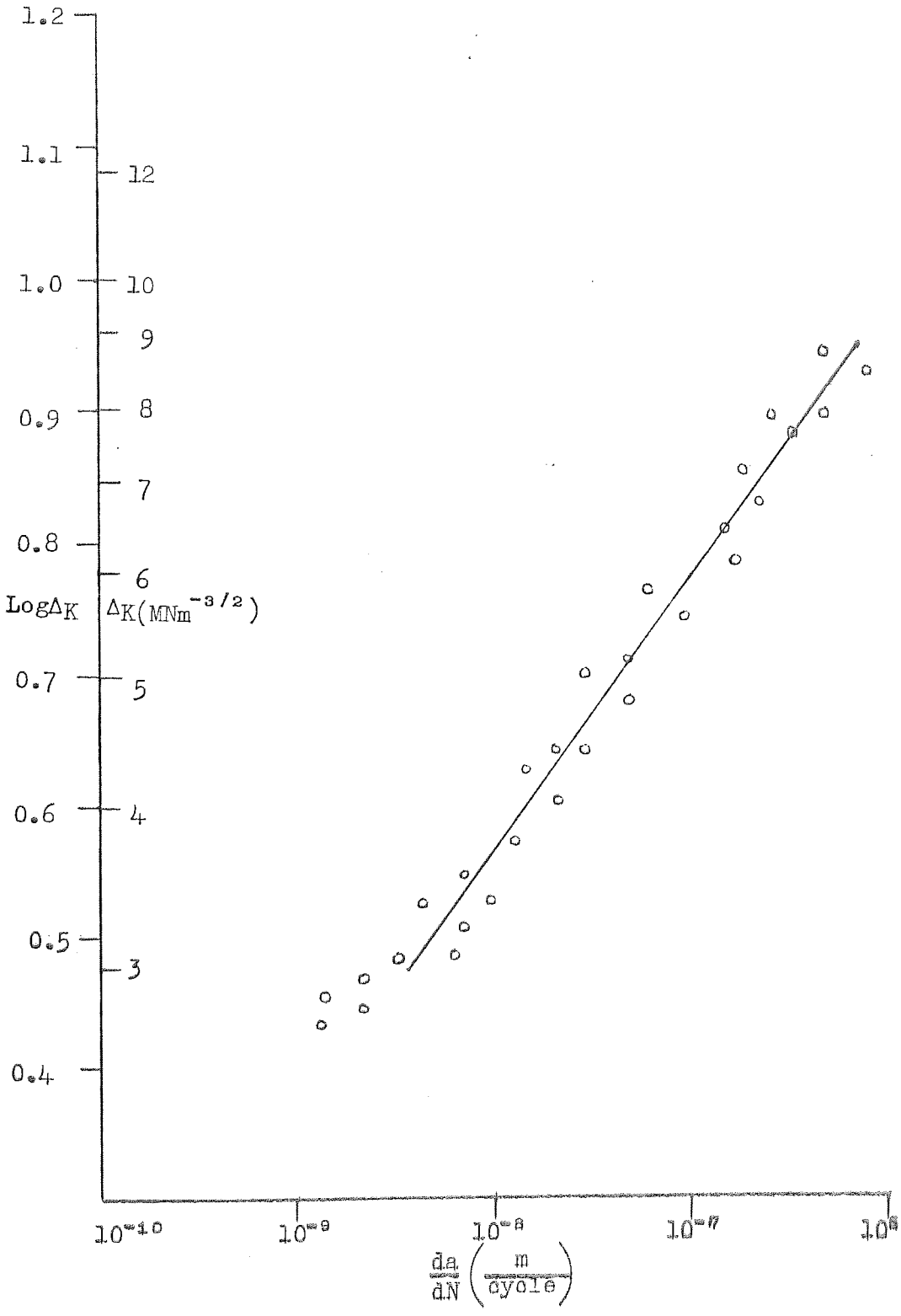

FIGURE 21 Effect of ΔK on Crack Growth Rate through the Weld Metal
Tested at 300°C, frequency 45Hz, after Stress-Relieving at 325°C
In the Linear Region:-

$$\frac{da}{dN} = 10^{-10.78}(\Delta K)^{5.25}$$

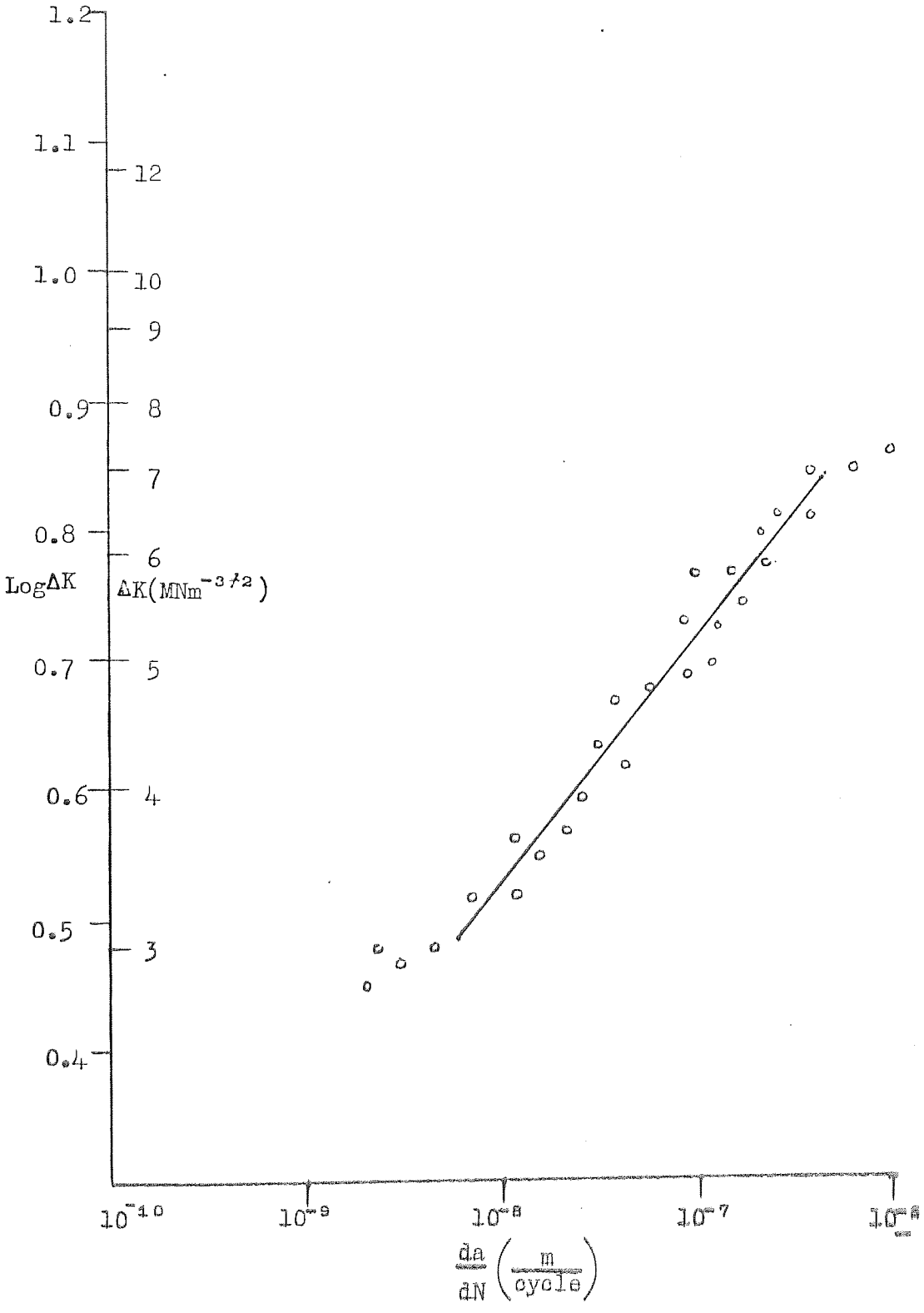

Figure 22. Crack Path through the Heat Affected Zone. Tested at Room Temperature in the As-Welded Condition. Magnification x 200.

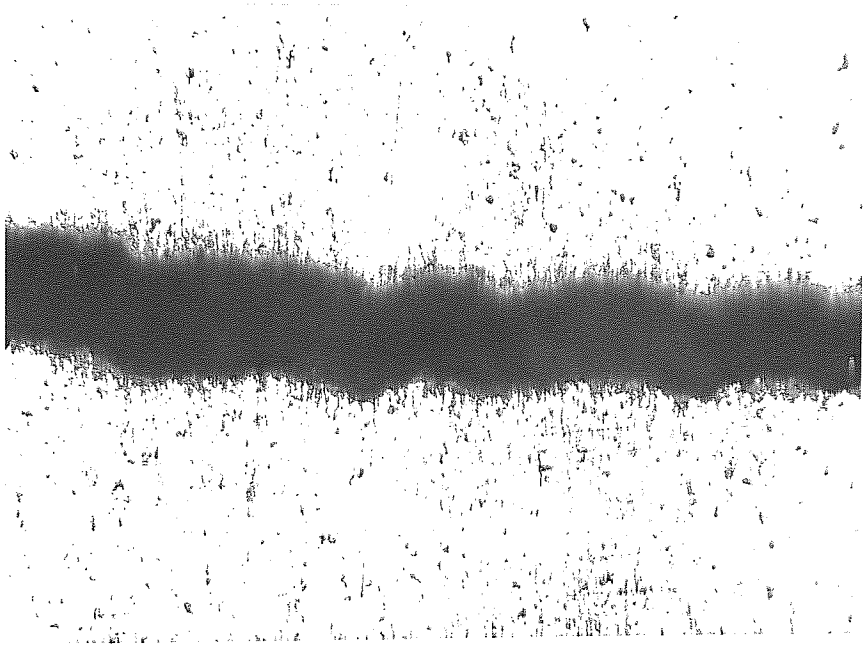

Figure 23. Crack Path through the Weld Metal. Tested at Room Temperature in the As-Welded Condition. Magnification x200.

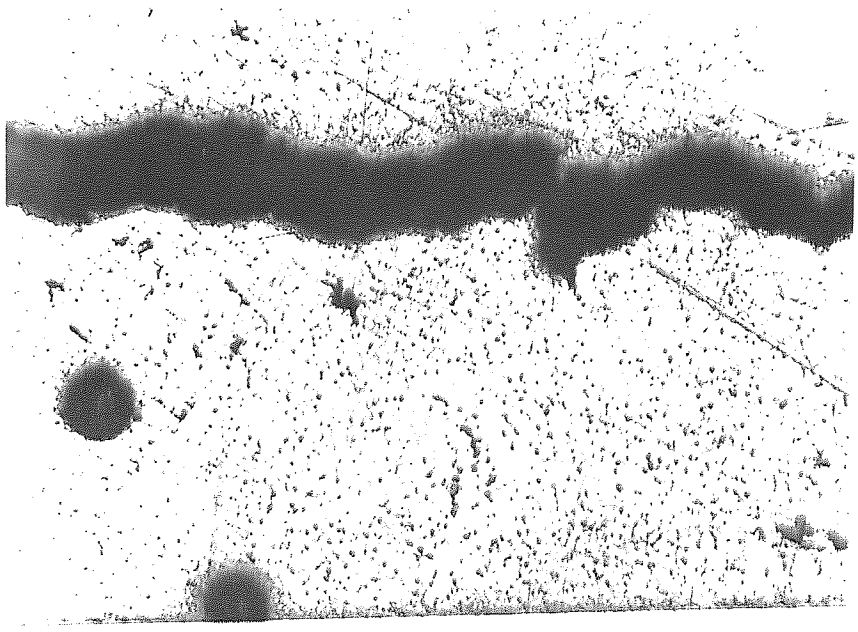

Figure 24. Fracture Surface in the Heat Affected Zone. Tested at Room Temperature after Stress-Relieving at 325°C. $\Delta K = 5\ MNm^{-3/2}$. Magnification x 650.

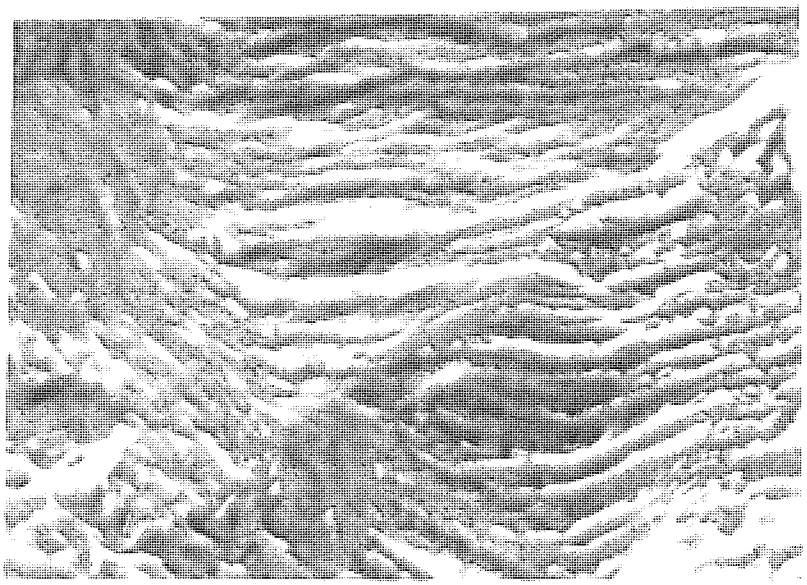

Figure 25. Fracture Surface in the Heat Affected Zone. Tested at Room Temperature after Stress-Relieving at 325°C. $\Delta K = 10\ MNm^{-3/2}$. Magnification x 650.

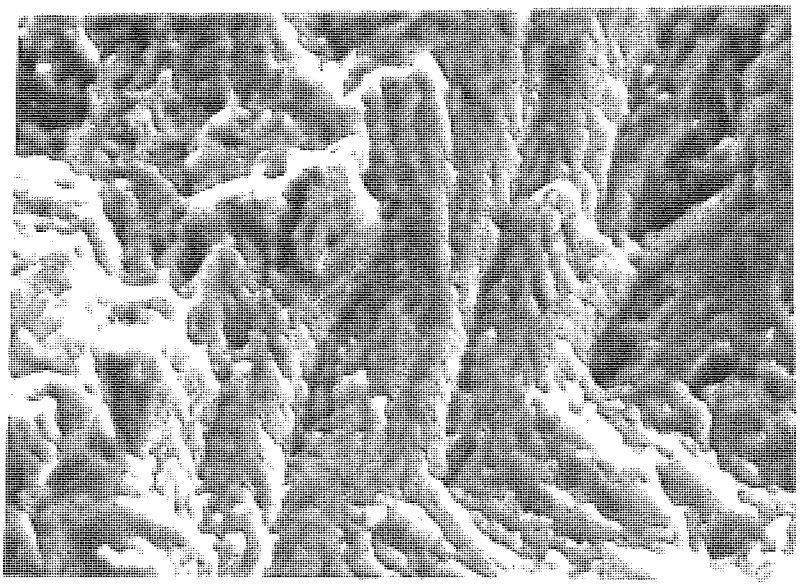

Figure 26. Fracture Surface in the Weld Metal. Tested at Room Temperature in the As-Welded Condition.
$\Delta K = 5 MNm^{-3/2}$. Magnification x 250.

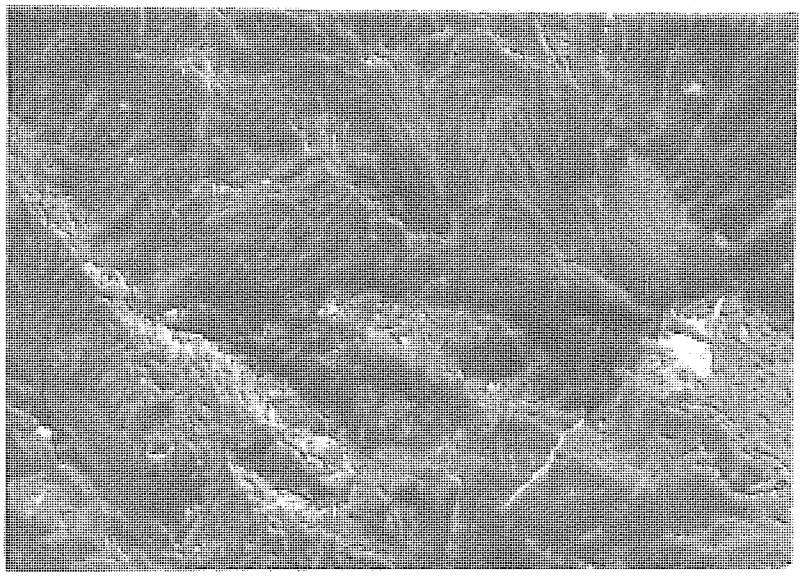

Figure 27. Fracture Surface in the Heat Affected Zone. Tested at Room Temperature in the As-Welded Condition.
$\Delta K = 5 MNm^{-3/2}$. Magnification x 250.

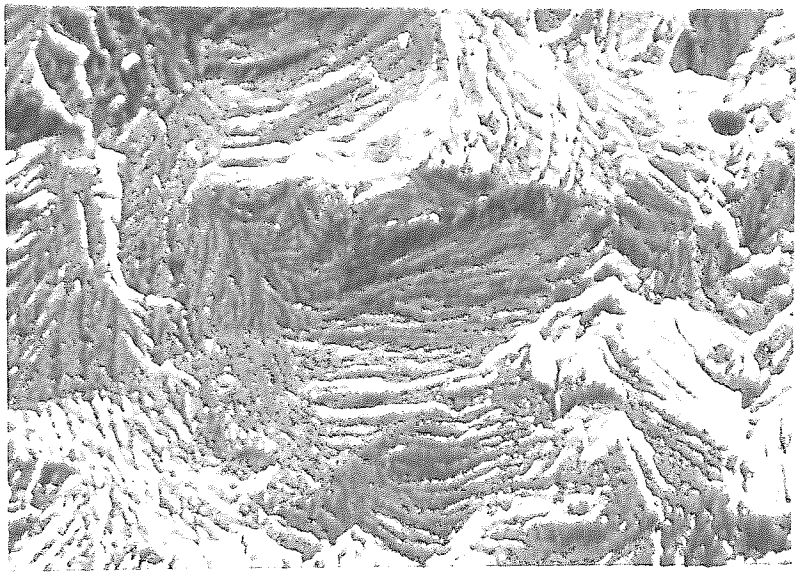

Figure 28. Crack Path through the Heat Affected Zone. Tested at Room Temperature after Stress-Relieving at 450°C. Magnification x 200.

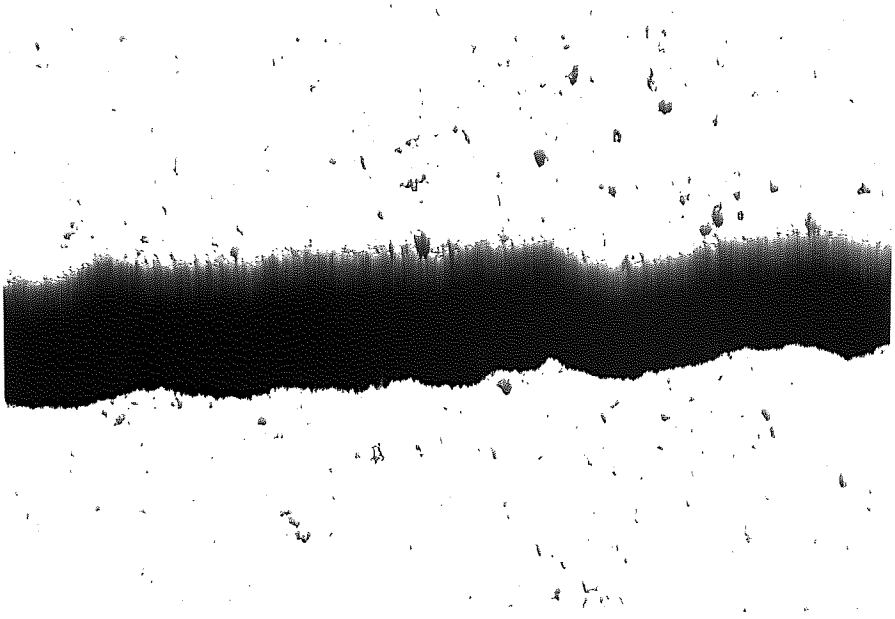

Figure 29 Crack Path through the Weld Metal. Tested at Room Temperature after Stress-Relieving at 450°C. Magnification x 200.

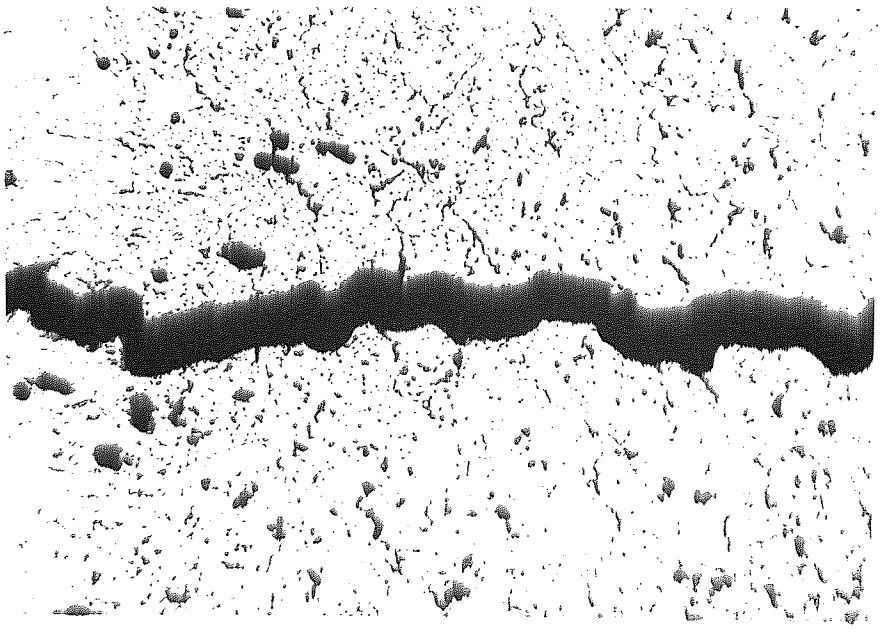

Figure 30 Crack Path through the Weld Metal. Tested at 300°C after Stress-Relieving at 325°C.

$\Delta K = 9\ MNm^{-3/2}$. Magnification x 200.

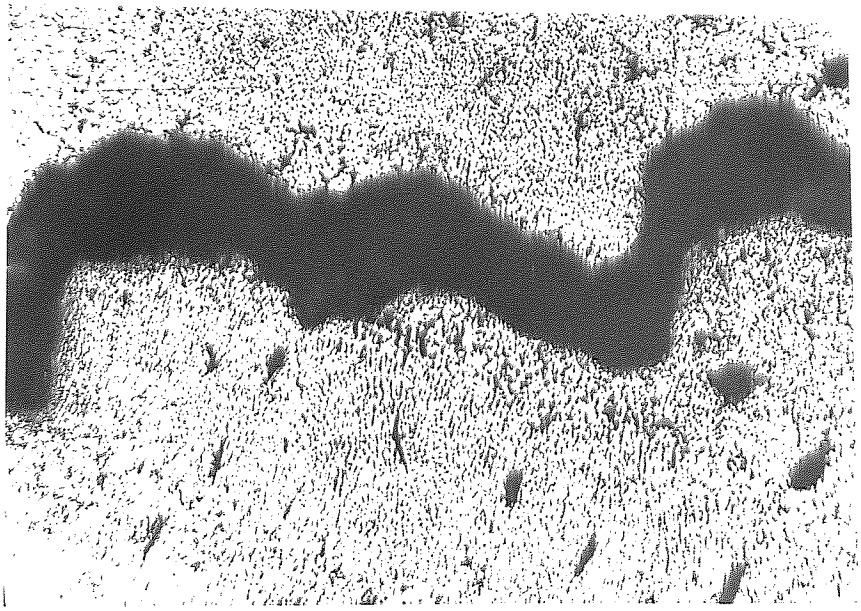

Figure 31. Crack Path through the Weld Metal. Tested at 300°C in the As-Welded Condition.

$\Delta K = 9MNm^{-3/2}$. Magnification x 100.

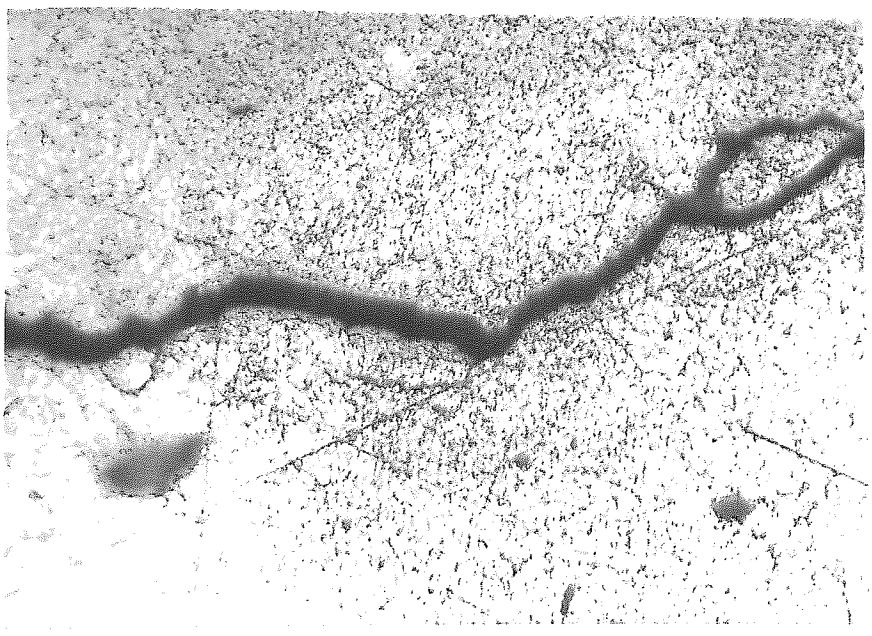

Figure 32. Fracture Surface in the Heat Affected Zone. Tested at 300°C in the As-Welded Condition.

$\Delta K = 9 MNm^{-3/2}$. Magnification x 250.

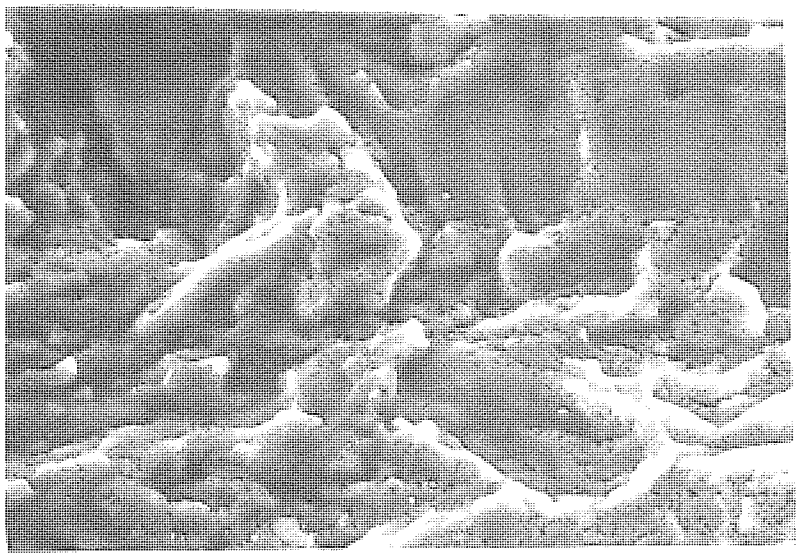

FIGURE 33 Determination of Fatigue Strength at 2 x 10^6 cycles for Welds containing Central Defects. Tested at Room Temperature after Stress-Relieving at 325°C.

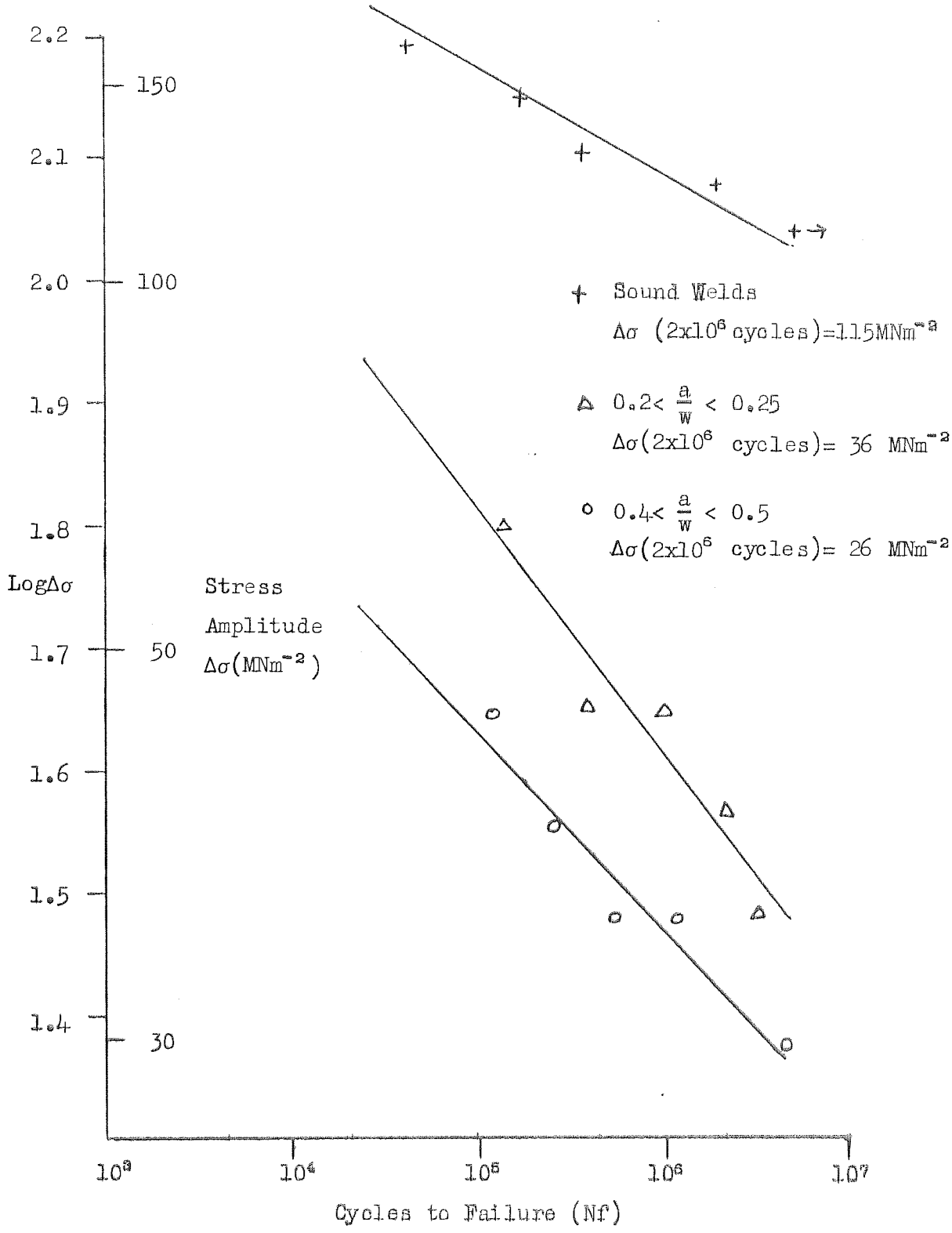

FIGURE 34 Determination of Fatigue Strength at 2 x 10^6 cycles for Welds containing Central Defects. Tested at 200°C after Stress-Relieving at 325°C.

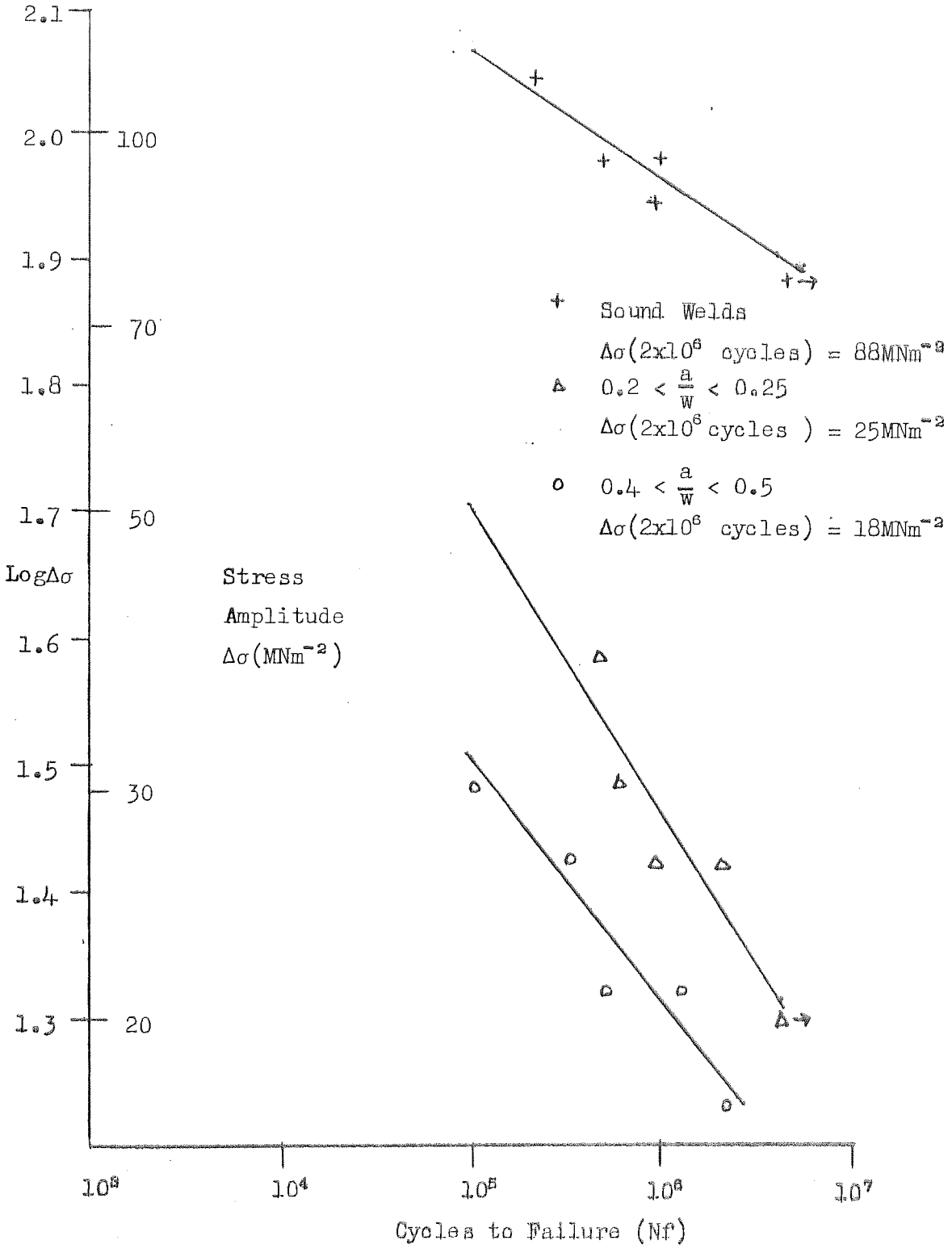

FIGURE 35 Determination of Fatigue Strength at 2×10^6 cycles for Welds containing Central Defects Tested at 300°C. after Stress-Relieving at 325°C.

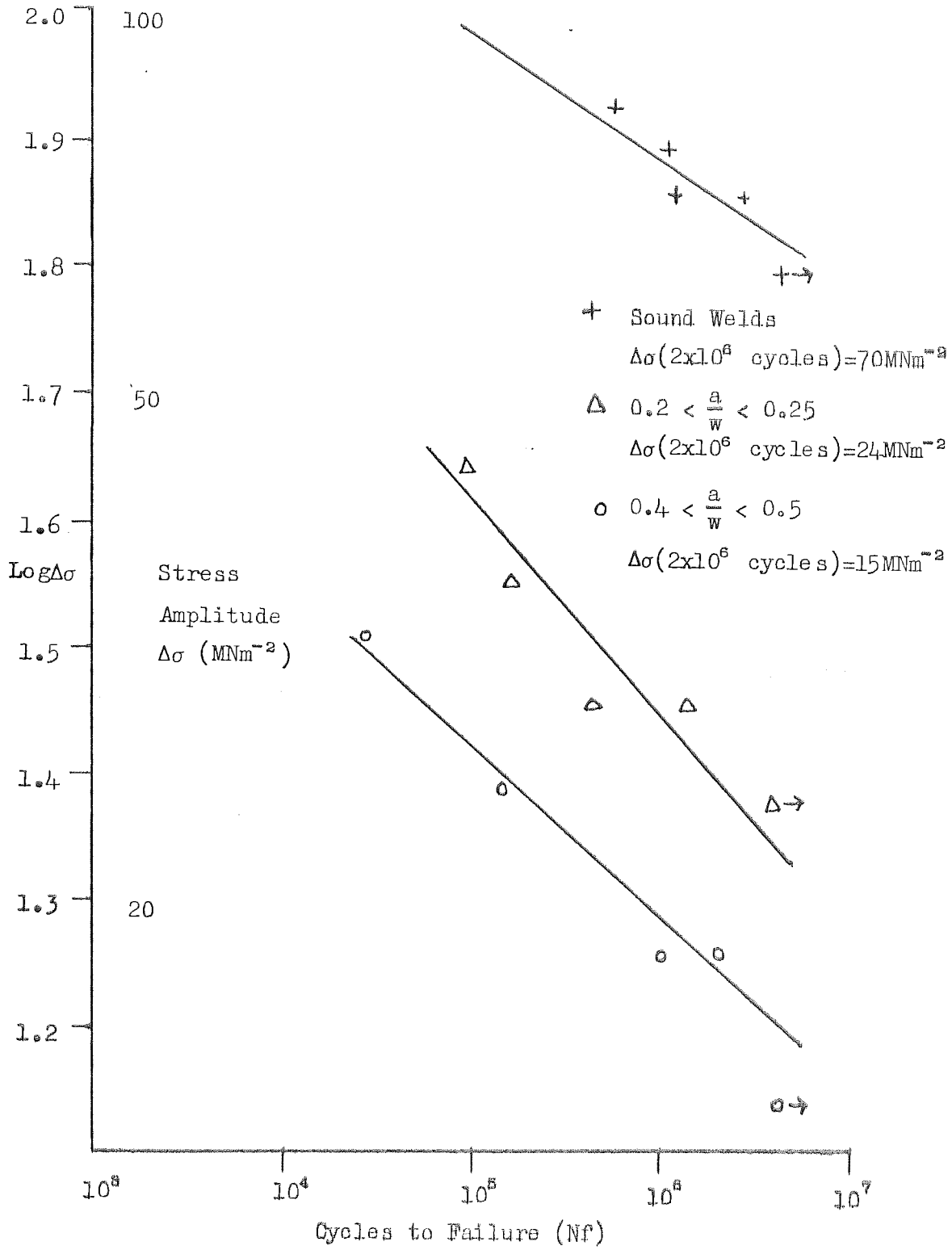

FIGURE 36 Effect of Defect Size on Fatigue Strength Reduction Factor Kf', measured at 2 x 10^6 cycles. Tested at Room Temperature.

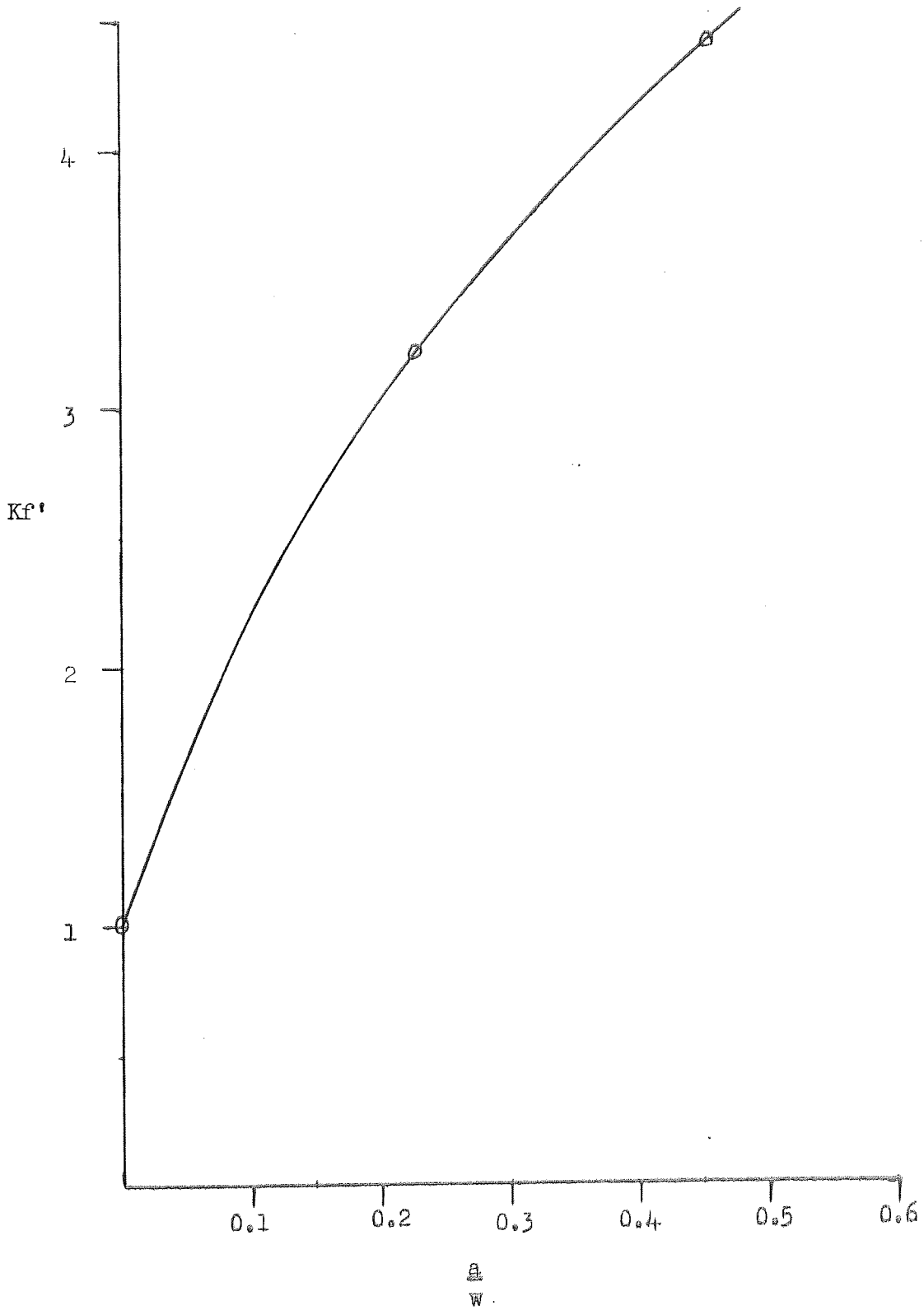

FIGURE 37 Effect of Defect Size on Fatigue Strength Reduction Factor Kf', measured at 2 x 10^6 cycles Tested at 200°C.

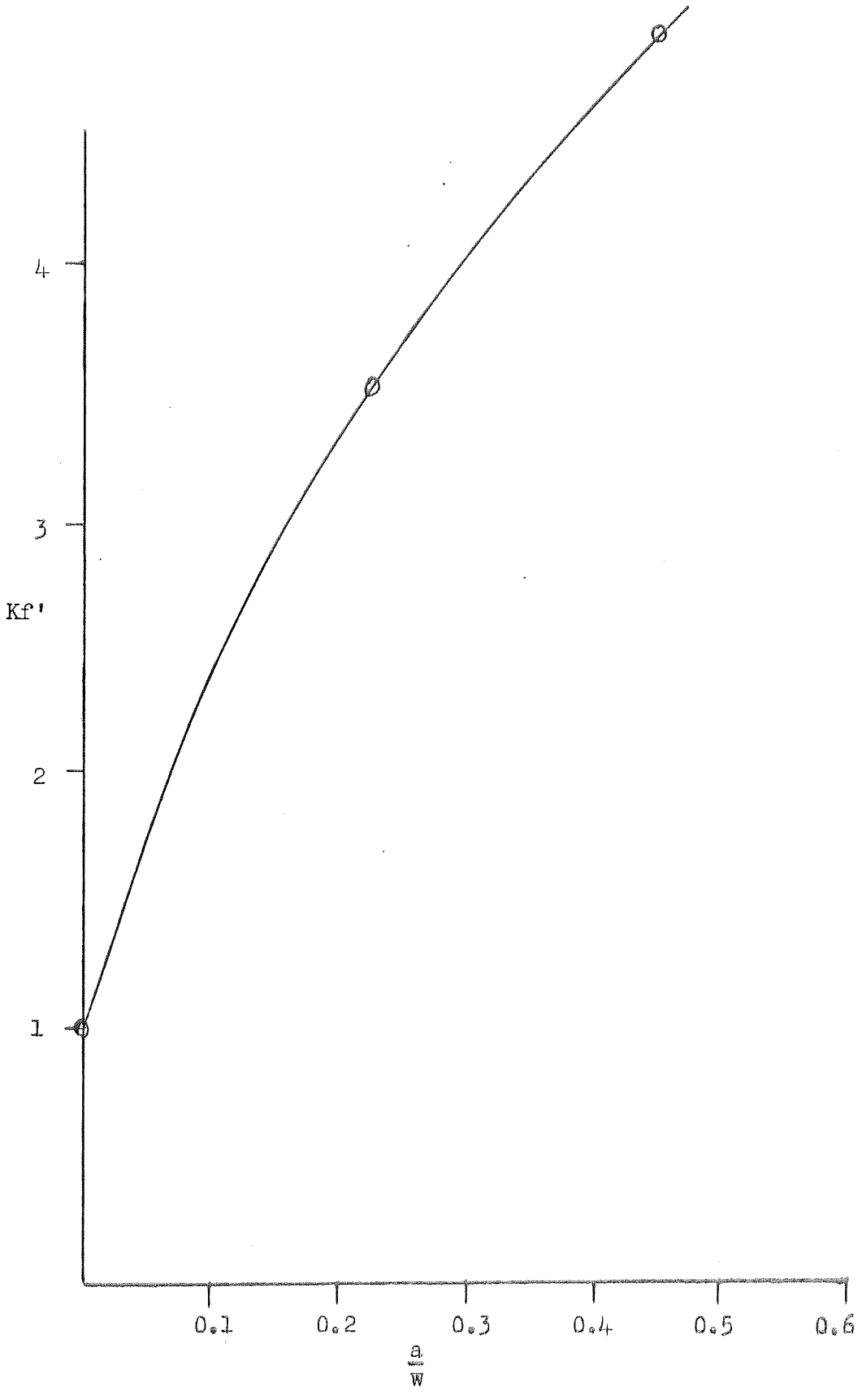

FIGURE 38 Effect of Defect Size on
Fatigue Strength Reduction Factor
Kf', measured at 2×10^6 cycles
Tested at 300°C

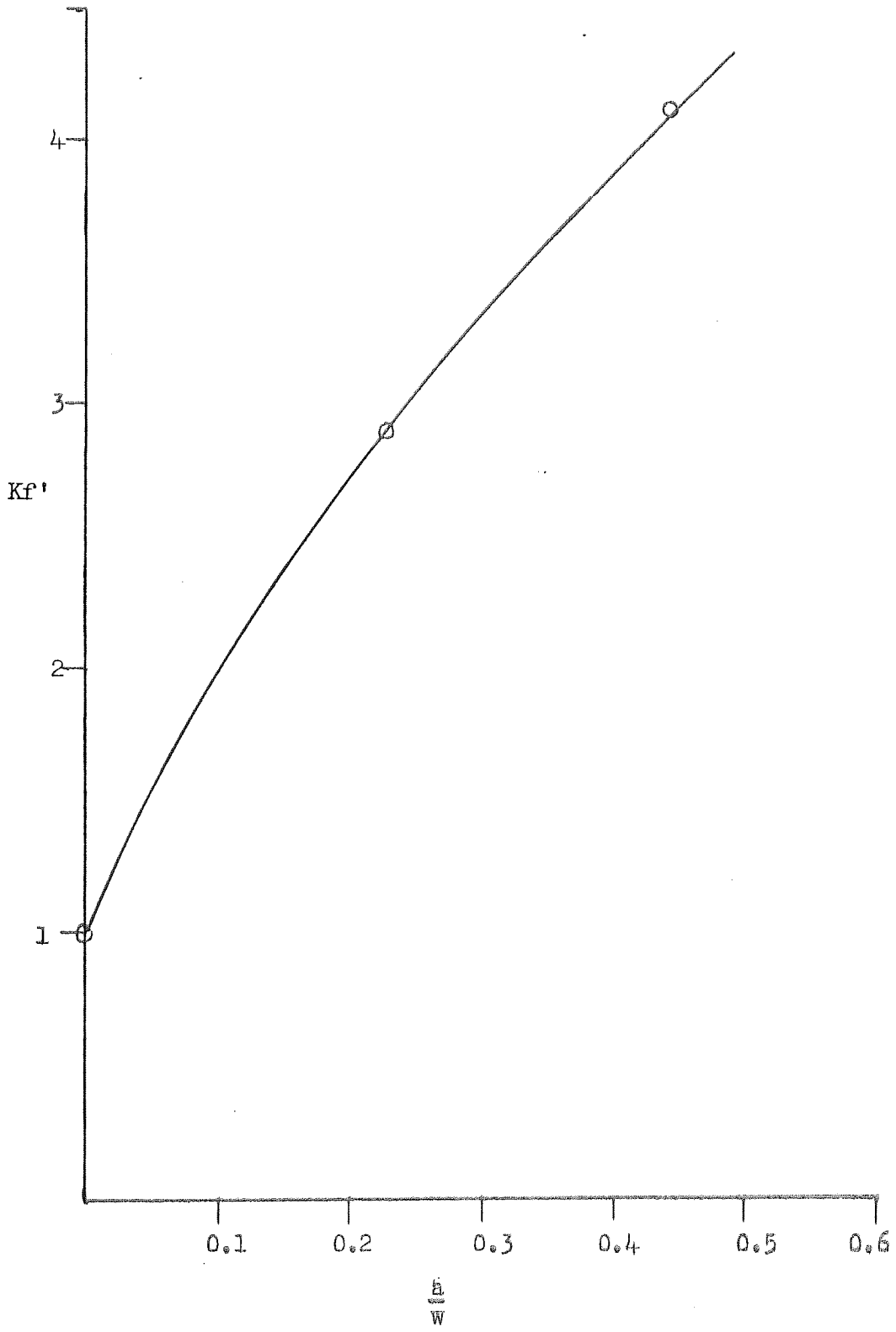

FIGURE 39A Effect of Reinforcement Angle (θ) on Fatigue Strength.
Tested at Room Temperature after Stress-Relieving at 325°C.
$130° < \theta < 140°$

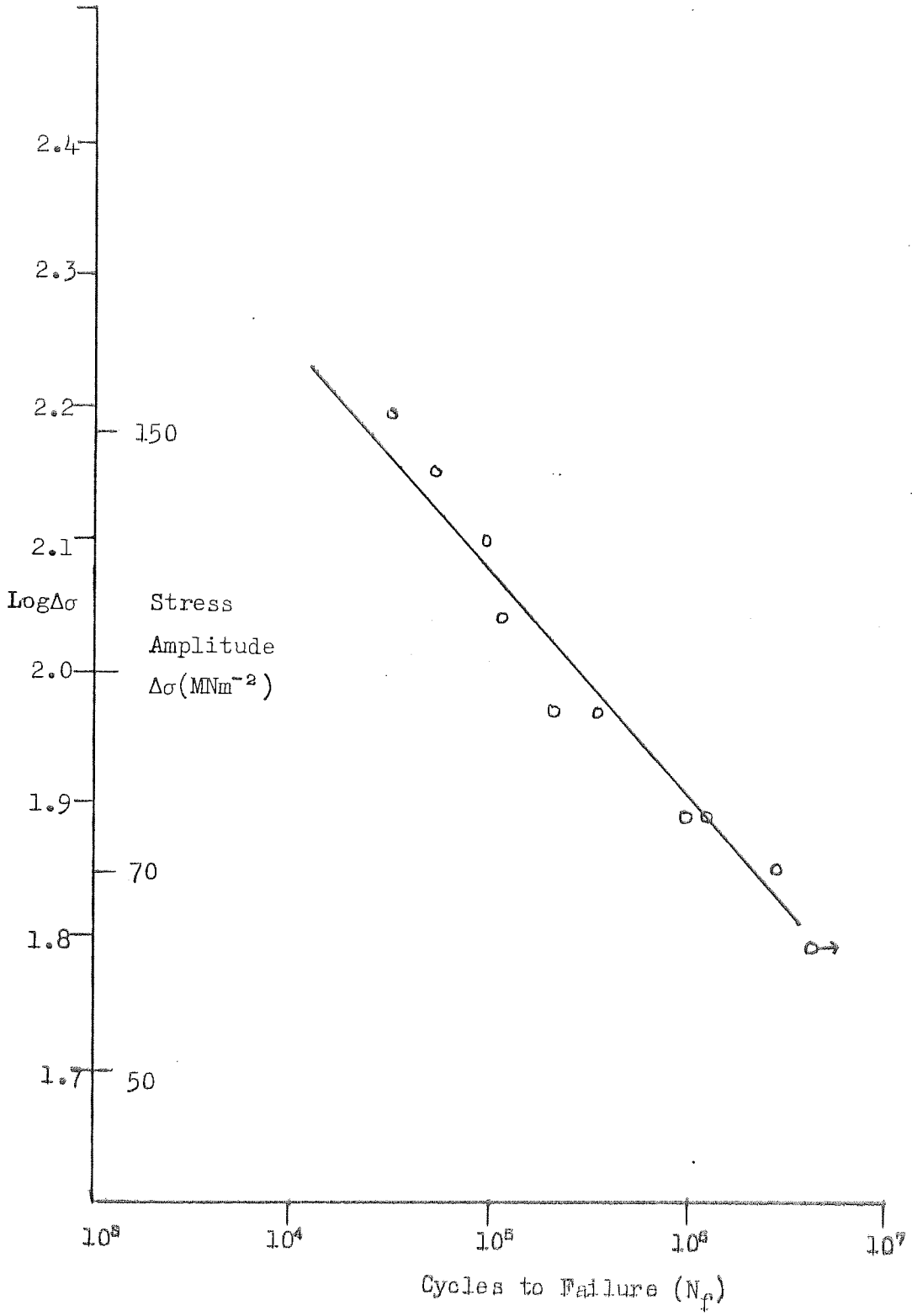

FIGURE 39B Effect of Reinforcement Angle (θ) on Fatigue Strength.
Tested at Room Temperature after Stress-Relieving at 325°C
$115° < \theta < 125°$.

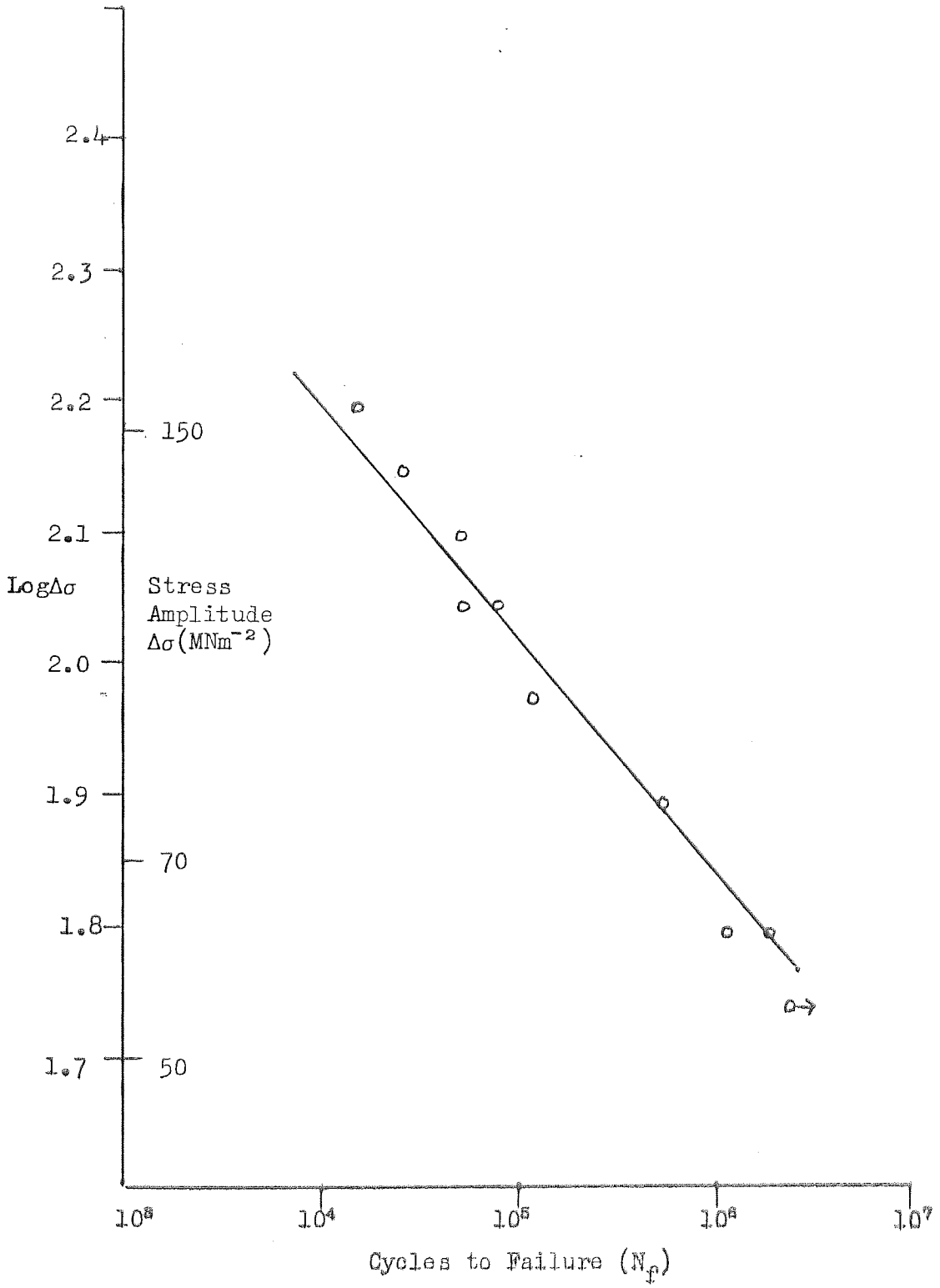

FIGURE 39C Effect of Reinforcement Angle (θ) on Fatigue Strength Tested at Room Temperature after Stress-Relieving at 325°C $100° < \theta < 110°$

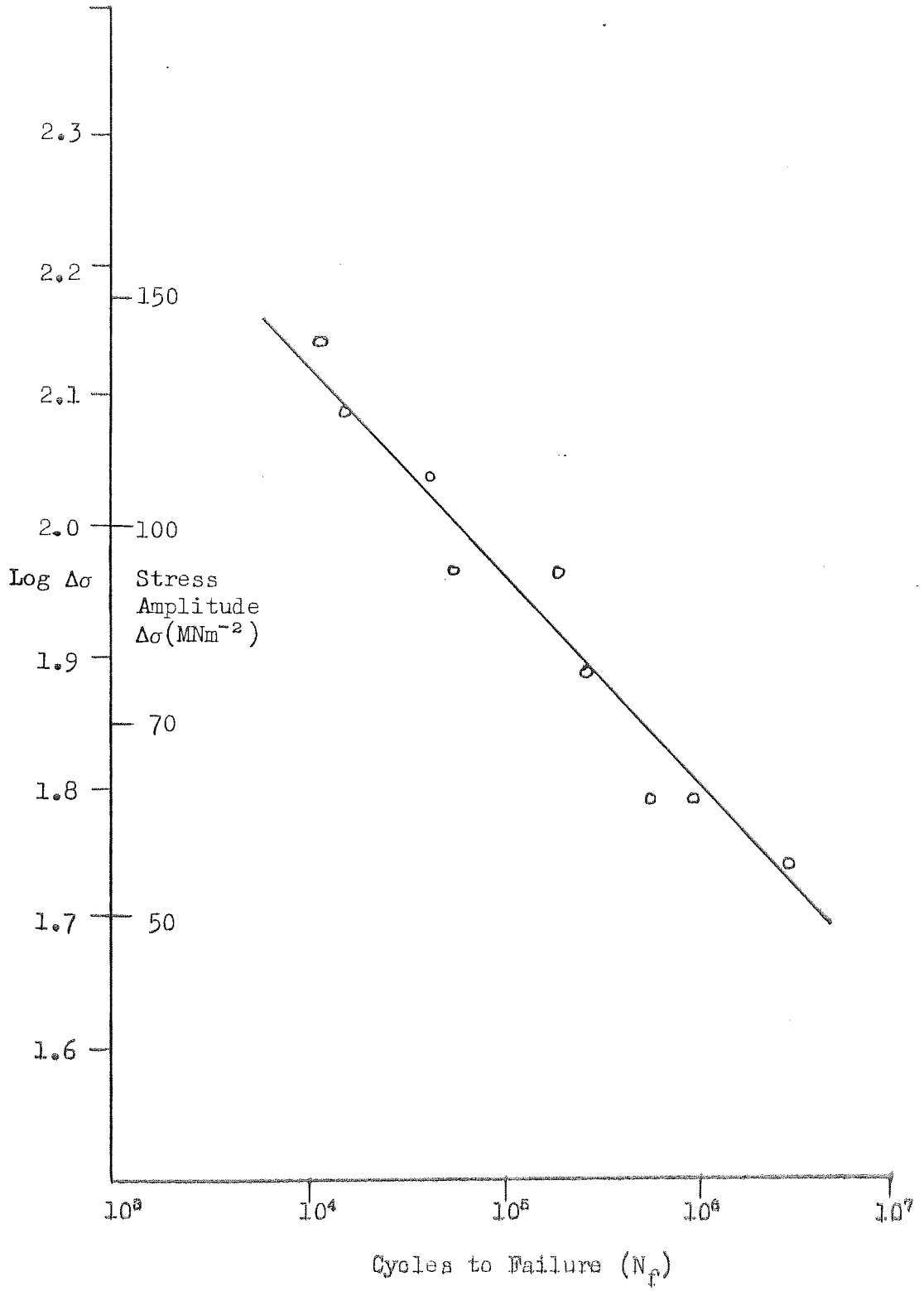

FIGURE 40A Effect of Reinforcement Angle (θ) on Fatigue Strength. Tested at 300°C after Stress-Relieving at 325°C $130° < \theta < 140°$.

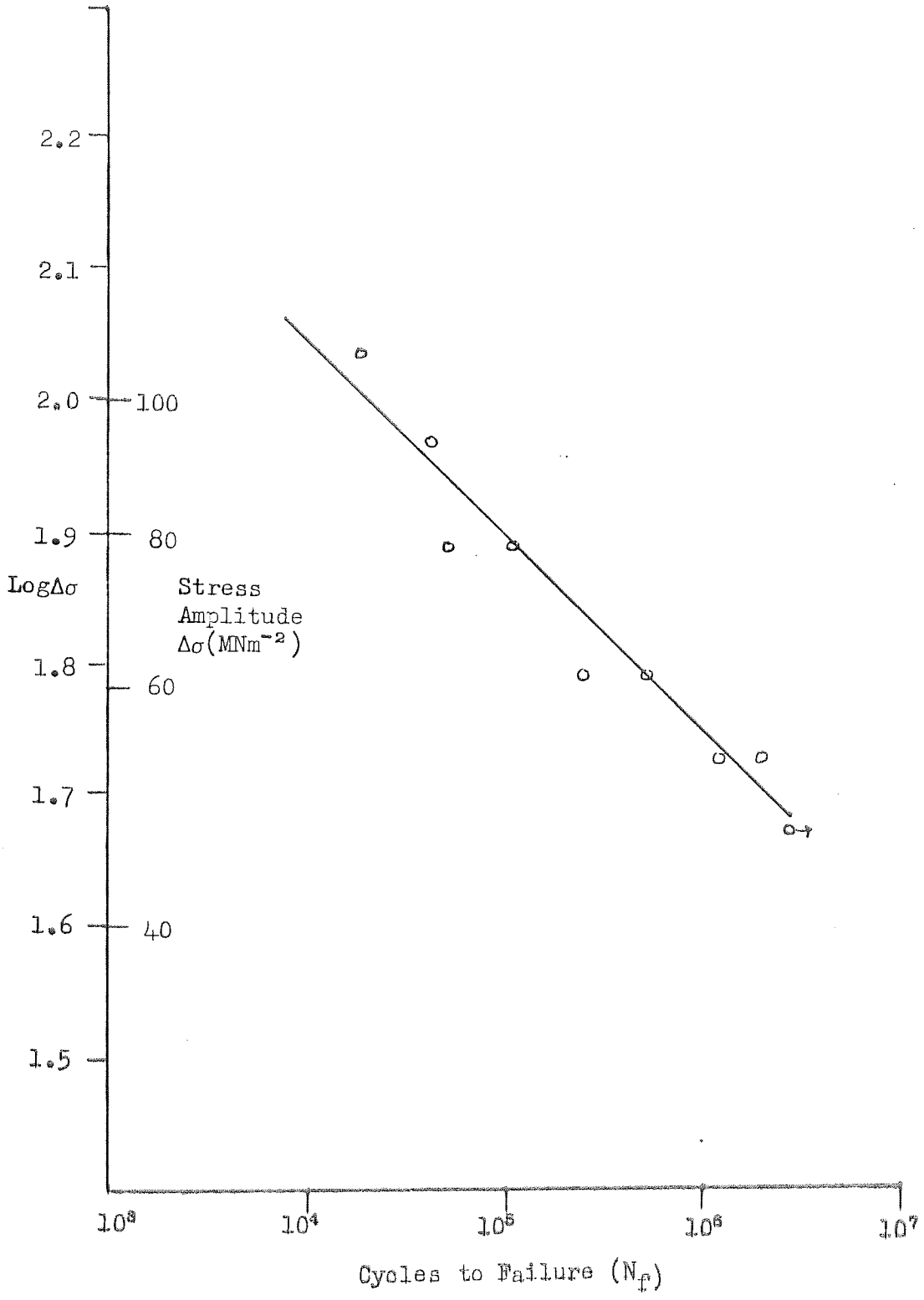

FIGURE 40B. Effect of Reinforcement Angle (θ) on Fatigue Life.
Tested at 300.C after Stress-Relieving at 325°C.
$115° < \theta < 125°$.

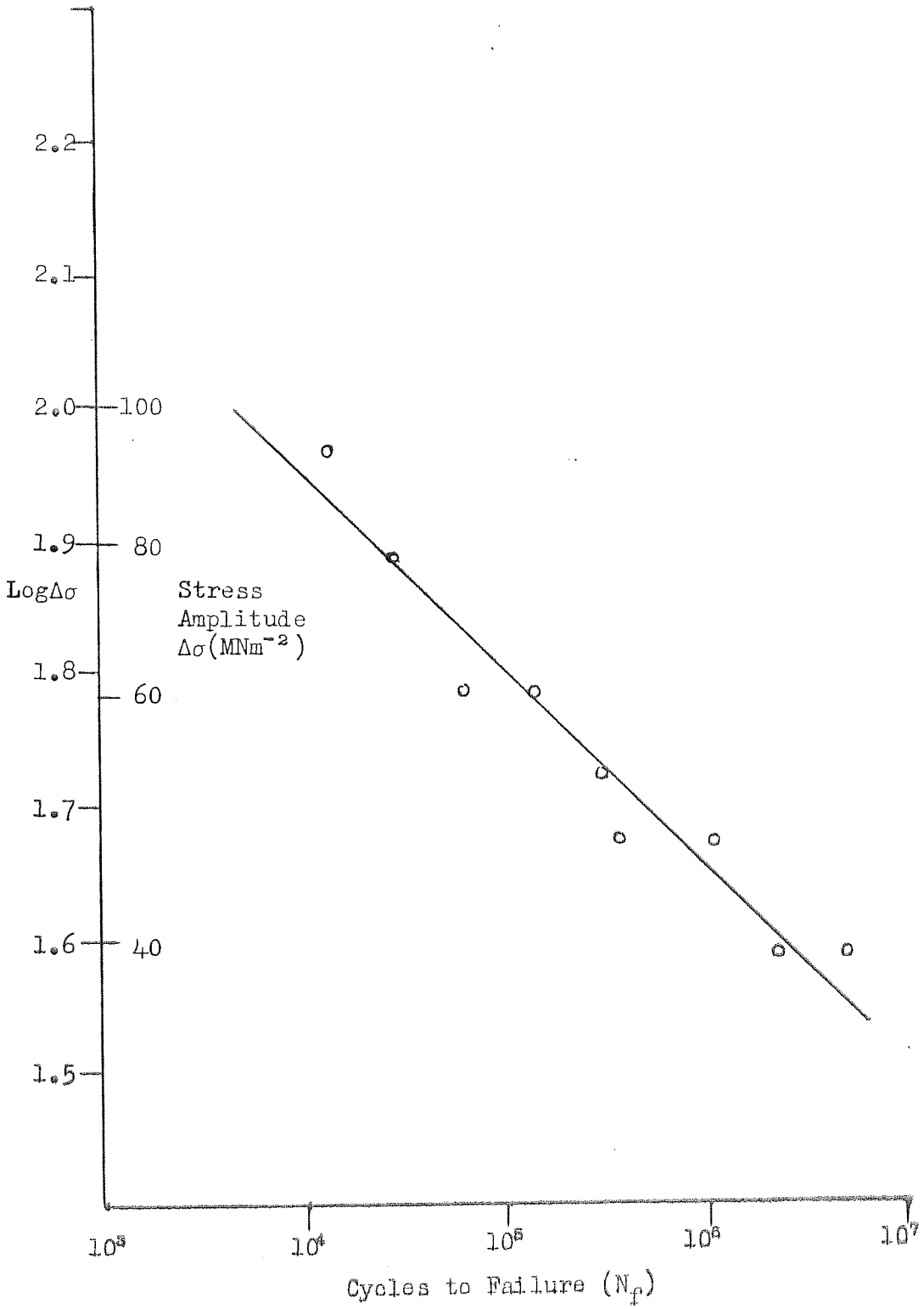

FIGURE 40C. Effect of Reinforcement Angle (θ) on Fatigue Strength. Tested at 300° after Stress-Relieving at 325°C. $100 < \theta < 110°$

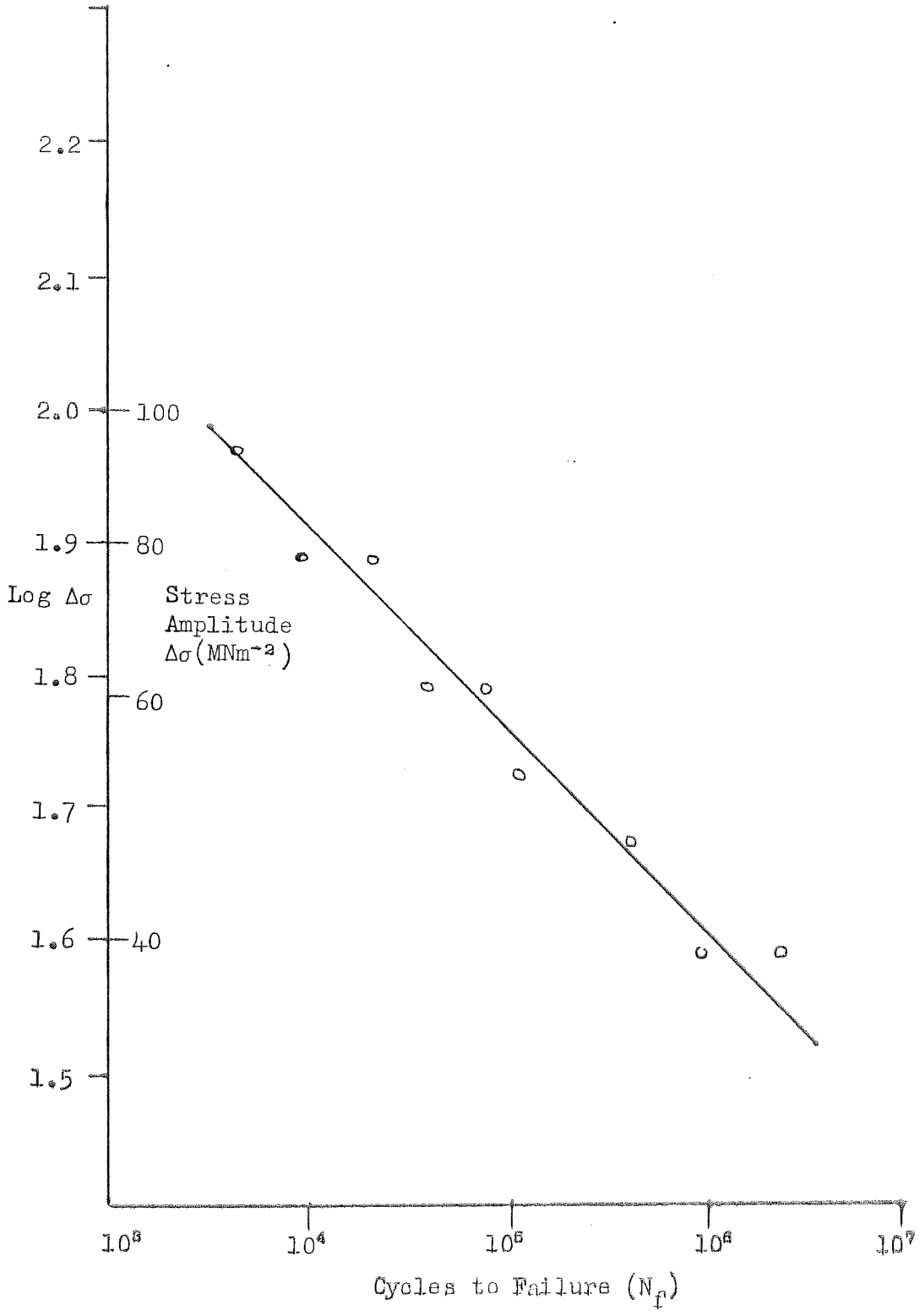

FIGURE 41. The Variables Relevant to the Amplification of Stress at a Symmetrical Projection

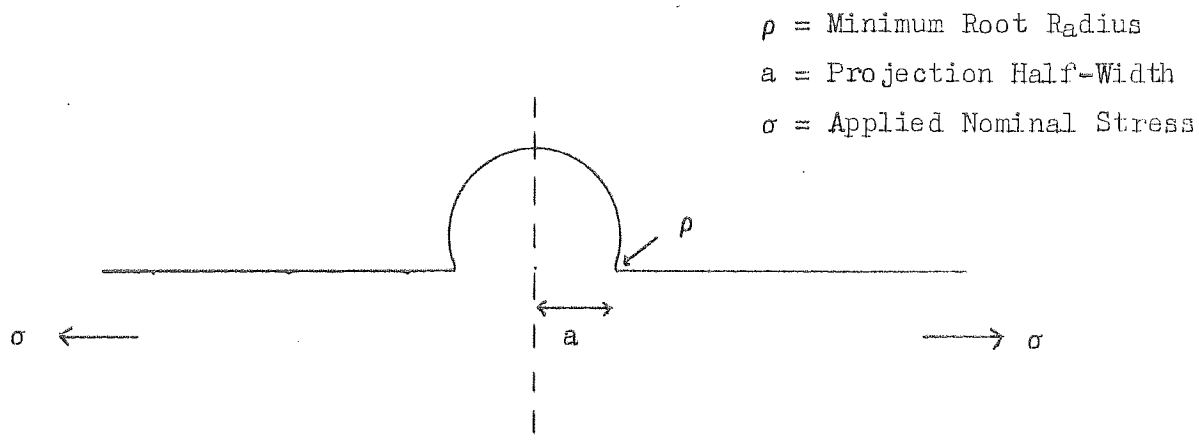

FIGURE 42. Amplification of Stress at the Root of the Projection, for the Configuration shown in Figure 41.

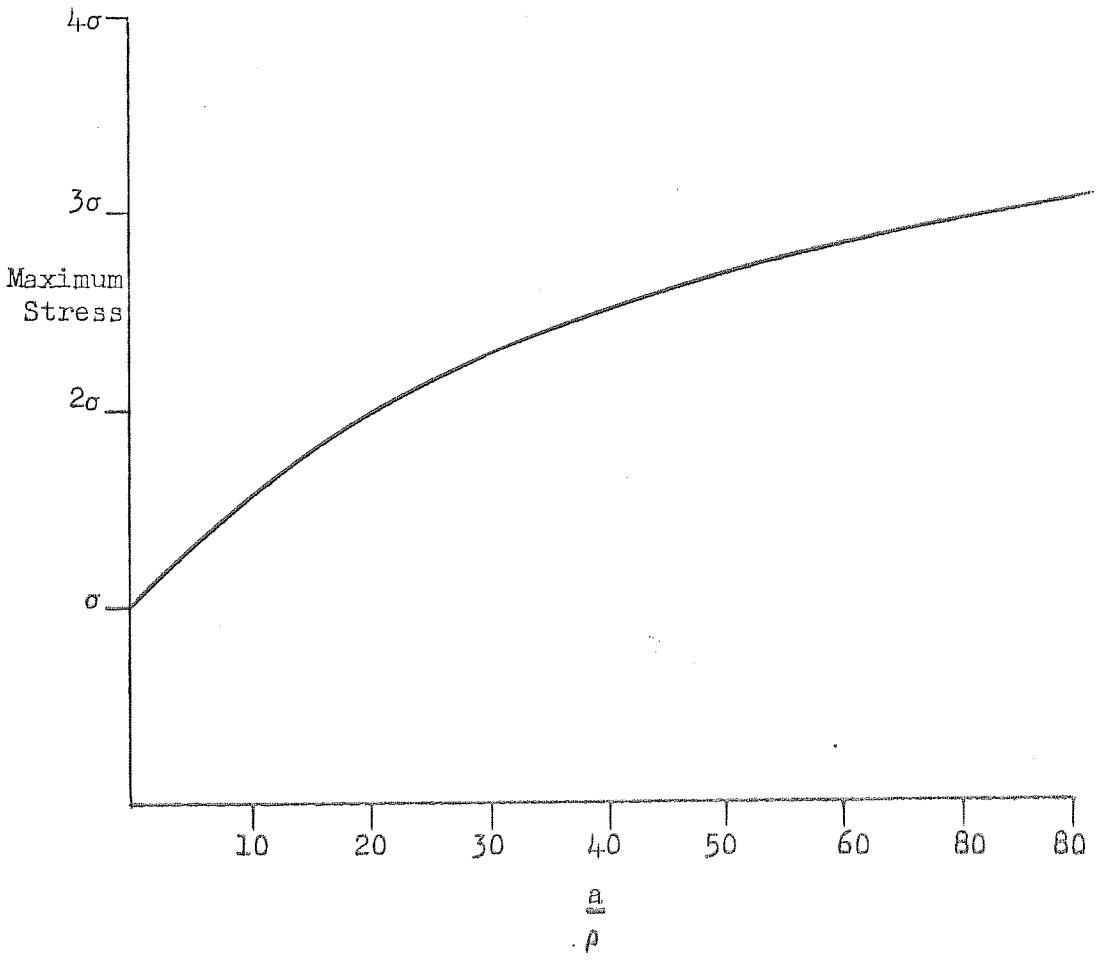

Figure 43. Crack Growth from the Weld Reinforcement.

θ = 140°C. Magnification x 50.

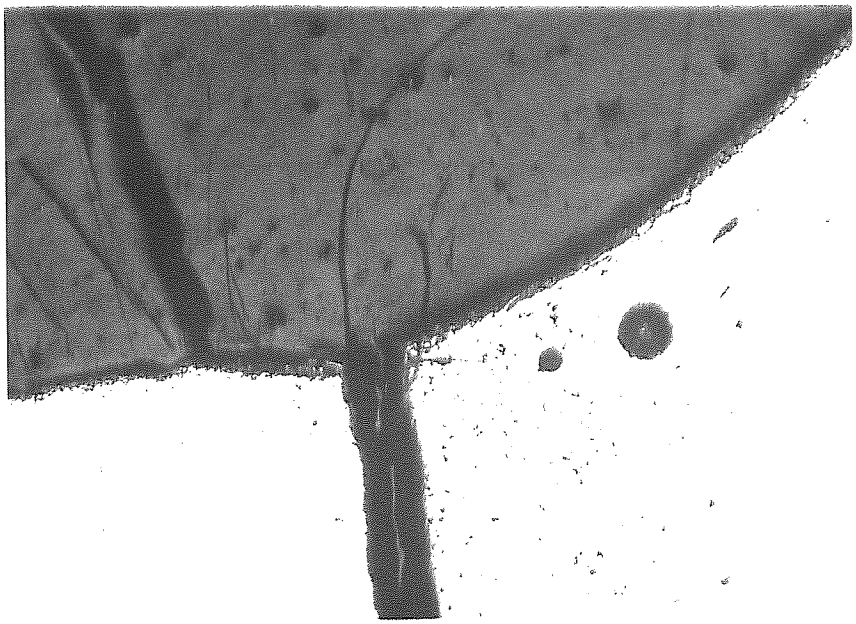

Figure 44. Crack Growth from the Weld Reinforcement.

θ = 125°. Magnification x 50

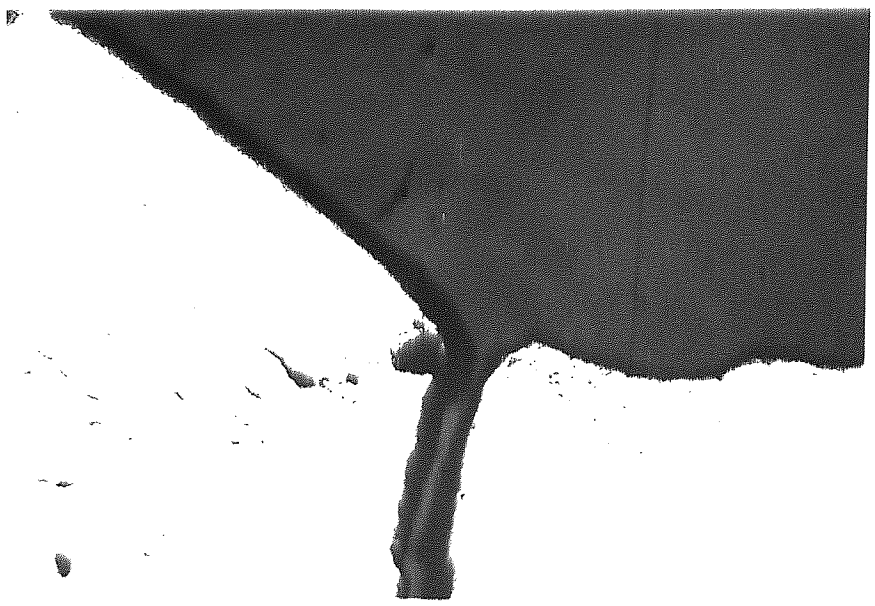

Figure 45. Crack Growth from the Weld Reinforcement

θ = 105°C. Magnification x 50.

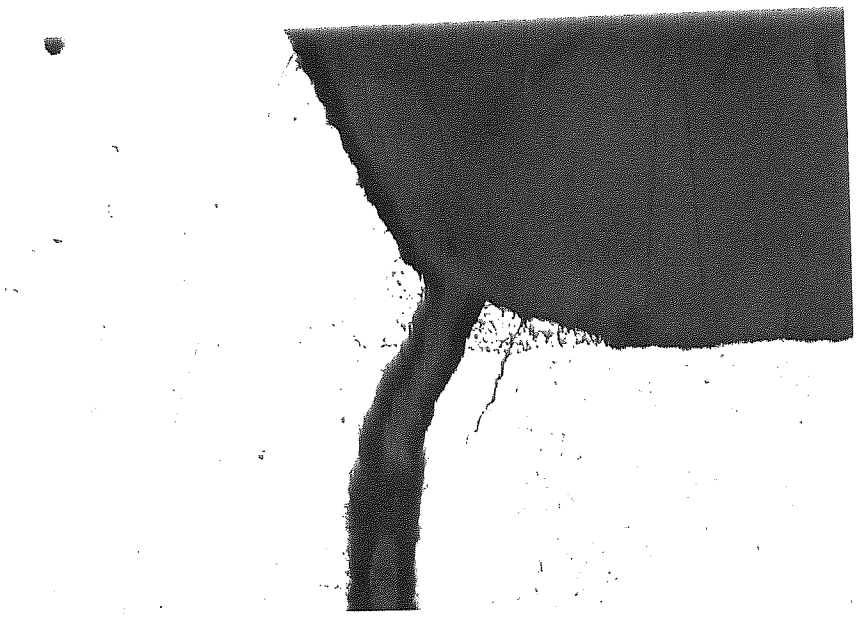

Figure 46. Fracture Surface in a Specimen containing a Central Defect. Magnification x 7.

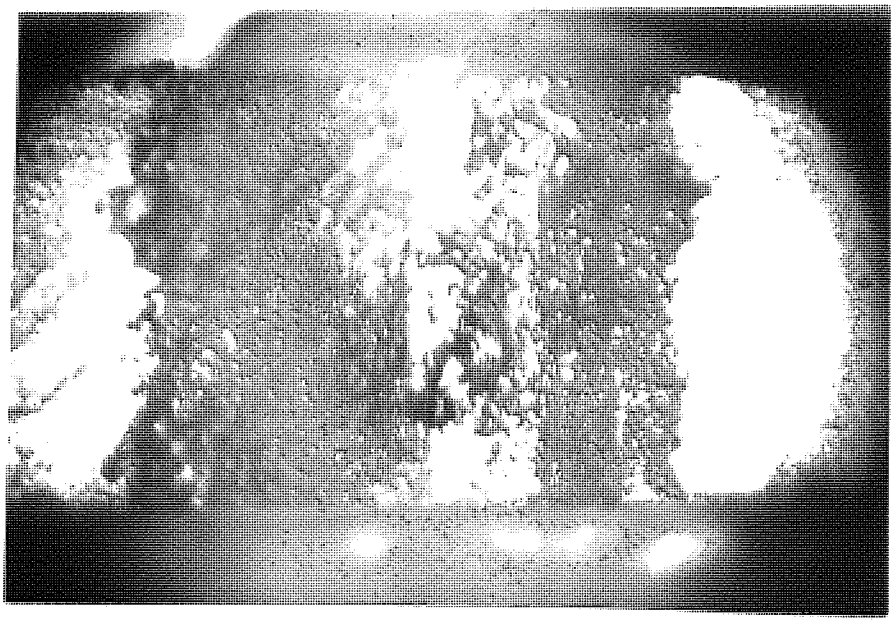

Figure 47. Boundary between Central Defect and Fracture Surface. Magnification x 120.

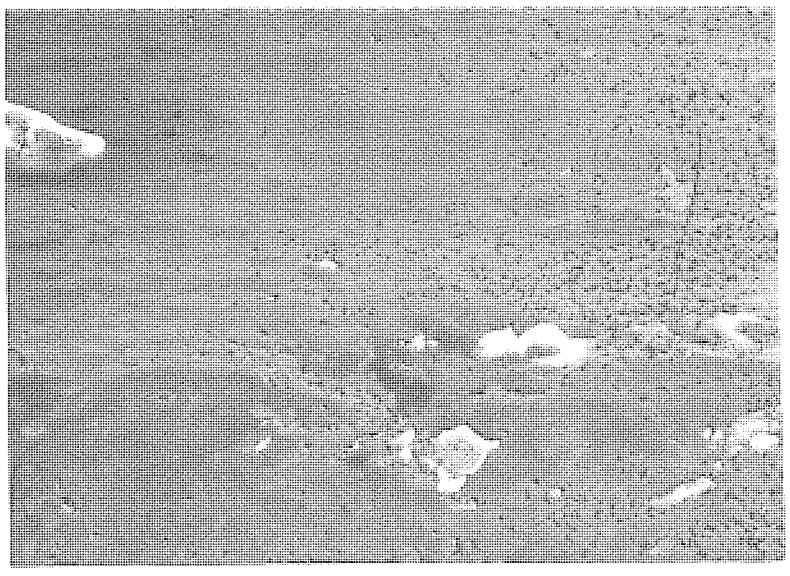

FIGURE 48 K-Callibration Curve for a Centre Cracked Plate under Uniform Tension

$$Y = 1.77\left[1-0.1\left(\frac{2a}{W}\right)+\left(\frac{2a}{W}\right)^2\right]$$

$$= \frac{K_I BW}{P\sqrt{a}}$$

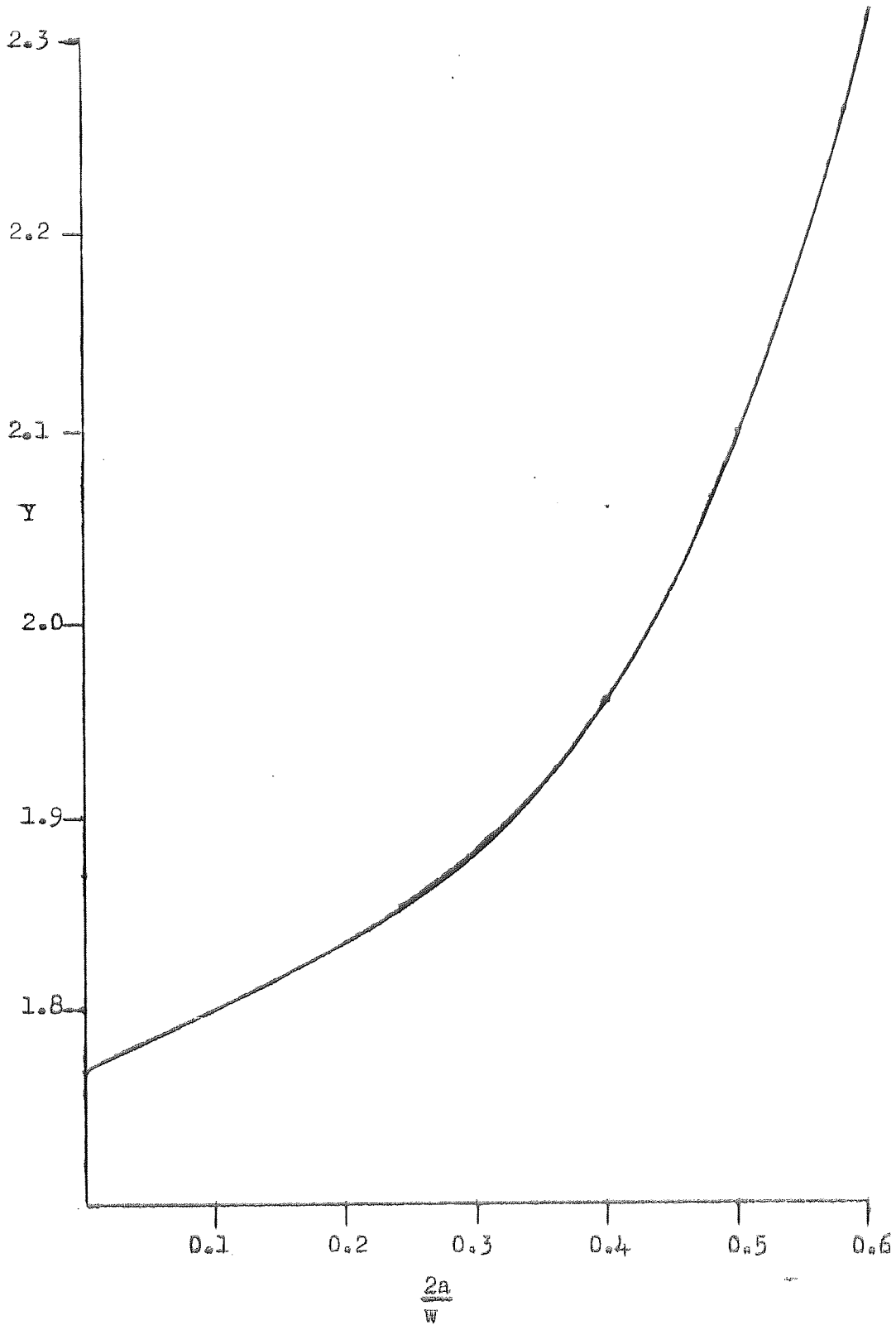

FIGURE 49 Effect of ΔK_o on Crack Initiation from Central Defects Tested at Room Temperature in the As-Welded Condition

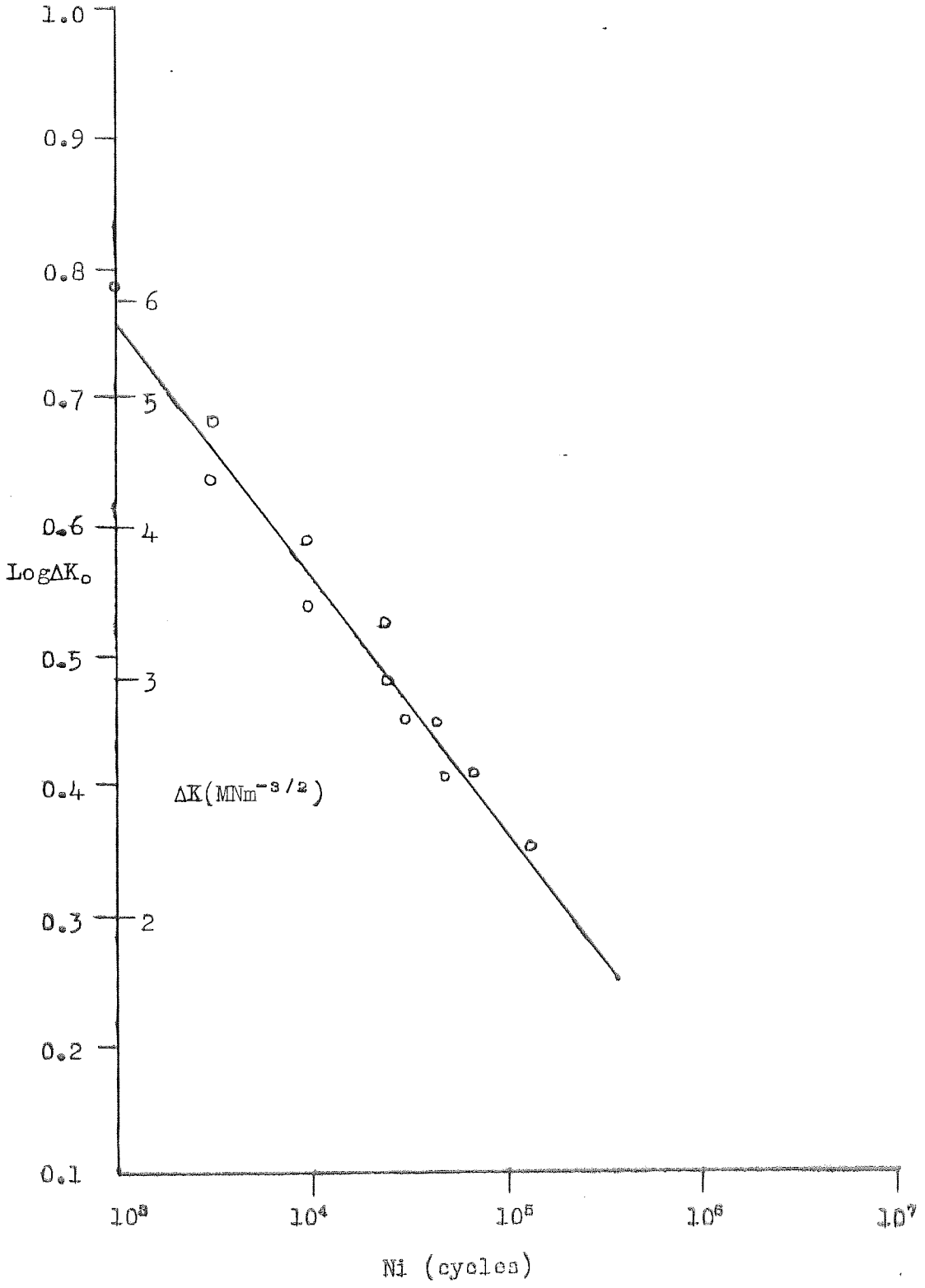

FIGURE 50 Effect of ΔK_o on Crack Initiation from Central Defects.
Tested at Room Temperature after Stress-Relieving at 325°C.

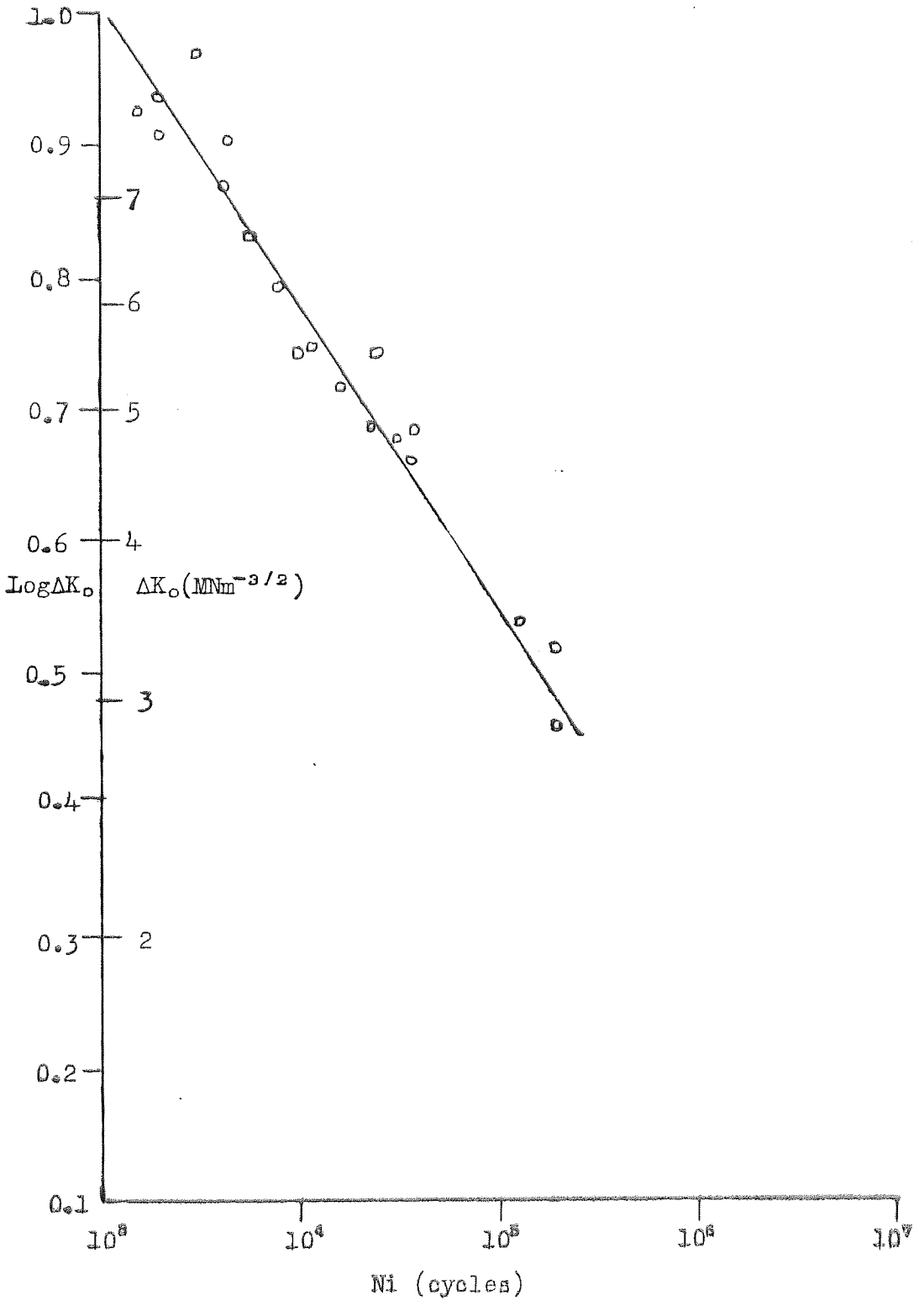

FIGURE 51 Effect of ΔK_o on Crack Initiation from Central Defects Tested at Room Temperature after Stress-Relieving at 450°C.

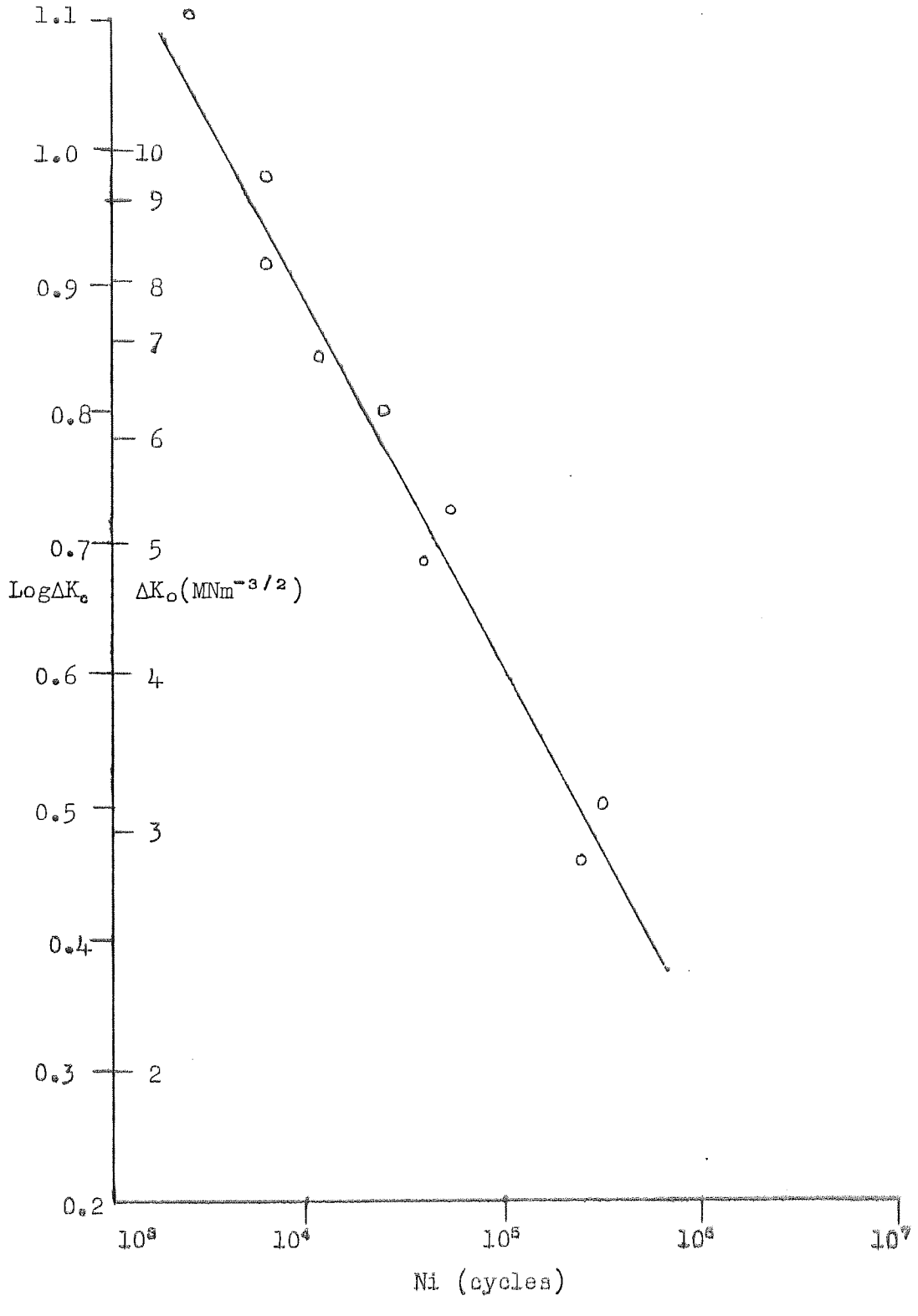

FIGURE 52 Effect of ΔK_o on Crack Initiation from Central Defects Tested at 200°C after Stress-Relieving at 325°C.

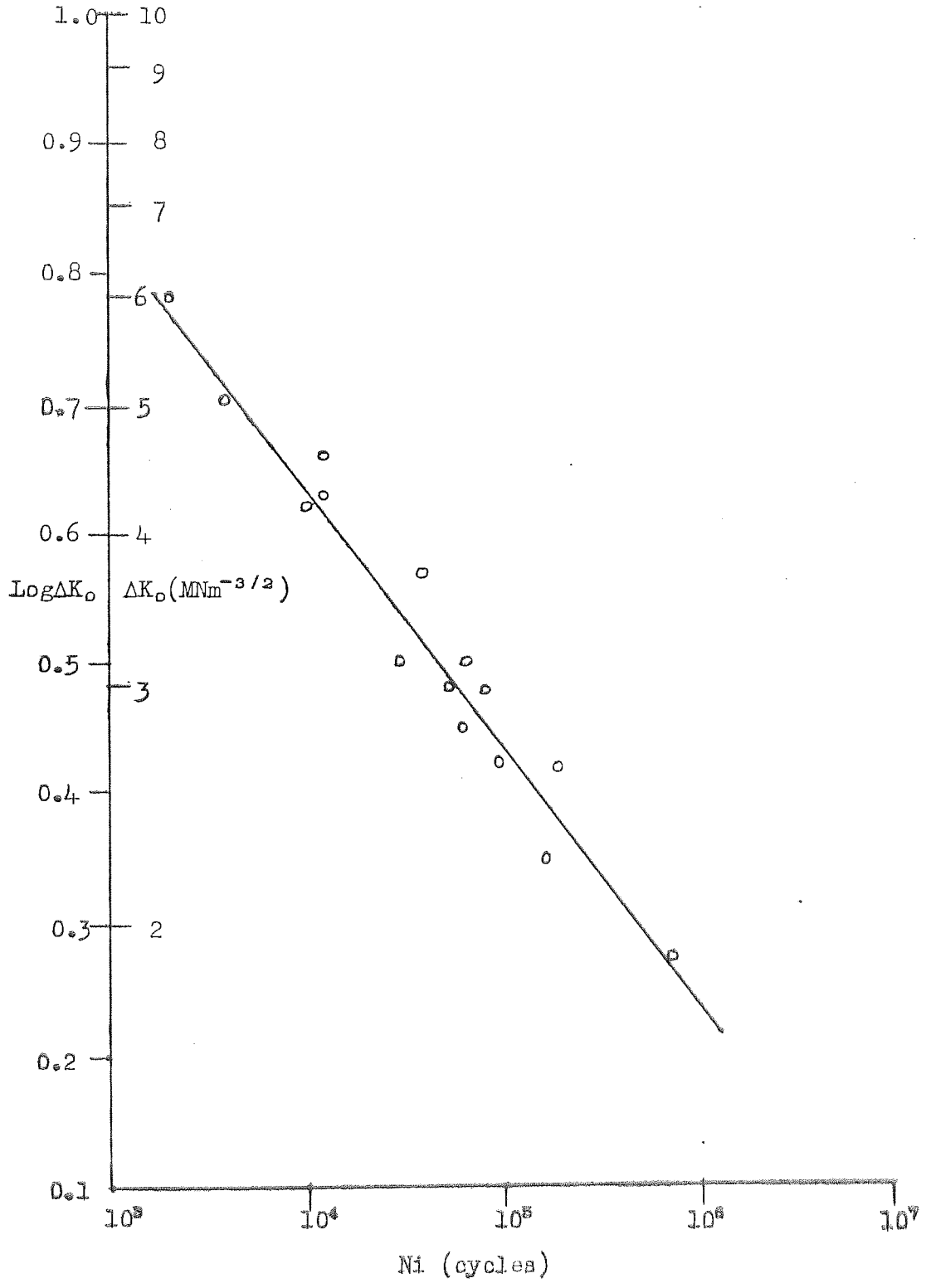

FIGURE 53 Effect of ΔK_o on Cycles to Initiate a Crack from Central Defects. Tested at 300°C after Stress-Relieving at 325°C.

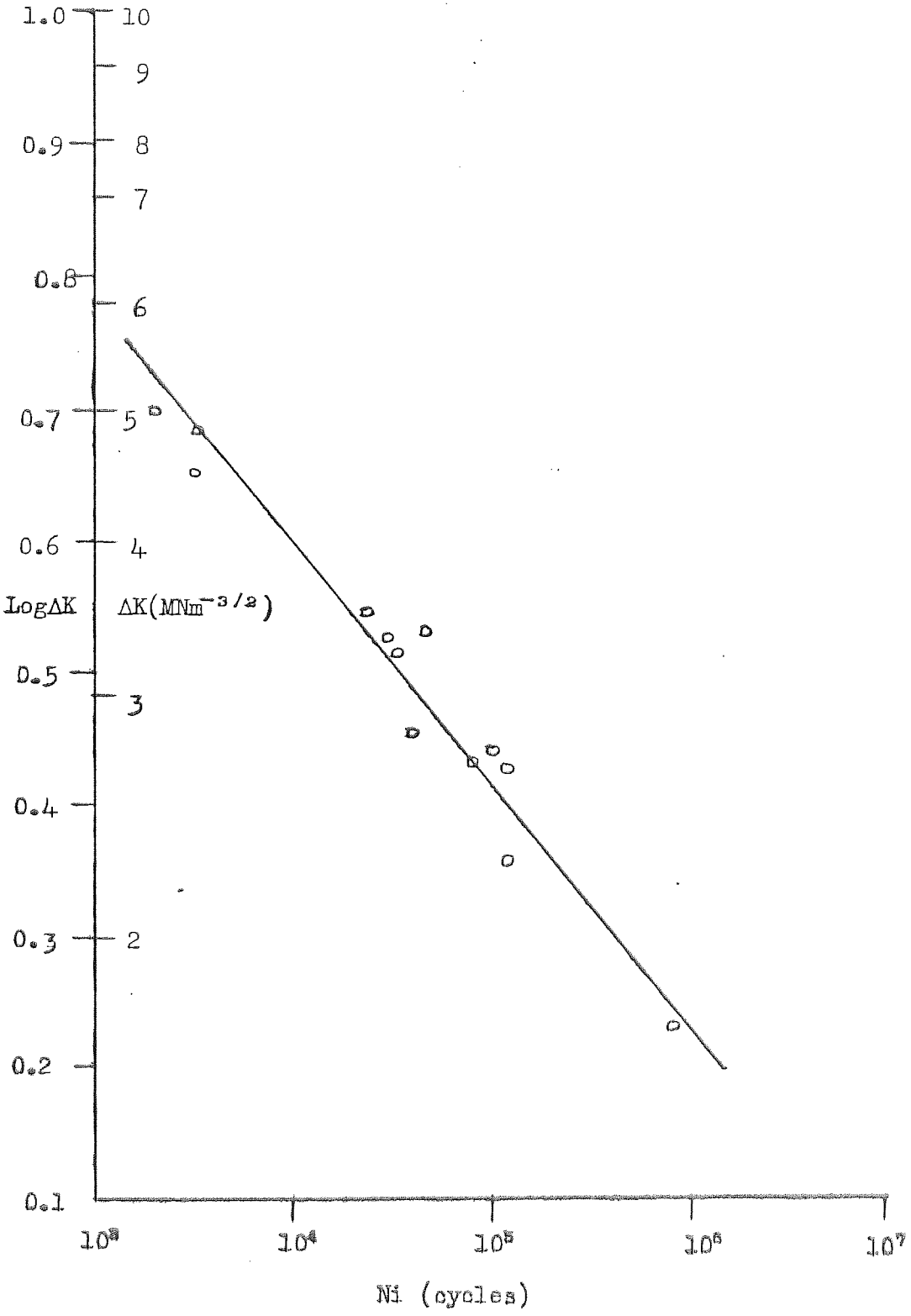

FIGURE 54 Effect of ΔK_o on Cycles to Inititate a crack from Central Defects Tested at 300°C after Stress-Relieving at 325°C.

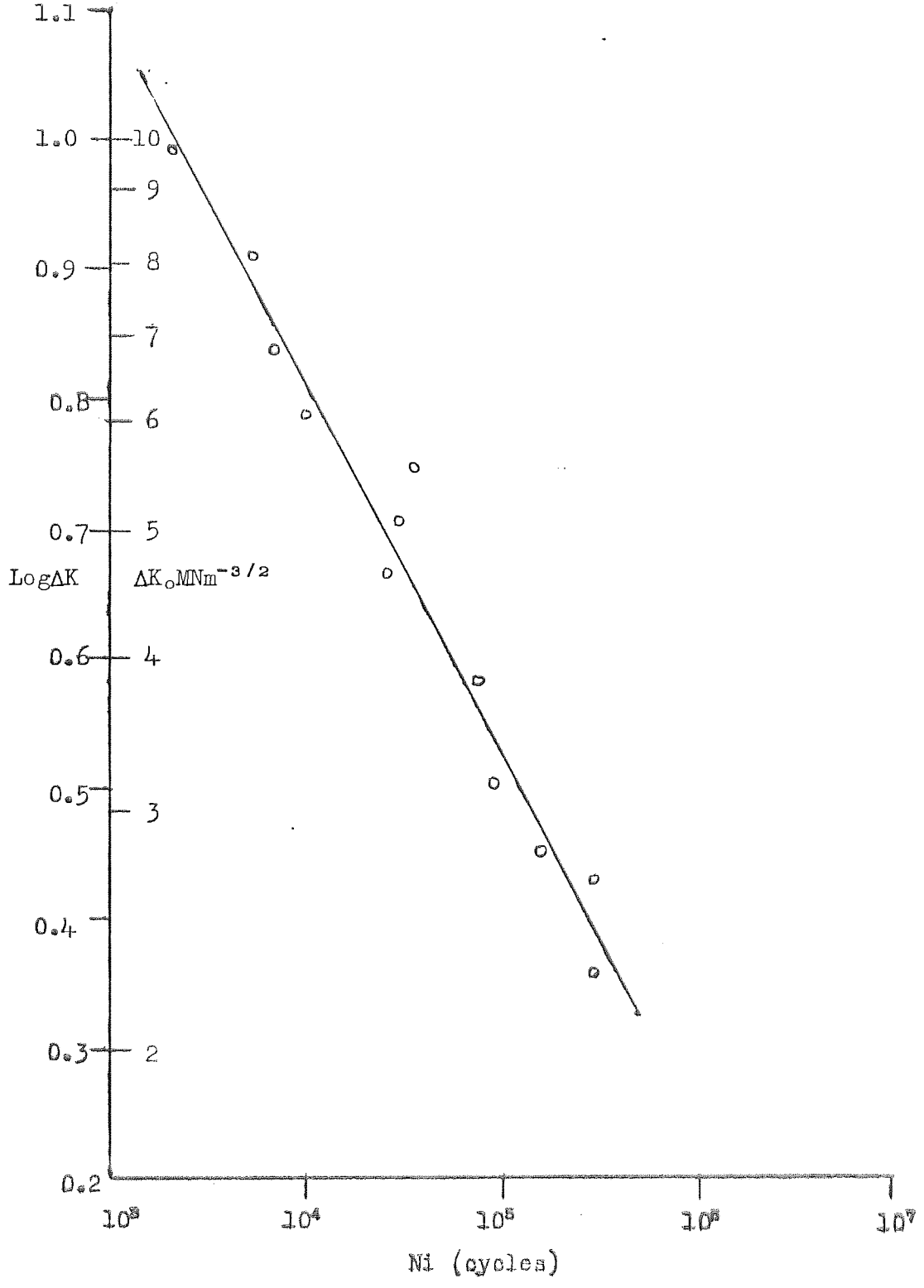

FIGURE 55 Effect of $K_f'\Delta\sigma$ on Crack Initiation from Central Defects Tested at Room Temperature after Stress-Relieving at 325°C.

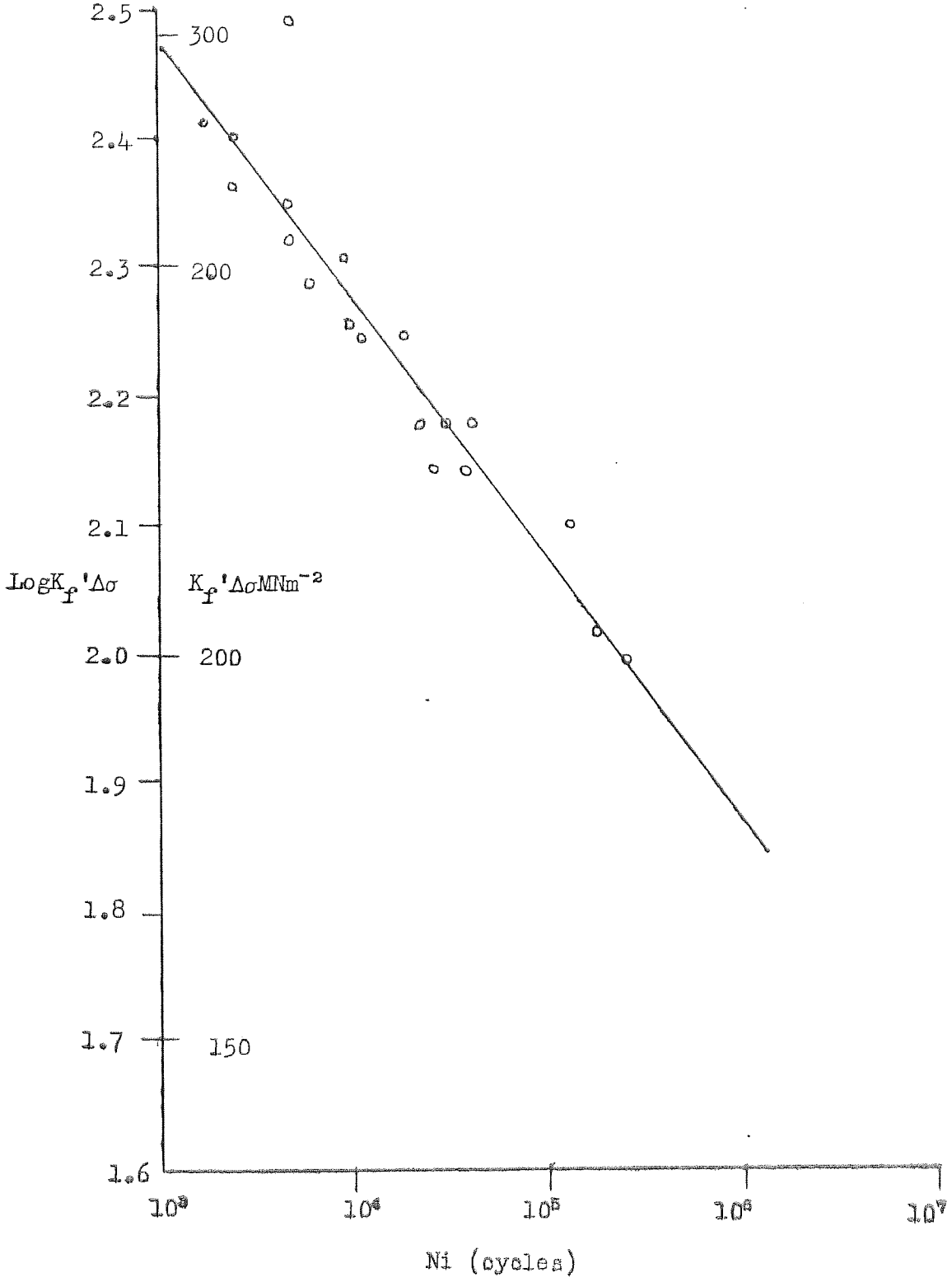

FIGURE 56 Effect of $K_f'\Delta\sigma$ on Crack Initiation from Central Defects Tested at 200°C after Stress-Relieving at 325°C.

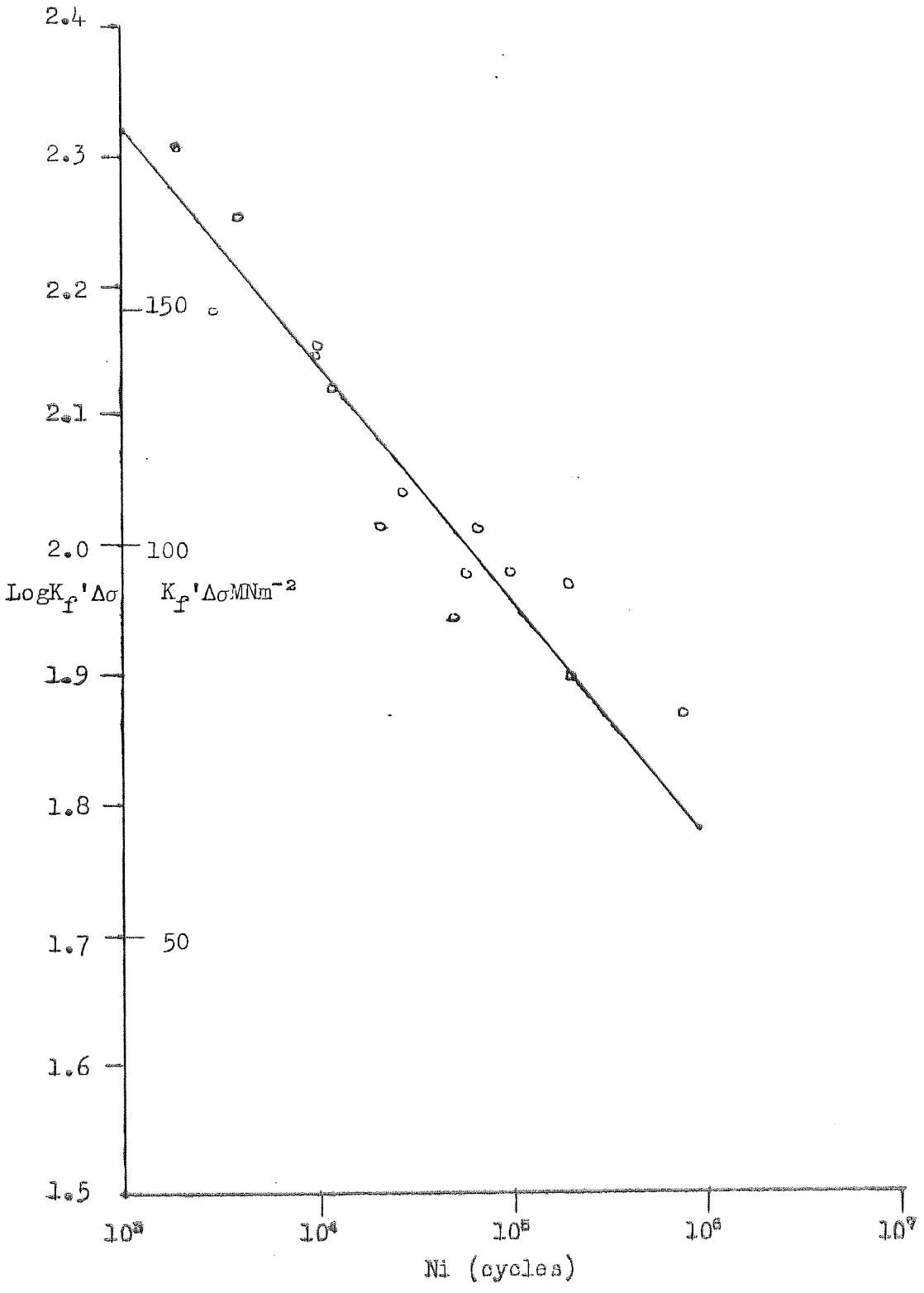

FIGURE 57 Effect of $K_f'\Delta\sigma$ on Crack Initiation from Central Defects Tested at 300°C after Stress-Relieving at 325°C.

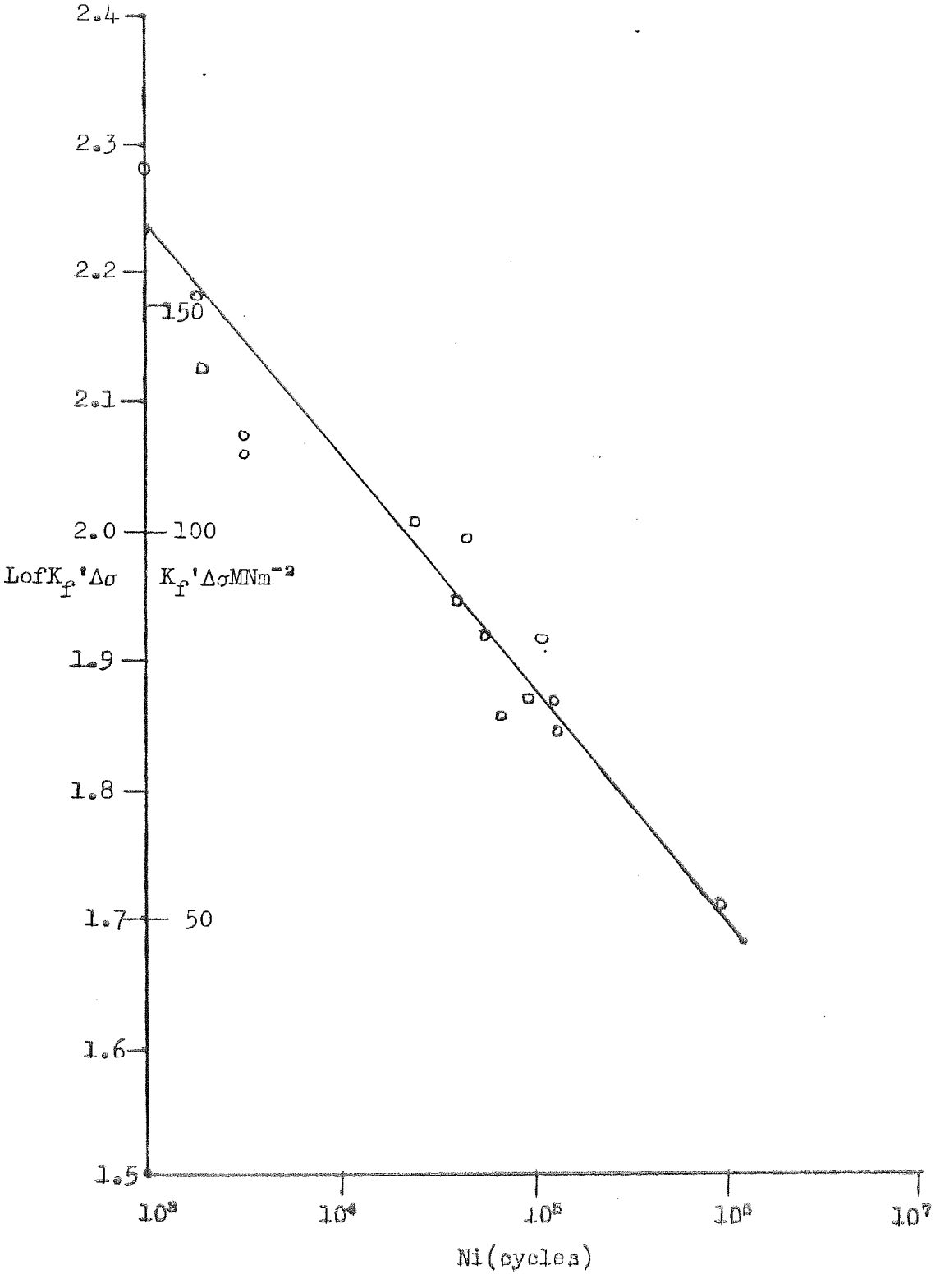

Figure 58. 'Intrusion' type Defect at the Reinforcement Root. Magnification x 75.

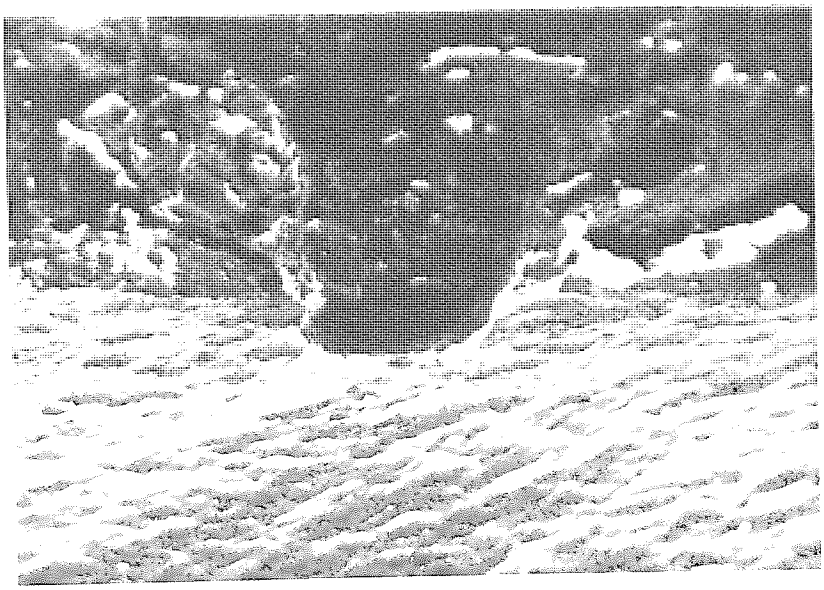

Figure 59. 'Inclusion' type Defect at the Reinforcement Root. Magnification x 75.

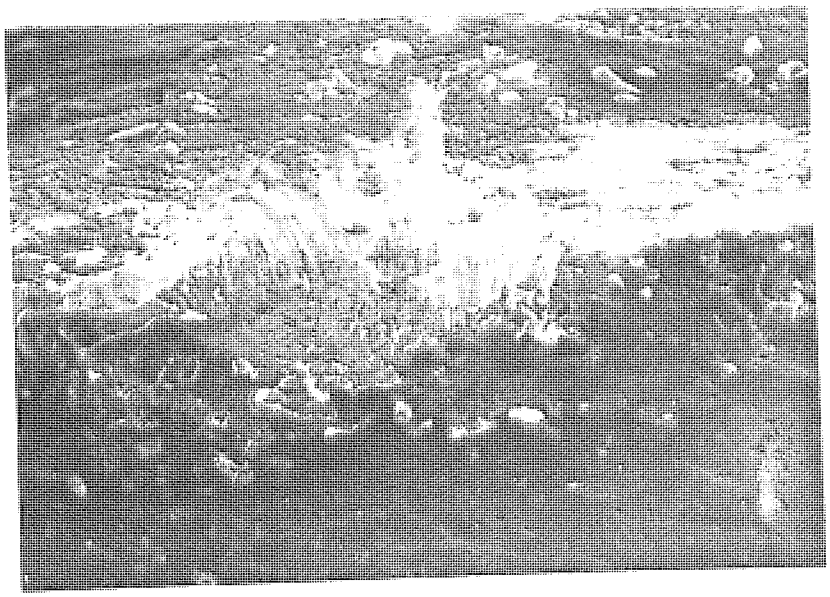

Figure 60. Pore Defect at the Reinforcement Root.

Magnification x 75.

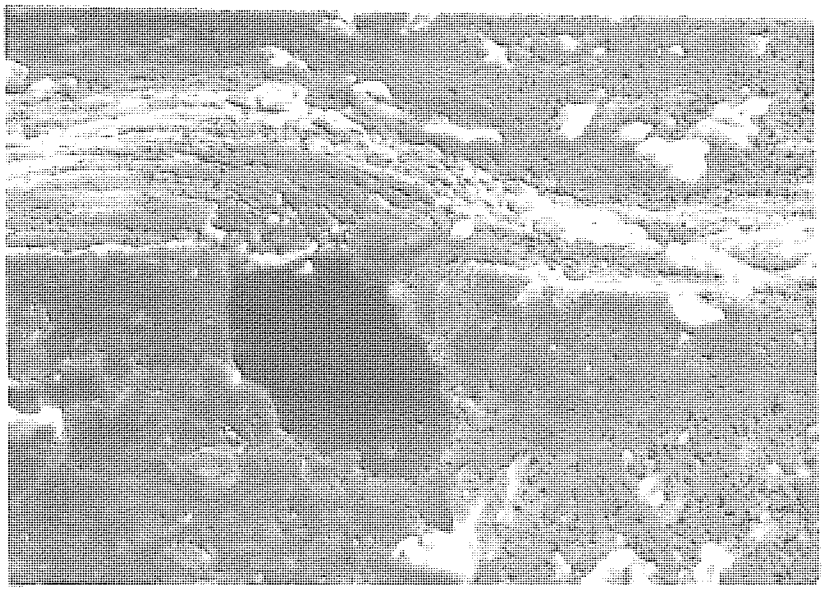

FIGURE 61 Stress Intensity Magnification, Mk, Resulting from the Reinforcement Stress Concentration.

1. $\theta = 105°$ (Estimated) (166)
2. $\theta = 120°$
3. $\theta = 135°$
4. $\theta = 150°$

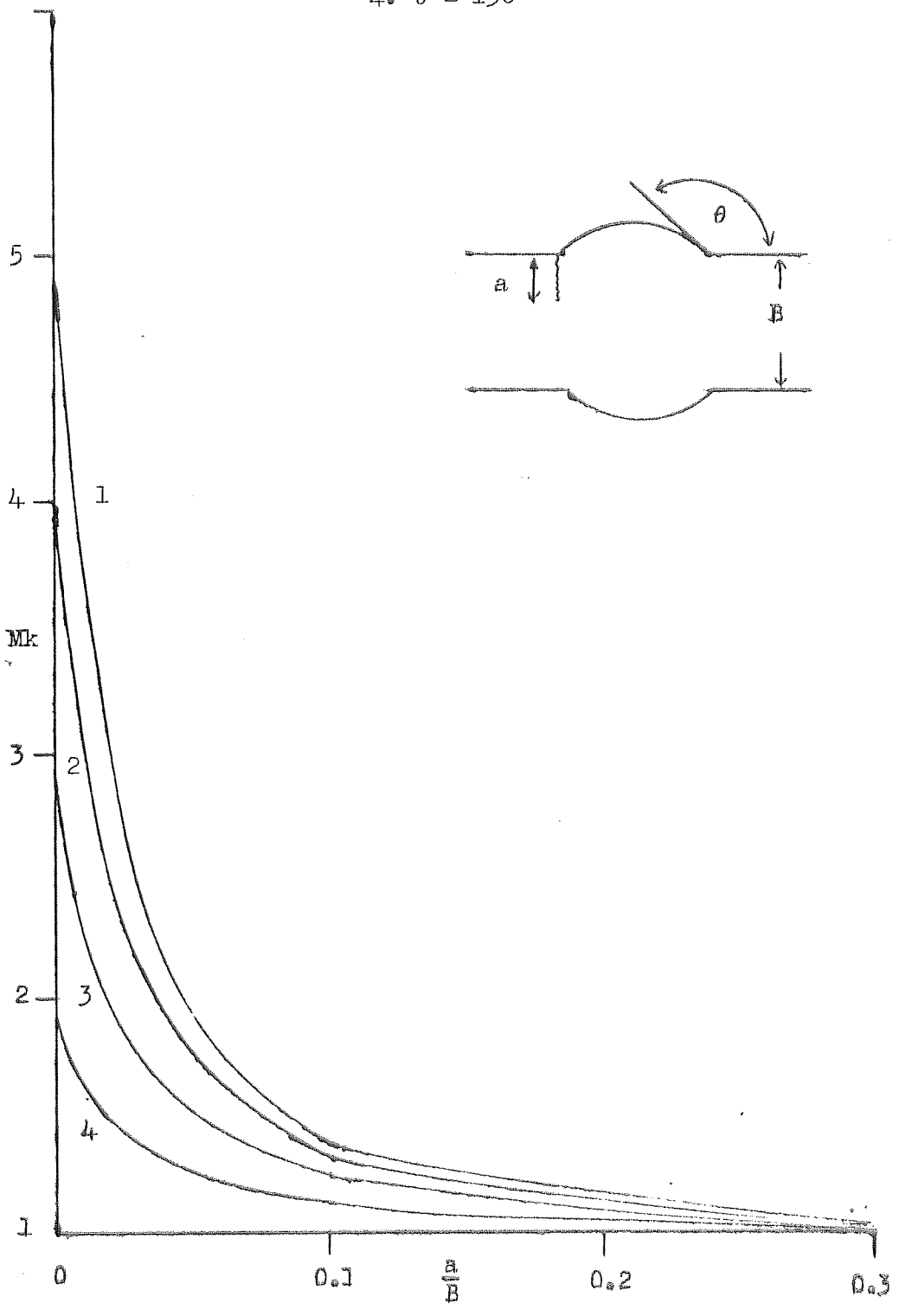

FIGURE 62 Stress Intensity Correction Term, $\frac{MsMt}{\Phi_o}$, as a Function of Crack Depth

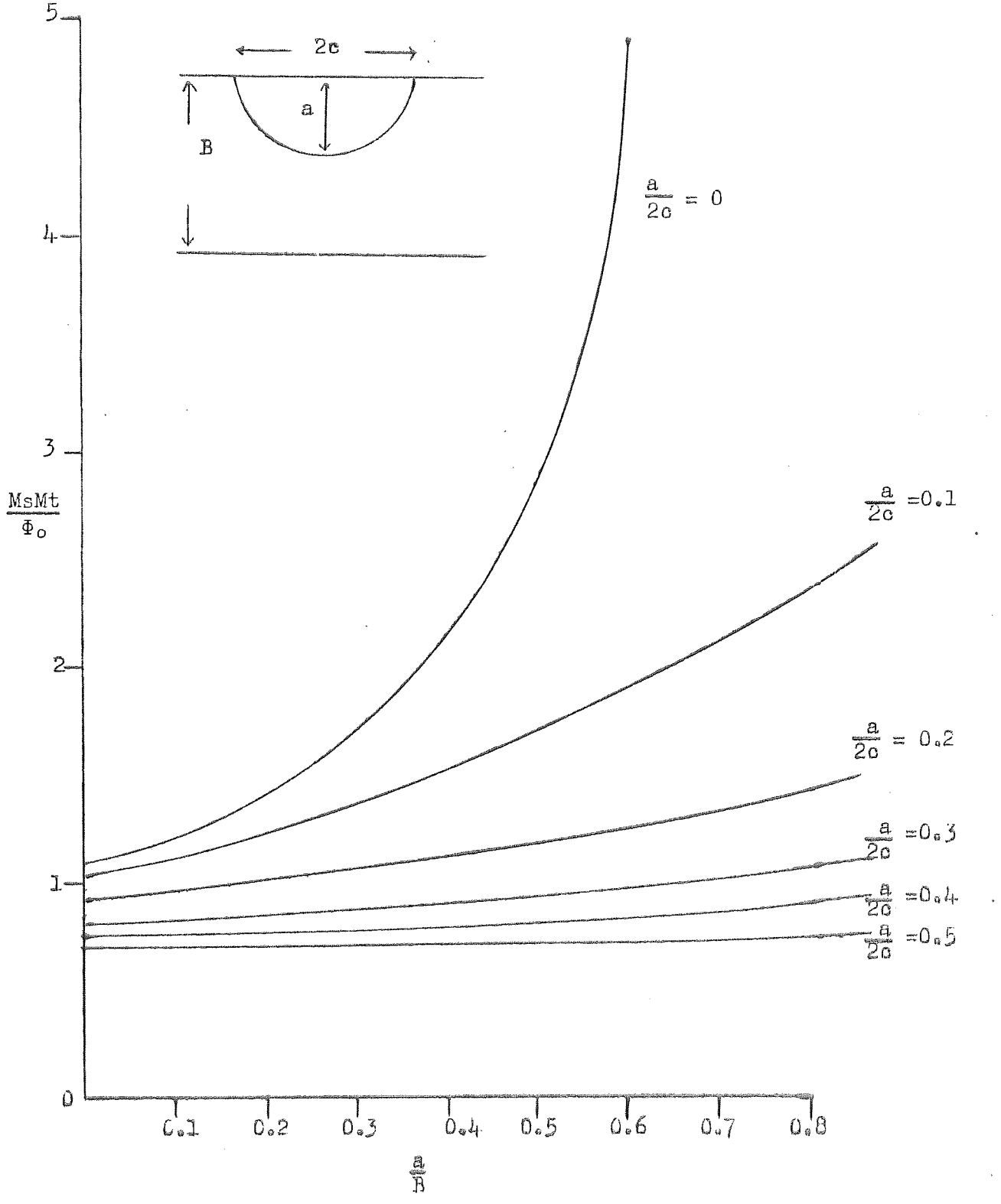

FIGURE 63 Effect of ΔK on Crack Initiation from Reinforcement Defects Tested at Room Temperature after Stress-Relieving at 325°C.

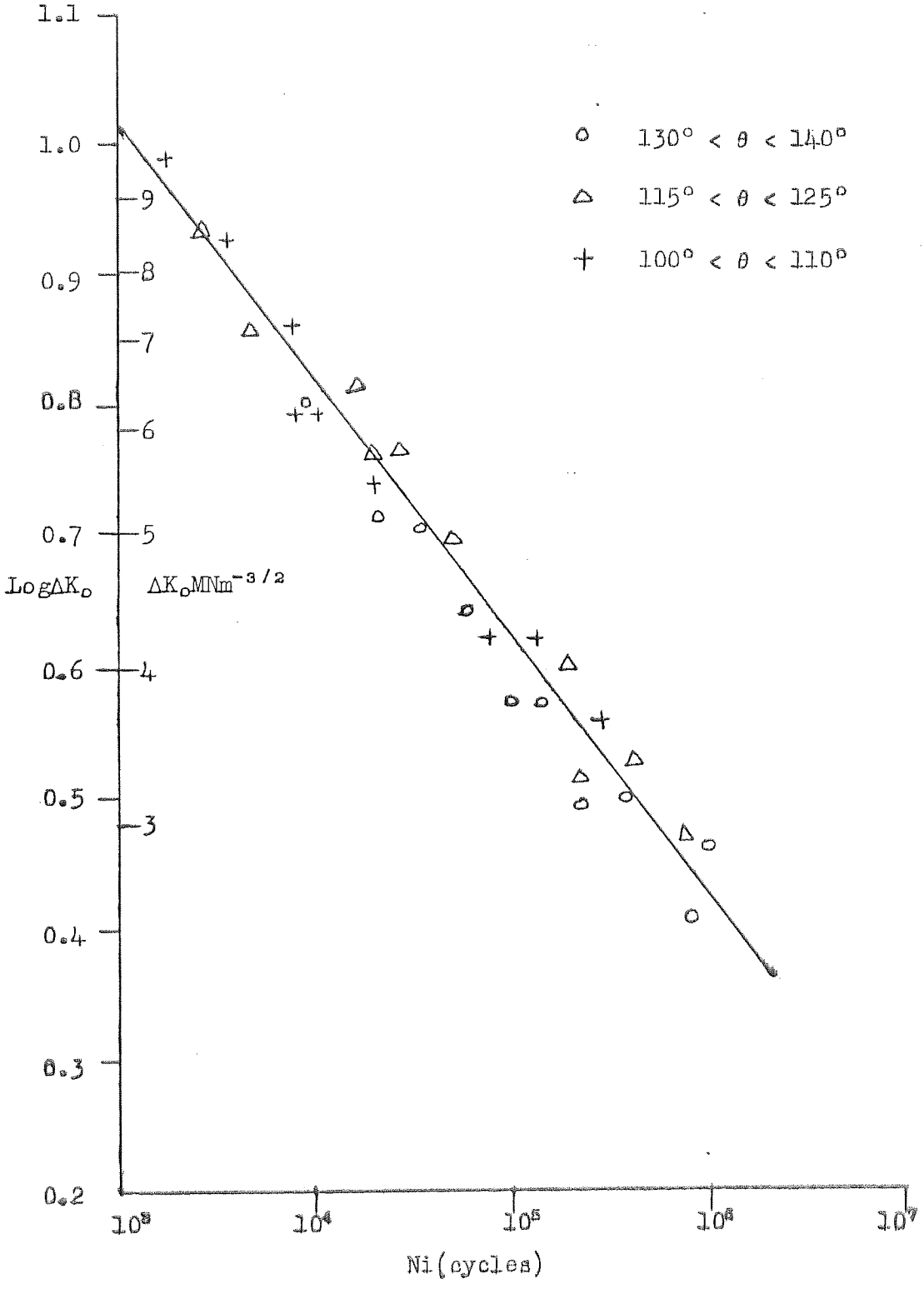

FIGURE 64 Effect of $K_t\Delta\sigma$ on Crack Initiation from Reinforcement Defects Tested at Room Temperature after Stress-Relieving at 325°C.

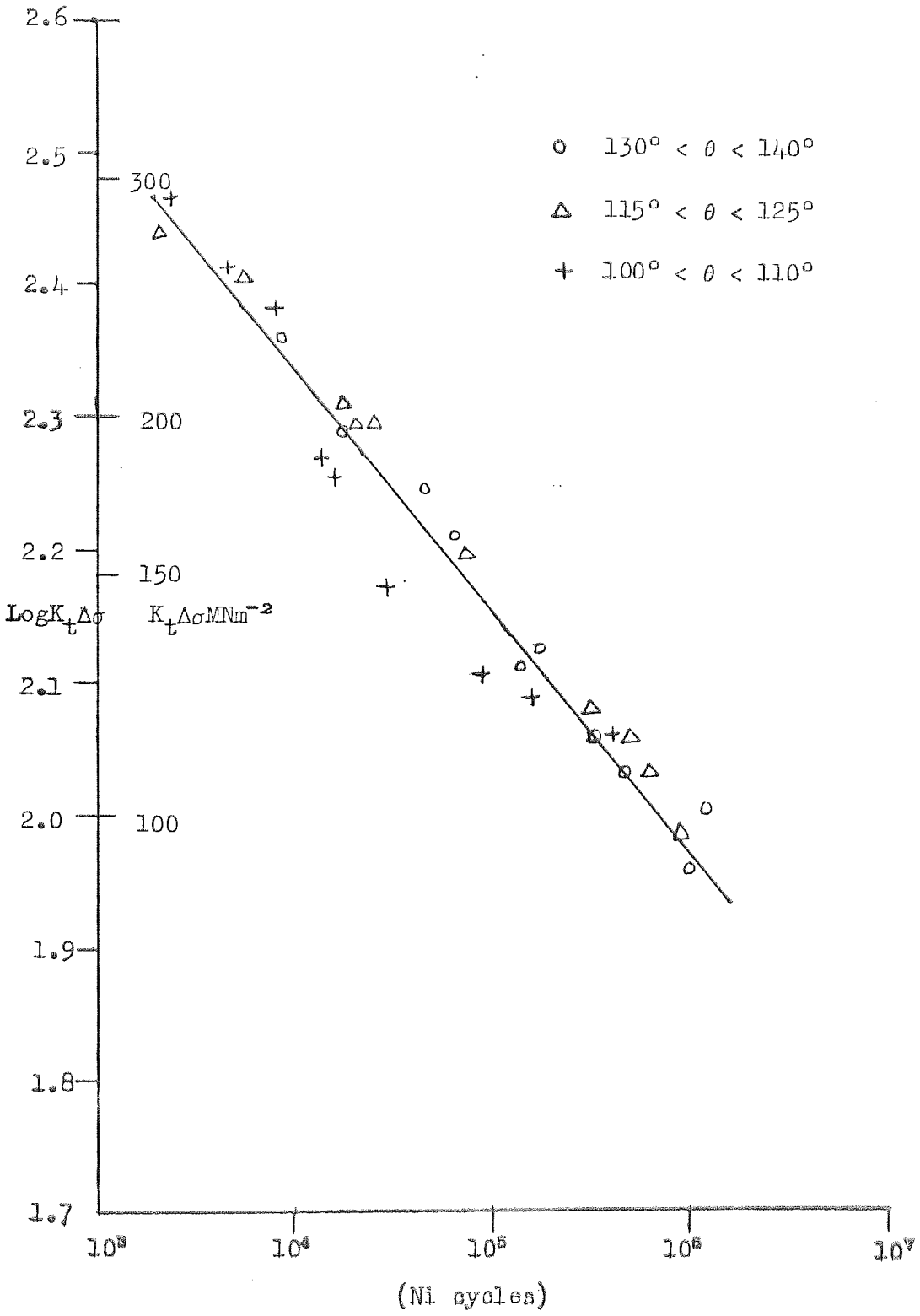

FIGURE 65 Effects of ΔK_o on Crack Initiation from Reinforcement Defects Tested at 300°C after Stress-Relieving at 325°C

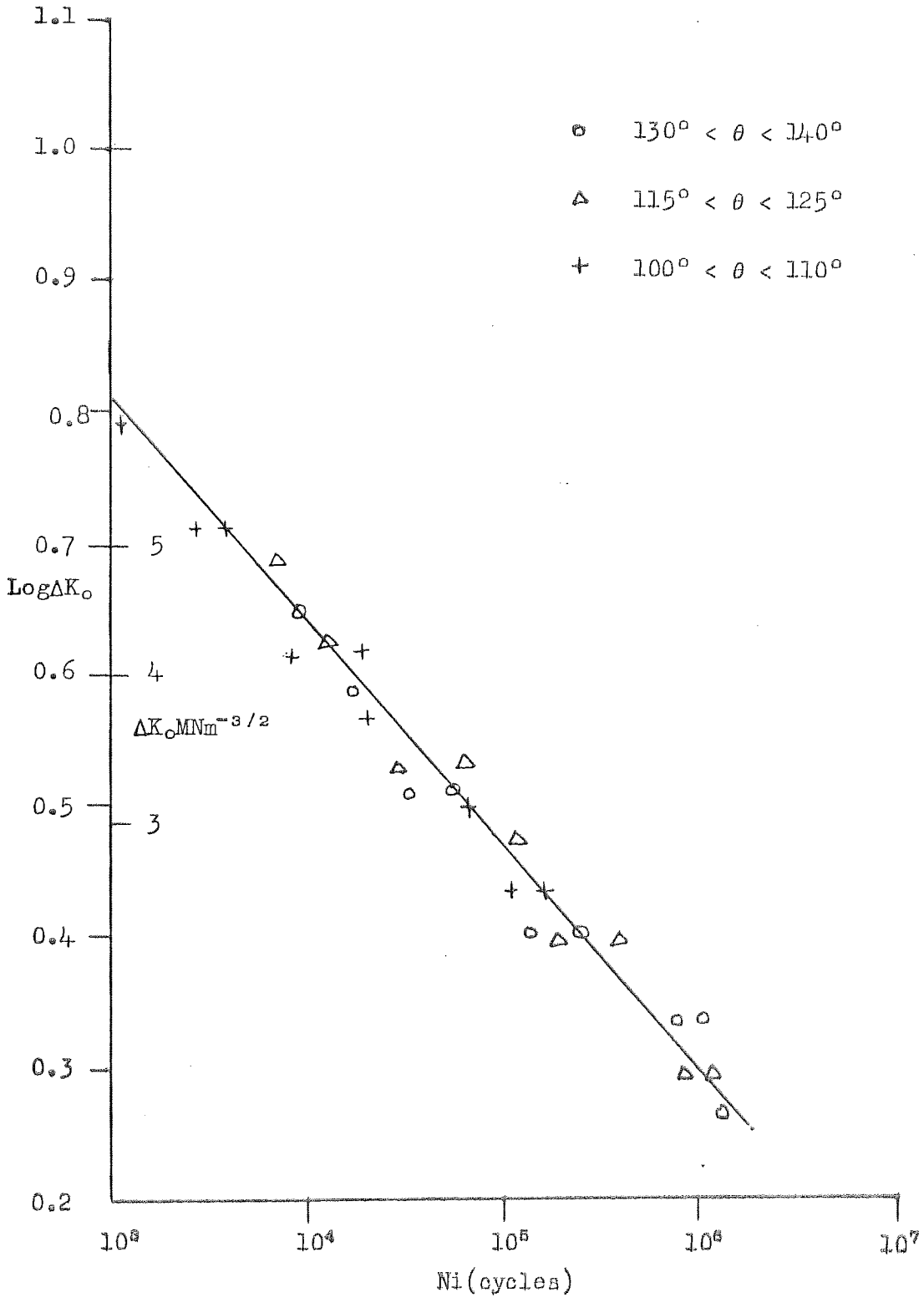

FIGURE 66 Effect of $K_t\Delta\sigma$ on Crack Initiation from Reinforcement Defects Tested at 300°C after Stress-Relieving at 325°C.

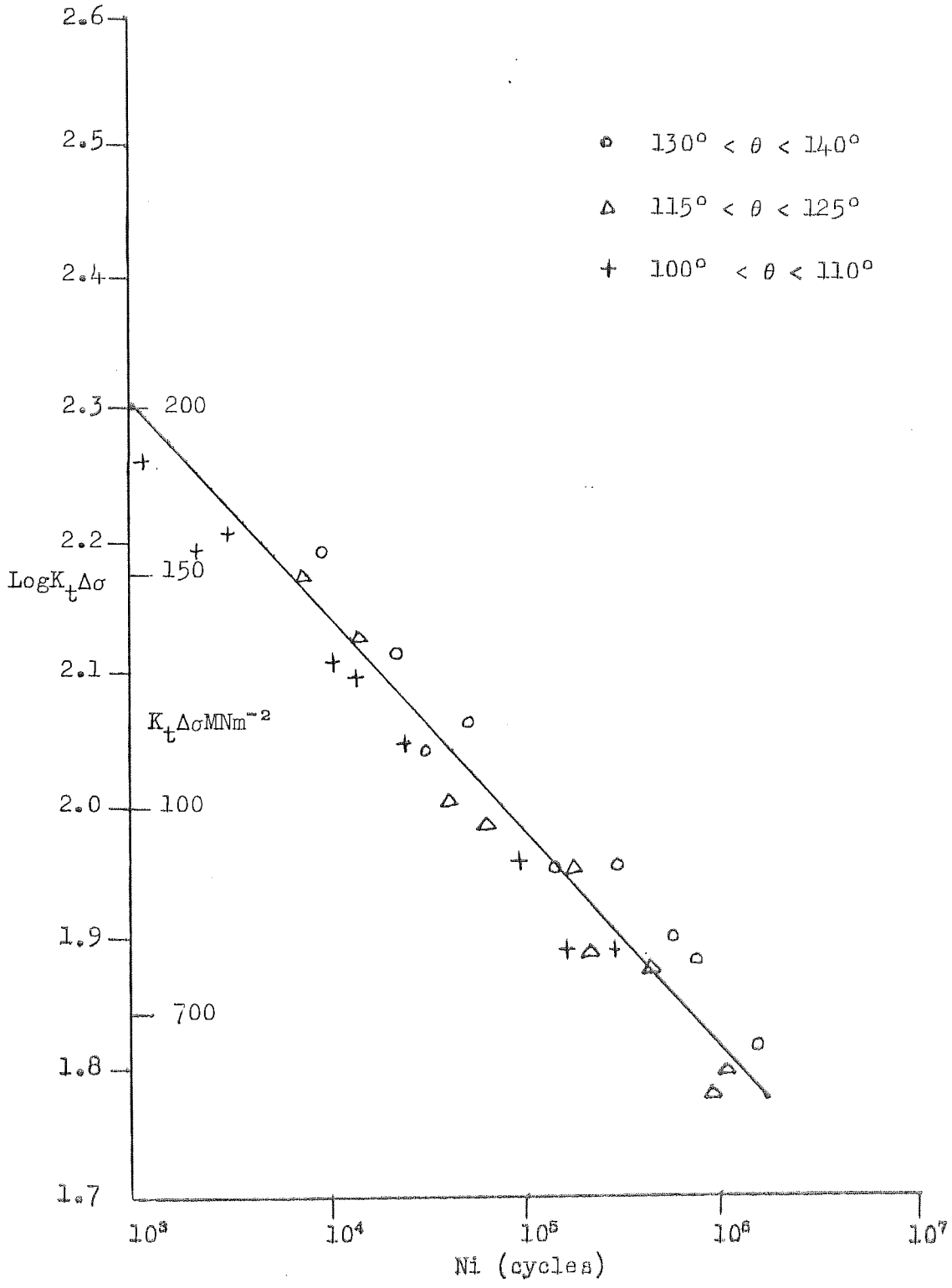

FIGURE 67 Effect of $\Delta\sigma^*$ on Crack Growth Cycles to Failure from Central Defects Tested at Room Temperature in the As-Welded Condition

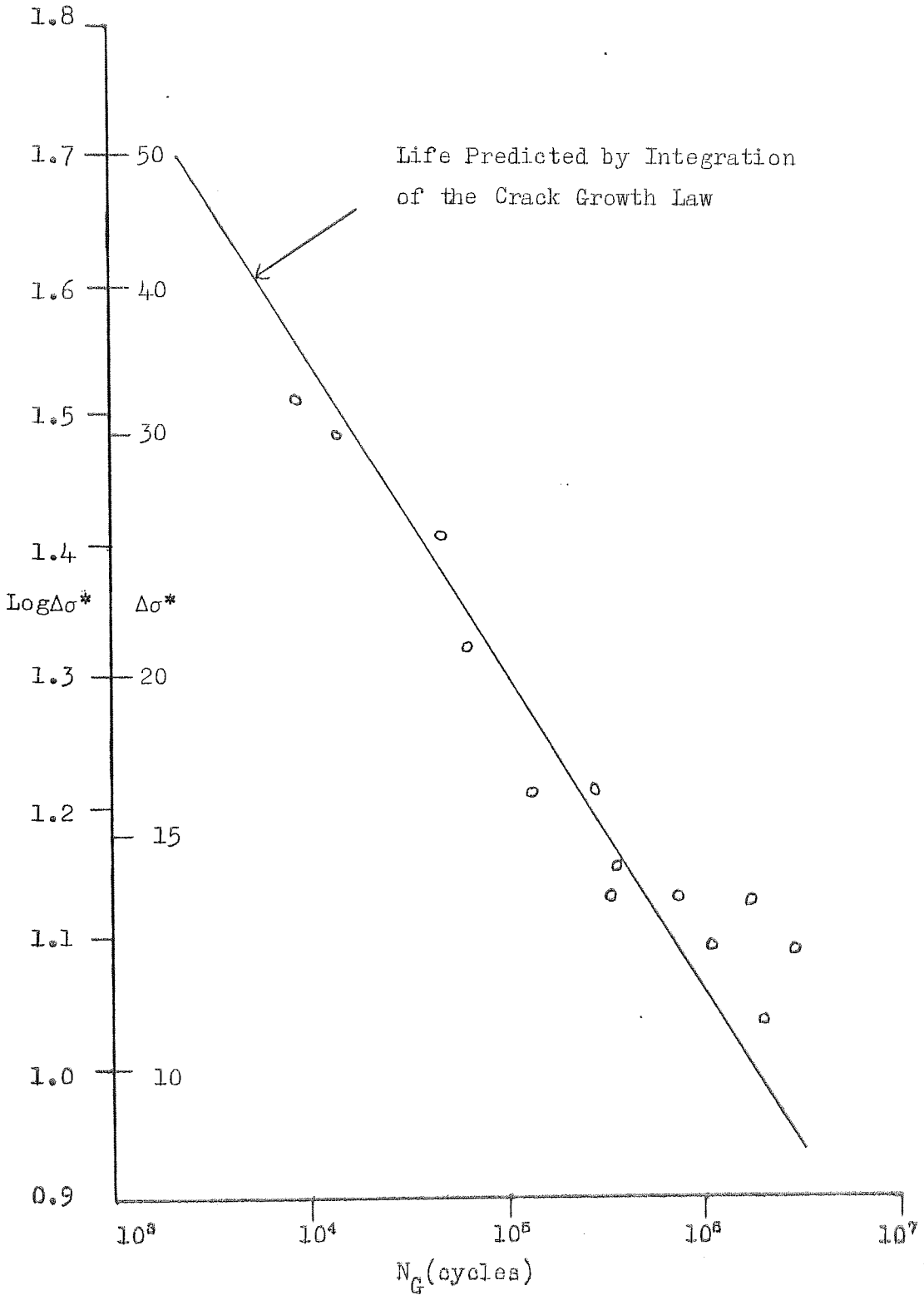

FIGURE 68 Effect of $\Delta\sigma^*$ on Cycles of Crack Growth to Failure from Central Defects Tested at Room Temperature after Stress-Relieving at 325°C.

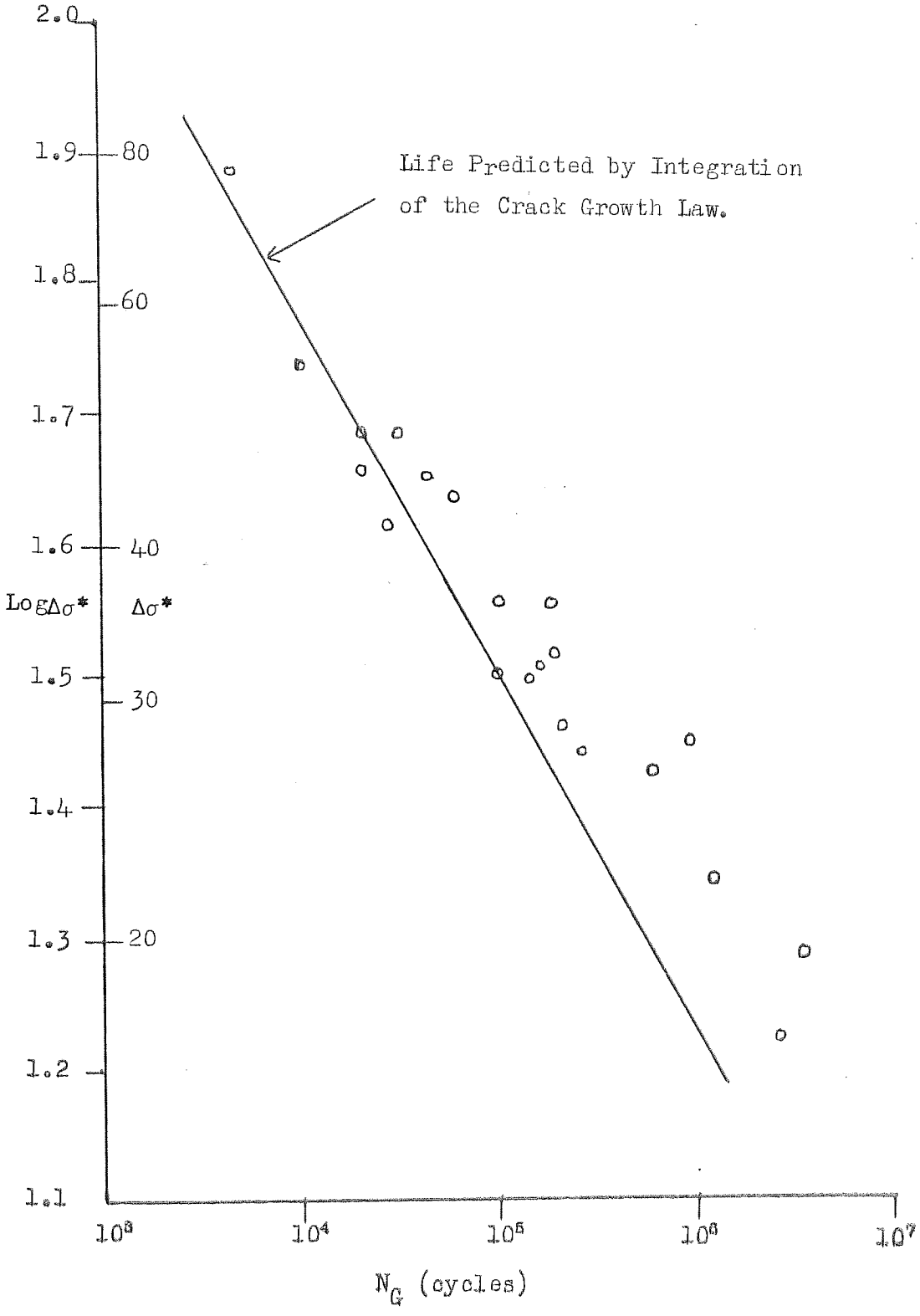

FIGURE 69 The Effect of $\Delta\sigma^*$ on Cycles of Crack Growth to Failure from Central Defects. Tested at Room Temperature after Stress-Relieving at 450°C.

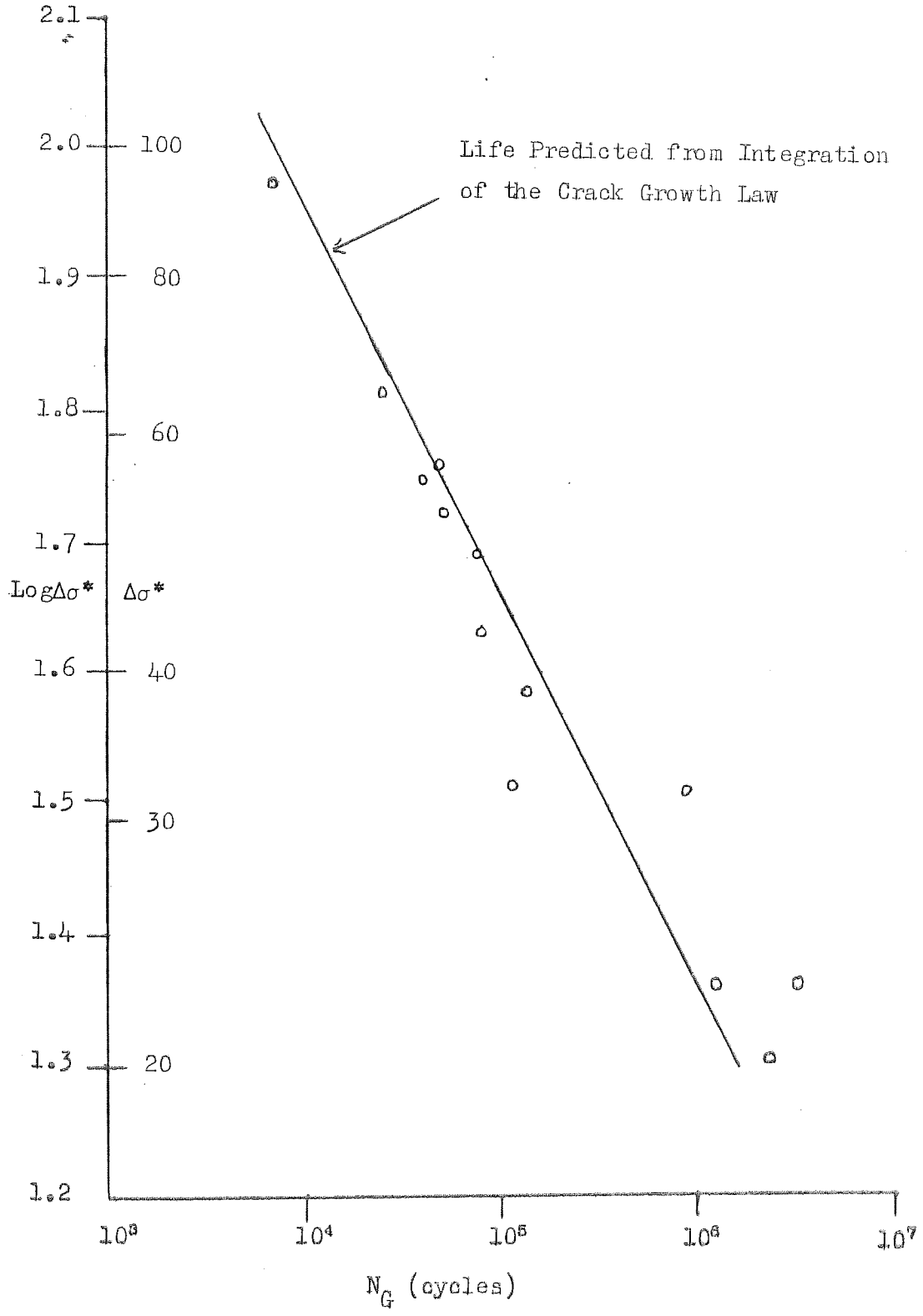

FIGURE 70 The Effect of $\Delta\sigma^*$ on Cycles of Crack Growth to Failure from Central Defects Tested at 200°C after Stress-Relieving at 325°C.

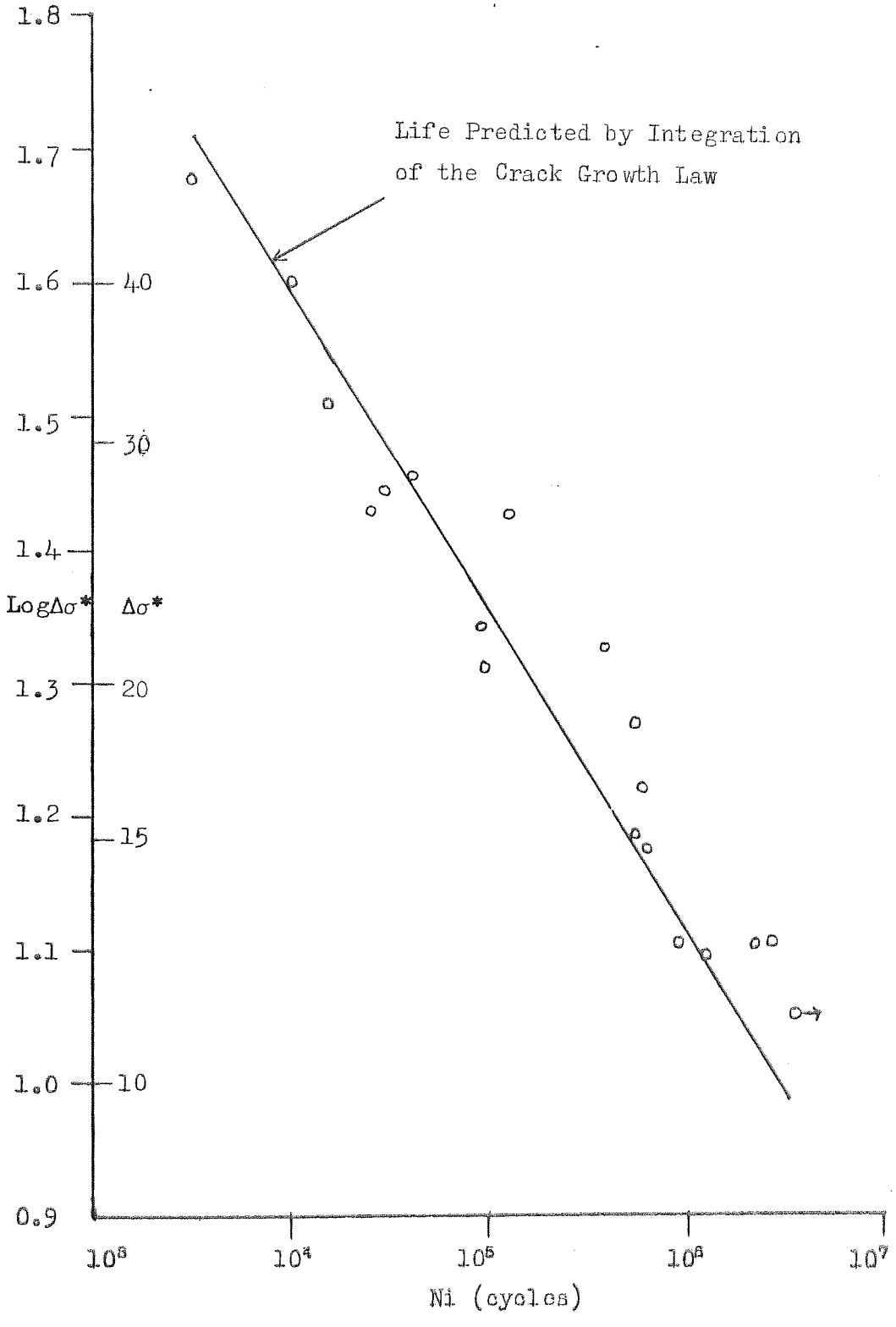

FIGURE 71 The effect of $\Delta\sigma^*$ on Cycles of Crack Growth to Failure from Central Defects. Tested at 300°C after Stress-Relieving at 325°C.

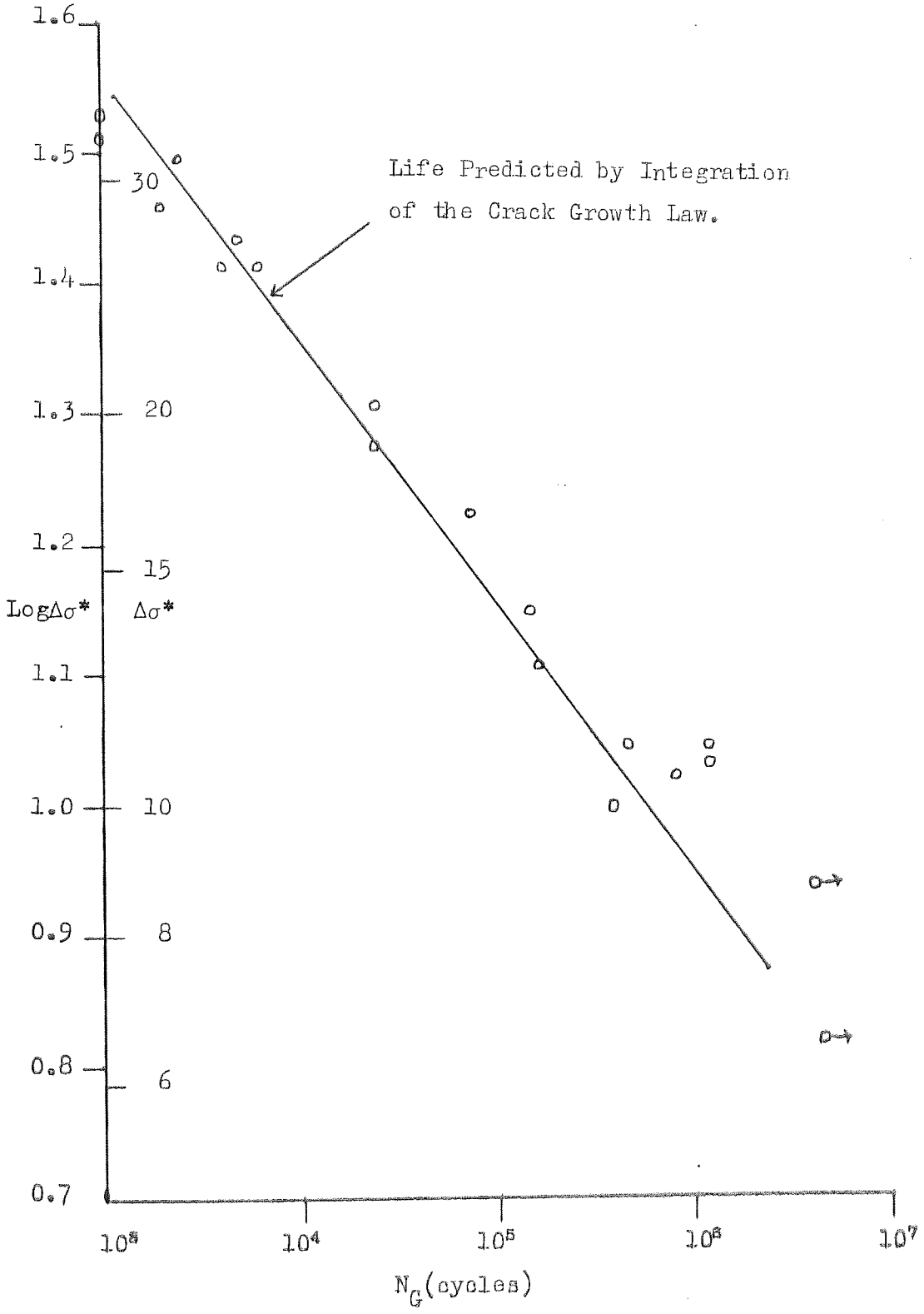

FIGURE 72 The Effect of $\Delta\sigma^*$ on Cycles of Crack Growth to Failure from Central Defects Tested at 300°C after Stress-Relieving at 450 °C.

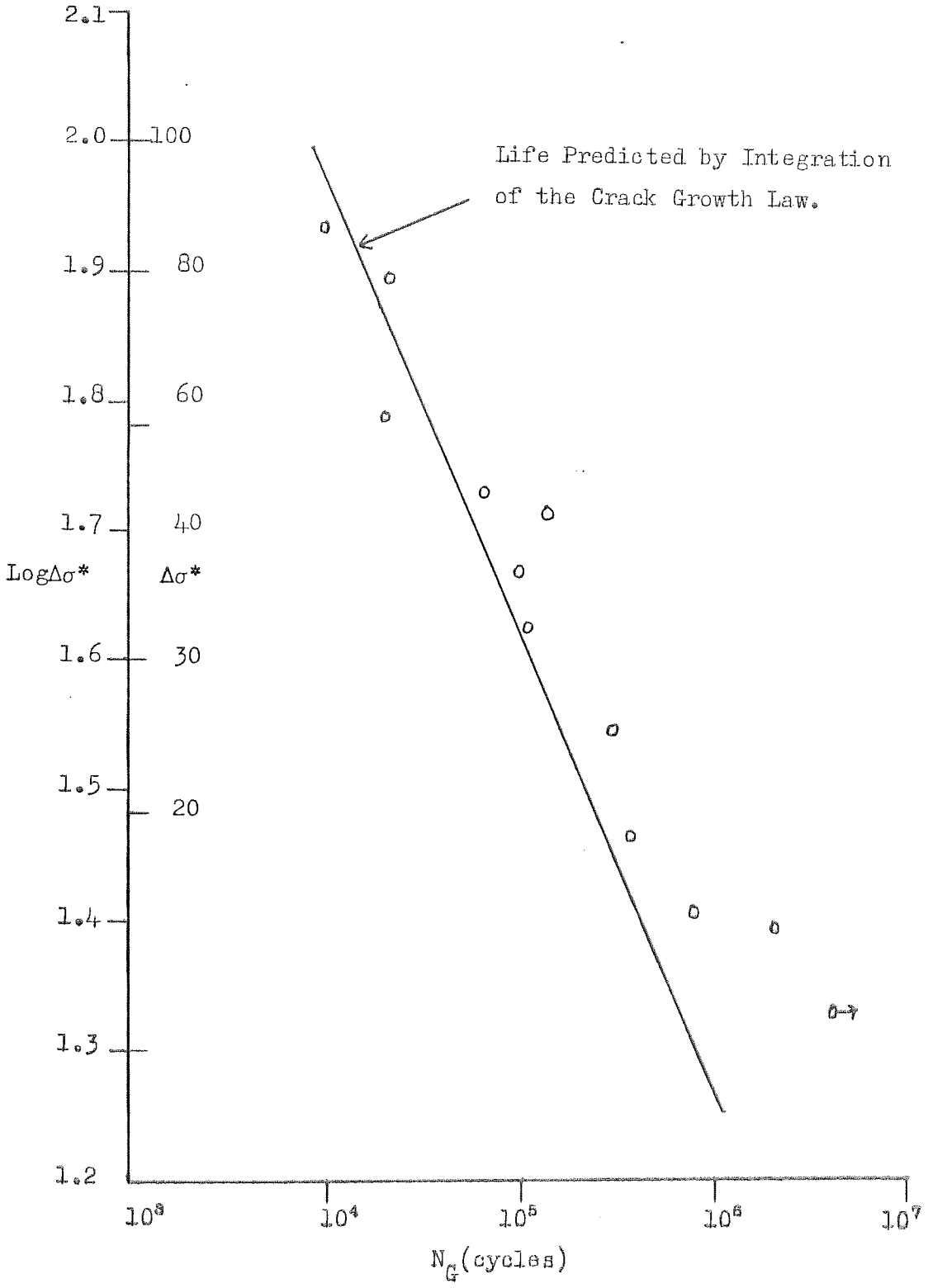

FIGURE 73 Effect of $\Delta\sigma^*$ on Cycles of Crack Growth to Failure from Reinforcement Defects. Tested at Room Temperature after Stress-Relieving at 325°C.

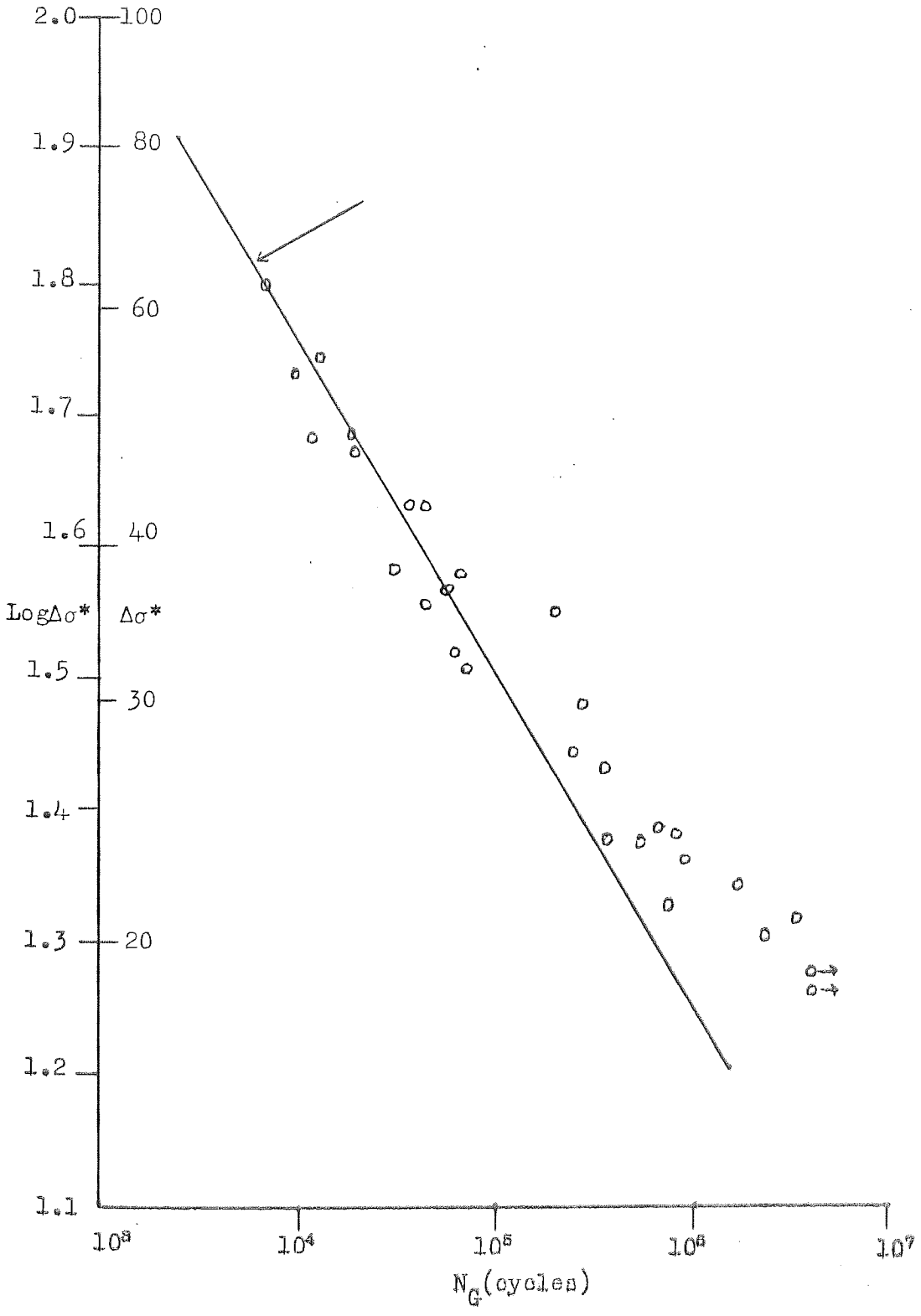

FIGURE 74 Effect of $\Delta\sigma^*$ on Cycles of Crack Growth to Failure from Reinforcement Defects Tested at 300°C after Stress-Relieving at 325°C.

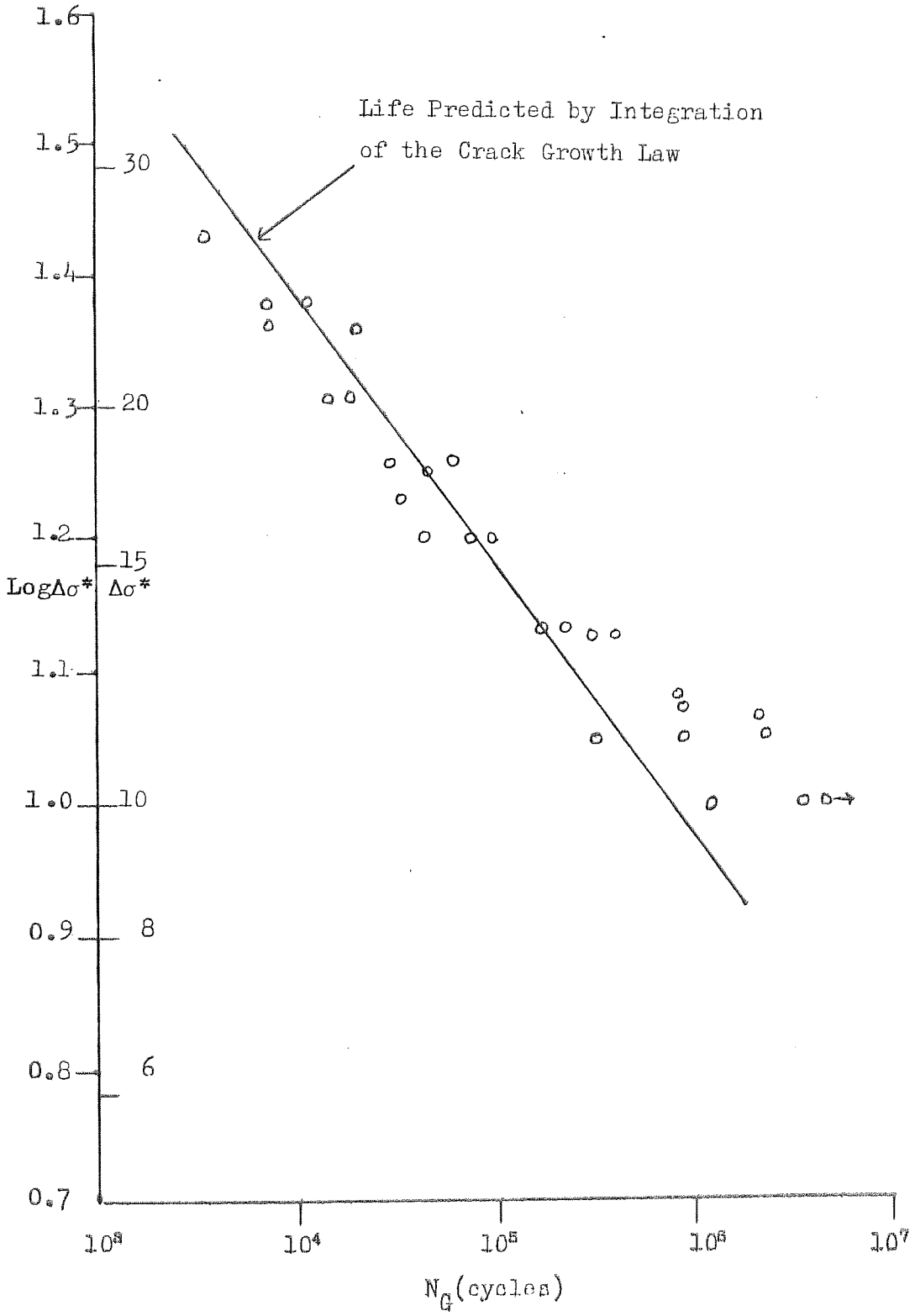

Figure 75. Multiple Initiation at the Reinforcement Root, Magnification x12.

FIGURE 76 The Effect of ΔK_o on Cycles to Initiate a Crack from Central and Reinforcement Defects.
Tested at Room Temperature after Stress-Relieving at 325°C.

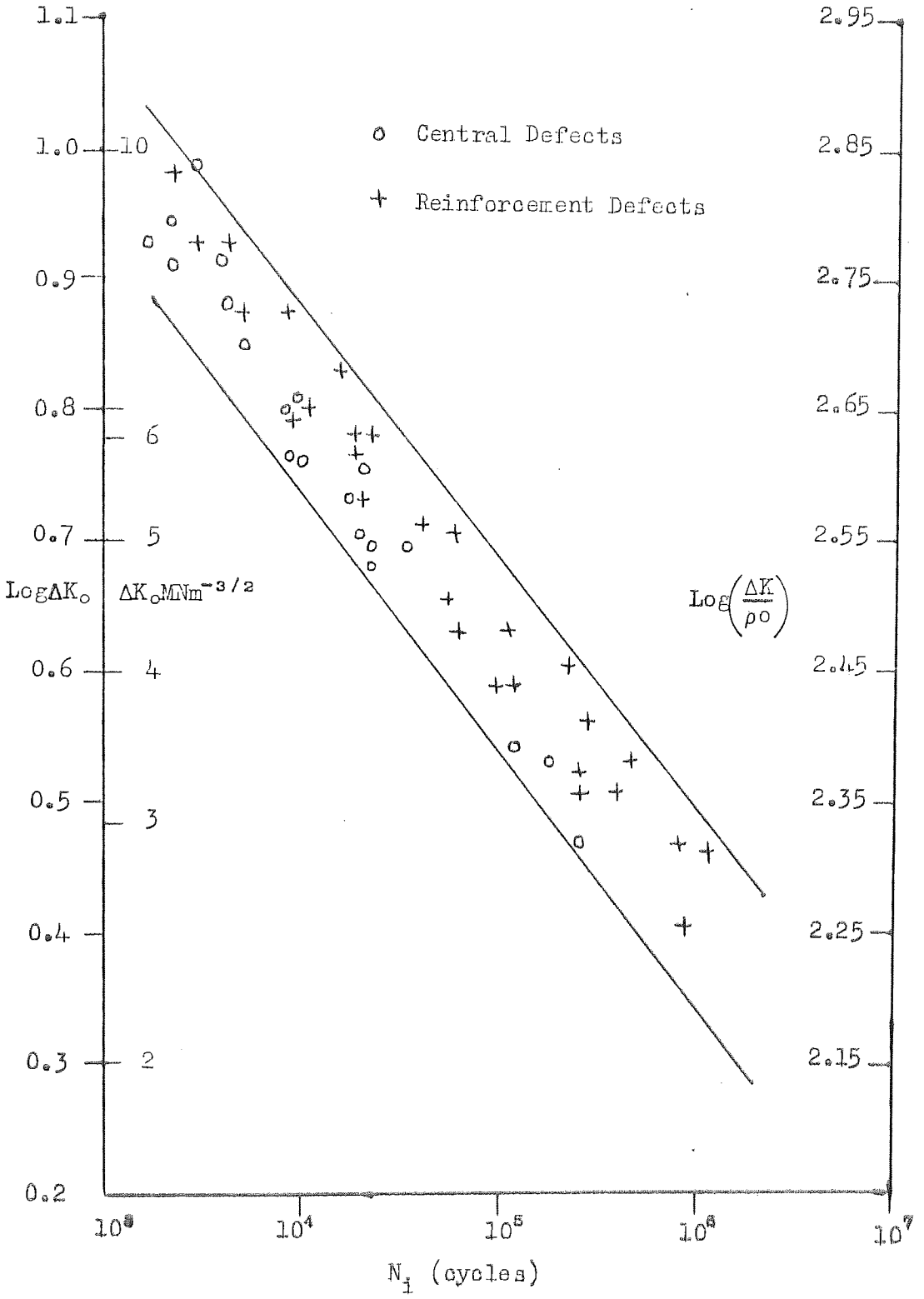

FIGURE 77 The Effect of $Kf'\Delta\sigma$ on Cycles to Initiate a crack from Central and Reinforcement Defects.
Tested at Room Temperature after Stress-Relieving at 325°C.

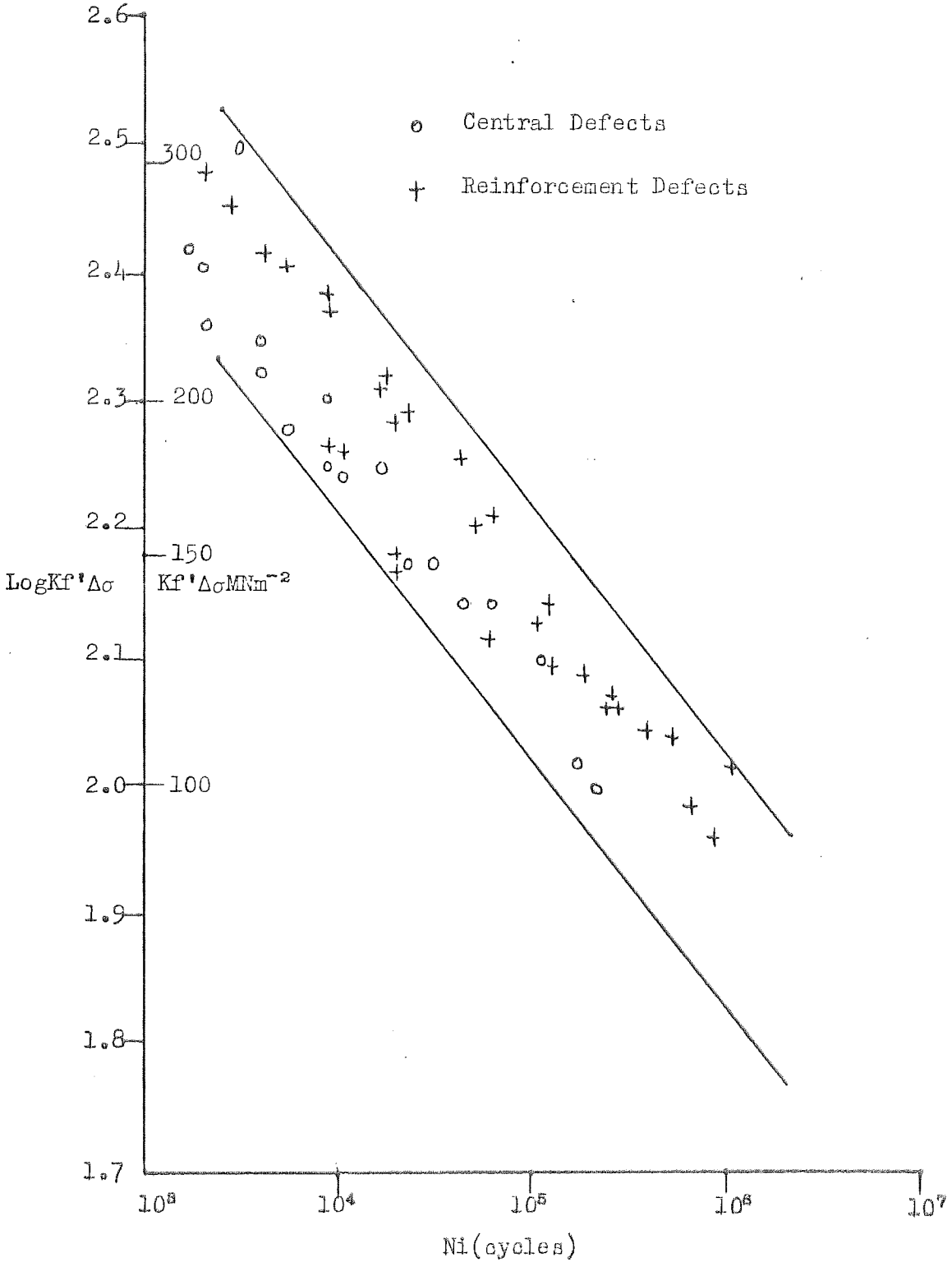

Figure 78. Crack Initiation from the Root of a Central Defect. Magnification x 200.

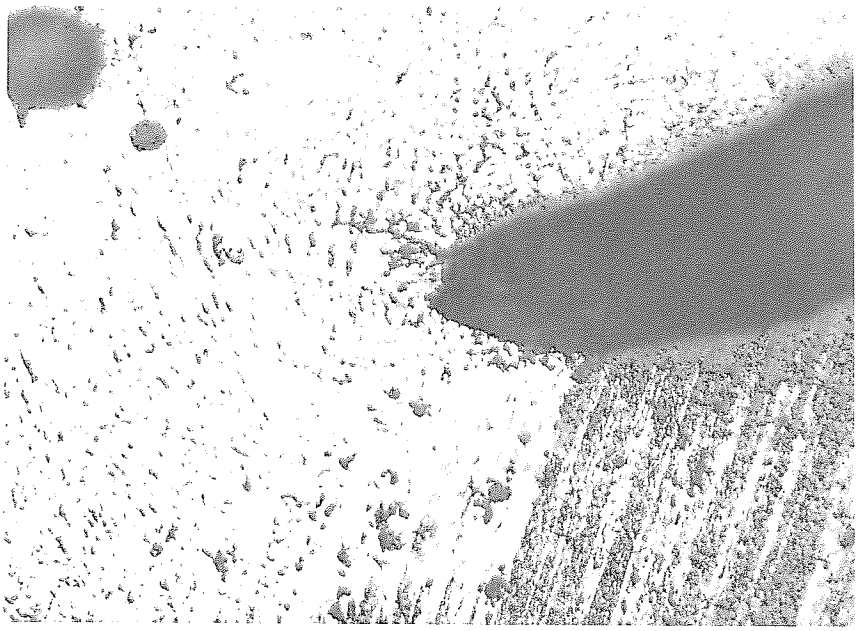

Figure 79. Crack Growth from the Root of a Central Defect. Magnification x 200.

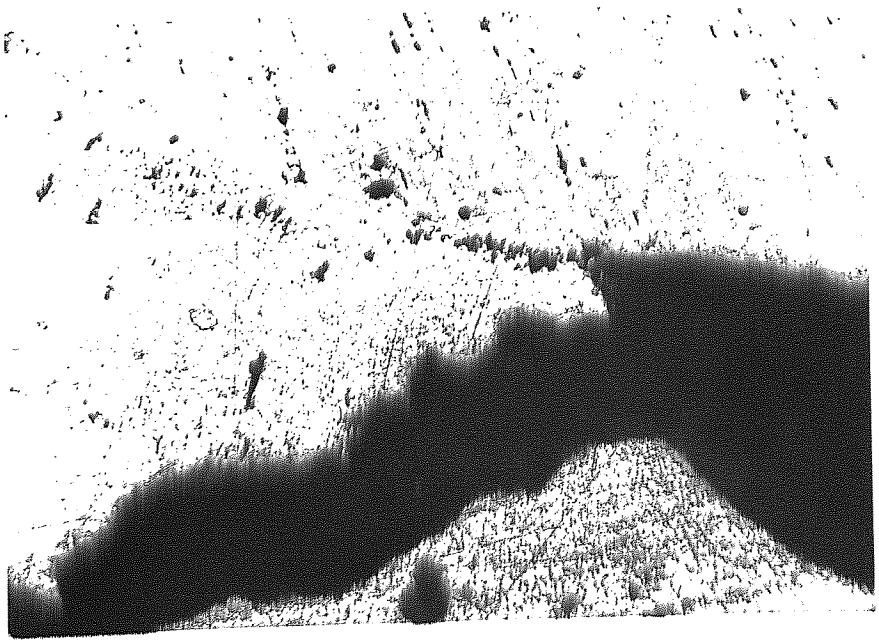

FIGURE 80 Comparison of $Kf\Delta\sigma$ and $\frac{\Delta K}{\rho^{\frac{1}{2}}}$ for Three Notch Geometries

1. Curve for elliptical through notches in infinite plates.
2. Curve for single edge notched tension and notched bend specimens
3. Line for $Kt\Delta\sigma = \frac{\Delta K}{\rho^{\frac{1}{2}}}$

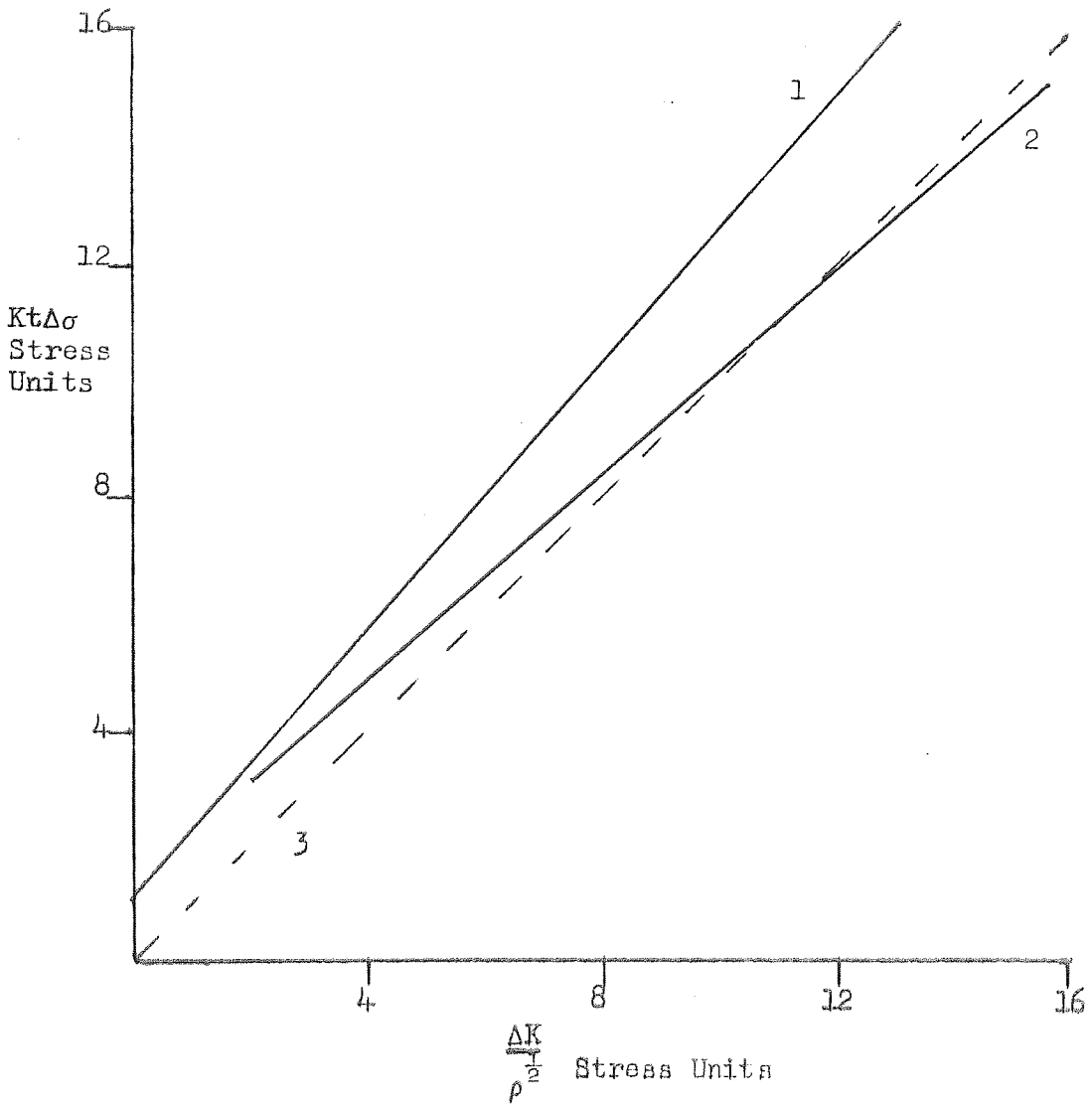

FIGURE 81 Comparison of $\frac{\Delta K}{\rho o}$ with $Kf'\Delta\sigma$ for the case of Central Defects Kf' is the fatigue strength reduction factor at 2×10^6 cycles.

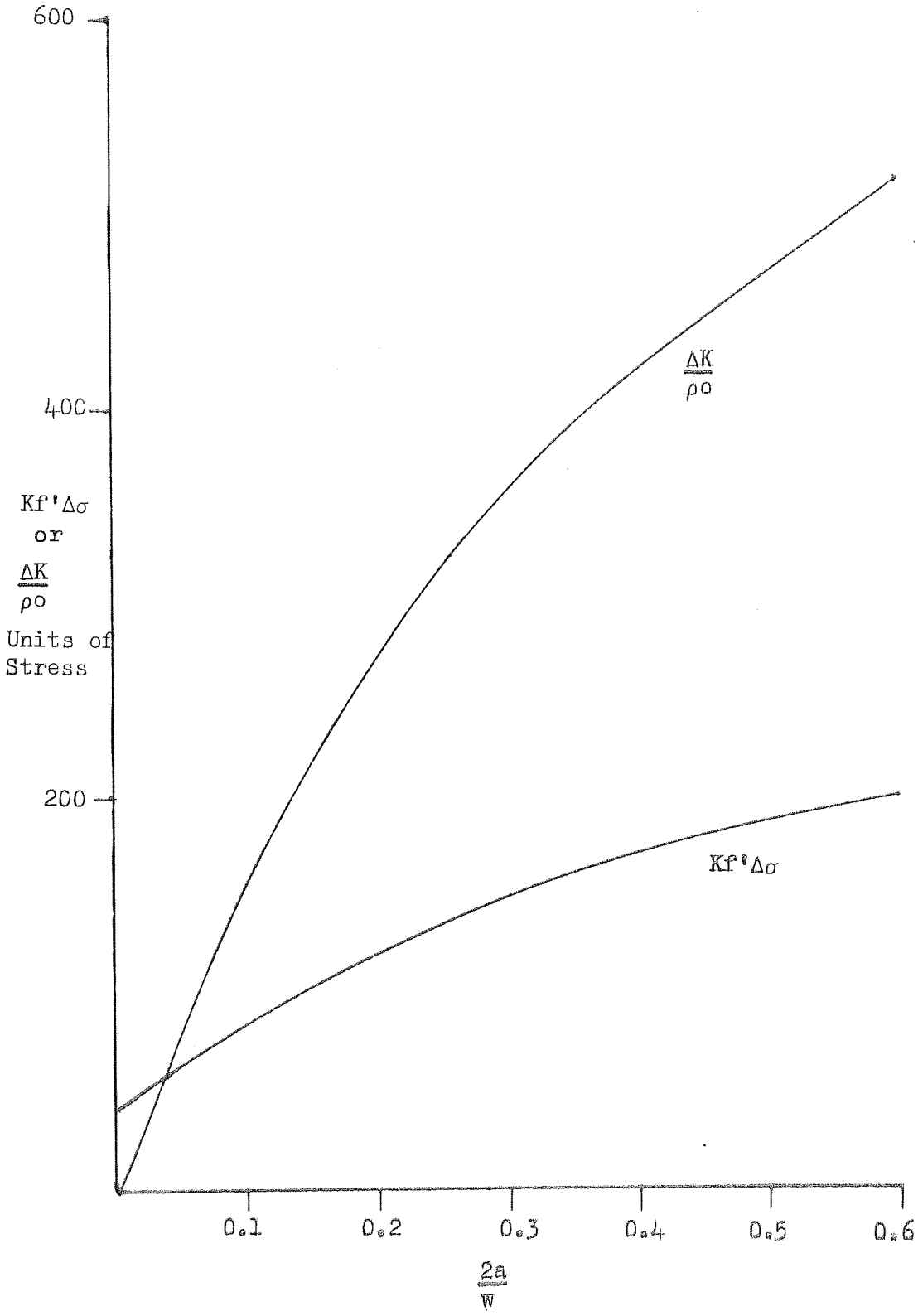

FIGURE 82 Comparison of $\frac{\Delta K}{\rho o}$ with $Kf'\Delta\sigma$ for the case of Reinforcement Defects Kf' is the fatigue strength reduction factor at 2×10^6 cycles.

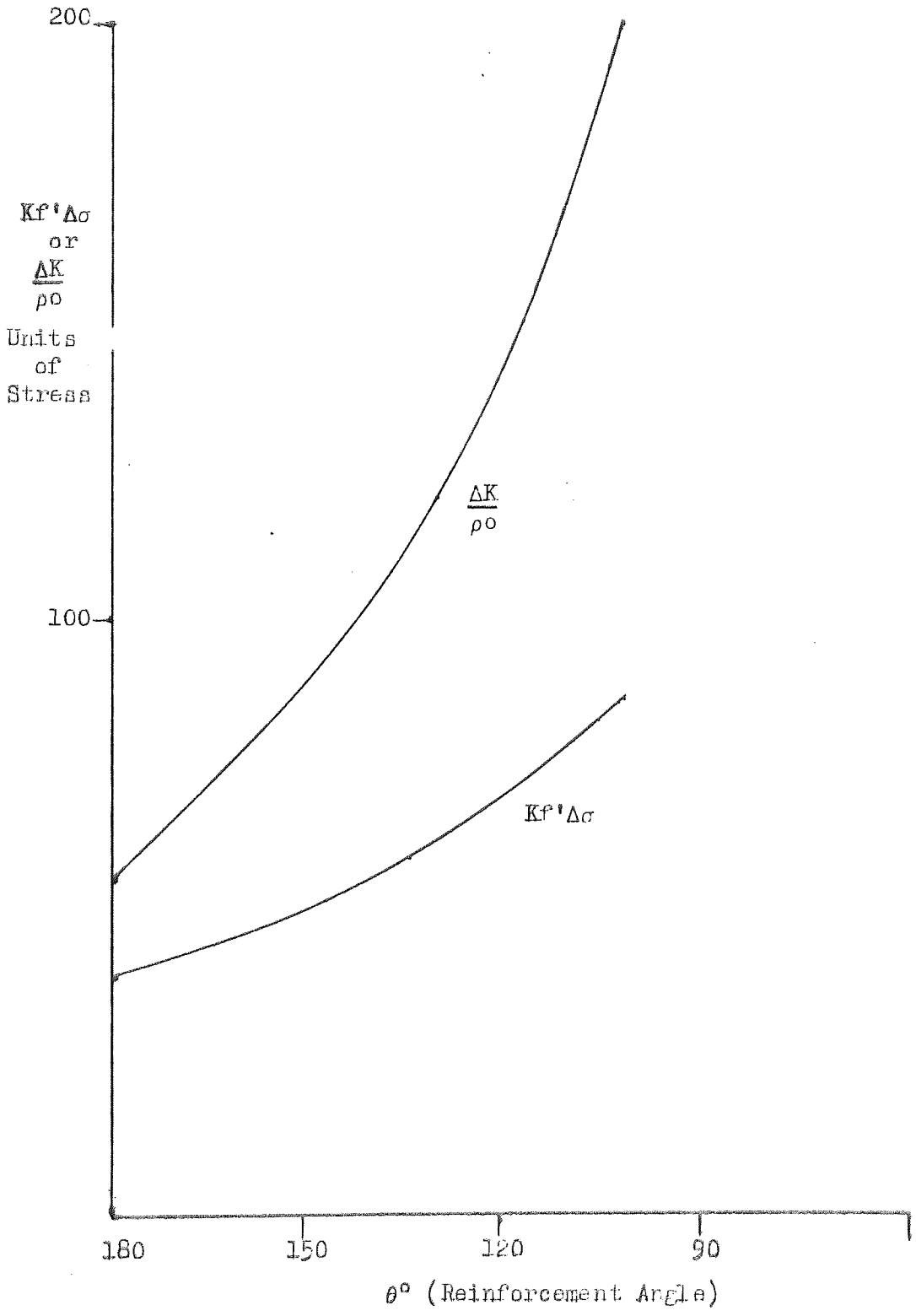

FIGURE 83 Correlation of Ni with $\frac{\Delta K}{\left(\frac{\rho}{\rho_o}\right)^{\frac{1}{2}}}$ for

Pearsons Data on Aluminium Alloy

BSL65

d = Notch Depth

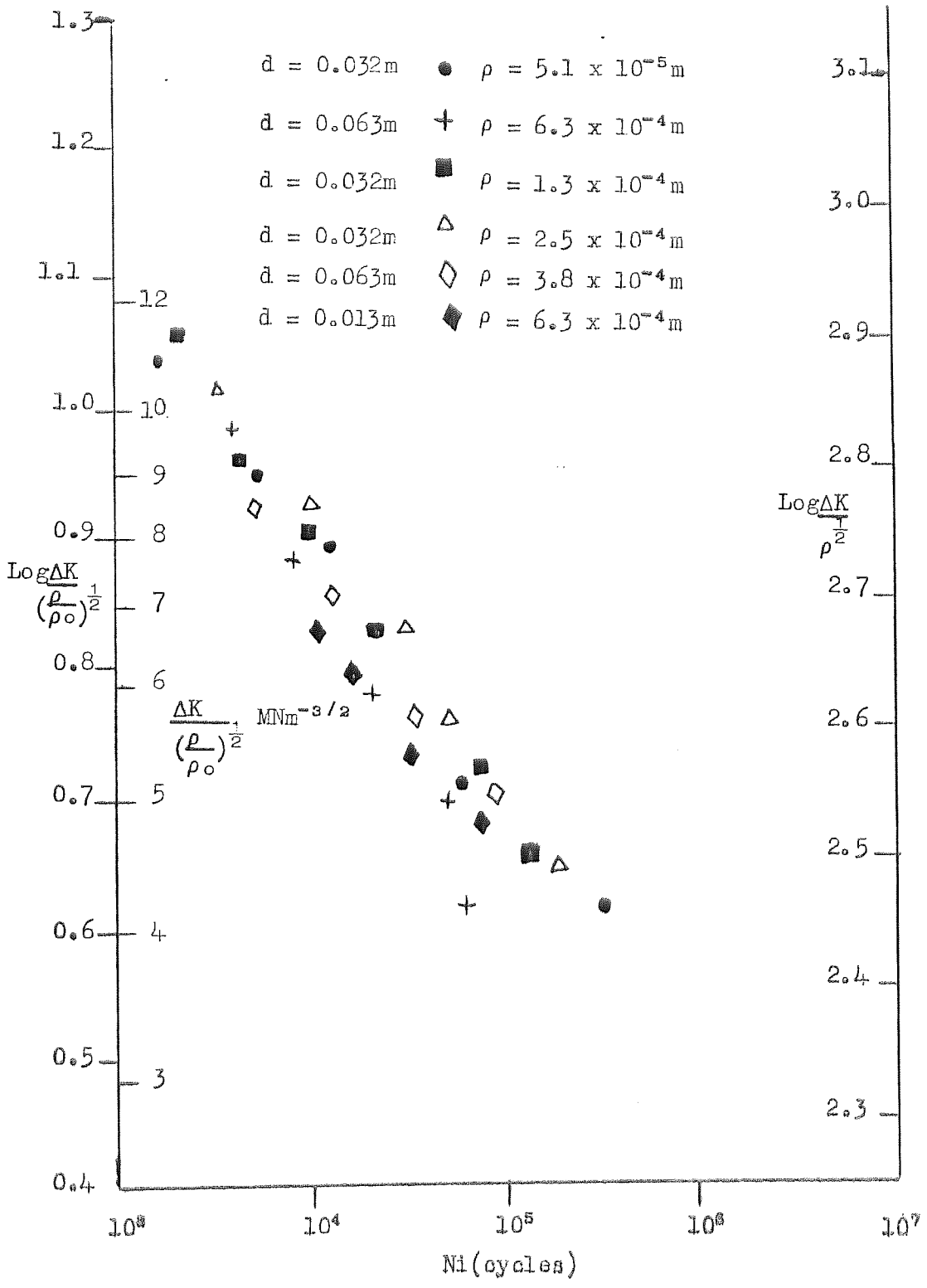

FIGURE 8. Correlation of Ni with $Kf'\Delta\sigma$ for Pearson's Data on Aluminium Alloy BSL65
d = Notch Depth

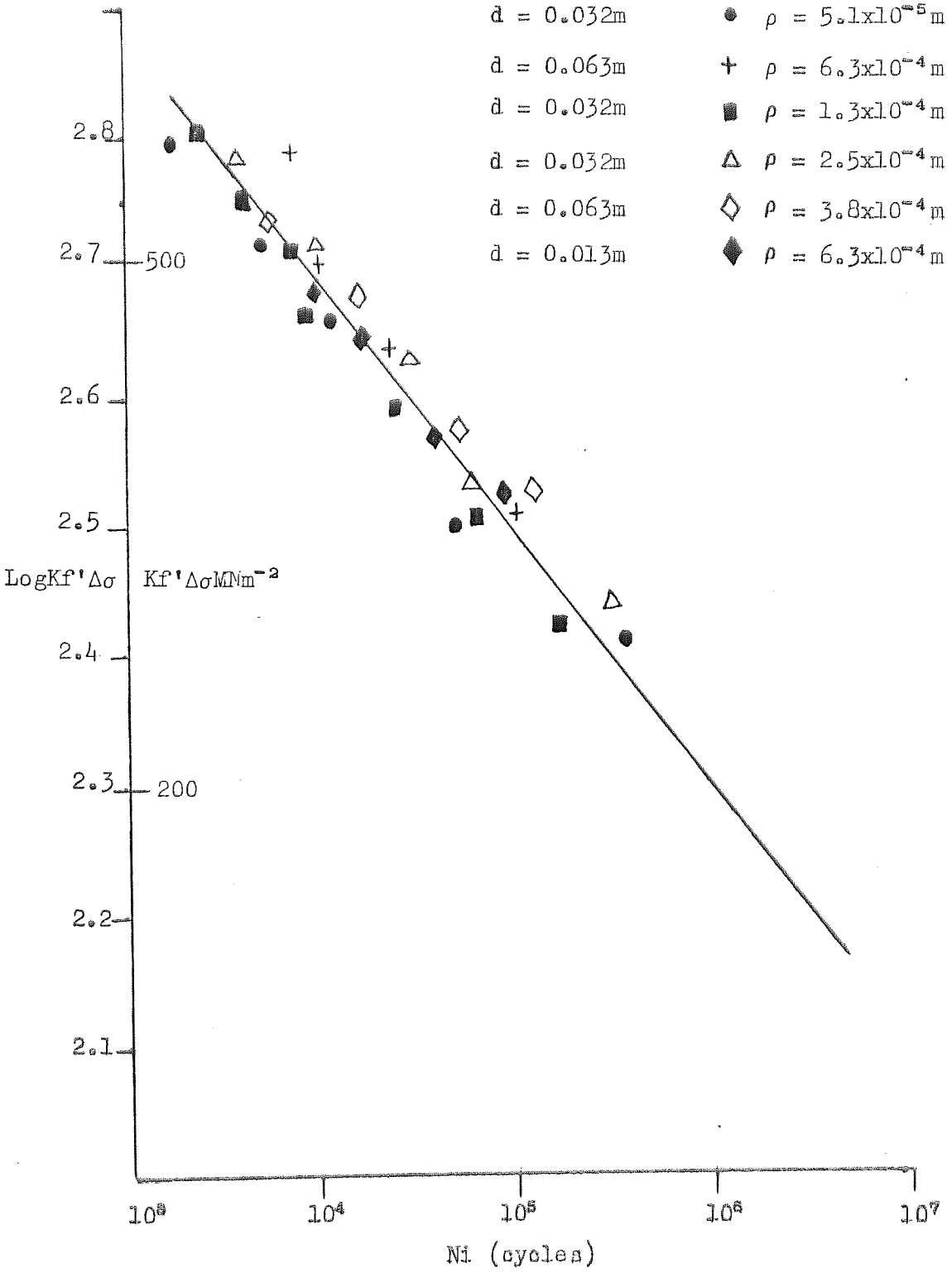

FIGURE 85 The Life to Failure Results of Dinsdale and Young on N8 Welds Containing Lack of Fusion - Re-analysed and Correlated with $\Delta\sigma^*$

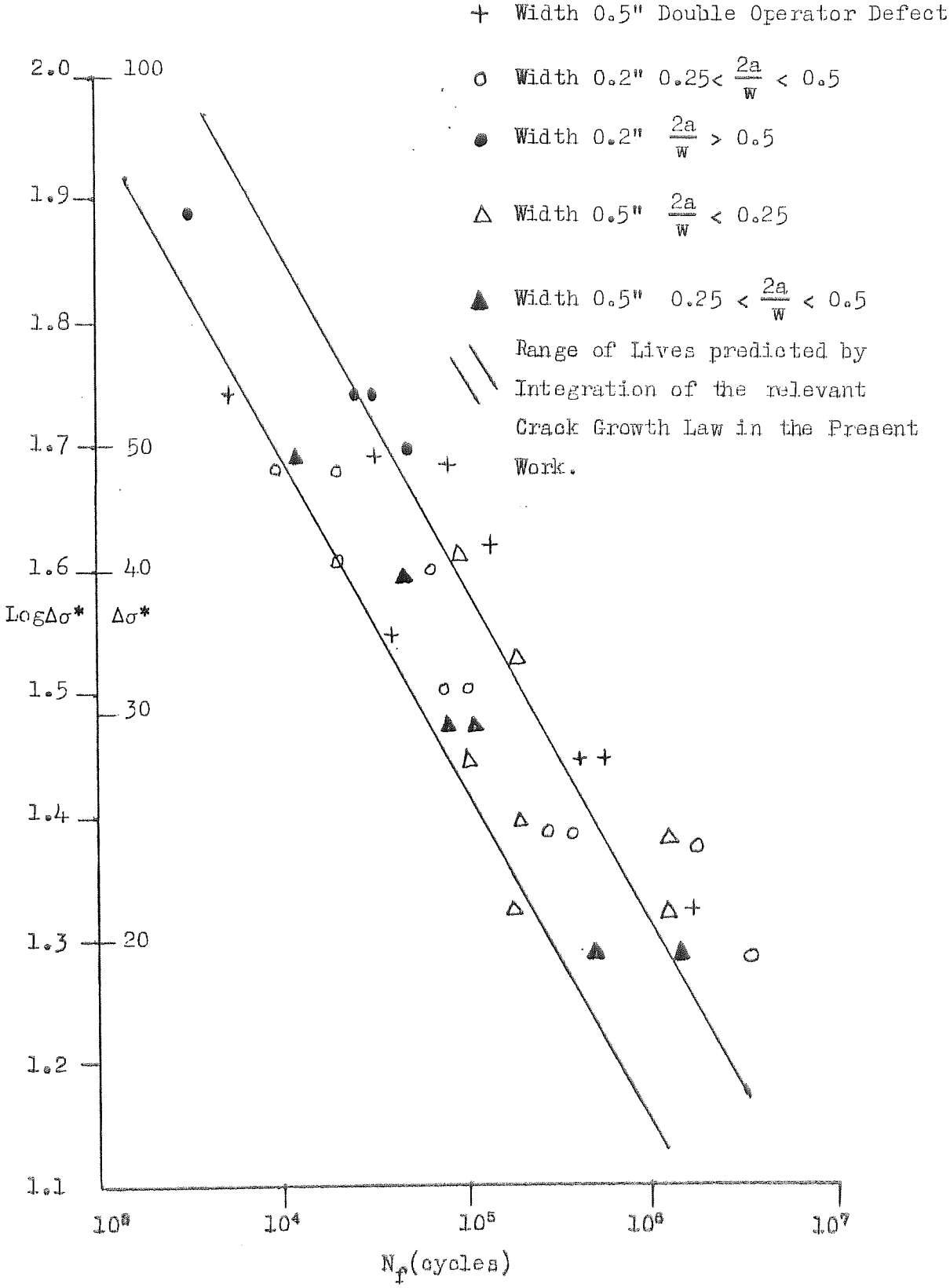

FIGURE 86 The Results of Dinsdale and Young on the Effect of Reinforcement Angle (θ) on the Fatigue Lives of N8 Welds - Re-analysed and correlated with $\Delta\sigma^*$

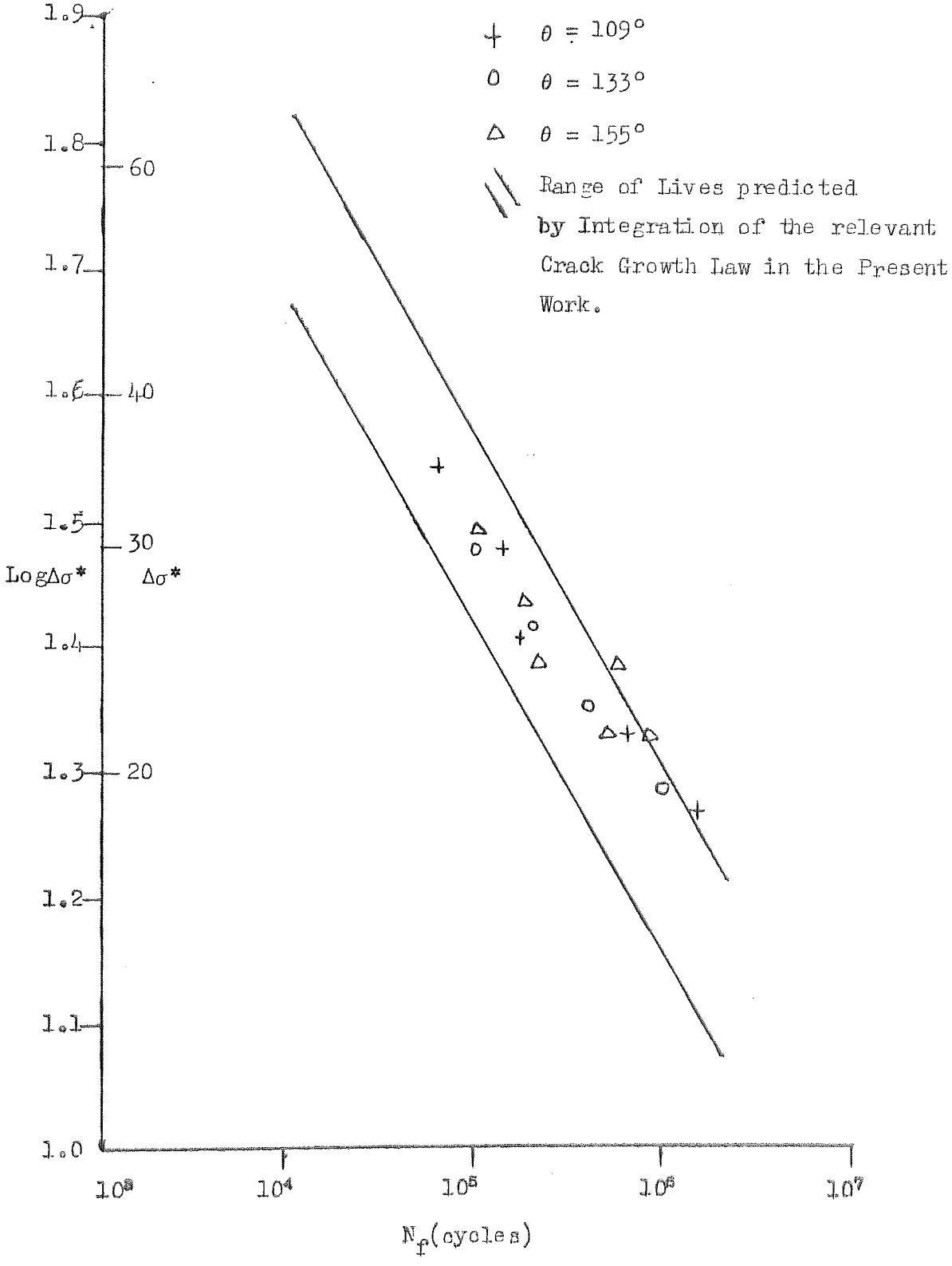

FIGURE 87 The Relationship between Initiation and Growth phases of the Fatigue Life, as a function of Weld Width, for Welds containing Central Defects of magnitude $\frac{2a}{w} = 0.3$

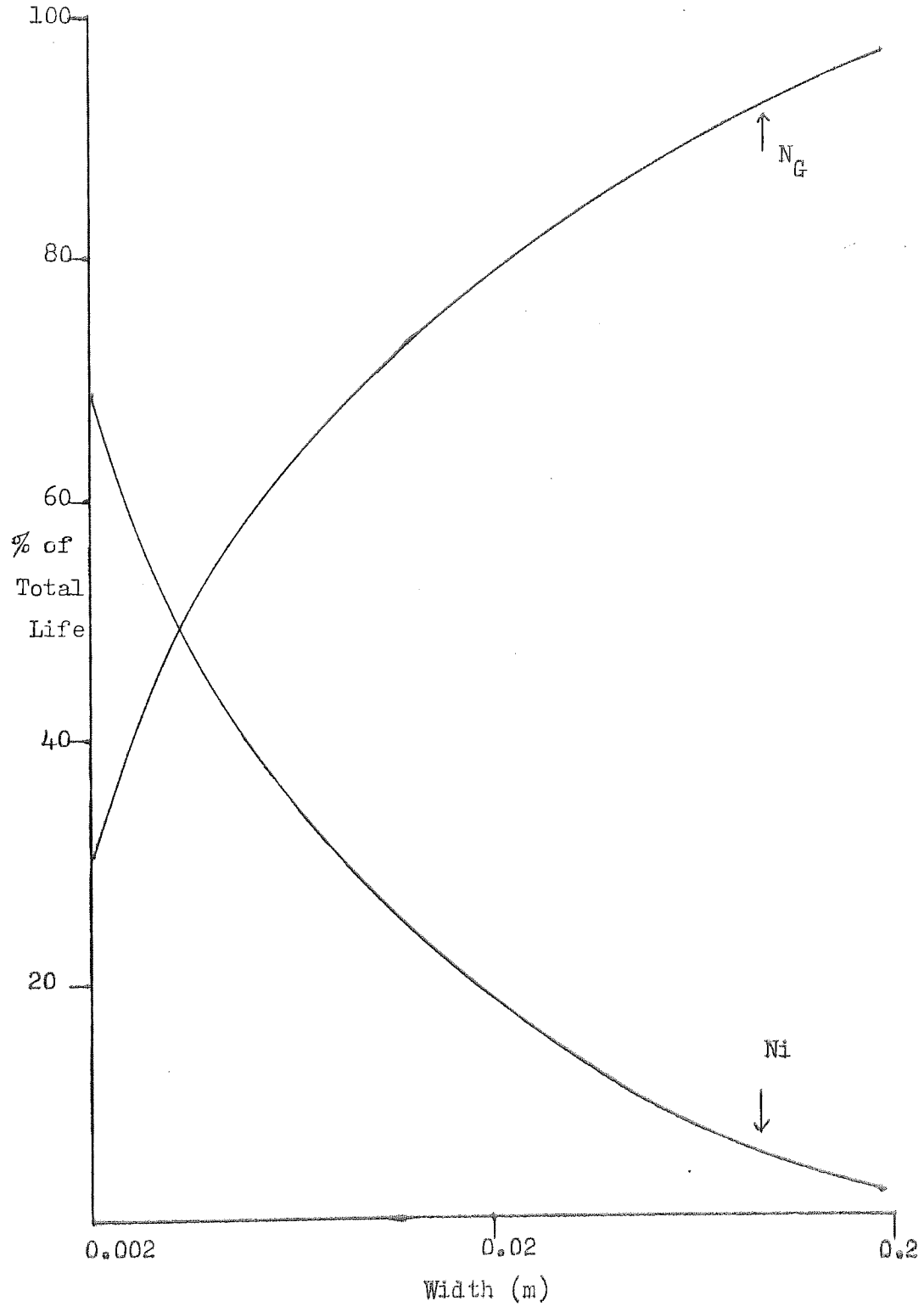

FIGURE 88 The Relationship between Initiation and Growth phases of the fatigue Life as a function of Weld Width, for Welds containing Central Defects of constant magnitude 2a = 0.003m.

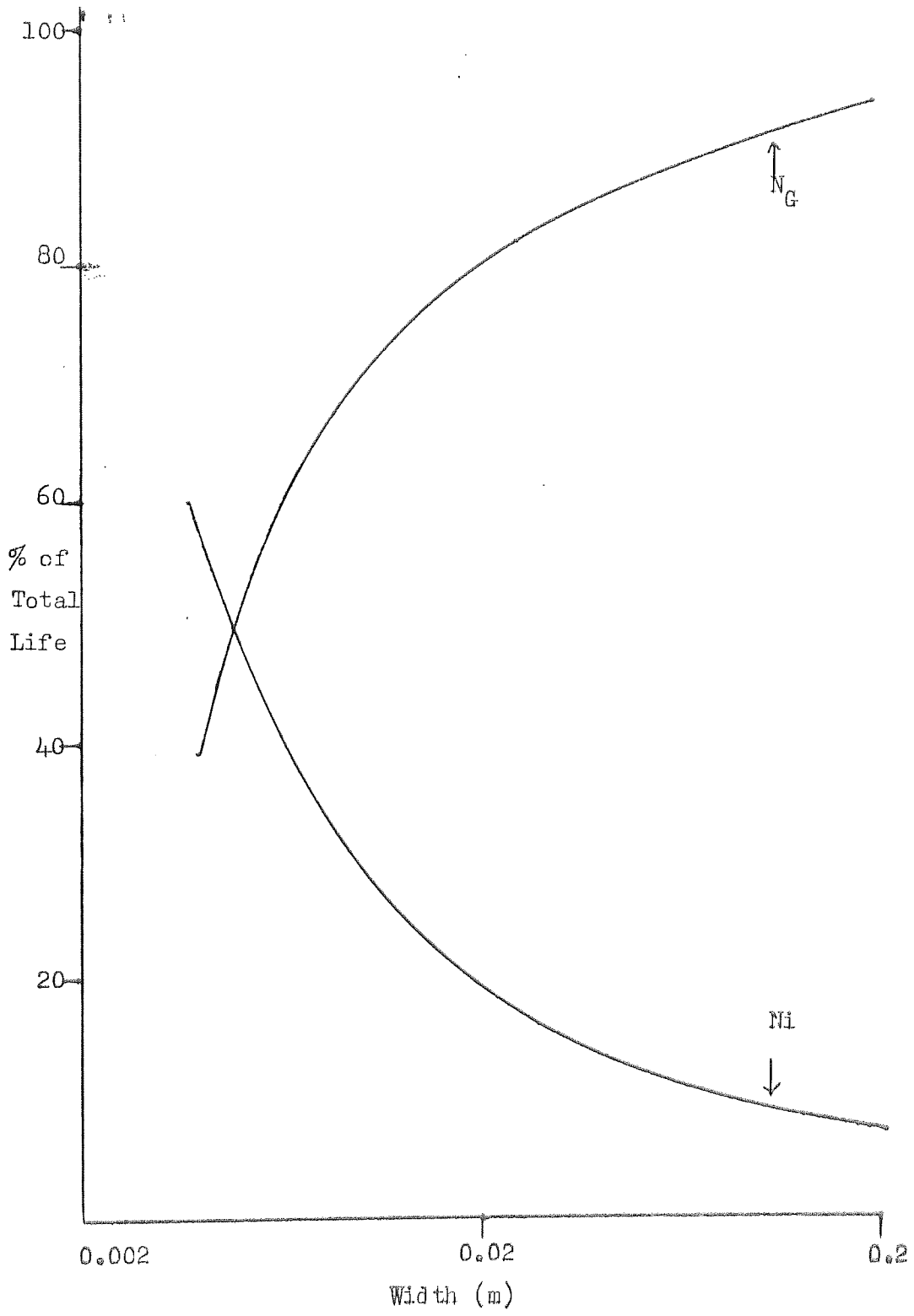

FIGURE 89 Rationalisation of the Effect of Stress-Relieving on the cycles of Crack Growth to Failure.

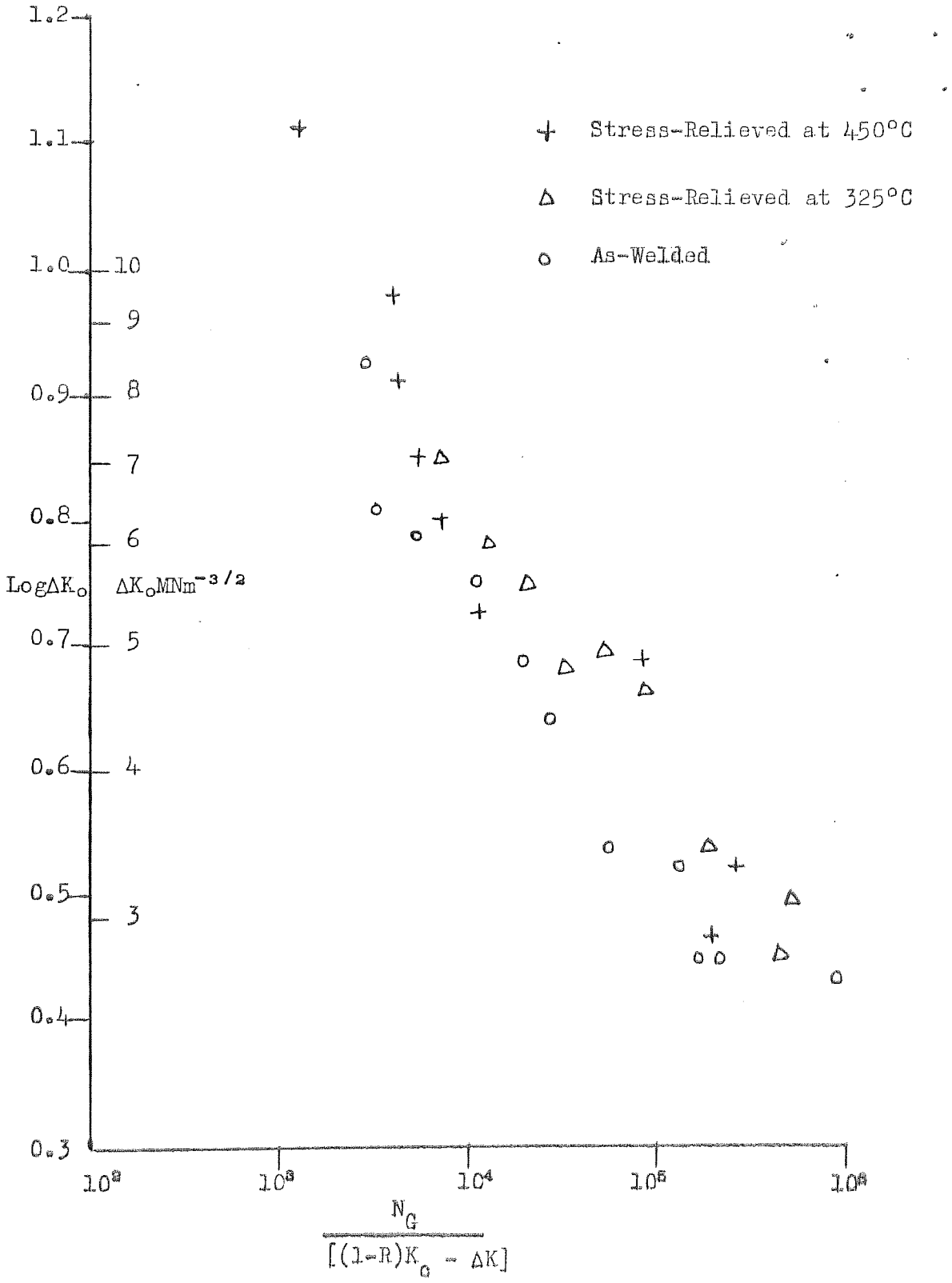

FIGURE 90 Rationalisation of the Effect of Stress-Relieving on the cycles to Initiate a Crack.

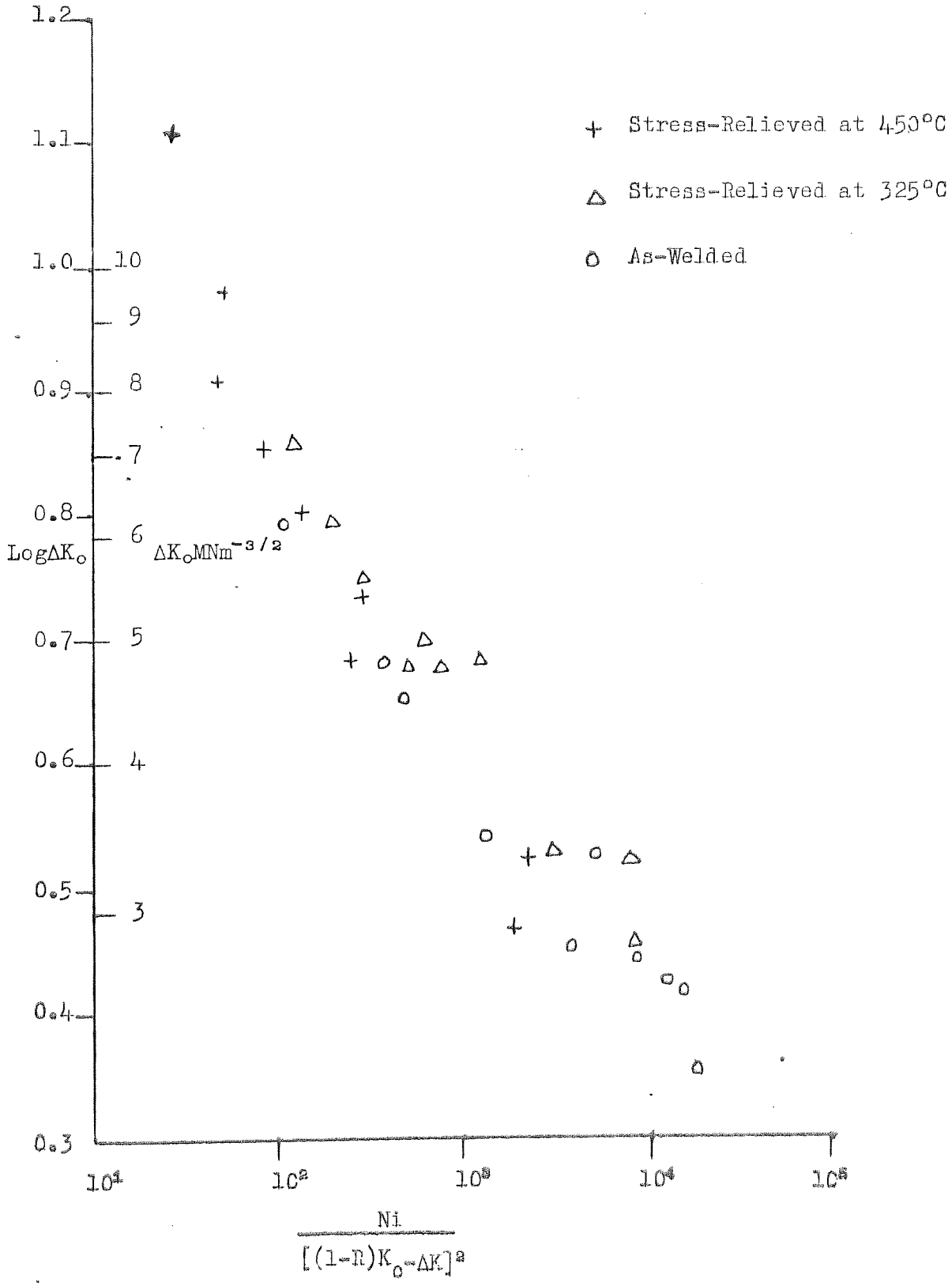

FIGURE 91 The Effect of Stress-Relieving on the Initiation Period as a Function of Width, for the case of a Weld containing a Central Defect of magnitude $\frac{2a}{w} = 0.3$

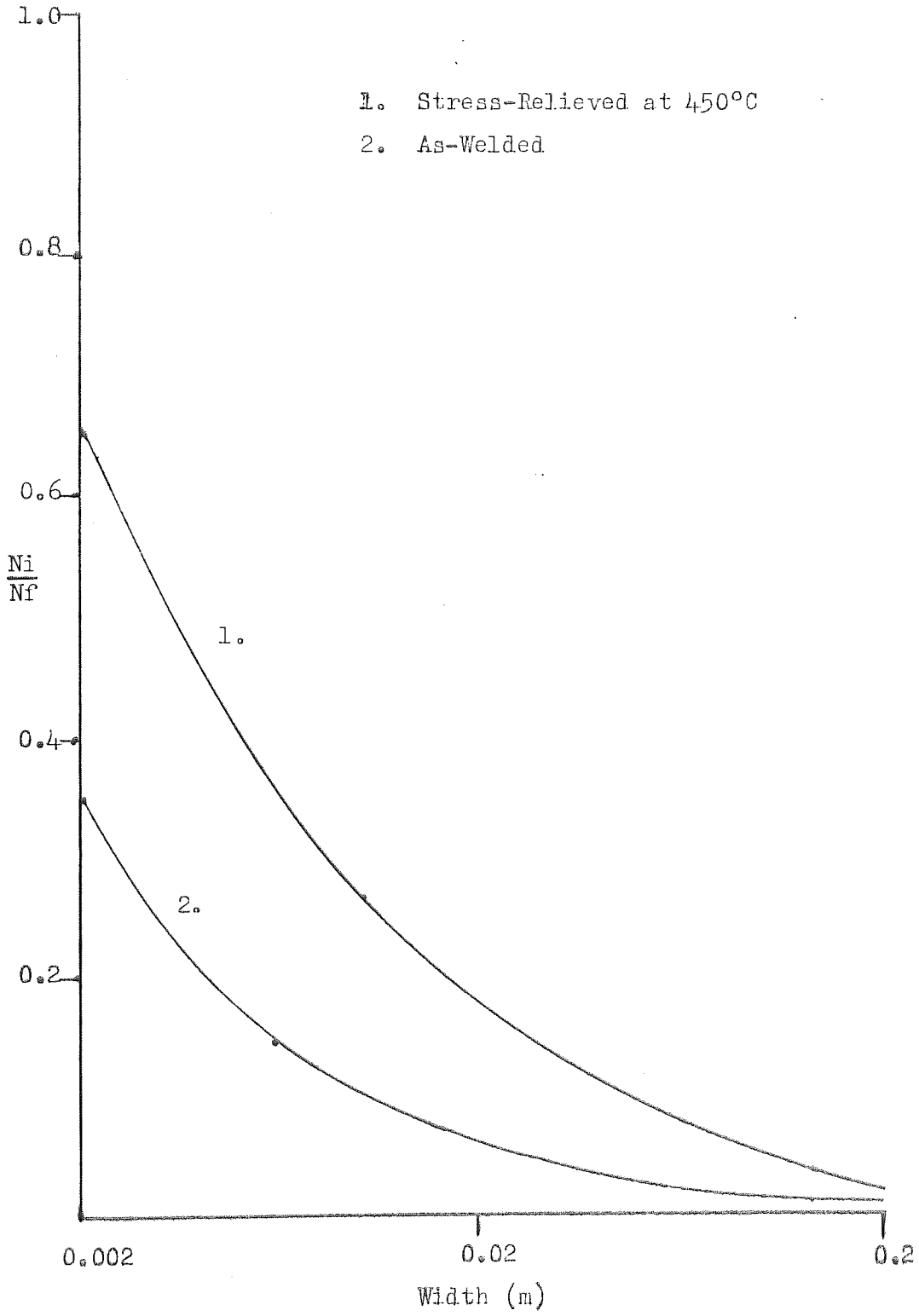

FIGURE 92 The Effect of Stress-Relieving on the Total Fatigue Life as a function of Width, for Welds containing Central Defects of Magnitude $\frac{2a}{W} = 0.3$, Tested at Room Temperature with $\Delta K_c = 5 MNm^{-3/2}$

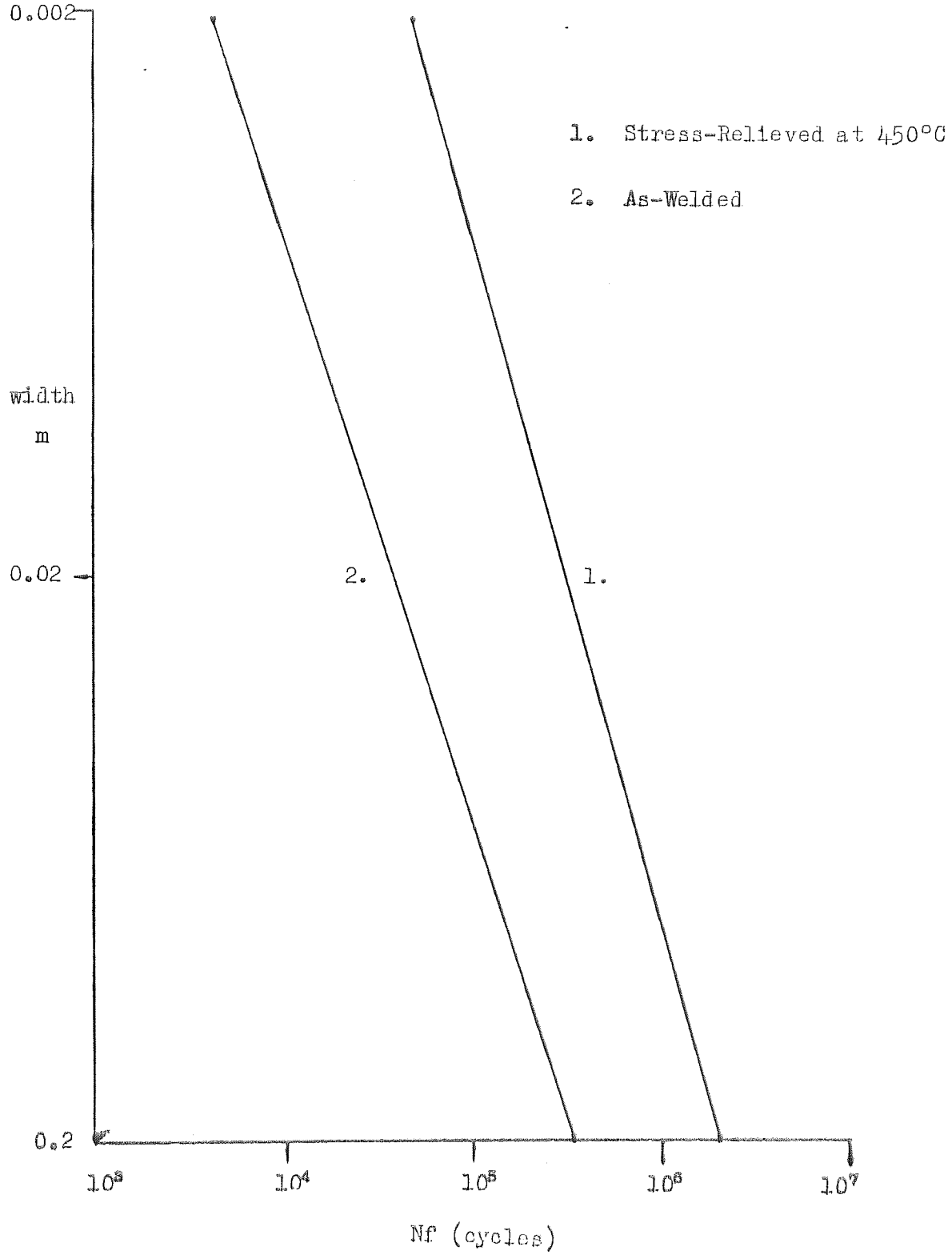

Appendices 1 and 2. The Value of the Crack Growth Integral, I, as a function of the Original Crack Size of a Central Defect

1. 'm' = 3.3
2. 'm' = 4.1

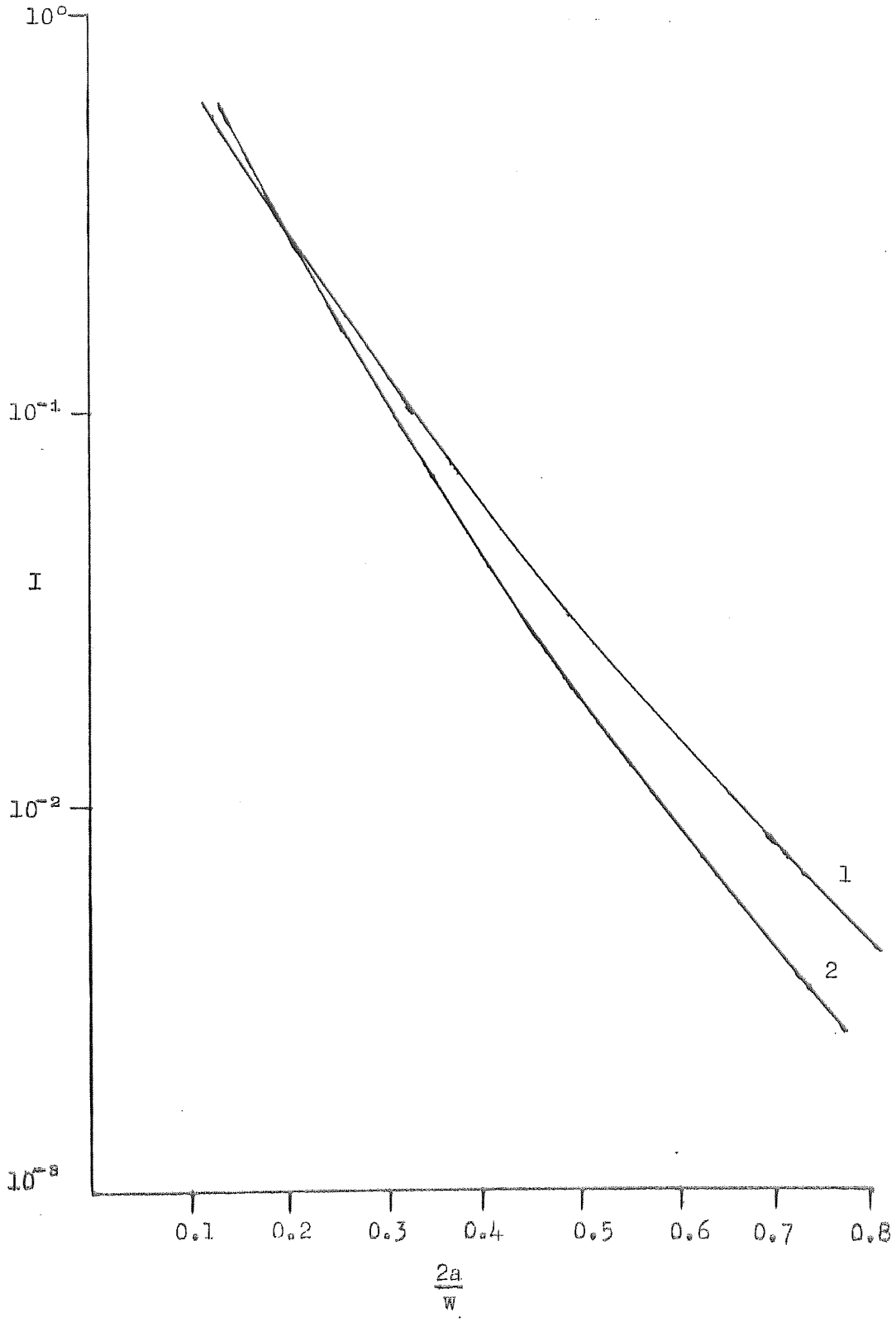

Appendices 3 and 4. The Value of the Crack Growth Integral, I, as a function of the Original Crack Size of a Central Defect

1. 'm' = 2.8
2. 'm' = 4.2

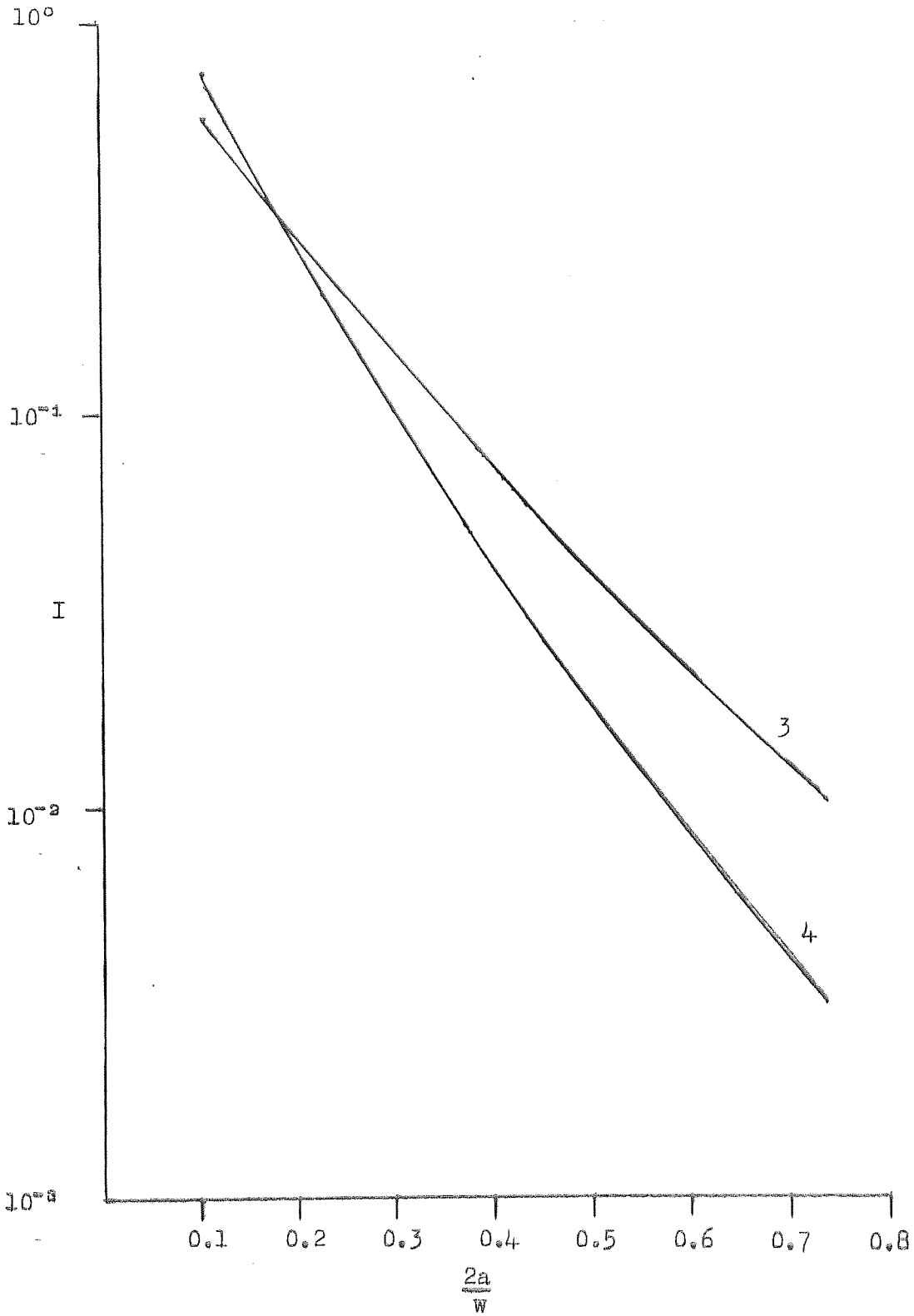

Appendices 5 and 6 The Value of the Crack Growth Integral, I, as a function of the Original Crack Size of a Central Defect

5. 'm' = 3.7
6. 'm' = 5.1

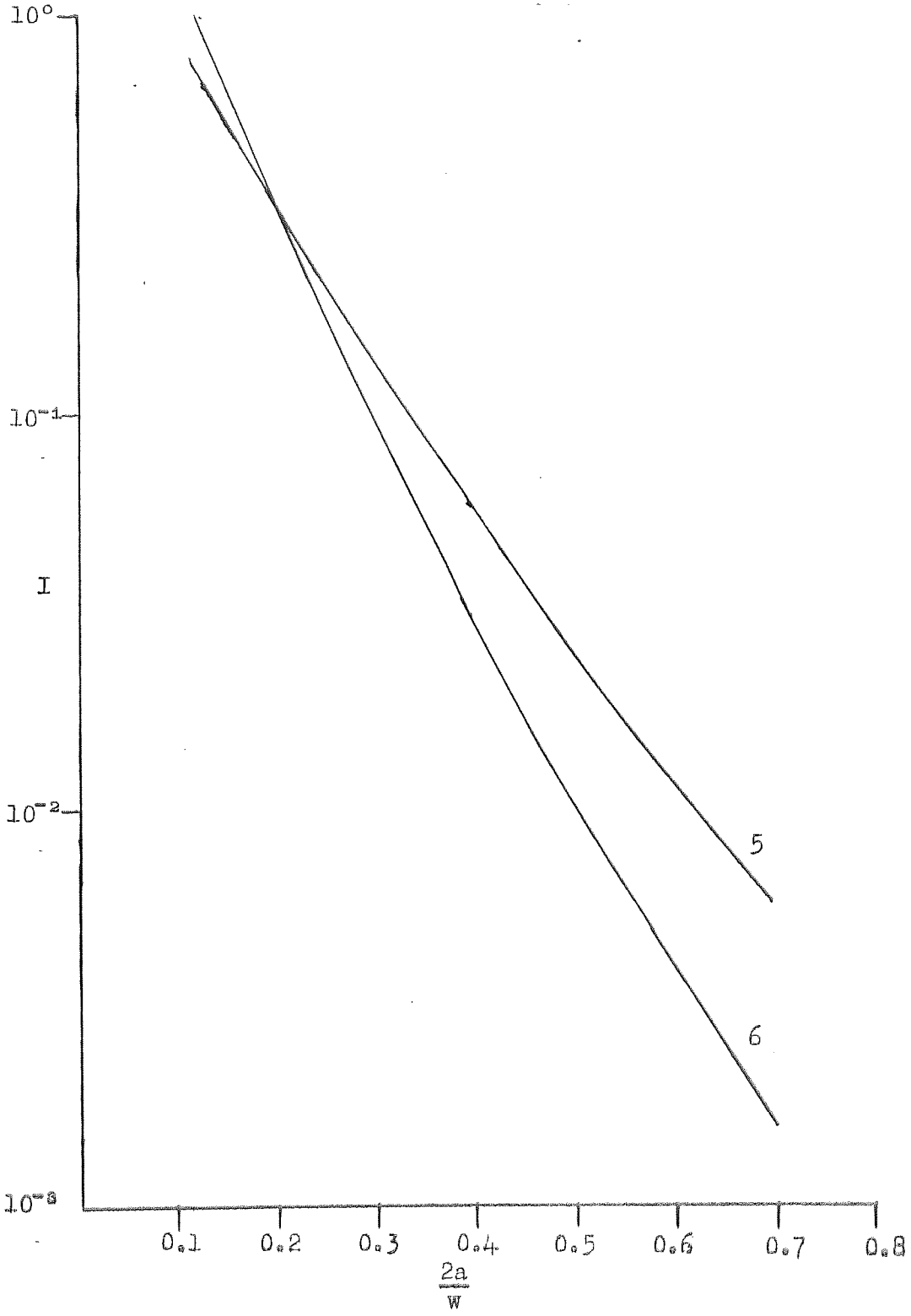

Appendix 7 The Value of the Crack Growth Integral, I, as a function of the original crack size, for the case of Reinforcement Defects at Room Temperature.

$\frac{a}{2c} = 0.3$

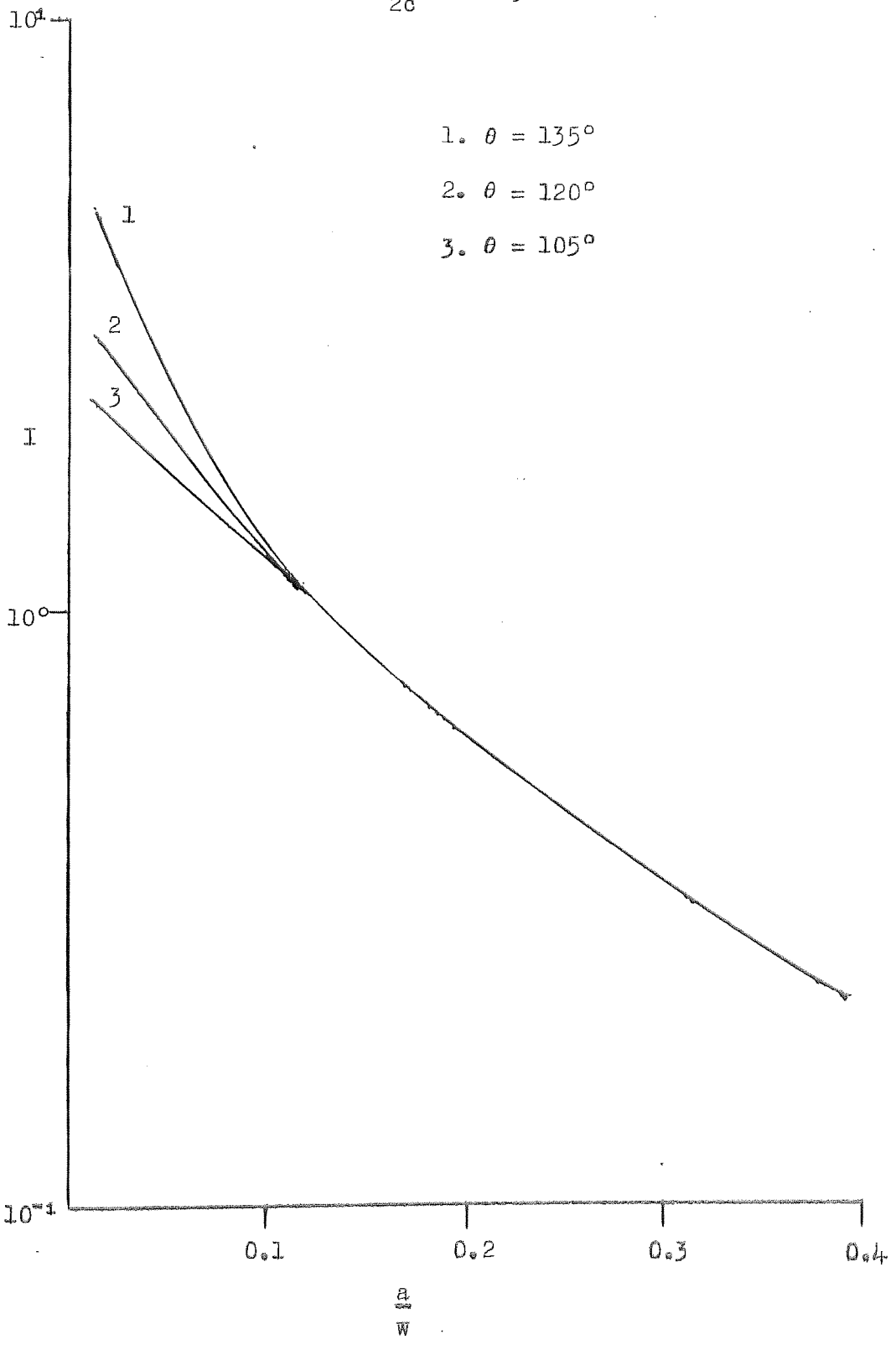

Appendix 8. The Value of the Crack Growth Integral, I, as a function of the original crack size, for the case of Reinforcement Defects at 300°C.

$\frac{a}{2c} = 0.3$

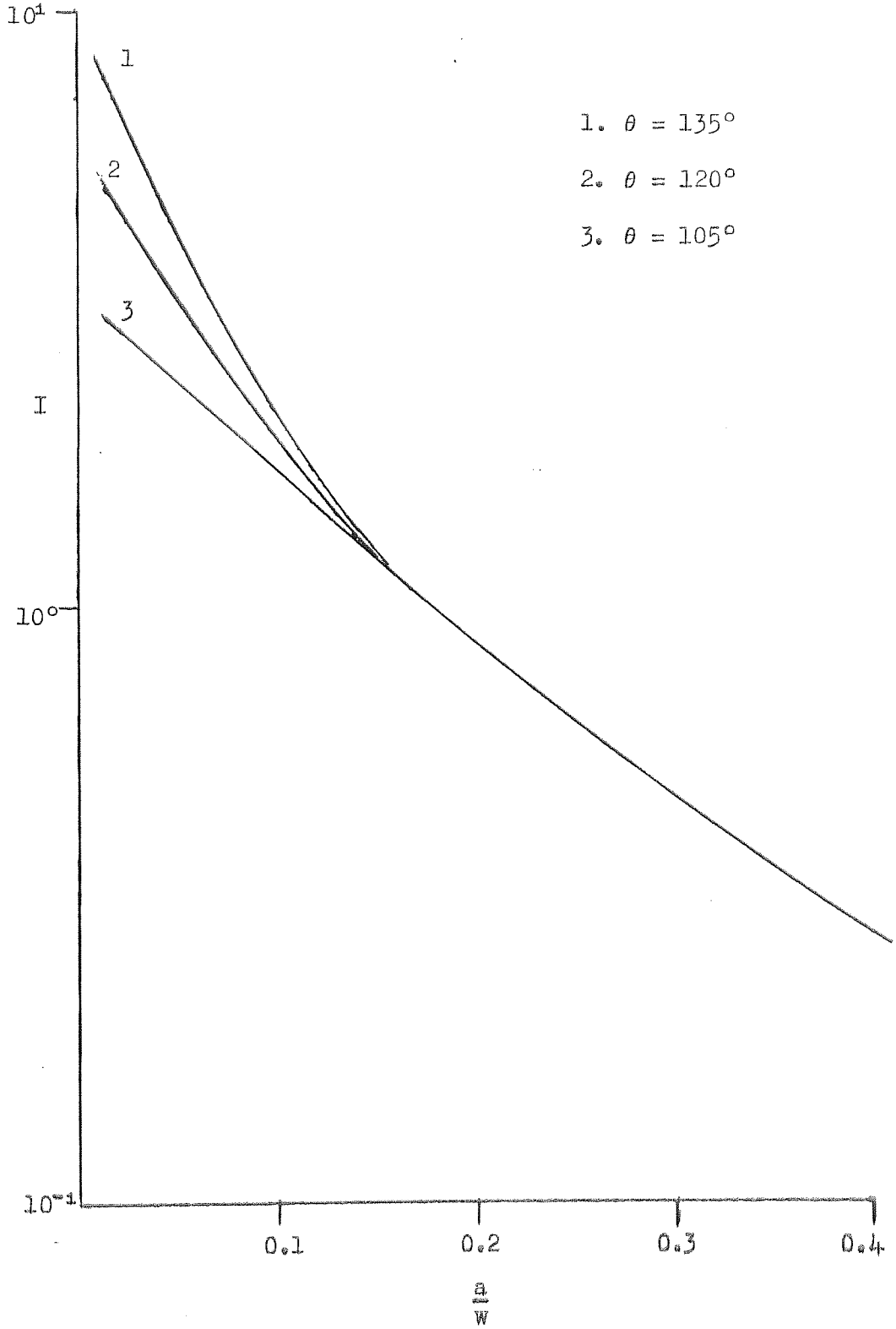

REFERENCES

1. J.A.Ewing and J.W.C.Humphrey. Phil.Trans A200,p 241 (1903).
2. H.J.Gough and D.Hanson. Proc.Roy.Soc. A104, p538 (1923)
3. E.Orowan Proc.Roy.Soc. A171,p79 (1939)
4. P.J.E.Forsyth. Proceedings of the Crack Propagation Symposium. Cranfield p.26 (1961)
5. P.J.E.Forsyth. International Conference on the Fatigue of Metals, London. Institution of Mechanical Engineers (1956)
6. L.J.Denver. Wright Air Development Centre Report No.56-408 (1957)
7. B.Chanley and T.J.Dolan. Am.Soc.Mech.Engineers - 'Metals Engineering - Design' p100 (1953)
8. L.J.Denver 'Interrelation of Fatigue Cracking, Damping and Notch Sensitivity' Rpt 56-408 (1957)
9. S.J.Maddox. Weld Res 10, p401-5 (1974)
10. C.A.Zappfe and C.O.Worden. Trans ASM 43, p 958 (1951)
11. C.Laird and G.C.Smith. Phil. Mag 7, p 847 (1962)
12. P.J.E.Forsyth and D.A.Ryder. Metallurgia 63, p 117 (1961)
13. Idem. Aircraft Engineering 32, p 96 (1960)
14. J.C.McMillan & R.M.N.Pelloux. ASTM STP 415, p 505
15. H.M.Westergaard. Trans ASME J.Appl.Mech. 61, p49 (1939)
16. G.R.Irwin. Structural Mechanics (Edited by Goodier and Hoff) p 557 (1960) Pergamon Press
17. A.A.Griffith. Phil Trans A221, p163 (1920)
18. G.R.Irwin. Fracturing of Metals ASM (Cleveland) (1948)
19. E.Orowan. Fatigue and Structure of Metals (MIT Symposium 1950) John Wiley and Sons. New York
20. W.F.Brown and J.E. Srawley. ASTM 410 (1966)
21. O.L.Bowie and D.M.Neal Technical Report AMRA TR65-20 (1965)
22. J.E.Srawley and B.Gross. Mats Research and Standards 7, p155 (1967)

23. J.R.Dixon and L.P.Pook. Nature 224, p 166 (1969)

24. A.M.Sullivan, Mats Research and Standards 7 p,20 (1967)

25. G.R.Irwin. Structural Mechanics (Edited by Goodier and Hoff) p557 (1960)Pergamon Press

26. D.J.Cartwright and D.P.Rooke. Eng.Frac.Mech.3 p563 (1974)

27. J.Weertman. Int.J.Fract.Mech. 5 p13 (1969)

28. N.A.Bilby, A.H.Cottrell and K.H.Swinden.Proc.Roy.Soc. A272 p 304 (1963)

29. B.A.Bilby and P.T.Heald. Proc.Roy.Soc. A305 p429 (1968)

30. L.N.McCartney and B.Gale. Proc.Roy.Soc.A333 (1973)

31. J.T.Barnby and F.M.Peace. Acta.Met.19 p1351 (1971)

32. Y.Komen and D.G.Brandon. Met Trans 1 p1663 (1970)

33. A.N.May. Nature 188 p173 (1960)

34. E.Smith. Proc.Roy.Soc.A229 p455 (1967)

35. A.R.Jack. 'Fatigue Cracking from Stress Concentrations in Mild Steel' Ph.D.Thesis. University of Aston (1971)

36. W.Weibull. SAAB TN25 (1954)

37. W.Weibull. The Aeronautical Research Institute of Sweden FFA Report 65 (1956)

37A. W.Weibull. Proceedings of Crack Propagation Symposium, Cranfield p 271 (1961)

38. M.A.Wilkins and G.C.Smith. Met.Sci.J.5 p139 (1971)

39. E.Taylor. Study of Low Cycle Fatigue Behaviour of Titanium Alloys University of Aston External Report (1973)

40. R.G.Forman. Eng.Fract.Mech.4 p333 (1972)

41. S.Pearson. R.A.E.Technical Report No.71109 (1971)

42. J.T.Barnby. K.Dinsdale and R.Holder. Institute of Physics and Metals Society. Conf on the Mechanisms and Physics of Fracture. Paper 26. Cambridge (1975)

43. S.S.Manson. Exp Mechs. p193 (1965)

44. T.H.Topper, R.M.Wetzel and J,Morrow. J.Mat 4. p200 (1969)

45. H.Neuber. J.Appl.Mech 83 p544 (1961)

46. J.Morrow. R.M.Wetzel and T.H.Topper. ASTM STP 462 p74 (1970)

47. C.B.V.Gowda, T.H.Topper and B.N.Leiss. Proc.Int.Conf on Mechanical Behaviour of Materials, Kyoto, Japan Vol.II p187 (1971)

48. S.J.Standick and J.Morrow ASTM STP 515. p229 (1972)

49. A.K.Head. Phil.Mag 44 p925 (1953)

50. W.Weibull. SAAB TN25 (1954)

51. W.Weibull. The Aeronautical Research Institute of Sweden FFA Report 65 (1956)

52. S.T.Rolfe and W.H.Munse. Weld Res.Supp.17 p131 (1963)

53. A.J.McEvily and W.Illg NACA-TN 4394 (1958)

54. N.E.Frost and J.S.Dugdale. J.Mech and Phys of Solids 6 p92 (1958)

55. N.E.Frost. Engineer 200 p464 (1955)

56. N.E.Frost and J.S.Dugdale. J.Mech and Phys of Solids 6 p92 (1958)

57. N.E.Frost and A.F.Greenan. N.E.L.Report 132 (1964)

58. N.E.Frost and K.Denton. N.E.L.Report 260 (1966)

59. N.E.Frost and J.R.Dixon. Int.J.Fract.Mech.3 p 301 (1967)

60. H.W.Liu. ASME Paper 60 - MET-11 (1960-

61. H.W.Liu. AR.L.Report 58 (1961)

62. P.C.Paris and F.Erdogan. Trans ASME 85 p121 (1963)

62A. P.C.Paris, M.P.Gomez and W.E.Anderson. The Trend in Engineering 13 p.9 (1960)

63. H.H.Johnson and P.C.Paris. Eng.Frac.Mech 1 p3 (1968)

64. G.A.Miller. Trans ASM 61 p442 (1968)

65. F.A.McLintock. Fracture of Solids. Interscience Publishers (New York) (1963)

66. J.M.Krafft. Applied Mats Research 3 p88 (1964)

67. J.M.Krafft. Trans A.SM 58 p691 (1965)

68. J.Weertman. Int. J.Fracture Mech. 2 p460 (1966)

69. R.K.Ham. Nature 212 p1568 (1966)

70. S.Pearson Nature 211 p1077 (1966)

71. N.E.Frost, L.P.Pooke, and K.Denton.Eng.Frac.Mech 3 p103 (1971)

72. S.Pearson. Eng.Frac.Mech.4 p9 (1972)

73. H.H.Johnson and P.C.Paris. Eng.Frac.Mech.1 p3 (1968)

74. W.G.Clarke Jr. J.Mat 6 p134 (1971)

75. R.G.Forman, V.E.Kearney, and R.M.Engle J.Bas.Enging. Trans ASME 89 p459 (1967)

76. C.M.Hudson and J.T.Scardinia. Eng.Fract.Mech.1 p429 (1969)

77. S.Pearson. R.A.E.Technical Report 69195 (1969)

78. N.E.Frost. First Int.Conf on Fracture. Vol.3 p1433 (1966)

79. M.R.Barren and R.P.Hurlebaus. Weld Res 5 p207-S (1971)

80. A.E.Asnis and G.A.Ivashchenko. Autom Weld 10 p32 (1967)

81. M.J.Openshaw M.Sc.Thesis. University of Aston (1973)

82. V.A.Shavyrin. Weld.Prod 1 p6 (1970)

83. W.O.Dinsdale and J.G.Young.Proc.Second Weld Conf. p153 (1970)

84. W.O.Dinsdale Brit.Weld J. 11 p22 (1964)

85. J.Martelee. Welding in the World 2 p122 (1969)

86. H.S.Reemsnyder. Weld Res.5 p213-5 (1969)

87. R.P.Newman and N.G.Dawes. Brit.Weld.J.12 p117 (1965)

88. T.R.Gurney. 'Fatigue of Welded Structures' Cambridge Press. p156 (1968)

89. W.O.Dinsdale and J.G.Young. Brit Weld J9 p482 (1962)

90. D.V.Lindh and G.M.Peshak. Weld.J. 48 p45-5 (1969)

91. G.A.Homes Arcos 15 p1951 (1938)

92. W.G.Warren. Weld.Res.6 p6 (1952)

93. L.S.Feldman. Weld Prod. 10 p15 (1970)

94. R.P.Newman. Trans.Inst. Marine Eng. 68 p153 (1956)

95. T.R.Gurney and S.J.Maddox Metal Construction 4 p418 (1972)

96. J.D.Harrison. Welding Institute Report Misc. March (1971)

97. J.D.Harrison. Welding Institute Report Misc. March (1972)

98. L.F.Coffin.Jr. Trans Am.Soc.Mech.Engrs. 76 p923 (1954)

99. S.S.Manson. Nat. Comm.Aero Tech.Note 2933 (1954)

100. R.W.Landgraf ASTM STP 467 p3 (1970)

101. S.I.Lui. J.J. Lynch, E.J.Ripling and G.Sachs Trans.Am. Inst. Min. metall Engrs. 175 p469 (1948)

102. V.D.Combs. ASTM STP 515 p3 (1971)

103. L.F.Coffin Jr. Appl. Materials Research 1 p 129 (1962)

104. D.Lee Metal Transactions 3 p315 (1972)

105. J.W.Aldrich and D.H.Avery. Sixteenth Sagamore Army Materials Research Conference (1969)

106. C.Laird and G.S.Smith. Phil Mag 8 p1945 (1963)

107. J.C.Grosskreutz. 'A critical review of micromechanisms in fatigue'. Fatigue - An Interdisciplinary Approach. Syracuse University Press, Syracuse N.Y. p 27

108. R.C.Boettner, C.Laird and J.G.McEvily. Trans Metall Soc. AIME 233 p 379 (1965)

109. B.Tompkins Phil Mag 18 p1041 (1968)

110. H.D.Solomon J.Materials 7 p299 (1972)

111. O.H.Basquin Proc.Am.Soc.Test Mater. 10 p625 (1910)

112. R.W.Swindeman ASTM STP 459 p31 (1968)

113. K.D.Sheffler and G.S.Doble. Symp on Fatigue at Elevated Temperatures ASTM STP (1972)

114. L.F.Coffin. Proc Second Int.Conf. on Fracture, Brighton p643 (1969)

115. L.F.Coffin. 'Corrosion Fatigue: Chemistry, Mechanics and Microstructure' NACE-2. National Association of Corrosion Engineers, Houston, p590 (1972)

116. L.F.Coffin.Jr. J.Materials 6 p388 (1971)

117. L.F.Coffin.Jr. Proc.Instn.Mech Engrs. 188 p120 (1974)

118. A.M.Van der Zanden. D.B.Robins and T.H.Topper ASTM STP 515 p268 (1972)

119. S.J.Maddox. Proc. Conf on Fatigue of Welded Structures. The Welding Institute (1970)

120. S.J.Maddox.Weld Institute Report E/50/72 (1973)

121. S.J.Maddox. Proc.Conf on Fatigue of Welded Structures, The Welding Institute (1970)

122. T.R.Gurney and S.J.Maddox. Metal Construction 4 p418 (1972)

123. S.J.Maddox. Welding Institute Report E/49/72 (1973)

124. J.D.Harrison. Met Con and B.W.J. 1 p333 (1969)

125. K.H.Frank Ph.D. Thesis. Lehigh University (1971)

126. S.J.Maddox. Weld Res 10 p401-s (1974)

127. F.V.Lawrence Jr. and J.B.Radzimiski. Weld Res. 6 p445-s (1970)

128. N.L.Person, Weld.Res. 7 p77-s (1971)

129. K.Jerram. 'Conf. on Fatigue of Welded Structures' Abingdon (Cambs) paper 2 p18 (1970)

130. M.J.Openshaw. M.Sc.Thesis. University of Aston (1973)

131. J.D.Harrison. Welding in the World 8 p168 (1970)

132. S.J.Maddox. To be published in Int.J.Fracture.

133. S.J.Maddox. Ph.D. Thesis. University of London (1972)

134. N.E.Frost. L.P.Pooke and K.Denton. Eng.Frac Mech.3. p103 (1971)

135. T.Yokobori. Tonoko University Sendai Japan 6 p19 (1969)

136. T.Ohmura, R.M.Pelloux and N.J.Grant. Eng.Frac.Mech.5.p909 (1973)

137. P.Shahinian, H.H.Smith and H.E.Watson. JMSLA.7 p 527 (1972)

138. L.A.James. ASTM STP.513. p218 (1972)

139. T.R.Gurney. 'Fatigue of Welded Structures' Cambridge Press (1968)

140. BISRA Open Report No. MG/EB/312/67.

141. A.R.Jack and D.E.Yeldham. CEGB Report No. 35D/MID/R/215/70 July (1970)

142. B.Gross, J.Srawley and W.F.Brown.Jr.Technical Note D2395.Nasa (1964)

143. H.Neuber. 'Theory of Notch Stresses' (1946)

144. R.G.Forman and A.S.Kobayashi. J.Bas.Eng.86 p93 (1964)

145. K.Tanaka. Eng.Frac.Mech.6 p493 (1974)

146. P.G.Forrest 'Fatigue of Metals' Pergamon Press p135 (1962)

147. R.E.Peterson 'Stress Concentration Design Factors' Wiley.J. New York (1953)

148. H.Neuber 'Theory of Notch Stresses' (1946)

149. P.Khun and H.F.Hardpath 'An Engineering Method for Estimating Notch Size Effect in Fatigue Tests on Steel' Nat.Adv.Co.Aero Tech. Note 2805 (1952)

150. J.R.Rise 'Fatigue Crack Propagation'ASTM STP 415 p247 (1966)

151. W.G.Clarke. Eng Frac Mech.1 p2 (1968)

152. N.E.Frost 'First International Conf on Fracture' Vol.3 p1433 (1966)

153. H.H.Johnson and P.C.Paris.Eng.Frac.Mech.1 p3 (1968)

154. B.Tomkins 'Proc.Conf on Mechanics and Mechanisms of Crack Growth' Cambridge April (1973)

155. N.E.Frost and J.R.Dixon. Int.J.Frac.Mech.3 p301 (1967)

156. L.P.Pook and N.E.Frost. Int.J.Frac.Mech 9 p53 (1973)

157. C.F.Tiffany and J.F.Masters. ASTM.STP 381 p249 (1965)

158. F.Jeglic, P.Niesson and J.D.Burns ASTM.STP 520 p139 (1973)

159. R.P.Wei. Int.J.Frac.Mech 4 p159 (1968)

160. M.Gell and G.R.Leverant ASTM STP 520 p37 (1973)

161. R.O.Ritchie 'Inst of Metallurgists Spring Meeting' Series 2 No10 Paper 8 p73 (1973)

162. M.F.Henry A.D.Soloman and L.F.Coffin Jr. 'Int Conf on Creep and Fatigue in Elevated Temperature Applications' Paper C182/73 (1973)

163. L.A.James. 'Fifth National Symposium on Fracture Mechanics' Urban. Illinois (1971)

164. J.Birbeck and K.Allery. Eng.Frac.Mech.4 p325 (1972)

165. Symposium on Strength and Ductility of Metals at Elevated Temperatures. A.S.T.M. S.T.P.128 (1952)

166. A.Robertson (Private Communication)